UNIVERSITÉ DU LUXEMBOURG

PhD-FSTM-2024-066
The Faculty of Science, Technology and Medicine

DISSERTATION

Presented on 06/09/2024 in ESCH-SUR-ALZETTE

to obtain the degree of

DOCTEUR DE L'UNIVERSITÉ DU LUXEMBOURG

EN BIOLOGIE

by

Candy Laura STEFFEN

Born on 11th October 1995 in Kyungsan City (South Korea)

DEVELOPMENT OF A PEPTIDE DISRUPTING NANOCLUSTERING OF H-RAS

Dissertation defence committee

Prof. Enrico Glaab (Chair)
University of Luxembourg, Esch-sur-Alzette, Luxembourg

Prof. Tom Grossmann (Vice-Chair)
Vrije Universiteit Amsterdam, Amsterdam, The Netherlands

Prof. Christina Kiel
University of Pavia, Pavia, Italy

Prof. Tobias Madl
Medical University of Graz, Graz, Austria

Prof. Daniel Abankwa (Dissertation supervisor)
University of Luxembourg, Esch-sur-Alzette, Luxembourg

UNIVERSITÉ DU LUXEMBOURG

Faculty of Science, Technology and Medicine

A dissertation by

Candy Laura STEFFEN

submitted to the University of Luxembourg

in partial fulfilment of the requirements for a degree of

Doctor of Philosophy

Approved by the dissertation defence committee:

Prof. Enrico Glaab (Chair)
University of Luxembourg Esch/Alzette, Luxembourg

Prof. Tom Grossmann (Vice-Chair)
Vrije Universiteit Amsterdam, Amsterdam, The Netherlands

Prof. Christina Kiel
University of Pavia, Pavia, Italy

Prof. Tobias Madl
Medical University of Graz, Graz, Austria

Prof. Daniel Abankwa (Dissertation supervisor)
University of Luxembourg, Esch/Alzette, Luxembourg

"Science, for me, gives a partial explanation for life. In so far as it goes, it is based on fact, experience and experiment."

- Rosalind Franklin

"Do not stop thinking of life as an adventure. You have no security unless you can live bravely, excitingly, imaginatively; unless you can choose a challenge instead of competence."

- Eleanor Roosevelt

“Nothing in life is to be feared, it is only to be understood. Now is the time to understand more, so that we may fear less.”

- Marie Curie

Dedication

This thesis is dedicated to my beloved parents, whose unwavering belief and support have shaped me into the person I am today. Thank you for encouraging me to pursue my dreams.

Table of Content

Acknowledgement

Firstly, I would like to express my sincerest gratitude and greatest respect to my supervisor and academic mentor, **Prof. Daniel Abankwa**, for allowing me to work on this stimulating thesis within an exceptional research group. Thank you for the unwavering supervision, invaluable guidance, and everything you have taught me during the last four years.

I am also profoundly grateful to my thesis committee members, **Prof. Enrico Glaab** and **Prof. Tom Grossmann** for providing me with their insightful advice and encouraging feedback during my PhD. I would like to acknowledge the external jury members of my defence committee, **Prof. Christina Kiel** and **Prof. Tobias Madl**, for taking the time to evaluate and examine my thesis.

I owe my deepest appreciation to my mentor, **Dr. Karolina Pavic**, for her kindness, support, encouragement, and the inspiring discussions we shared over the past years. A special thanks to **Dr. Ganesh Babu Manoharan** for training me at the start of my PhD, enabling me to become the researcher I am today. I would like to especially thank all the current members, **Dr. Elisabeth Schaffner-Reckinger, Dr. Sara Bottone, Dr. Rohan Chippalkatti, Christina Laurini, Bianca Parisi, Carla Duval, Atanasio Gomez Mulas** and **Göksu Oral Tüzün,** and past members, **Dr. Sunday Ojochegbe Okutachi, Dr. Farah Kouzi, Dr. Vladislav Stramiska, Marie Catillon, and Nesrine Ben Fredj** and **Dr. Pelin Kaya**, of the Cancer Cell Biology and Drug Discovery group, as well as all the bachelor and master students I encountered during my PhD. You all made my experience unique and unforgettable. Thank you for all your encouraging support, helpful advice and assistance and the fun moments we spent together. My deepest appreciation goes to the multi-talented **Christina** and research specialist **Marie** for always giving me invaluable assistance and significant troubleshooting. The biggest thank you to **Bianca** and **Sara** for the countless coffee breaks filled with conversations about science, laughter, and life, and for their precious friendship. *Grazie mille alle mie italiane preferite*.

To all my dearest friends, thank you for all your understanding and patience, and for standing by myside along the ups and downs of my PhD. Merci fir all är onendlech grouss Ënnerstëtzung.
Last but not least, I express my heartfelt appreciation to my family and friends. Without your unwavering support and greatest patience, I would not have become the person I am today. Merci **Mamma**, **Papa** a **Kevin**, mir hu gelaacht a gekrasch, geféiert a gegranzt. Ech weess et war net ëmmer einfach mat mir déi läscht Joren, mee ouni iech wier et net gaangen. Merci och dir **Ben**, fir deng grouss Gedold, däi Versteesdemech an deng Ënnerstëtzung.

Thank you all! Merci iech all!

List of figures

List of tables

List of abbreviations

AKT	Protein Kinase B (PKB)
AML	Acute myeloid leukaemia
ARF	ADP ribosylation factors
ASPP2	Apoptosis-stimulating of p53 protein family member 2
ATP	Adenosine triphosphate
AUC	Area under the curve
BRET	Bioluminescence Resonance Energy Transfer
CAM	Calmodulin
CR	Conserved region
CRD	Cysteine rich domain
CRD	Carbohydrate recognition domain
DARPin	Designed Ankyrin Repeat Protein
DSS	Drug sensitivity score analysis
E3-ligase	E3 ubiquitin ligase
EC50	Half maximal effective concentration
EMA	European Medicines Agency
ERK	Extracellular signal regulated kinase
FDA	U.S. Food and Drug Administration
FITC	Fluorescein isothiocyanate
FLIM	Fluorescence life-time imaging microscopy
FP	Fluorescence polarisation
FRET	Förster Resonance Energy Transfer
FTase	Farnesyltransferase
FTI	FTase inhibitors
G-domain	GTPase domain
Gal1	Galectin-1
Gal3	Galectin-3
GAP	GTPase activating proteins
GDP	Guanosine 5'-diphosphate
GEF	guanine exchange factors
GFP	Green fluorescent protein
GGT-1	Geranylgeranyltransferase I
GTP	Guanosine 5'-triphosphate
GTPase	Guanosine triphosphatases
H-Ras	Harvey rat sarcoma viral oncogene homolog
HIV1	Human immunodeficiency virus 1 or Lentivirus humimdef1
HK1	Hexokinase 1
HNSCC	Head and neck squamous cell carcinoma
HVR	Hypervariable region
IC50	Half maximal inhibitory concentration
ICMT	Isoprenylcysteine carboxylmethyltransferase
K-Ras	Kirsten rat sarcoma viral oncogene homolog
KD	Kinase domain

LC-MS	Liquid chromatography–mass spectrometry
MAPK	Mitogen-activated protein kinase
MEK	Mitogen-activated protein kinase kinase
mTOR	Mammalian target of Rapamycin
N-Ras	Neuroblastoma Ras viral oncogene homolog
NF1	Neurofibromin 1
NPM1	Nucleophosmin-1
NSCLC	Non-small-cell lung cancer
ORP	Oxysterol-related protein
PAT	Palmitoyl acyl transferase
PDB	Protein data bank
PDE6D	Retinal rod rhodopsin-sensitive cGMP 3',5'-cyclic phosphodiesterase subunit δ
PI3K	Phosphatidylinositol 3-kinase
PLCε	Phospholipase C-ε
POI	Protein of interest
PROTAC	Proteolysis Targeting Chimeras
PtdSer	Phosphatidylserine
QRET	Quenching resonance energy transfer
RA	Ras association domain
RAB	Ras-related protein
Raf	RAF proto-oncogene serine/threonine-protein kinase
Rafi	Raf inhibitors
RALGDS	Ral guanine nucleotide dissociation stimulator
RAN	Ras-related nuclear protein
Ras	Rat sarcoma
RASSF	Ras-association domain family
RBD	Ras binding domain
RCE1	Ras converting enzyme 1
RET	Resonance energy transfer
RHO	Ras homolog
RIN1	Ras and Rab interactor 1
RLuc	*Renilla* Luciferase
RTK	Receptor tyrosine kinases
SHOC-2	Leucine-rich repeat protein
SOS	Son of Sevenless
TIAM	T-lymphoma invasion and metastasis-inducing protein 1
TRPML1	Lysosomal Ca^{2+}-releasing mucolipin-1

Affidavit

I hereby confirm that the PhD thesis entitled “Development of a peptide disrupting nanoclustering of H-Ras” has been written independently and without any other sources than cited.

Luxembourg, 26th of July 2024 Candy Laura STEFFEN

List of Publications and Manuscripts

This thesis is based on publications and manuscripts, which are referred to in the text by their roman numbers:

I. Review publication (shared first author)

Steffen CL*, Kaya P*, Schaffner-Reckinger E*, Abankwa D. Eliminating oncogenic RAS: back to the future at the drawing board. Biochem Soc Trans. 2023 Feb 27;51(1):447-456. doi: 10.1042/BST20221343. PMID: 3668843

* These authors contributed equally

II. Research article (shared first author)

Steffen CL*, Manoharan Gb*, Pavic K, Yeste-Vázquez A, Knuuttila M, Arora N, Zhou Y, Härmä H, Gaigneaux A, Grossmann TN, Abankwa DK. Identification of an H-Ras nanocluster disrupting peptide. Commun Biol 7, 837 (2024). doi: 10.1038/s42003-024-06523-9.

* These authors contributed equally

III. Research article accepted in *STAR protocol* (shared first author)

Duval CJ*, **Steffen CL*,** Pavic K, Abankwa DK. Protocol to measure and analyze protein interactions in mammalian cells using Bioluminescence Resonance Energy Transfer. (05.09.2024)

Preprint available on bioRxiv doi: https://doi.org/10.1101/2024.07.05.602189

* These authors contributed equally

Abstract

The three oncogenes *KRAS, NRAS* and *HRAS* are mutated in 19 % of all cancer cases. Ras proteins were considered undruggable for a long time due to their shallow surface lacking druggable pockets. However, after decades of long and hard efforts, two allele-specific inhibitors against K-RasG12C were recently approved by the U.S. Food and Drug Administration (FDA) and European Medicines Agency (EMA) for non-small cell lung carcinoma (NSCLC). While *KRAS* is often mutated in lung, pancreas and colon cancer, *HRAS* is frequently mutated in bladder and head and neck cancer adding up to 250 000 new cancer cases per year worldwide. Next to therapies focusing on signalling downstream of mutant H-Ras, the farnesyl transferase inhibitor tipifarnib is the only approved inhibitor for H-Ras mutant cancer types. Despite these recent advances in therapies, patients rapidly develop resistances against these targeted therapies highlighting the need for novel broad spectrum targeting approaches.

Ras is organized into plasma membrane signalling hubs, called nanoclusters, which are the exclusive recruitment sites for effectors, such as Raf proteins. Ras nanoclusters are highly dynamic epicentres of mitogen-activated protein kinase (MAPK) signalling cascade. The canonical MAPK signalling downstream of Ras proteins regulates cellular processes such as proliferation, apoptosis, differentiation, etc. and is frequently dysregulated in human cancers (Guo et al., 2020).

Previously, our research group proposed that active H-Ras nanoclusters are stabilized by Raf dimers, and this complex can be further enhanced by Galectin-1 (Gal1) dimers (Blazevits et al., 2016). We demonstrated that Gal1 does not harbour a farnesyl binding pocket, thus does not bind to H-Ras directly, but instead engages with the Ras binding domain (RBD) of Raf. Given that nanoclustering determines MAPK output, the stabilization of Raf dimers by dimeric Gal1 was proposed as explanation for the observed increased MAPK signalling. In line with MAPK signalling driving cancer progression, patients with H-Ras mutant cancers that have a high Gal1 level display a poorer survival. Therefore, targeting the Raf/ Gal1 protein interface may represent a novel opportunity to inhibit enhanced H-Ras signalling.

We here identified the 52-amino acid L5UR-peptide and its 23-mer core fragment as an H-Ras nanocluster disrupting agent. L5UR binds with low micromolar affinity to the B-Raf RBD at a site that disrupts the B-Raf-RBD/ Gal1 interface. We have investigated the activity of L5UR and L5URcore in Bioluminescence Resonance Energy Transfer (BRET). This technique is typically used to study protein-protein interactions in intact cells and it is a suitable method to study Ras nanocluster organization. L5UR and L5URcore disrupt H-Ras nanoclustering-BRET, as well as Gal1/ RBD interaction BRET. Cell-permeable variants of the peptide decrease MAPK-signalling output and cell viability in H-Ras mutant cancer cell lines. The L5UR peptide may therefore represent a starting point for the development of chemical-biological tools that disrupt H-Ras nanoclustering and signalling.

Aims and objectives of the thesis

The Ras small GTPases are mutated in 19 % of all cancer cases worldwide (Prior et al., 2020). Since the discovery of Ras in the 1980s (Cox & Der, 2010), major research efforts have focused on directly or indirectly targeting Ras proteins. Despite recent breakthroughs, patients rapidly develop resistances against available specific inhibitors (Kwan et al., 2022). Hence, there is still a major need for alternative approaches to treat Ras mutant cancer.

Amongst the first targeting strategies, numerous research attempts focused on inhibiting the membrane anchorage necessary for Ras activity and developing methods to target downstream effector proteins. At the plasma membrane, Ras organises into proteo-lipid signalling complexes, called nanoclusters, which function as recruitment sites for at least Rad effector proteins. The best studied Ras nanocluster modulator is the small lectin, Gal1 (Pavic et al., 2022). Gal1 is involved in various extracellular processes. However, in the intracellular context Gal1 executes a different role. At micromolar concentrations, Gal1 can dimerize and thus stabilize H-Ras nanoclusters in a stacked dimer with Raf, as it binds its RBD domain (Blazevits et al., 2016). Thus, high Gal1 levels would stabilize Ras signalling complexes. High Gal1 levels are found in H-Ras mutant cancers, e.g., thymoma, bladder and head and neck cancers, and are associated with poorer survival rates of patients (Steffen et al., 2024). As H-Ras nanocluster-dependent signalling is enhanced by Gal1 binding to the RBD, their protein-protein interaction interface represents a promising target site. The research conducted for my thesis focuses on the development of a peptide binding at this protein-protein interaction interface in order to selectively target H-Ras nanoclustering and H-Ras driven cancers. We used BRET to study Ras nanoclusters and other relevant protein-protein interactions in intact cells. We therefore prepared a detailed published protocol to share with the research community. This inhibitory peptide, L5UR, affects Gal1-enhanced H-Ras signalling in H-Ras mutant cancer cell lines and more broadly inhibits 2D cell proliferation.

Therefore, the specific aims of this thesis are:

- To identify Ras targeting opportunities by a thorough and extensive literature review studying direct Ras binders of macromolecular nature either to inhibit Ras or explore the surface for new binding sites.
- To develop and characterize a peptide, which binds at the Gal1/ RBD interface to reduce Gal1-enhanced H-Ras nanoclusters and signalling in H-Ras mutant cancer cells.
- To prepare a comprehensive protocol describing the BRET method applied in this thesis to study protein-protein interaction.

Section A: Material and methods

1. Material

Table 1: Cell lines

Cell line	Tissue / Tumour Type	Mutation	Manuscript
Human cell line, HEK293-EBNA (HEK)	Human embryonic kidney	/	II, III
Human cell line, MIA PaCa-2	Pancreas/ Carcinoma	KRAS-G12C	II
Human cell line, Hs 578T	Breast/ Carcinoma	HRAS-G12D	II
Human cell line, T24	Urinary tract/ Carcinoma	HRAS-G12V	II
Hamster, BHK-21	Baby Hamster Kidney	/	II

Table 2: Recombinant DNA

Recombinant DNA	Manuscript
C413-E36_CMV promoter (Entry clone for Multisite Gateway Cloning)	II
C453-E04_CMV promoter (Entry clone for Multisite Gateway Cloning)	II
pDest-305 (Destination vector for Multisite Gateway Cloning)	II
pDest-312 (Destination vector for Multisite Gateway Cloning)	II
pDest-527 (Destination vector for Multisite Gateway Cloning)	II
C231-E13_RLuc8-stop (Entry clone for Multisite Gateway Cloning)	II
C511-E03_RLuc8-no stop (Entry clone for Multisite Gateway Cloning)	II
pDONR235-GFP2_stop (Entry clone for Multisite Gateway Cloning)	II
pDONR257-GFP2_no stop (Entry clone for Multisite Gateway Cloning)	II
Hs. K-Ras4BG12V (mutated P01116-2) (Entry clone for Multisite Gateway Cloning)	II
Hs. H-RasG12V (mutated P01112-1) (Entry clone for Multisite Gateway Cloning)	II
Hs. ARAF (P10398) (Entry clone for Multisite Gateway Cloning)	II
Hs. BRAF (P15056) (Entry clone for Multisite Gateway Cloning)	II
Hs. RAF1(P04049) (Entry clone for Multisite Gateway Cloning)	II
pDONR221-hGal1 (P09382) (Entry clone for Multisite Gateway Cloning)	II
pDONR221-hNGal1 (mutated P09382) (Entry clone for Multisite Gateway Cloning)	II
pDONR221-C-RBD (aa 56-131 of P04049) (Entry clone for Multisite Gateway Cloning)	II
pDONR221-B-RBD (aa 155-227 of P15056) (Entry clone for Multisite Gateway Cloning)	II
pDest305-CMV-GFP2- K-Ras4BG12V (mutated P01116-2)	II, III
pDest305-CMV-RLuc8- K-Ras4BG12V (mutated P01116-2)	II, III
pDest305-CMV-GFP2- H-RasG12V (mutated P01112-1)	II
pDest305-CMV-RLuc8- H-RasG12V (mutated P01112-1)	II
pDest305-CMV-hGal1 (P09382)	II
pDest305-CMV-RLuc8-Gal1 (P09382)	II
pDest305-CMV-GFP2-Gal1 (P09382)	II
pDest305-CMV-RLuc8-N-hGal1 (mutated P09382)	II

pDest305-CMV-GFP2-N-hGal1 (mutated P09382)	II
pEF-A-RBD-GFP2 (aa 19-91 of P10398)	II
pEF-B-RBD-GFP2 (aa 155-227 of P15056)	II
pEF-C-RBD-GFP2 (aa 56-131 of P04049)	II
pClontech-C-L5UR (P15814-1)	II
pEF-L5UR-SNAP (aa 38-89 of P15814-1)	II
pEF-mutL5UR-SNAP (mutated aa 38-89 of P15814-1)	II
pEF-SNAP	II
pDest305-CMV-GFP2-B-Raf (P15056)	II
pDest305-CMV-GFP2-C-Raf (P04049)	II
pDest305-CMV-GFP2-A-Raf (P10398)	II
pEF-A-RBD-D75A-GFP2 (mutated aa 19-91 of P10398)	II
pEF-B-RBD-D211,213A-GFP2 (mutated aa 155-227 of P15056)	II
mGFP-rtGal1 (P11762)	II
mRFP-C-RBD (aa 56-131 of P04049)	II
mGFP-H-RasG12V (mutated P01112-1)	II
mCherry-H-RasG12V (mutated P01112-1)	II
mRFP-C-RBD-D117A (mutated aa 56-131 of P04049)	II
pcDNA3-rtGal1 (P11762)	II
pcDNA3-N-rtGal-1 (mutated P11762)	II
pcDNA-Hygro-Anginex	II
pDest527-His-hGal1 (P09382)	II
pGEX4T2-B-RBD (aa 155-227 of P15056)	II
pGEX2T-C-RBD (aa 50-134 of P04049)	II
pGEX4T2	II
pcDNA3.1(-)	II, III
pDest305-CMV-mNeonGreen- H-RasG12V (mutated P01112-1)	II
pDest305-CMV-NanoLuc- H-RasG12V (mutated P01112-1)	II
pcDNA3-RLucF1-BRAF-RLucF2 (P15056)	II
pDest305-CMV- RLuc8	III
pDest312-CMV- GFP2	III

Table 3: Antibodies

Antibody	**Source**	**Manuscript**
mouse monoclonal anti-Galectin 1 (E2)	Santa Cruz Biotechnology	II
mouse monoclonal Lambda 5 (A-1)	Santa Cruz Biotechnology	II
rabbit polyclonal GST	Cell Signaling	II
rabbit polyclonal anti-SNAP	New England Biolabs	II
mouse monoclonal anti-B-Raf (F-7)	Santa Cruz Biotechnology	II
rabbit polyclonal anti-C-Raf (C-12)	Santa Cruz Biotechnology	II
rabbit polyclonal anti-PI3K p110α	Cell Signaling	II
mouse monoclonal anti-RASSF7 (C-6)	Santa Cruz Biotechnology	II
rabbit polyclonal anti-RASSF9	Invitrogen	II

rabbit polyclonal anti-ASPP2	Bethyl	II
rabbit polyclonal anti-GAPDH	Sigma-Aldrich	II
mouse monoclonal anti-B-actin	Sigma-Aldrich	II
mouse monoclonal anti-phospho-p44/42 MAPK (Erk1/2) (Thr202/Tyr204) (E10)	Cell Signaling Technology	II
p44/42 MAPK (Erk1/2) Rabbit pAb	Cell Signaling Technology	II
rabbit monoclonal anti-phospho-AKT(S473) (D9E)	Bioke	II
mouse monoclonal anti-AKT(pan) (40D4)	Bioke	II
IRDye 680LT Goat anti-Mouse IgG1-Specific Secondary Antibody	Li-Cor Biosciences	II
IRDye 800CW Goat anti-Mouse IgG Secondary Antibody	Li-Cor Biosciences	II
IRDye 680RD Goat anti-Rabbit IgG Secondary Antibody	Li-Cor Biosciences	II
IRDye 800CW Goat anti-Rabbit IgG Secondary Antibody	LI-Cor Biosciences	II

Table 4: Compounds, proteins, and peptides

Compounds, proteins and peptides	**Source**	**Manuscript**
Benzethonium chloride	Sigma-Aldrich	II
Trametinib	MedChem Express	II
Fluorescein- isothiocyanate labelled L5UR	Pepmic Co., China	II
L5UR	Pepmic Co., China	II
mutL5UR	Pepmic Co., China	II
L5URcore	Pepmic Co., China	II
Biotinylated L5UR	(Steffen et al., 2024)	II
TAT-L5URcore	(Steffen et al., 2024)	II
TAT-mutL5URcore	(Steffen et al., 2024)	II
TAT	(Steffen et al., 2024)	II
Eu-L5URcore	(Steffen et al., 2024)	II
GST-B-RBD	(Steffen et al., 2024)	II
B-RBD	(Steffen et al., 2024)	II
C-RBD	(Steffen et al., 2024)	II
GST	(Steffen et al., 2024)	II
His-Gal1	(Steffen et al., 2024)	II

2. Methods

Table 5: Methods

Methods	**Manuscript**
Expression constructs	II, III
Protein purification	II
Fluorescence Polarization	II
Immunoblotting	II
Cell Viability Assay and Drug Sensitivity Score (DSS) analysis	II
Bioluminescence Resonance Energy transfer assay	II, III

Section B: Synopsis

1. Synopsis – Introduction

1.1. Human Ras superfamily and related G-proteins

The Ras superfamily comprises more than 170 genes encoding small guanosine triphosphatases (GTPases), categorized into five subfamilies, RAS, RHO, ARF, RAB, and RAN. In addition, the heterotrimeric Gα subunit, closely related in sequence and function, is considered part of the Ras superfamily. However, unlike G-proteins, these subunits function as monomeric units (Claing, 2013; Colicelli, 2004). The members of this superfamily regulate various cellular processes including cytoskeletal structure and migration, vesicular transport, and nuclear transport (Bernal Astrain et al., 2022).

The oncoproteins K-Ras, H-Ras and N-Ras belong to the subfamily of Ras proteins and have been subject to intense research scrutiny. The three Ras oncogenes encode four different Ras proteins due to the two splice variants of the K-Ras transcript, K-Ras4A and K-Ras4B. Phylogenetically, the Ras proto-oncogenes originate from *KRAS*. Evolutionarily its duplication has led to the rise of *HRAS*, whereas the duplication of *HRAS* created *NRAS*. The isoform *KRAS4A* is the product of the duplication and insertion of the 4th exon of *NRAS* into the 3rd intron of *KRAS4B* (Garcia-Espana & Philips, 2023).

1.1.1. Ras proteins function as molecular switches at the plasma membrane

The four ubiquitously expressed Ras proteins, K-Ras4A, K-Ras4B, N-Ras and H-Ras, are highly homologous, sharing 82-90 % of their sequence identity. Notably, their first 82 amino acids are completely identical (Ahearn et al., 2018). These globular, single-domain proteins are composed of 188 amino acids for K-Ras4B and 189 amino acids for H-, N- and K-Ras4A. They mainly differ in the C-terminal hypervariable region (HVR), which plays a crucial role in the membrane anchorage of Ras. The CAAX motif included in the HVR undergoes different post-translational modifications, among others prenylation, to predominantly anchor Ras at the plasma membrane (Hobbs et al., 2016). The C in the CAAX motif represents a cysteine residue, A typically represents aliphatic residues and X can be any type of amino acid (Wright & Philips, 2006). The sequence variations in the HVR dictate the different post-translational modifications and lipid anchor attachments for each isoform (**Figure 1**) (Zhou & Hancock, 2015).

Prior to Ras activation, the four Ras proteins are irreversibly farnesylated by the farnesyltransferase (FTase) on the conserved cysteine in the HVR. Alternatively, K- and N-Ras, but not H-Ras, can be prenylated by geranylgeranyl transferase I (GGT-1). The farnesylation is followed by the cleavage of the amino acids AAX of the CAAX motif effectuated by the Ras converting enzyme 1 (RCE1) and lastly

the carboxymethylation of the cysteine residue by the isoprenylcysteine carboxylmethyltransferase (ICMT) (**Figure 2**). K-Ras4B, with its lysine-rich polybasic region, does not require further modifications and is translocated from the endoplasmic reticulum to the plasma membrane with the help of trafficking chaperones like Calmodulin (CaM) or Retinal rod rhodopsin-sensitive cGMP 3',5'-cyclic phosphodiesterase subunit δ (PDE6D) (Ahearn et al., 2011). In contrast, K-Ras4A, N-Ras and H-Ras, are palmitoylated at the Golgi prior to shuttling to the plasma membrane (Campbell & Philips, 2021). N- and K-Ras4A are monopalmitoylated on Cys180 and Cys181 respectively, and H-Ras is dually palmitoylated (**Figure 1, Figure 2**) (Campbell & Philips, 2021). The diverse lipid anchors determine the trafficking itineraries of each isoform (Mo et al., 2018).

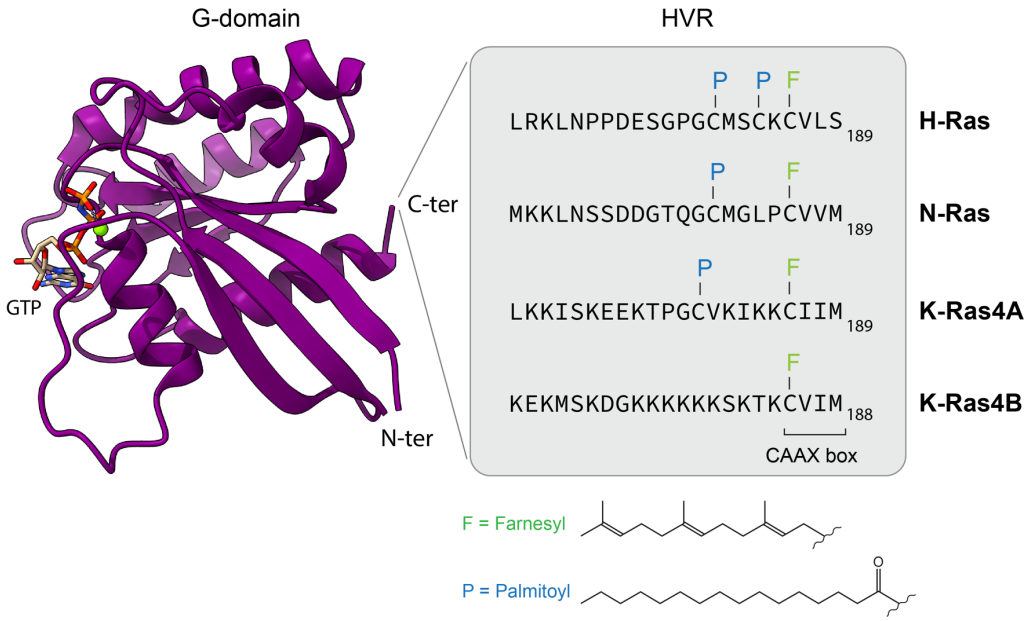

Figure 1. Comparison of structural diversity of the HVR of Ras proteins. *G-domain of GTP-loaded H-Ras (PBD code 4EFL) on the left and sequences of Ras isoform HVR and lipid modifications on the right (adapted from Van et al., 2021).*

The G-domain, ranging from amino acid 1 to 166, is commonly subdivided into lobe 1 (residues 1 – 85) and lobe 2 (86 – 166) (Gorfe et al., 2008). The conserved N-terminal lobe 1, also termed effector lobe, contains the P loop and the two switch regions, I and II, and engages in binding to effectors (Vatansever et al., 2016). The allosteric lobe (lobe 2) is more variable and interacts with the membrane (Grant et al., 2011). A third switch region, involving the β2-β3 loop and helix α5, influences the reorientation of GTP-loaded Ras at the membrane through helix α4 and the HVR (Abankwa, Hanzal-Bayer, et al., 2008).

Ras GTPases function as molecular switches, cycling between an inactive GDP-bound state and an active GTP-bound state (Hennig et al., 2015; Vetter & Wittinghofer, 2001). Once anchored at the plasma membrane, Ras is activated by exchanging GDP for GTP. This reaction is mediated by guanine

nucleotide exchange factors (GEF), e.g. Son of Sevenless (SOS) (Buday & Downward, 1993). SOS binding induces a conformational change in the flexible switch I and II regions, displacing the catalytic magnesium ion (Mg^{2+}) and decreasing nucleotide affinity (Bos et al., 2007). GDP is released from the nucleotide binding site of Ras. Given the higher intracellular abundance of GTP (10- to 50-fold excess) in most cell types, GTP rapidly replaces GDP in the nucleotide binding site (Hennig et al., 2015). This binding induces another conformational change, stabilizing the active state of Ras.

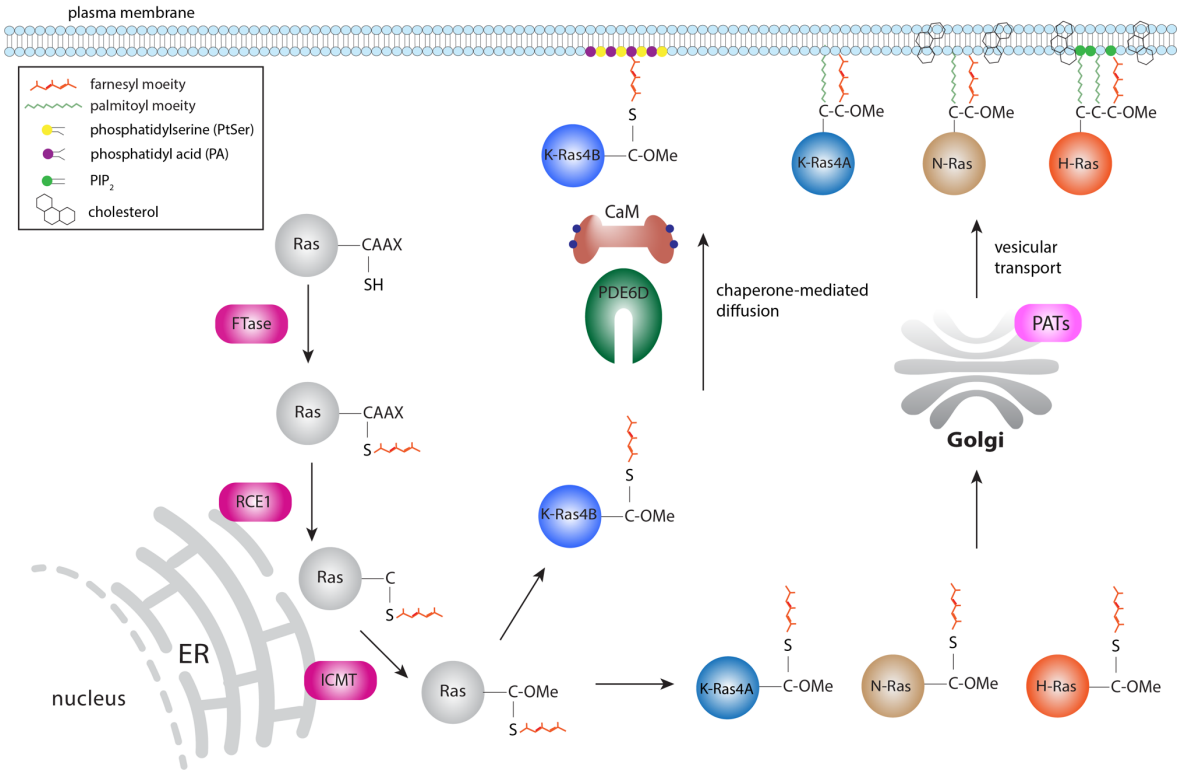

Figure 2. Overview of Ras post-translational modifications. *All four Ras isoforms are farnesylated at the CAAX motif, followed by the removal of "-AAX" by the RCE1 and carboxymethylation by the ICMT. K-Ras4A, N-Ras and H-Ras are palmitoylated at the Golgi before they are shuttled to the plasma membrane. C represents cysteine residue (adapted from Pavic et al., 2022).*

The activation process is tightly regulated by upstream factors to ensure the appropriate cellular response. The active, membrane-bound Ras proteins then engage with downstream effectors and activate downstream signalling pathways (Simanshu et al., 2017). Dysregulation of Ras and subsequent perturbance of its downstream signalling pathways are hallmarks of many human cancers. These disturbances can occur via various mechanism, including mutations in Ras and/ or its regulators or overexpression of Ras pathway components leading to amplification of the signalling. After effector recruitment, Ras is inactivated through the hydrolysis of GTP via their intrinsic GTPase activity, which can be enhanced by GTPase activating proteins (GAPs), for instance

neurofibromin 1 (NF1). Thus, Ras cycles between an “on-state”, GTP-bound, and “off-state”, GDP-bound (Hennig et al., 2015)

1.2. Ras effector proteins

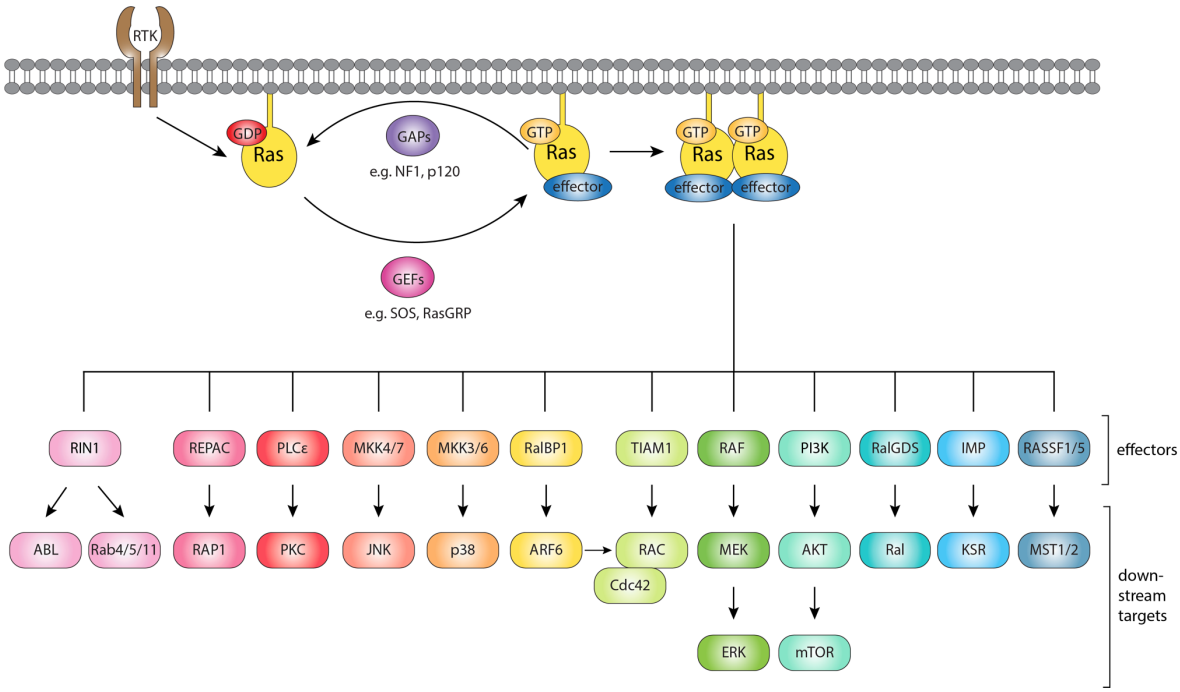

***Figure 3. Overview of known Ras effector proteins and their downstream targets**. Upon exchange of GDP to GTP, effector proteins compete for Ras binding. Ras nanoclusters at the plasma membrane act as recruitment sites for Raf effector proteins (adapted from Kiel et al., 2021).*

Proteins are categorized as canonical Ras effector proteins, if they contain at least one domain that directly binds to Ras, either a Ras binding domain (RBD-) or a Ras association (RA-) domain. These Ras binding domains (RBD) typically have a ubiquitin-like fold (Kiel et al., 2021). Ras effector proteins are binding Ras in a GTP-loading dependent manner and compete for Ras binding (Smith, 2023). Recently more than 50 putative RBD-containing proteins have been identified in the human proteome through sequence homology with most assumed to interact with the four Ras isoforms (Smith, 2023). Recently, also proteins missing the RBD or RA domains have been identified as Ras effector proteins, such as SHOC2 and hexokinase 1 (HK1) (Amendola et al., 2019; Bonsor & Simanshu, 2024). The most studied Ras effector proteins are shown in **Figure 3** (Kiel et al., 2021). Ras effector proteins link specific downstream signal outputs to Ras, which can result in completely opposite outcomes, such as normal development or Ras-driven tumorigenesis (Smith, 2023). Effector proteins bind to the switch I and II regions of Ras. Upon hydrolysis of GTP to GDP, they are released from binding to Ras due to the conformational change of the switch I and II regions. The

interaction between Ras and its effectors is often of low affinity; however the binding time might be increased by trapping the effectors in the actin mesh surrounding Ras nanoclusters at the plasma membrane (Abankwa & Gorfe, 2020; Kiel et al., 2021). However, for many of these identified Ras interactors, the exact binding mechanism is still not fully understood.

1.2.1. Structure of Ras effector protein Raf

The three Raf paralogs play a central role in the MAPK pathway, initiating the three-tiered signalling cascade that next activates the mitogen-activated protein kinase kinase (MEK) and the extracellular signal regulated kinase (ERK). This pathway, downstream of Ras, regulates a wide array of cellular and physiological processes, such as organismal development, cell cycle regulation, proliferation, differentiation, survival, and apoptosis. The Raf kinases, A-, B- and C-Raf, are highly homologous, but encoded by three different genes (Cook & Cook, 2021).

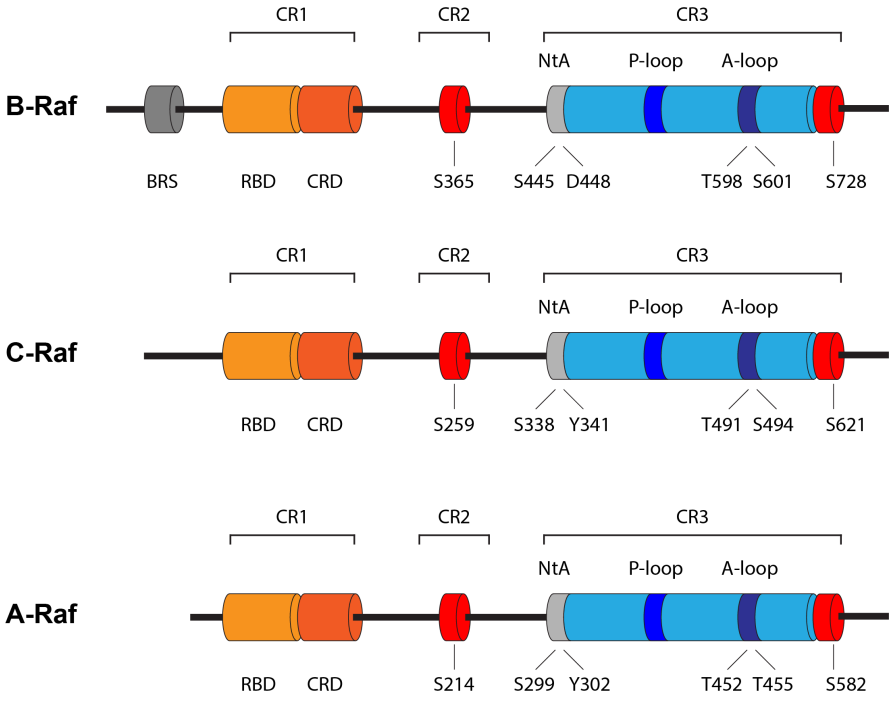

Figure 4. Schematics of structural features of the three Raf proteins. *Raf proteins are characterized by the three conserved regions (CR1, CR2 and CR3). The schematics display relative positions of conserved structural elements, such as Ras Binding Domain (RBD), Cysteine-rich domain (CRD), B-Raf specific region (BSR), glycine-rich phosphorylation loop (P-loop), activation loop (A-loop), N-terminal acidic region (NtA) and phosphorylation sites (Cook & Cook, 2021; Lavoie & Therrien, 2015; Martinez Fiesco et al., 2022; Park et al., 2019; Roskoski, 2010).*

Raf protein structure is divided into N-terminal regulatory domain and C-terminal kinase domain (KD), which contains three conserved regions (CR), CR1, CR2 and CR3 (**Figure 4**). CR1 comprises of

the RBD, which interacts with GTP-loaded Ras and a zinc-binding cysteine-rich domain (CRD), involved in Ras/ Raf interaction at the plasma membrane. CR2 is located within the N-terminal regulatory domain of Raf and is composed of a threonine- and serine-rich stretch (Lavoie & Therrien, 2015). CR2 contains a conserved serine (**Figure 4**), which upon phosphorylation binds 14-3-3 dimers together with a C-terminal conserved serine residue (Cook & Cook, 2021). CR3 comprises the C-terminal KD and facilitates the binding and phosphorylation of MEK1/ 2 (Shaw et al., 2014). The KD includes the catalytic domain DFG, which marks the start of the activation loop, and the regulatory αC-helix, which undergo conformational changes upon activation of Raf (Cook & Cook, 2021; Shaw et al., 2014). Additionally, αC-helix contains the RKTR motif (R506, K507, T508 and R509 in B-Raf), which is important for modulating Raf dimerization (Karoulia et al., 2017). Within the CR3, the phosphorylation loop (P-loop) is crucial for adenosine triphosphate (ATP) binding, while the activation loop (A-loop) is involved in the kinase function (Cook & Cook, 2021). The conserved N-terminal acidic region (NtA), located at the start of the activation loop, is essential for Raf dimerization and varies between B-Raf and A-/ C-Raf (Cook & Cook, 2021).

1.2.2. Raf activation and dimerization

The Raf kinases reside as autoinhibited monomers in the cytoplasm and are activated through multi-step process upon recruitment to the plasma membrane by active Ras. Specifically, autoinhibited B-Raf exists in a complex with 14-3-3 dimers and MEK. Unlike 14-3-3, MEK is not required for maintaining B-Raf in its autoinhibited state (Martinez Fiesco et al., 2022). In the autoinhibited state, the N-terminal region represses the C-terminal kinase. This inhibition is stabilized by the binding of a 14-3-3 dimer to the conserved serine in the CR2 region and to a second serine C-terminally located (Lavoie & Therrien, 2015; Park et al., 2019). Furthermore, the RBD of B-Raf remains accessible and binds GTP-loaded Ras even in the autoinhibited state. A current model of Raf activation suggests that a steric clash and electrostatic repulsion between 14-3-3 and Ras occurs at the RBD/ 14-3-3 binding interface. This repulsion dislodges the RBD and CRD, buried in the centre of the autoinhibited complex, thus resulting in the release of 14-3-3 from the conserved serine in CR2 (S365 for B-Raf) (Martinez Fiesco et al., 2022). Thus, the freed up CRD could contact Ras, as well as the plasma membrane, and stabilize the Ras-Raf complex (**Figure 5**). The membrane localisation and contact are required for dislodging the CRD and opening the autoinhibited Raf complex (Park et al., 2023). During phosphorylation of the activation loop, the conformation of the DFG motif switches from "out" to "in" followed by a conformational change in the αC-helix from "in" to "out." These changes induce the formation of an active Raf state (Cook & Cook, 2021).

The Raf opening alone is insufficient for Raf activation; instead, Raf activation is mediated by formation of Raf homo- and heterodimers at a conserved side-to-side interface (Lavoie et al., 2013; Park et al., 2023). During dimerization, the positively charged RKTR motif in the αC-helix interacts

with the NtA region of the phosphorylated partner Raf protein (Cook & Cook, 2021). It is hypothesized that the dephosphorylation of B-Raf at S365 by the SHOC2 phosphatase complex inhibits closing of Raf monomers, enhancing the lifetime of open inactive Raf monomers. This prevention leads to the accumulation and rearrangement into active dimers (Park et al., 2023).

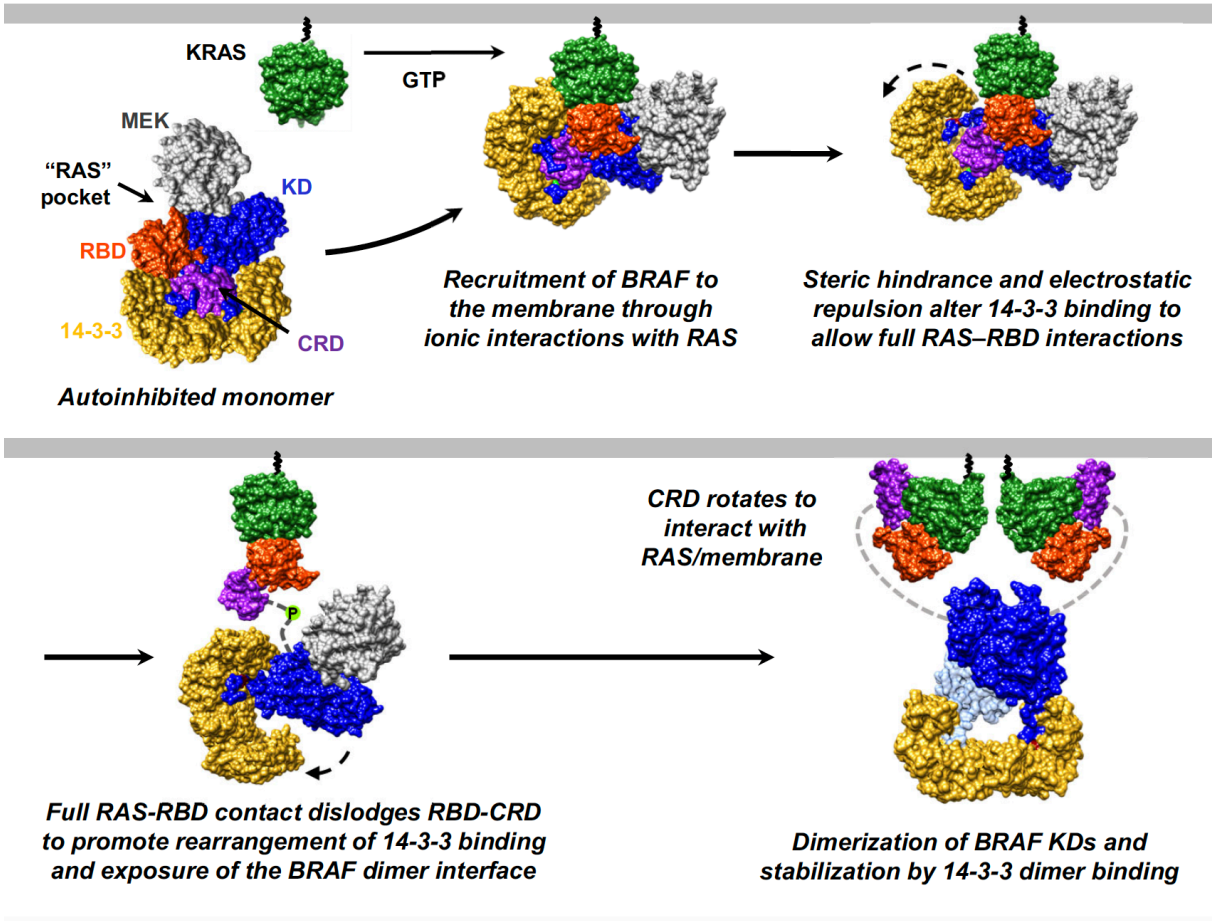

Figure 5. B-Raf monomer to dimer transition model. *The autoinhibited B-Raf monomer is recruited to the plasma membrane via ionic interactions between RBD and the switch I region of Ras upon Ras activation. The steric clashes and electrostatic repulsion between the RBD and the 14-3-3 facilitate the conformational changes dislodging the RBD/CRD. This promotes the rearrangement of 14-3-3 binding, revealing the pS365 site and the B-Raf dimer interface. The rotation of the CRD further stabilizes the interaction with the membrane and K-Ras and thus exposes the KD. The KD then dimerizes and adopts the active catalytic conformation stabilized by 14-3-3 dimer binding to the pS729 sites on B-Raf (from Martinez Fiesco et al., 2022).*

1.2.3. Raf inhibitors and paradoxical activation

Given its frequent implication in tumorigenesis, many research efforts have focused on developing inhibitors against Raf kinases, particularly targeting the B-RafV600E mutation commonly found in melanoma, thyroid, glioblastoma, colon, and lung cancer (Holderfield et al., 2014). A broad set of

inhibitors against dysregulated Raf have been developed. The Raf inhibitors (Rafi) can be categorized into three types: type I, type I ½ and type II (**Figure 6**) (Cook & Cook, 2021). The type I Rafi are first-generation inhibitors and mostly ATP-binding competitors (**Figure 6A**) (Holderfield et al., 2014). Type I ½ inhibitors, such as vemurafenib (PLX4032) and dabrafenib (GSK2118436) have been developed and demonstrated impressive potency against metastatic melanomas with B-RafV600E allele (**Figure 6A**) (Bollag et al., 2010; Chapman et al., 2011). Additionally, vemurafenib has been shown to be highly effective in B-RafV600E-dependent melanoma harbouring low Ras activity levels. However, both vemurafenib and dabrafenib, have surprisingly exhibited weak inhibition activity in cancer with receptor tyrosine kinases (RTK) or Ras mutations (Durrant & Morrison, 2018). Patients rapidly develop distinct resistance mechanisms against these kinds of inhibitors (Lavoie et al., 2013). A subset of cells promptly develops resistance mechanism via expressing different splice variants of B-RafV600E, lacking the exons 4-8, including the RBD (Poulikakos et al., 2011). These mutant isoforms dimerize independently of Ras and are insensitive to Raf inhibitors (Poulikakos & Rosen, 2011). In non-saturating conditions, the inhibitor binds one Raf protomer of either a homo- or heterodimer, inhibiting one member, but transactivates the drug-free Raf protomer (**Figure 6A**) (Poulikakos et al., 2010). Furthermore, it has been shown that drug-binding limits the kinase lobes in movement. Thus, the generated static dimer interface facilitates the formation of dimers at the plasma membrane (Lavoie et al., 2013). More understanding of this mechanism was given by extensive structure/ function studies. The type I ½ inhibitors stabilize the KD in the DFG-in/ αC-helix-out conformation required for dimerization and induce paradoxical activation of Raf (Karoulia et al., 2016). All dimer promoting inhibitors, inducing paradoxical activation, bind B-Raf with altering the orientation of R506 side chain, located in the RKTR motif of αC-helix (Durrant & Morrison, 2018). This conformational change of R506 leads to a disruption of a critical salt-bridge, which stabilises dimeric Raf complexes (Karoulia et al., 2016).

Since then, overcoming the paradoxical activation of Raf became the major focus. Most drug development efforts have focused on developing inhibitors of both monomers and dimers of Raf, binding the DFG-out/ αC-helix-in conformation, named pan-Raf or type II inhibitors (**Figure 6B**) (Durrant & Morrison, 2018). For example, pan-Raf inhibitor LY3009120 blocks MEK activation driven by Ras mutants, B-RafV600E monomers, and non-B-RafV600E dimers in melanoma and colorectal cancer (Peng et al., 2015; Vakana et al., 2017). Another strategy is the development of inhibitors, which do not promote dimerization, called paradox breakers. The company Plexxikon focused on optimizing the type I ½ inhibitor vemurafenib to generate the paradox breakers PLX7904 and PLX8394, which inhibit ERK activation in melanoma cell lines with N-Ras mutation (**Figure 6C**) (Zhang et al., 2015). It is thought that the paradox breakers prevent dimerization by causing steric hindrance at the dimer interface.

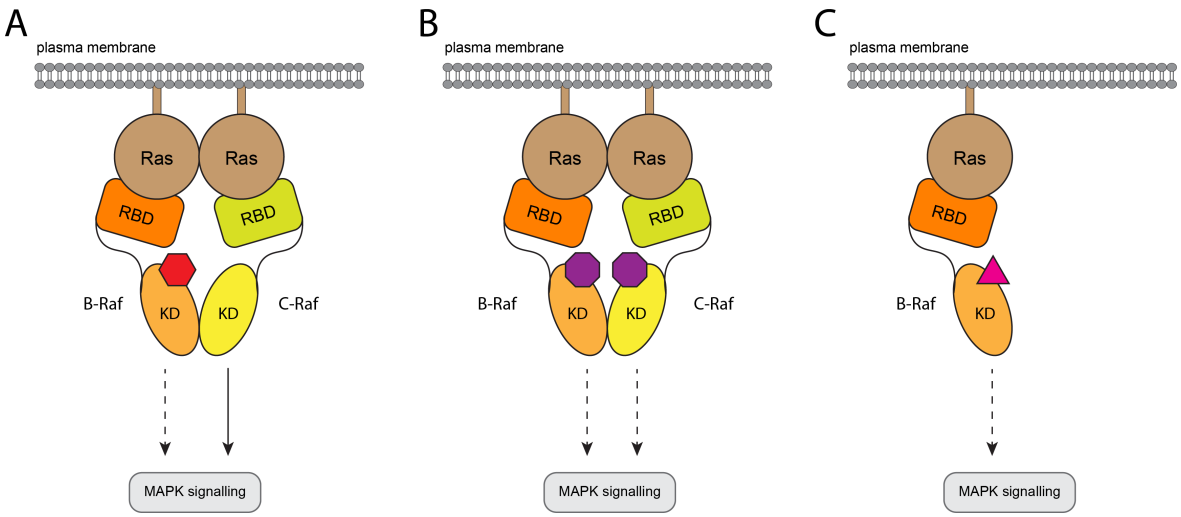

Figure 6. Overview of Raf inhibitor models. *(A) Type I and I ½ inhibitors can induce paradoxical activation. (B) Type II pan-Raf inhibitors alter the αC-helix orientation, thus preventing/ disrupting dimerization. (C) Paradox breakers are non-dimer promoting inhibitors, because they may cause steric hindrance at the dimer interface (adapted from Durrant & Morrison, 2018).*

Considering the extensive efforts on overcoming the paradoxical Raf activation with the design of next-generation inhibitors, other targeting approaches have emerged. Targeting Ras/ Raf interface demonstrates a plausible alternative, given the prerequisite of Ras binding for Raf dimerization. Designing peptides, mimicking the Raf dimer interface, may prevent Ras-driven heterodimerization and subsequent downstream signalling (Durrant & Morrison, 2018). Currently the inhibitor dabrafenib, specifically targeting B-RafV600E, in combination with the MEK inhibitor trametinib is approved by both the FDA and EMA for treatment of patients with melanoma, anaplastic thyroid carcinoma, non-small-cell lung cancer (NSCLC) and low-grade glioma (Gouda & Subbiah, 2023).

1.3. Ras nanoclusters and nanocluster modulators

1.3.1. Ras organises into nanoclusters at the plasma membrane

Once RAS is translocated to the inner leaflet of the membrane, the proteins laterally segregate and assemble into nanoclusters. The active nanoclusters, formed by GTP-loaded Ras proteins, are the exclusive sites of effector recruitment, forming highly dynamic epicentres of the Ras signalling cascade (Zhou et al., 2018). Nanoclusters consist of two to three Ras proteins and have an approximate size of 9 nm. Their lifetime varies according to their activation state (Abankwa & Gorfe, 2020). A nanocluster of inactive Ras has an approximate lifetime of only 0.1 seconds, which is 10 time less than the average lifetime of an active nanocluster (1 second) (Zhou & Hancock, 2015) Inactive Ras moves more freely at the plasma membrane than activated Ras. The Ras dynamics on the membrane are governed by activation state dependent orientations of Ras (**Figure 6**) (Abankwa

& Gorfe, 2020). The membrane orientation of the G-domain may contribute to determining Ras isoform diversity, as it constitutes a first selectivity filter for effector engagement (Abankwa, Gorfe, et al., 2008; Zhou & Hancock, 2018). To express this conformational switch of membrane-bound Ras, the balance model was proposed. GDP-loaded H-Ras at the plasma membrane is stabilized by R169 and K170 in the HVR. Upon activation, the HVR shifts the orientation of the G-domain, and membrane anchorage is stabilized by contacts between R128 and R135 located in the helix α4 (Abankwa, Hanzal-Bayer, et al., 2008).

The non-random organisation into nanoclusters correlates with the organisation of lipid microdomains. Ras nanocluster formation is highly regulated by different phospholipid species in the plasma membrane. The isoforms have distinct preferences for lipid environment. Both K-Ras nanoclusters and membrane anchorage require specific phosphatidylserine (PtdSer) -rich environment at the plasma membrane (Zhou & Hancock, 2015).

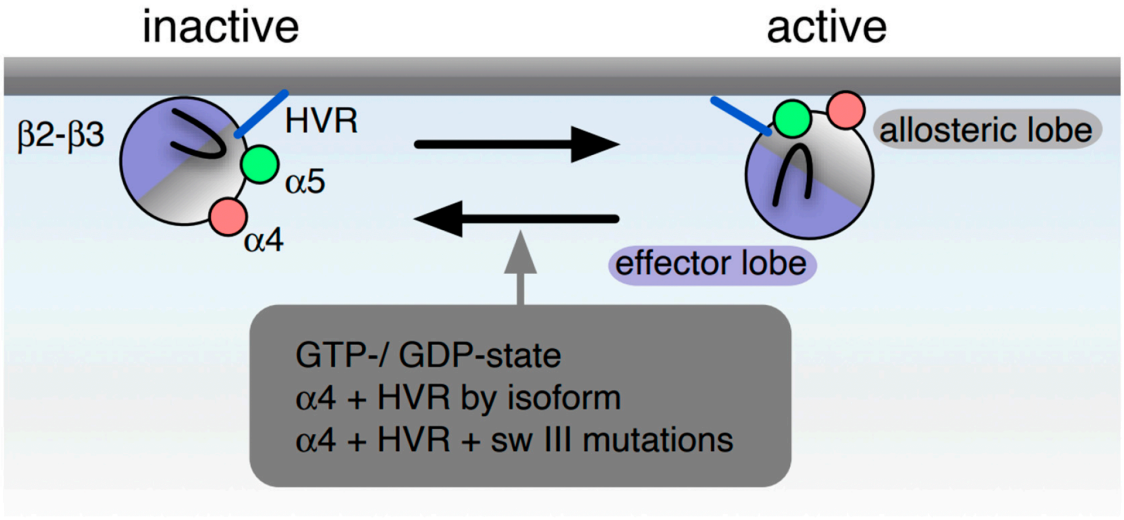

Figure 7. Model of Ras orientation at the plasma membrane*. The distinct orientation states of Ras at the membrane are supported by computational and experimental data. GDP-bound (inactive) Ras contacts the membrane predominantly through the lipid-modified HVR (blue). In the GTP-bound (active state), the helix α4 (pink) transiently maintains contacts with the membrane. The switch III region contains the β2- β3 loop (black), also known as interswitch region, and helix α5 (green) (from Abankwa & Gorfe, 2020).*

1.3.2. Ras nanocluster modulating proteins

Ras nanocluster are versatile lipid-based signalling platforms modulated by a variety of scaffolds or modulators, which are unrelated and structurally diverse. The ensemble of known modulators counts only around half a dozen members (Pavic et al., 2022). As advancements continue in

identifying Ras interaction partners, more modulators are being discovered. Not all modulators influence all four Ras isoforms due to their diverse nature (Pavic et al., 2022). For example, H-Ras nanoclusters are positively regulated by Gal1 dimers, shifting the signalling output from the PI3K pathway toward enhanced MAPK signalling, thus driving tumorigenicity in H-Ras mutant tumours (Blazevits et al., 2016; Posada et al., 2017).

Apoptosis-stimulating p53 protein family member 2 (ASPP2) is a multifunctional protein involved in apoptosis and cell cycle regulation and has been identified as a novel Ras nanocluster modulator (Iosub-Amir & Friedler, 2014; Wang et al., 2013). ASPP2 binds H-Ras, K-Ras, and N-Ras, positively mediating nanoclustering by increasing both pERK1/2 and pAKT levels. Full-length ASPP2 contains an N-terminal ubiquitin-like domain similar to the RBD or RA domains of Ras effector proteins (Posada et al., 2016). ASPP2 co-immunoprecipitates with H-RasG12V, enhancing downstream Raf-mediated signalling. The α-helical middle domain is necessary for Ras nanocluster modulation (Posada et al., 2016). Specifically in combination with Gal1 enhancing-effect on H-RasG12V, ASPP2 shifts the cellular response away from Gal1-induced growth promotion (Posada et al., 2016). However, ASPP2 is not only tied to Ras, but interacts also with effector proteins of the RAS superfamily containing the RA-domain, for instance RASSF7, RASSF8, RASSF9, and RASSF10 (Dhanaraman et al., 2020). The Ras effector proteins RASSFs are known to directly interact with the small GTPase of the RAS superfamily. The precise selectivity of the RASSFs for the more than 160 members of the RAS superfamily still needs to be unfolded. The RASSFs are known to interact directly with the small GTPase of the RAS superfamily, linking Ras signalling to the pro-apoptotic Hippo pathway. This interaction occurs either by forming complexes with the Hippo kinase ortholog MST1 (RASSF1-6) or oligomers with the p53-regulating proteins ASPP1 or ASPP2. Specifically, RASSF5 is known to bind both H-Ras and K-Ras. Due to recent evidence, it cannot be excluded that RASSF1, via heterodimers with RASSF5, mediates H-, K-, and N-Ras signalling.(Dhanaraman et al., 2020; Rezaei Adariani et al., 2021).

The lateral segregation and organization of Ras into nanoclusters are tightly regulated by interactions with membrane lipids. Oxysterol-related proteins ORP5 and ORP8, which maintain the PtdSer content on the plasma membrane, indirectly regulate K-Ras nanoclusters, as K-Ras harbours a selectivity for PtdSer. Inhibiting ORP5 and ORP8 results in the mis-localization of K-Ras and reduced nanoclustering (Kattan et al., 2019).

The lysosomal Ca^{2+}-releasing mucolipin-1 (TRPML1) channel belongs to the transient receptor potential channels (Yang et al., 2020). The non-selective cation channel TRPML1 is involved in various membrane-trafficking processes, such as autophagic vesicle-lysosome fusion, lysosome reformation and lysosomal exocytosis. Besides its trafficking activity, the TRPML1 gene, *MCOLN1*, has been found as a signature gene in H-Ras mutant cancers (Jung et al., 2019). TRPML1 is required

for cancer cells expressing mutant H-Ras. TRPML1 plays a role in the maintenance of the plasma membrane cholesterol levels. Inhibition of TRPML1 with the inhibitor ML-SI1 decreases H-Ras nanoclustering and reduces pERK1/ 2 signalling (Jung et al., 2019).

The pentameric protein Nucleophosmin-1 (NPM1) is a multidomain protein of the nuclear chaperone family (Lopez et al., 2020). In acute myeloid leukaemia (AML) NPM1 is frequently mutated, leading to its abnormal cytoplasmic distribution (Liso et al., 2008). NPM1 and its interaction partner nucleolin have been identified as K-Ras4B interactors and can increase plasma membrane localization of K-Ras4B (Inder et al., 2009). Additionally, NPM1 increases oncogenic and wild-type K-Ras4B nanoclustering (Inder et al., 2010). The exact mechanism of action, however, remains unknown.

The RAS superfamily member DIRAS3 shares high homology with Ras and plays an important role in cancer development, including cell migration, growth and apoptosis (Li et al., 2019). DIRAS3 directly binds to Ras, and the formation of Ras-DIRAS3 heteromers disrupts nanocluster formation and subsequent Raf activation, inhibiting the transformation and growth of cancer cells (Sutton et al., 2019).

1.3.3. Galectins as nanocluster modulators

Lectins are small glycan-binding proteins identified by at least one evolutionarily conserved carbohydrate binding site (Yu et al., 2023). The galectin family, a subset of lectins, is characterized by a high affinity for β-galactosides (Shimada et al., 2020). There are 15 different galectins in mammals, but only 11 can be found in humans (Lau et al., 2022). Most galectins are present across various tissue and cell types and are synthesized on free polysomes (Shimada et al., 2020). They can shuttle between the cytoplasm and nucleus and are often found in the extracellular matrix. Depending on their localization, galectins play roles in apoptosis, cell differentiation, proliferation, adhesion, and migration (Shi et al., 2022). By binding to glycocarbohydrates, galectins mediate cell-to-cell interactions, as well as cell-to-matrix interactions.

The 15 galectins can be classified in three groups (Ebrahim et al., 2014). The prototype group contains a single carbohydrate recognition domain (CRD). The second group is the tandem-repeat-type. These galectins contain two distinct carbohydrate binding sites. The last group of galectins consists of only one member, namely the chimeric Galectin-3 (Gal3) (Troncoso et al., 2023).

The best-studied nanocluster modulator is Gal1, which increases H-RasG12V nanoclustering and will be discussed in a later chapter. Another galectin family member, Gal3, has been studied in the context of K-Ras4B nanoclusters (Shalom-Feuerstein et al., 2008). Through its 120 amino acid N-terminal extension, Gal3 can form dimers or even multimers (Lau et al., 2022; Troncoso et al., 2023). Gal3 can be secreted to the extracellular milieu, where it is involved in cell-matrix interactions and plays a role in modulating the immune response, inflammation, and tumour progression

(Shimada et al., 2020). Inside cells, Gal3 stabilizes active K-Ras nanoclustering (Elad-Sfadia et al., 2004). This interaction promotes downstream signalling pathways, such as the MAPK pathway, impacting cell adhesion and migration. By modulating the Ras pathway, Gal3 enhances also the activation of cell survival signals, therefore inhibiting apoptotic processes (Shi et al., 2022).
As there are 15 human galectins, other family members may play unknown roles in Ras nanocluster modulation. For instance, Galectin-7 (Gal7) and Galectin-8 (Gal8) were recently discovered in the K-Ras4B interactome (Elad-Sfadia et al., 2004; Kovalski et al., 2019). However, the exact mechanism in which they modulate Ras nanoclusters remains to be determined.

1.4. Galectin-1 in cancer

Gal1 is about 14.5 kD in size and is found as a non-covalent homodimer (Cho & Cummings, 1996). The 135 amino acid long protein is encoded by the gene *LGALS1* (Pfeffer et al., 2023). The Gal1 dimer interface comprises a 22-strand anti-parallel β-sandwich (Yu et al., 2023). The functional differences of Gal1, depending on its location, may be due to the oxidation state of its six cysteine residues (Yu et al., 2023). For example, oxidized monomeric Gal1 reduces T-cell apoptosis activity but loses its ability to bind lactose (Guardia et al., 2014). There is a positive correlation between Gal1 levels and tumour invasiveness or metastasis in various cancers (Shimada et al., 2020). In human breast cancer, Gal1 expression correlates positively with tumour grade, with Grade III tumours having 3.5 times more Gal1-positive cells than Grade I tumours (Dalotto-Moreno et al., 2013; Ebrahim et al., 2014). Gal1 expression in various tumour types, e.g. prostate, melanoma, and brain gliomas, correlates with presence of high angiogenesis, especially in advanced stages of the diseases (Compagno et al., 2014; Ebrahim et al., 2014; Lefranc et al., 2011; Mathieu et al., 2012; Verschuere et al., 2014).
In addition to its roles in tumour progression, Gal1 is the best-characterized H-Ras nanocluster modulator. A prenyl-binding pocket was previously proposed on the surface of Gal1, suggesting that it could directly bind farnesylated Ras proteins and act as a nanocluster modulator (Rotblat et al., 2004). However, Gal1 binds with 106 nM affinity to the RBD of the effector protein C-Raf (Blazevits et al., 2016). To stabilize H-Ras nanoclusters through RBD interaction, Gal1 requires an intact dimer interface. A stacked dimer model was proposed, where H-Ras dimers in complex with Raf dimers are stabilized through Gal1 dimers. This stabilisation of the signalling complex of mutant H-Ras with Raf leads to an increased oncogenic MAPK signalling output (Blazevits et al., 2016).

Gal1, along with other galectins, have been the target of extensive efforts to develop inhibitors to alleviate Gal1 extra- and intracellular activities (Johannes et al., 2018). Currently three different categories of inhibitors target carbohydrate binding of Gal1: modified mono-and di-saccharides containing galactose or its mimics, synthetic glycodendrimers and non-saccharide-based inhibitors

(Blanchard et al., 2016). Since galectins recognize galactose and di- and oligosaccharides containing galactose, most drug development has focused on synthetically modifying galactosides, lactosides, and their mimics. However, the highly conserved carbohydrate-binding site of galectins makes it challenging to specifically target one galectin (Blanchard et al., 2016). These modified glycans often exhibit lower affinity for galectins, resulting in less potent inhibitors. Given the implication of Gal1 in tumour angiogenesis and the difficulties in generating specific Gal1 inhibitors, the peptide anginex and its peptidomimetic OTX008 were designed. Both the peptide and the peptidomimetic exhibit anti-tumour activity by inhibiting angiogenesis and inducing apoptosis or inhibiting cell cycle progression, cell invasion and proliferation respectively (Astorgues-Xerri et al., 2014; Griffioen et al., 2001; Thijssen et al., 2010). All the above-mentioned inhibitors, however, target only the extracellular activity of Gal1 and inhibitors for intracellular Gal1-mediated processes are still needed.

1.5. H-Ras in cancer

K-Ras is the most frequently mutated with occurrence in 19 out of 29 cancer types translating to 75 % of Ras mutant cancer types. N-Ras mutation primarily occur in melanoma and account for 17 % of Ras mutant cancers. In contrast, H-Ras mutations are responsible for only 7 % of Ras mutant cancers, affecting a relatively small subset, including head and neck and bladder carcinomas. Generally, the abundance of Ras mutants correlates with Ras protein expression (Hood et al., 2023). Despite K-Ras being the most frequently mutated Ras isoform in cancer, H-Ras mutations affect approximately 230 000 cancer patients globally (Prior et al., 2020).

Oncogenesis promoted by mutated Ras is typically due to gain-of-function missense mutations at hotspot codons 12, 13, or 61 (Prior et al., 2012). Single base changes at these codons result in constitutively active Ras variants, including G12D, G12V, G12C, G13D, and Q61R. Approximately 70% of all Ras-mutant cancer patients have one of these five mutations at these hotspot codons (Prior et al., 2020).The most frequent mutation is K-RasG12D (34.1 %), followed by K-RasG12V, which accounts for 23.1 %, K-RasG13D (12.8 %), K-RasG12C (11.5 %) and H-RasG12V (10.2 %) (Hunter et al., 2015). These constitutively active Ras mutants have enhanced GTP-binding due to impairment of GAP-activity and/ or faster GTP-exchange rate (Smith et al., 2013). For instance, G12V mutants are predicted to be hyperactive due to insensitivity to GAP-mediated GTP hydrolysis, whereas K-RasG13D displays a faster nucleotide exchange rate (Hunter et al., 2015). Ras expression varies by isoform, tissue type, and mutations, and not all mutants share the same stability in their active state. Thus, Ras oncogenesis occurs only under a subset of optimal conditions. Excessive Ras signalling may lead to senescence or cell death rather than tumour progression, while insufficient Ras signalling may not trigger tumorigenesis (Pershing et al., 2015; Sarkisian et al., 2007; Serrano et al., 1997). K-Ras, but not H-Ras expression, is crucial to mouse embryonic development (Koera et

al., 1997; Yan et al., 1998). K-Ras knockout mice die between embryonic day 12.5 and birth, whereas H-Ras knockout mice are born and growing normally. These data suggest that H-Ras might operate through different signal transduction proteins compared to the other isoforms (Koera et al., 1997). Every year more than 650 000 new cases of head and neck squamous cell carcinoma (HNSCC) are reported (Shu et al., 2020). Moreover, H-Ras mutants are frequently expressed in thyroid, bladder and prostate cancers. These cancer types carry mutations exclusively at codons 12 and 61 (Prior et al., 2012). Ras isoforms differ not only in expression and prevalence but also in their interactions with various effector proteins and subsequent downstream signalling pathways. Beyond its role in the MAPK pathway, H-Ras has been tied to the PI3K-AKT pathway promoting oncogenic transformation (Suire et al., 2002). For instance, H-RasQ61R mutation has been shown to drive a cancerous phenotype followed by the activation of the PI3K-AKT-mTOR pathway (Geyer et al., 2018).

Despite the approximately 90 % sequence homology among the four Ras isoforms, expression and activation of each isoforms vary, leading to different cellular responses and treatment sensitivities. Notably, initial inhibitors targeting prenylation and subsequent membrane anchorage have been ineffective for both K- and N-Ras, as they can bypass FTase inhibitors through geranylgeranylation (Zhang et al., 1997). In contrast, H-Ras is not a suitable substrate for GGT-I and is exclusively dependent on farnesylation. Thus H-Ras remains sensitive to FTase inhibitors (FTI) and currently the only approved inhibitor against H-Ras mutant cancers is the farnesyl transferase inhibitor tipifarnib (Gilardi et al., 2020).

1.6. Targeting oncogenic Ras

The therapeutic strategies for targeting oncogenic Ras are thoroughly discussed in the review, manuscript I, section C appendix of original publications (Steffen et al., 2023).

Eliminating oncogenic RAS - Back to the future at the drawing board

Candy Laura Steffen[#], Pelin Kaya[#], Elisabeth Schaffner-Reckinger[#], Daniel Abankwa*

Cancer Cell Biology and Drug Discovery Group, Life Sciences Research Unit, University of Luxembourg, L-4362, Esch-sur-Alzette, Luxembourg
* corresponding author

Correspondence: daniel.abankwa@uni.lu

# These authors contributed equally to the manuscript.

2. Synopsis – Results and discussion

2.1. Eliminating oncogenic RAS: back to the future at the drawing board (I)

In this review, manuscript I (Section C, appendix I), we conducted an in-depth analysis of different inhibitors and binders of Ras focusing on directly targeting oncogenic Ras. Our evaluation highlights significant advancements in the development of covalent and non-covalent small molecules binding Ras with promising activities. The development of non-covalent inhibitors based on existing covalent small molecules builds a robust approach to generate non-allele-specific inhibitors with the potential to overcome resistances.

The description of four distinct allosteric binding pockets on the Ras surface significantly facilitated the evolution of these molecules. Furthermore, we described the importance of Ras binders of macromolecular nature, such as antibodies, monobodies, affimers, and DARPins, which have led to the discovery of novel binding sites and Ras inhibition principles. Additionally, we analysed the utility of reversible small molecules in novel targeting strategies, such as degraders against Ras. The emerging PROTAC (Proteolysis Targeting Chimeras) technology employs recruitment of E3-ligases to a protein of interest and tagging it via ubiquitination for degradation by the proteasome. The specific degradation of mutated Ras may reduce toxicity given the more controlled drug action due to spatio-temporal expression of some E3-ligases in different cell types.

2.1.1. Development of clinical inhibitors targeting Ras not mentioned in Manuscript I

In the above-mentioned review, we described the significant discoveries made in the advancement of targeted therapies against Ras. Since then, more inhibitors have been designed and tested, with several entering clinical trials in phases I or II. The company Revolution Medicine has made notable progress in designing covalent inhibitors against different K-Ras mutants, which functions as molecular glues. Specifically, the compounds RMC-6291 forms a tricomplex with GTP-loaded K-RasG12C and cyclophilin A, sterically blocking Ras interactions and downstream signalling. RMC-9805 applies the same mechanism, but targets K-RasG12D instead of K-RasG12C (Jiang et al., 2024; Long et al., 2024; Schulze et al., 2023). Additionally, Revolution Medicine has developed a panRAS(ON) multi-selective non-covalent inhibitor (RMC-6236), which is also under clinical investigation (Jiang et al., 2024). A related panRAS(ON) molecular glue compound is currently under development (Holderfield et al., 2024). These RAS(ON) multi-selective inhibitors enable the targeting of a broader range of Ras-addicted cancers.

Furthermore, the covalent K-RasG12C inhibitors Divarasib (GDC-6036, Genentech), Garsorasib (D-1553, InventisBio), JDQ443 (Novartis) and MK1084 (Merck) have entered clinical trials and show promising results in blocking oncogenic Ras signalling and anti-tumour activity (Desai et al., 2024; Li et al., 2023; Ma et al., 2024; Sacher et al., 2023; Shi et al., 2023; Weiss et al., 2022).

The protein-protein interaction inhibitor targeting the SOS1/ K-RasG12C interface, MRTX0902 (Mirati Therapeutics) has recently entered clinical trial phase I. MRTX0902 increases the GDP-loaded fraction of K-RasG12C and in combination with adagrasib (MRTX849) significantly enhances antitumor activity (Ketcham et al., 2022). The K-RasG12D PROTAC ASP3082 (Astellas Pharma) prevents K-RasG12D-mediated signaling through targeted degradation of K-RasG12D (Nagashima et al., 2022). Their compound binds K-RasG12D on one end and recruits an E3 ligase on the other, forming a ternary complex. The protein is subsequently ubiquitinated and degraded by the proteasome, leading to inhibition of the tumor growth in mice (Nagashima et al., 2022).

The 11-mer cyclic peptide LUNA18 is panRas inhibitor resulting from the optimization of a hit discovered with mRNA display library (Tanada et al., 2023). The cyclic peptide is orally bioavailable and inhibits the interaction between inactive Ras and GEFs, explaining its antitumor activity. However, the peptide alone, was not sufficient to inhibit cell proliferation in cells, which have activating mutations downstream of Ras (Sase et al., 2024). Combination treatment with K-RasG12C inhibitors and LUNA18 decreases cell proliferation more effectively than either agent alone (Michisaka et al., 2024). The cyclic peptide has entered clinical trial phase I and shows great potential.

2.2. Identification of an H-Ras nanocluster disrupting peptide (II)

Contrary to previous publications, Gal1 does not interact directly with H-Ras via its farnesyl tail. A previous study using fluorescence polarization showed that H-Ras binds farnesyl-binding protein PDE6D, but not Gal1. Furthermore, through FRET it was established that the Gal1/ Raf-RBD interaction is the mechanism behind the stabilizing effect of Gal1 on H-RasG12V nanoclusters (Blazevits et al., 2016). Here I describe the identification of a peptide targeting the intracellular, H-Ras nanocluster stabilising function of Gal1. We have established the direct binding of this peptide to the RBD domain of not only B- and C-Raf, but also interestingly to other RBD- or RA-domain containing Ras effector proteins. Furthermore, we showed that our peptide interferes with and downregulates H-Ras nanoclustering and cell viability of different cancer cell lines.

2.2.1. Validation of the proposed structural model of Gal1/ RBD interaction

Here, we validated the proposed stacked dimer model as a target (**Manuscript II, Fig. 1a**) using our BRET assay. We demonstrated the increase in H-RasG12V nanoclustering upon addition of increasing concentrations of Gal1 (**Manuscript II, Fig.1 b**). We confirmed that Gal1 is a dimer under our expressing conditions (**Manuscript II, Fig. 1c**) and observed a preference of Gal1 for the RBD of B-Raf over C- and A-Raf (**Manuscript II, Fig. 1d, Fig. S1a**). The D113A and D117A mutations in the C-RBD have led to a significant loss of binding to Gal1, in line with the proposed computational model (**Manuscript II, Fig. S1b**). We therefore introduced analogous mutations in the RBD domains of A- and B-Raf to further confirm this computational model (**Manuscript II, Fig S1c, d, e**). The results of the split-luciferase assay suggest that Gal1 facilitates the B-Raf opening to a similar extent as SNAP-HRasG12V (**Manuscript II, Fig. 1e**). In summary, when functioning as a dimer, Gal1 might further stabilize H-RasG12V nanoclusters, similar to the effect observed with ON-state Raf inhibitors. In the context for the stacked dimer model, our data suggest the involvement of Gal1 in Raf activation and/ or stabilisation of dimers.

2.2.2. Identification of a peptide targeting the RBD/ Gal1 binding interface

After having validated the binding between Gal1 and RBD, we continued to characterize a previously described peptide. The 52-mer peptide, L5UR, has been reported by Elantak et al to bind with low (310 µM) affinity to Gal1 at the back side of the carbohydrate binding site (Elantak et al., 2012). This binding site overlaps with the binding interface of RBD and Gal1 (**Manuscript II, Fig. S1b**). Therefore, we hypothesised that L5UR could act as a Gal1/ RBD interface inhibitor. The analysis of data from the PanCanAtlas database has shown a poorer survival rate with higher Gal1 levels (**Manuscript II, Fig. S2a**). Using FRET, we studied the effect of L5UR expression on Gal1/ RBD binding, as well as H-RasG12V nanoclustering (**Manuscript II, Fig. 2a, b**). The control peptide anginex and its analogue compound OXT-008 did not affect the Gal1/ RBD FRET (**Manuscript II, Fig. 2a**). Using a biotinylated

L5UR peptide, we performed pulldown assays. Interestingly, L5UR pulled down not only Gal1 but also GST-B-Raf-RBD independently (**Manuscript II, Fig. 2c**). Moreover, we demonstrated the direct binding of L5UR and GST-B-Raf-RBD, but not GST alone via FP establishing a K_D of 7 µM and confirmed these findings in a quenching resonance energy transfer (QRET) assay using L5URcore conjugated with a nonadentate europium chelate (Eu-L5URcore), whilst Eu-L5URcore could not be saturated by His-Gal1 (**Manuscript II, Fig. 2d and Fig. S2c, d, e**). The L5UR peptide has six positively charged arginine residues, suggesting an electrostatic nature of its binding to the RBD. Seven charge reversal mutations in the core region were introduced to generate the loss-of-function mutant mutL5UR (**Manuscript II, Fig. 2f**). Indeed, the mutL5UR lost its potency to displace F-L5UR from GST-B-Raf-RBD, as well as C-Raf-RBD, in competitive FP (**Manuscript II, Fig. 2e and Fig. S2f**). In summary, we determined that L5UR and L5URcore bind the RDB of B- and C-Raf with low micromolar affinity. This interaction seems to be largely influenced by several positively charged residues in the core region, as the binding is significantly reduced in the mutL5UR variant.

2.2.3. SNAP-tagged L5UR interferes with H-Ras nanoclustering at the Gal1/ RBD interface

To investigate the potency of L5UR, we functionalised the peptide by adding a SNAP-tag at the C-terminus (**Manuscript II, Fig. 3a, b**). Using immunoblotting, we confirmed a linear increase in the expression of L5UR-SNAP variants with increasing amounts of transfected DNA (**Manuscript II, Fig. S3a**). Genetically expressed L5UR and L5UR-SNAP decreased both Gal1/ RBD- and H-RasG12V nanoclustering-BRET to a similar extent. As expected, mutL5UR-SNAP, as well as the SNAP-tag alone, did not affect this interaction (**Manuscript II, Fig. 3b, c**). After analysing endogenous Gal1 levels in different cell lines, we observed that HEK293-EBNA cells are devoid of Gal1 (**Manuscript II, Fig. S3d**). However, L5UR and L5UR-SNAP reduced H-RasG12V nanoclustering-BRET to similar levels (**Manuscript II, Fig. S3c**). The SNAP-H-RasG12V control reduced the H-RasG12V nanoclustering-BRET by 85 % (**Manuscript II, Fig. S3e**). To study potential Ras isoform selectivity, we tested the L5UR constructs in K-Ras nanoclustering-BRET, finding that neither of the L5UR constructs affected this BRET pair significantly (**Manuscript II, Fig. S3f**). With classical electron microscopy-based Ras nanoclustering analysis performed on membrane sheets of Gal1-expressing BHK cells, we confirmed H-Ras nanocluster disrupting activity of L5UR and L5UR-SNAP (**Manuscript II, Fig. 3d**). Considering the potentially electrostatic interaction between L5UR and the RBD, we investigated its engagement with other RBD or RA-containing proteins in a pulldown assay. Using L5UR-SNAP as bait, we did not only pulldown B- and C-Raf, but also the catalytic subunit of PI3Kα. The pan-Ras nanocluster scaffold RBD-containing ASPP2, as well as its two interaction partners RASSF7 and RASSF9, were also captured by L5UR-SNAP (**Manuscript II, Fig. 3e**). L5UR-SNAP engagement with multiple RBD- or RA-containing proteins may suggest that it is still an immature tool and may appear as a liability, but nevertheless it represents a starting point to develop novel binders disrupting Ras nanoclustering.

2.2.4. TAT-L5URcore interferes with Ras-mediate signalling and cell proliferation

We rendered the L5URcore peptide cell-permeable by adding a cell-penetrating group. Here, we used the cell-penetrating group TAT, which is 12 amino acids long and derived from a Human immunodeficiency virus 1 (HIV1) protein. The cell-penetrating TAT group facilitates cellular peptide uptake (**Manuscript II, Fig. 4a**). To validate the cell penetration and on-target activity, we tested the TAT-tagged variants compared to the non-tagged peptides in our BRET system. Both the H-RasG12V nanoclustering and Gal1/ RBD BRET were dose-dependently decreased by increasing concentrations of TAT-L5URcore. None of the control peptides (TAT-mutL5URcore, TAT alone, non-labelled peptides) affected these interactions as measured by BRET (**Manuscript II, Fig. 4b, c**).

To study the effect of TAT-L5URcore on cell signalling and proliferation, we chose two cell lines with high Gal1 levels and H-Ras mutations, T24 and Hs 578T, as they were expected to respond best. Additionally, we tested the effect of our peptide on control cell lines, K-Ras mutant MIA PaCa-2 and HEK293-EBNA cells. Indeed, we observed reduced EGF-induced cellular pERK- and pAKT-levels with TAT-L5URcore in T24 and Hs 578T (**Manuscript II, Fig. 5a, b, e, f**). In the K-Ras mutant cell line MIA PaCa-2, TAT-L5URcore did not affect pERK levels but decreased pAKT-levels (**Manuscript II, Fig. 5 c, g**). Non-transformed HEK293-EBNA cells showed slightly increased levels of pERK and pAKT levels after addition of TAT-L5URcore (**Manuscript II, Fig. 5 d, h**). Furthermore, we evaluated the effect of these peptides on the cell viability and quantitatively compared the still weak activity of the peptides calculating the area under the curve (AUC) and subsequent drug sensitivity score (DSS_3) (**Manuscript II; Fig. 6 a e**) (Potdar et al., 2023). The viability of all four cell lines was affected by TAT-L5URcore, but less by TAT-mutL5URcore and TAT alone. This broad effect on cell proliferation is consistent with the fact that L5UR engages various other proteins containing RBD or RA domains (**Manuscript II, Fig. 3e**). In conclusion, these results suggest that our L5UR-based peptides interfere with several signalling pathways relevant for cell proliferation and survival.

2.3. Protocol to measure and analyze protein interactions in mammalian cells using Bioluminescence Resonance Energy Transfer (III)

In Manuscript III, we comprehensively describe a general protocol for the Bioluminescence Resonance Energy Transfer (BRET) assay to study protein-protein interactions in living cells.

Bioluminescence is an intrinsic phenomenon that occurs in marine organisms, for example the sea pansy *Renilla reniformis* and jellyfish *Aequorea victoria* (Pfleger & Eidne, 2006). Its principle is based on the occurring resonance energy transfer (RET) phenomenon between two photoactive molecules. To study interactions between two proteins of interest (POI) with BRET, one POI needs to be tagged with a bioluminescent energy donor and the other one with a fluorescent energy acceptor. After addition of a substrate, the donor catalyses the oxidation of the substrate, producing energy (Dacres et al., 2012). This excited-state energy can be transferred to the interaction partner tagged with the fluorescent energy acceptor through a non-radiative resonance process occurring only at a proper orientation and a permissive distance (typically less than 10 nm) (Kobayashi et al., 2019). Additionally, the emission spectrum of the donor needs to sufficiently overlap with the excitation spectrum of the acceptor.

Here, we describe the use of enhanced BRET2 (eBRET2), employing the luciferase Rluc8 and fluorescent acceptor GFP2 together with coelenterazine 400a as a substrate. BRET is an important tool to study transient interactions as well as interactions involving membrane proteins. Since the BRET signal originates from an enzymatic reaction, the risk of autofluorescence or photobleaching, which frequently occurs in FRET, are avoided. This technique allows us to study the interactions between two proteins in cells in their physiological environment. Dense packing of Ras in nanoclusters at the plasma membrane can be studied using eBRET2, by tagging Ras proteins with Rluc8 and GFP2. Our protocol provides detailed instructions for conducting donor saturation-titration BRET experiments using K-Ras nanoclustering-BRET sensors and a conventional microplate reader. In these experiments, a constant amount of RLuc8-tagged donor construct is co-expressed with increasing amounts of GFP2-tagged acceptor construct and the BRET ratio is plotted against the acceptor/ donor ratio. As true saturation is typically not reached in cells, we introduced the BRETtop value, representing the highest BRET ration within a defined range of acceptor/ donor expression signal ratios to characterize the strength or probability of the interaction. A modulation of the interaction can be observed as a change in the BRET signal. We typically use the compound mevastatin as a control, which is an inhibitor of the mevalonate pathway that affects cholesterol levels and subsequently inhibits the membrane localization of Ras (Endo, 2017). A drop in the BRET signal following mevastatin treatment can result from any process upstream of Ras nanoclustering. Therefore, any manipulation that affects Ras lipid modification, proper trafficking, or lateral

organization in nanoclusters can be detected with this assay. However, it is not possible to conclude that Ras or related proteins are present as dimers or other oligomers based on BRET results. To further improve the method, the expression signal ratio can be calibrated to reflect actual protein stoichiometries and total expression levels. This can be achieved by employing a fusion protein of the BRET pair with a long linker that prevents BRET, thereby ensuring the signal ratio represents a fixed 1:1 protein stoichiometry. Furthermore, using a purified acceptor protein preparation of known concentration can help correlate the signals to precise concentration equivalents.

3. Conclusions and perspectives

3.1. Conclusion

The oncogene Ras has been studied for decades and has been a major focus of recent drug development efforts. Ras was considered undruggable due to its lack of druggable pockets on its shallow surface. However, in 2011, the Gorfe group identified four potential low-affinity allosteric binding pockets on the Ras surface by computational simulations (Grant et al., 2011). We conducted an in-depth study of covalent and non-covalent Ras inhibitors. With the development of the first covalent small molecule against K-RasG12C, the switch II pocket was identified (Ostrem et al., 2013). Since then, the chemical scaffold introduced with ARS-1620 led to the development of more compounds that bind Ras either covalently or non-covalently (Janes et al., 2018). Sotorasib and adagrasib have been approved by the corresponding authorities, while others have entered clinical trials. Moreover, we have established the importance of macromolecular binders in drug development and their limited potential as drug candidates. Macromolecular binders can be used to identify novel binding sites, even if these sites are not distinct binding cavities. These macromolecular binders engage larger regions, such as the Ras dimer interface or effector binding site, after sterically hindering engagement with other interaction partners. The drawback of macromolecular binders is that they are currently not suitable for pharmacological targeting of intracellular targets like Ras due to low cell permeability. However, they remain essential proof-of-concept tools for target site identification with application in both cellular and *in vivo* models.

Peptides serve as natural intermediates between macromolecules and small molecule inhibitors. Considering the role of naturally occurring peptides in controlling major physiological events and their greater chemical diversity, it is not surprising that designing therapeutic peptides is a growing drug development field (Lau & Dunn, 2018; Wang et al., 2022). Several Ras-binding peptides have been developed, averaging about 14 amino acids in length. Compared to monobodies or affimers, peptides can be linear or cyclic when chemically synthesized. Cyclization of peptides enhances their stability. Depending on their size and composition, peptides can overcome complications of intracellular delivery. Recent studies have shown that it is possible to use peptides as drugs. For instance, the cyclic peptide LUNA18 is currently under clinical investigation as a pan-Ras inhibitor (Sase et al., 2024).

Our L5UR peptides validate the Gal1/ RBD binding interface as a drug target to interfere with Gal1-enhanced H-RasG12V nanoclustering. L5UR engages multiple RBD- and RA-containing proteins associated with Ras signalling. To validate the activity of L5UR on signalling and cancer cell proliferation, we designed a cell-penetrating version of L5UR that can be added to cells similarly to small molecule compounds. With TAT-L5URcore, we have developed a tool compound that can be used to further study Gal1-enhanced H-Ras nanoclusters. It remains unclear how Gal1 stabilizes and

how L5UR disrupts H-Ras nanoclusters, but L5UR targeting the Gal1/ RBD binding interface provides insights into how Gal1 positively modifies H-Ras nanoclusters.

3.2. Perspectives

To better understand and validate the mechanism of action of L5UR, one could work on obtaining structural information using the peptide and either of its binding partners (RBD or Gal1), or even structural data of the RBD/ Gal1 complex. An actual structure of RBD/ Gal1 could be compared to the model previously proposed by our group (Blazevits et al., 2016), and by extension the predicted L5UR binding site relative to the RBD. Alternatively, one could introduce point mutations either in L5UR or on the RBD at the predicted binding interface. Once having identified a reliable peptide/ protein interface, it will be possible to shorten and modify the peptide further to obtain the shortest possible variant, which still retains activity.

With liquid chromatography-mass spectroscopy (LC-MS), one could envision to perform proteomic studies and analyse the proteins binding to L5UR-SNAP, and mutL5UR and SNAP alone as controls and establish a mass-spectroscopy (MS) hit list of the pulled-down interaction partners. With this hit list, it would be possible to compare the sequences of the hits, to eventually determine a common denominator of where the peptide could bind.

Based on the obtained targets, one could design peptidomimetics. Peptidomimetics are synthetic molecules that mimic the structure and functionality of native peptides (Del Gatto et al., 2021). Compared to native peptides, peptidomimetics can have a more versatile design due to the possibility of incorporating non-natural amino acids and chemical modifications. They often overcome complications such as low bioavailability and proteolysis (Paul et al., 2021).

Moreover, one could use the obtained peptides and peptidomimetics with the emerging PROTAC technology. PROTACs are heterobifunctional small molecules consisting of two ligands connected by a linker: one ligand is a warhead recruiting a POI, while the second ligand recruits an E3 ligase (E3), thus forming a tricomplex (Zeng et al., 2021). The simultaneous binding of the PROTAC to the POI and the E3 ligase induces ubiquitination of the POI and subsequent degradation of the POI by the ubiquitin-proteasome (Bekes et al., 2022). Currently, the K-RasG12D PROTAC ASP3082 is in clinical trials (Nagashima et al., 2022). Degrading the POI may be a promising opportunity to increase drug activity. One could use L5UR, or an L5UR-based peptidomimetic, as a PROTAC warhead to degrade Raf in cells and inhibit Raf-mediated signalling. PROTACs employ an event-driven mechanism, in contrast to classical small molecule inhibitors, which use an occupancy-driven mechanism (Bouvier et al., 2024). The main difference between these mechanisms is that PROTACs induce the degradation of the target protein and can thus be recycled and reused. PROTACs do not necessarily need to block activity through binding to the active site or by initiating an allosteric conformational change leading to loss of activity. Degrading the POI and thus removing the protein entirely,

eliminates also possible scaffolding functions the protein might have. Under saturating conditions, the phenomenon called the hook effect might occur, where PROTAC-POI and PROTAC-E3 complexes form instead of the tricomplex preventing efficient degradation (Bouvier et al., 2024). To avoid the hook effect, one should always test a wide range of concentrations to determine the optimal amount with highest activity.

Given the latest advancement, growing investment and recent interest in PROTACs, it is evident that that targeted protein degradation could play a key role in future drug development, potentially offering new treatment options to patients across various indications.

4. Glossary

Terms	Definition
Affirmers	Engineered small non-antibody proteins designed to bind proteins with nanomolar affinity.
Allele-specific inhibitor	Therapeutic agent selectively targeting and inhibiting a specific allele of a gene.
Antibodies	Y-shaped large proteins of the immunoglobulin superfamily neutralizing antigens.
BRET	*In cellulo* bioluminescence-based technique to study protein-protein interaction.
Cell Viability Assay	Technique to assess cell growth and proliferation after treatment.
Cell-penetrating group	Short sequence facilitating entrance of a cargo through the plasma membrane.
Circular Dichroism Spectra	Spectroscopy-based method measuring differences in absorbance used to examine structures of peptides and proteins.
DARPin	Engineered antibody mimetics derived from natural ankyrin repeat proteins exhibiting specific affinities.
Drug Sensitivity Score (DSS) analysis	Measurement of an area under the curve to determine reduced viability of cancer cells after response to various treatments.
Electron microscopic analysis of Ras-nanoclustering	Electron microscopy-based technique to study gold-plated membrane grits to evaluate Ras nanoclusters.
Farnesylation	Post-translational modification adding a farnesyl group via the enzyme farnesyltransferase.
Fluorescence Lifetime Imaging Microscopy (FLIM)-FRET	Approach for measuring FRET using lifetime microscopy on living cells.
Fluorescence Polarization	Fluorescence-based method to study protein interactions *in vitro* via measuring variations in polarized light.
Gateway Cloning	Cloning method developed by Invitrogen using a multi-vector system to generate novel recombinant DNA vectors.
Immunoblotting	Biochemical method to analyse and identify a mixture of proteins using antibodies after separation by electrophoresis.
In vitro pulldown	Method to study protein-protein interaction using an immobilized protein bait capturing potential interaction partners from a protein mixture.
Inner leaflet of the plasma membrane	Inner layer of the lipid bilayer of the plasma membrane contacting the cytoplasm.
Monobody	Synthetic protein derived from the human fibronectin scaffold type III domain.
OFF-state inhibitor	Inhibitor specifically targeting the inactive state (OFF-state) of the target protein.
ON-state inhibitor	Inhibitor specifically targeting the active state (ON-state) of the target protein.

Peptidomimetic	Synthetic compound designed to mimic a peptide.
PROTAC	Heterobifunctional molecule containing a warhead binding to a protein of interest, a linker, and an E3-ligase recruiting moiety.
Proteomics	Large-scale experimental analysis of proteins and proteomes.
Quenching Resonance Energy Transfer (QRET) assay	Method to study protein-protein interaction using a single-label, typically used for inhibitor screening and interaction studies

5. References

Abankwa, D., & Gorfe, A. A. (2020). Mechanisms of Ras Membrane Organization and Signaling: Ras Rocks Again. *Biomolecules*, *10*(11). https://doi.org/10.3390/biom10111522

Abankwa, D., Gorfe, A. A., & Hancock, J. F. (2008). Mechanisms of Ras membrane organization and signalling: Ras on a rocker. *Cell Cycle*, *7*(17), 2667-2673. https://doi.org/10.4161/cc.7.17.6596

Abankwa, D., Hanzal-Bayer, M., Ariotti, N., Plowman, S. J., Gorfe, A. A., Parton, R. G., McCammon, J. A., & Hancock, J. F. (2008). A novel switch region regulates H-ras membrane orientation and signal output. *EMBO J*, *27*(5), 727-735. https://doi.org/10.1038/emboj.2008.10

Ahearn, I., Zhou, M., & Philips, M. R. (2018). Posttranslational Modifications of RAS Proteins. *Cold Spring Harb Perspect Med*, *8*(11). https://doi.org/10.1101/cshperspect.a031484

Ahearn, I. M., Haigis, K., Bar-Sagi, D., & Philips, M. R. (2011). Regulating the regulator: post-translational modification of RAS. *Nat Rev Mol Cell Biol*, *13*(1), 39-51. https://doi.org/10.1038/nrm3255

Amendola, C. R., Mahaffey, J. P., Parker, S. J., Ahearn, I. M., Chen, W. C., Zhou, M., Court, H., Shi, J., Mendoza, S. L., Morten, M. J., Rothenberg, E., Gottlieb, E., Wadghiri, Y. Z., Possemato, R., Hubbard, S. R., Balmain, A., Kimmelman, A. C., & Philips, M. R. (2019). KRAS4A directly regulates hexokinase 1. *Nature*, *576*(7787), 482-486. https://doi.org/10.1038/s41586-019-1832-9

Astorgues-Xerri, L., Riveiro, M. E., Tijeras-Raballand, A., Serova, M., Rabinovich, G. A., Bieche, I., Vidaud, M., de Gramont, A., Martinet, M., Cvitkovic, E., Faivre, S., & Raymond, E. (2014). OTX008, a selective small-molecule inhibitor of galectin-1, downregulates cancer cell proliferation, invasion and tumour angiogenesis. *Eur J Cancer*, *50*(14), 2463-2477. https://doi.org/10.1016/j.ejca.2014.06.015

Bekes, M., Langley, D. R., & Crews, C. M. (2022). PROTAC targeted protein degraders: the past is prologue. *Nat Rev Drug Discov*, *21*(3), 181-200. https://doi.org/10.1038/s41573-021-00371-6

Bernal Astrain, G., Nikolova, M., & Smith, M. J. (2022). Functional diversity in the RAS subfamily of small GTPases. *Biochem Soc Trans*, *50*(2), 921-933. https://doi.org/10.1042/BST20211166

Blanchard, H., Bum-Erdene, K., Bohari, M. H., & Yu, X. (2016). Galectin-1 inhibitors and their potential therapeutic applications: a patent review. *Expert Opin Ther Pat*, *26*(5), 537-554. https://doi.org/10.1517/13543776.2016.1163338

Blazevits, O., Mideksa, Y. G., Solman, M., Ligabue, A., Ariotti, N., Nakhaeizadeh, H., Fansa, E. K., Papageorgiou, A. C., Wittinghofer, A., Ahmadian, M. R., & Abankwa, D. (2016). Galectin-1 dimers can scaffold Raf-effectors to increase H-ras nanoclustering. *Sci Rep*, *6*, 24165. https://doi.org/10.1038/srep24165

Bollag, G., Hirth, P., Tsai, J., Zhang, J., Ibrahim, P. N., Cho, H., Spevak, W., Zhang, C., Zhang, Y., Habets, G., Burton, E. A., Wong, B., Tsang, G., West, B. L., Powell, B., Shellooe, R., Marimuthu, A., Nguyen, H., Zhang, K. Y., . . . Nolop, K. (2010). Clinical efficacy of a RAF inhibitor needs broad target blockade in BRAF-mutant melanoma. *Nature*, *467*(7315), 596-599. https://doi.org/10.1038/nature09454

Bonsor, D. A., & Simanshu, D. K. (2024). RAS and SHOC2 Roles in RAF Activation and Therapeutic Considerations. *Annu Rev Cancer Biol*, *8*, 97-113. https://doi.org/10.1146/annurev-cancerbio-062822-030450

Bos, J. L., Rehmann, H., & Wittinghofer, A. (2007). GEFs and GAPs: critical elements in the control of small G proteins. *Cell*, *129*(5), 865-877. https://doi.org/10.1016/j.cell.2007.05.018

Bouvier, C., Lawrence, R., Cavallo, F., Xolalpa, W., Jordan, A., Hjerpe, R., & Rodriguez, M. S. (2024). Breaking Bad Proteins-Discovery Approaches and the Road to Clinic for Degraders. *Cells*, *13*(7). https://doi.org/10.3390/cells13070578

Buday, L., & Downward, J. (1993). Epidermal growth factor regulates the exchange rate of guanine nucleotides on p21ras in fibroblasts. *Mol Cell Biol*, *13*(3), 1903-1910. https://doi.org/10.1128/mcb.13.3.1903-1910.1993

Campbell, S. L., & Philips, M. R. (2021). Post-translational modification of RAS proteins. *Curr Opin Struct Biol*, *71*, 180-192. https://doi.org/10.1016/j.sbi.2021.06.015

Chapman, P. B., Hauschild, A., Robert, C., Haanen, J. B., Ascierto, P., Larkin, J., Dummer, R., Garbe, C., Testori, A., Maio, M., Hogg, D., Lorigan, P., Lebbe, C., Jouary, T., Schadendorf, D., Ribas, A., O'Day, S. J., Sosman, J. A., Kirkwood, J. M., . . . Group, B.-S. (2011). Improved survival with vemurafenib in melanoma with BRAF V600E mutation. *N Engl J Med*, *364*(26), 2507-2516. https://doi.org/10.1056/NEJMoa1103782

Cho, M., & Cummings, R. D. (1996). Characterization of monomeric forms of galectin-1 generated by site-directed mutagenesis. *Biochemistry*, *35*(40), 13081-13088. https://doi.org/10.1021/bi961181d

Claing, A. (2013). beta-Arrestins: modulators of small GTPase activation and function. *Prog Mol Biol Transl Sci*, *118*, 149-174. https://doi.org/10.1016/B978-0-12-394440-5.00006-1

Colicelli, J. (2004). Human RAS superfamily proteins and related GTPases. *Sci STKE*, *2004*(250), RE13. https://doi.org/10.1126/stke.2502004re13

Compagno, D., Gentilini, L. D., Jaworski, F. M., Perez, I. G., Contrufo, G., & Laderach, D. J. (2014). Glycans and galectins in prostate cancer biology, angiogenesis and metastasis. *Glycobiology*, *24*(10), 899-906. https://doi.org/10.1093/glycob/cwu055

Cook, F. A., & Cook, S. J. (2021). Inhibition of RAF dimers: it takes two to tango. *Biochem Soc Trans*, *49*(1), 237-251. https://doi.org/10.1042/BST20200485

Cox, A. D., & Der, C. J. (2010). Ras history: The saga continues. *Small GTPases*, *1*(1), 2-27. https://doi.org/10.4161/sgtp.1.1.12178

Dacres, H., Michie, M., Wang, J., Pfleger, K. D., & Trowell, S. C. (2012). Effect of enhanced Renilla luciferase and fluorescent protein variants on the Forster distance of Bioluminescence resonance energy transfer (BRET). *Biochem Biophys Res Commun*, *425*(3), 625-629. https://doi.org/10.1016/j.bbrc.2012.07.133

Dalotto-Moreno, T., Croci, D. O., Cerliani, J. P., Martinez-Allo, V. C., Dergan-Dylon, S., Mendez-Huergo, S. P., Stupirski, J. C., Mazal, D., Osinaga, E., Toscano, M. A., Sundblad, V., Rabinovich, G. A., & Salatino, M. (2013). Targeting galectin-1 overcomes breast cancer-associated immunosuppression and prevents metastatic disease. *Cancer Res*, *73*(3), 1107-1117. https://doi.org/10.1158/0008-5472.CAN-12-2418

Del Gatto, A., Cobb, S. L., Zhang, J., & Zaccaro, L. (2021). Editorial: Peptidomimetics: Synthetic Tools for Drug Discovery and Development. *Front Chem*, *9*, 802120. https://doi.org/10.3389/fchem.2021.802120

Desai, J., Alonso, G., Kim, S. H., Cervantes, A., Karasic, T., Medina, L., Shacham-Shmueli, E., Cosman, R., Falcon, A., Gort, E., Guren, T., Massarelli, E., Miller, W. H., Jr., Paz-Ares, L., Prenen, H., Amatu, A., Cremolini, C., Kim, T. W., Moreno, V., . . . Han, S. W. (2024). Divarasib plus cetuximab in KRAS G12C-positive colorectal cancer: a phase 1b trial. *Nat Med*, *30*(1), 271-278. https://doi.org/10.1038/s41591-023-02696-8

Dhanaraman, T., Singh, S., Killoran, R. C., Singh, A., Xu, X., Shifman, J. M., & Smith, M. J. (2020). RASSF effectors couple diverse RAS subfamily GTPases to the Hippo pathway. *Sci Signal*, *13*(653). https://doi.org/10.1126/scisignal.abb4778

Durrant, D. E., & Morrison, D. K. (2018). Targeting the Raf kinases in human cancer: the Raf dimer dilemma. *Br J Cancer*, *118*(1), 3-8. https://doi.org/10.1038/bjc.2017.399

Ebrahim, A. H., Alalawi, Z., Mirandola, L., Rakhshanda, R., Dahlbeck, S., Nguyen, D., Jenkins, M., Grizzi, F., Cobos, E., Figueroa, J. A., & Chiriva-Internati, M. (2014). Galectins in cancer: carcinogenesis, diagnosis and therapy. *Ann Transl Med*, *2*(9), 88. https://doi.org/10.3978/j.issn.2305-5839.2014.09.12

Elad-Sfadia, G., Haklai, R., Balan, E., & Kloog, Y. (2004). Galectin-3 augments K-Ras activation and triggers a Ras signal that attenuates ERK but not phosphoinositide 3-kinase activity. *J Biol Chem*, *279*(33), 34922-34930. https://doi.org/10.1074/jbc.M312697200

Elantak, L., Espeli, M., Boned, A., Bornet, O., Bonzi, J., Gauthier, L., Feracci, M., Roche, P., Guerlesquin, F., & Schiff, C. (2012). Structural basis for galectin-1-dependent pre-B cell receptor (pre-BCR) activation. *J Biol Chem*, *287*(53), 44703-44713. https://doi.org/10.1074/jbc.M112.395152

Endo, A. (2017). Discovery and Development of Statins. *Natural Product Communications*, *12*(8), 1934578X1701200801. https://doi.org/10.1177/1934578x1701200801

Garcia-Espana, A., & Philips, M. R. (2023). Origin and Evolution of RAS Membrane Targeting. *Oncogene*, *42*(21), 1741-1750. https://doi.org/10.1038/s41388-023-02672-z

Geyer, F. C., Li, A., Papanastasiou, A. D., Smith, A., Selenica, P., Burke, K. A., Edelweiss, M., Wen, H. C., Piscuoglio, S., Schultheis, A. M., Martelotto, L. G., Pareja, F., Kumar, R., Brandes, A., Fan, D., Basili, T., Da Cruz Paula, A., Lozada, J. R., Blecua, P., . . . Reis-Filho, J. S. (2018). Recurrent hotspot mutations in HRAS Q61 and PI3K-AKT pathway genes as drivers of breast adenomyoepitheliomas. *Nat Commun*, *9*(1), 1816. https://doi.org/10.1038/s41467-018-04128-5

Gilardi, M., Wang, Z., Proietto, M., Chilla, A., Calleja-Valera, J. L., Goto, Y., Vanoni, M., Janes, M. R., Mikulski, Z., Gualberto, A., Molinolo, A. A., Ferrara, N., Gutkind, J. S., & Burrows, F. (2020). Tipifarnib as a Precision Therapy for HRAS-Mutant Head and Neck Squamous Cell Carcinomas. *Mol Cancer Ther*, *19*(9), 1784-1796. https://doi.org/10.1158/1535-7163.MCT-19-0958

Gorfe, A. A., Grant, B. J., & McCammon, J. A. (2008). Mapping the nucleotide and isoform-dependent structural and dynamical features of Ras proteins. *Structure*, *16*(6), 885-896. https://doi.org/10.1016/j.str.2008.03.009

Gouda, M. A., & Subbiah, V. (2023). Expanding the Benefit: Dabrafenib/Trametinib as Tissue-Agnostic Therapy for BRAF V600E-Positive Adult and Pediatric Solid Tumors. *Am Soc Clin Oncol Educ Book*, *43*, e404770. https://doi.org/10.1200/EDBK_404770

Grant, B. J., Lukman, S., Hocker, H. J., Sayyah, J., Brown, J. H., McCammon, J. A., & Gorfe, A. A. (2011). Novel allosteric sites on Ras for lead generation. *PLoS One*, *6*(10), e25711. https://doi.org/10.1371/journal.pone.0025711

Griffioen, A. W., van der Schaft, D. W., Barendsz-Janson, A. F., Cox, A., Struijker Boudier, H. A., Hillen, H. F., & Mayo, K. H. (2001). Anginex, a designed peptide that inhibits angiogenesis. *Biochem J*, *354*(Pt 2), 233-242. https://doi.org/10.1042/0264-6021:3540233

Guardia, C. M., Caramelo, J. J., Trujillo, M., Mendez-Huergo, S. P., Radi, R., Estrin, D. A., & Rabinovich, G. A. (2014). Structural basis of redox-dependent modulation of galectin-1 dynamics and function. *Glycobiology*, *24*(5), 428-441. https://doi.org/10.1093/glycob/cwu008

Guo, Y. J., Pan, W. W., Liu, S. B., Shen, Z. F., Xu, Y., & Hu, L. L. (2020). ERK/MAPK signalling pathway and tumorigenesis. *Exp Ther Med*, *19*(3), 1997-2007. https://doi.org/10.3892/etm.2020.8454

Hennig, A., Markwart, R., Esparza-Franco, M. A., Ladds, G., & Rubio, I. (2015). Ras activation revisited: role of GEF and GAP systems. *Biol Chem*, *396*(8), 831-848. https://doi.org/10.1515/hsz-2014-0257

Hobbs, G. A., Der, C. J., & Rossman, K. L. (2016). RAS isoforms and mutations in cancer at a glance. *J Cell Sci*, *129*(7), 1287-1292. https://doi.org/10.1242/jcs.182873

Holderfield, M., Deuker, M. M., McCormick, F., & McMahon, M. (2014). Targeting RAF kinases for cancer therapy: BRAF-mutated melanoma and beyond. *Nat Rev Cancer*, *14*(7), 455-467. https://doi.org/10.1038/nrc3760

Holderfield, M., Lee, B. J., Jiang, J., Tomlinson, A., Seamon, K. J., Mira, A., Patrucco, E., Goodhart, G., Dilly, J., Gindin, Y., Dinglasan, N., Wang, Y., Lai, L. P., Cai, S., Jiang, L., Nasholm, N., Shifrin, N., Blaj, C., Shah, H., . . . Singh, M. (2024). Concurrent inhibition of oncogenic and wild-type RAS-GTP for cancer therapy. *Nature*, *629*(8013), 919-926. https://doi.org/10.1038/s41586-024-07205-6

Hood, F. E., Sahraoui, Y. M., Jenkins, R. E., & Prior, I. A. (2023). Ras protein abundance correlates with Ras isoform mutation patterns in cancer. *Oncogene*, *42*(15), 1224-1232. https://doi.org/10.1038/s41388-023-02638-1

Hunter, J. C., Manandhar, A., Carrasco, M. A., Gurbani, D., Gondi, S., & Westover, K. D. (2015). Biochemical and Structural Analysis of Common Cancer-Associated KRAS Mutations. *Mol Cancer Res*, *13*(9), 1325-1335. https://doi.org/10.1158/1541-7786.MCR-15-0203

Inder, K. L., Hill, M. M., & Hancock, J. F. (2010). Nucleophosmin and nucleolin regulate K-Ras signaling. *Commun Integr Biol*, *3*(2), 188-190. https://doi.org/10.4161/cib.3.2.10923

Inder, K. L., Lau, C., Loo, D., Chaudhary, N., Goodall, A., Martin, S., Jones, A., van der Hoeven, D., Parton, R. G., Hill, M. M., & Hancock, J. F. (2009). Nucleophosmin and nucleolin regulate K-Ras plasma membrane interactions and MAPK signal transduction. *J Biol Chem*, *284*(41), 28410-28419. https://doi.org/10.1074/jbc.M109.001537

Iosub-Amir, A., & Friedler, A. (2014). Protein–protein interactions of ASPP2: an emerging therapeutic target. *MedChemComm*, *5*(10), 1435-1443.

Janes, M. R., Zhang, J., Li, L. S., Hansen, R., Peters, U., Guo, X., Chen, Y., Babbar, A., Firdaus, S. J., Darjania, L., Feng, J., Chen, J. H., Li, S., Li, S., Long, Y. O., Thach, C., Liu, Y., Zarieh, A., Ely, T., . . . Liu, Y. (2018). Targeting KRAS Mutant Cancers with a Covalent G12C-Specific Inhibitor. *Cell*, *172*(3), 578-589 e517. https://doi.org/10.1016/j.cell.2018.01.006

Jiang, J., Jiang, L., Maldonato, B. J., Wang, Y., Holderfield, M., Aronchik, I., Winters, I. P., Salman, Z., Blaj, C., Menard, M., Brodbeck, J., Chen, Z., Wei, X., Rosen, M. J., Gindin, Y., Lee, B. J., Evans, J. W., Chang, S., Wang, Z., . . . Singh, M. (2024). Translational and Therapeutic Evaluation of RAS-GTP Inhibition by RMC-6236 in RAS-Driven Cancers. *Cancer Discov*, *14*(6), 994-1017. https://doi.org/10.1158/2159-8290.CD-24-0027

Johannes, L., Jacob, R., & Leffler, H. (2018). Galectins at a glance. *J Cell Sci*, *131*(9). https://doi.org/10.1242/jcs.208884

Jung, J., Cho, K. J., Naji, A. K., Clemons, K. N., Wong, C. O., Villanueva, M., Gregory, S., Karagas, N. E., Tan, L., Liang, H., Rousseau, M. A., Tomasevich, K. M., Sikora, A. G., Levental, I., van der Hoeven, D., Zhou, Y., Hancock, J. F., & Venkatachalam, K. (2019). HRAS-driven cancer cells are vulnerable to TRPML1 inhibition. *EMBO Rep*, *20*(4). https://doi.org/10.15252/embr.201846685

Karoulia, Z., Gavathiotis, E., & Poulikakos, P. I. (2017). New perspectives for targeting RAF kinase in human cancer. *Nat Rev Cancer*, *17*(11), 676-691. https://doi.org/10.1038/nrc.2017.79

Karoulia, Z., Wu, Y., Ahmed, T. A., Xin, Q., Bollard, J., Krepler, C., Wu, X., Zhang, C., Bollag, G., Herlyn, M., Fagin, J. A., Lujambio, A., Gavathiotis, E., & Poulikakos, P. I. (2016). An Integrated Model of RAF Inhibitor Action Predicts Inhibitor Activity against Oncogenic BRAF Signaling. *Cancer Cell*, *30*(3), 485-498. https://doi.org/10.1016/j.ccell.2016.06.024

Kattan, W. E., Chen, W., Ma, X., Lan, T. H., van der Hoeven, D., van der Hoeven, R., & Hancock, J. F. (2019). Targeting plasma membrane phosphatidylserine content to inhibit oncogenic KRAS function. *Life Sci Alliance*, *2*(5). https://doi.org/10.26508/lsa.201900431

Ketcham, J. M., Haling, J., Khare, S., Bowcut, V., Briere, D. M., Burns, A. C., Gunn, R. J., Ivetac, A., Kuehler, J., Kulyk, S., Laguer, J., Lawson, J. D., Moya, K., Nguyen, N., Rahbaek, L., Saechao, B., Smith, C. R., Sudhakar, N., Thomas, N. C., . . . Marx, M. A. (2022). Design and Discovery of MRTX0902, a Potent, Selective, Brain-Penetrant, and Orally Bioavailable Inhibitor of the SOS1:KRAS Protein-Protein Interaction. *J Med Chem*, *65*(14), 9678-9690. https://doi.org/10.1021/acs.jmedchem.2c00741

Kiel, C., Matallanas, D., & Kolch, W. (2021). The Ins and Outs of RAS Effector Complexes. *Biomolecules*, *11*(2). https://doi.org/10.3390/biom11020236

Kobayashi, H., Picard, L. P., Schonegge, A. M., & Bouvier, M. (2019). Bioluminescence resonance energy transfer-based imaging of protein-protein interactions in living cells. *Nat Protoc*, *14*(4), 1084-1107. https://doi.org/10.1038/s41596-019-0129-7

Koera, K., Nakamura, K., Nakao, K., Miyoshi, J., Toyoshima, K., Hatta, T., Otani, H., Aiba, A., & Katsuki, M. (1997). K-ras is essential for the development of the mouse embryo. *Oncogene*, *15*(10), 1151-1159. https://doi.org/10.1038/sj.onc.1201284

Kovalski, J. R., Bhaduri, A., Zehnder, A. M., Neela, P. H., Che, Y., Wozniak, G. G., & Khavari, P. A. (2019). The Functional Proximal Proteome of Oncogenic Ras Includes mTORC2. *Mol Cell*, *73*(4), 830-844 e812. https://doi.org/10.1016/j.molcel.2018.12.001

Kwan, A. K., Piazza, G. A., Keeton, A. B., & Leite, C. A. (2022). The path to the clinic: a comprehensive review on direct KRAS(G12C) inhibitors. *J Exp Clin Cancer Res*, *41*(1), 27. https://doi.org/10.1186/s13046-021-02225-w

Lau, J. L., & Dunn, M. K. (2018). Therapeutic peptides: Historical perspectives, current development trends, and future directions. *Bioorg Med Chem*, *26*(10), 2700-2707. https://doi.org/10.1016/j.bmc.2017.06.052

Lau, L. S., Mohammed, N. B. B., & Dimitroff, C. J. (2022). Decoding Strategies to Evade Immunoregulators Galectin-1, -3, and -9 and Their Ligands as Novel Therapeutics in Cancer Immunotherapy. *Int J Mol Sci*, *23*(24). https://doi.org/10.3390/ijms232415554

Lavoie, H., & Therrien, M. (2015). Regulation of RAF protein kinases in ERK signalling. *Nat Rev Mol Cell Biol*, *16*(5), 281-298. https://doi.org/10.1038/nrm3979

Lavoie, H., Thevakumaran, N., Gavory, G., Li, J. J., Padeganeh, A., Guiral, S., Duchaine, J., Mao, D. Y., Bouvier, M., Sicheri, F., & Therrien, M. (2013). Inhibitors that stabilize a closed RAF kinase domain conformation induce dimerization [10.1038/nchembio.1257]. *Nat Chem Biol*, *9*(7), 428-436. https://doi.org/10.1038/nchembio.1257

Lefranc, F., Mathieu, V., & Kiss, R. (2011). Galectin-1-mediated biochemical controls of melanoma and glioma aggressive behavior. *World J Biol Chem*, *2*(9), 193-201. https://doi.org/10.4331/wjbc.v2.i9.193

Li, X., Liu, S., Fang, X., He, C., & Hu, X. (2019). The mechanisms of DIRAS family members in role of tumor suppressor. *J Cell Physiol*, *234*(5), 5564-5577. https://doi.org/10.1002/jcp.27376

Li, Z., Song, Z., Zhao, Y., Wang, P., Jiang, L., Gong, Y., Zhou, J., Jian, H., Dong, X., Zhuang, W., Cang, S., Yang, N., Fang, J., Shi, J., Lu, J., Ma, R., Wu, P., Zhang, Y., Song, M., . . . Lu, S. (2023). D-1553 (Garsorasib), a Potent and Selective Inhibitor of KRAS(G12C) in Patients With NSCLC: Phase 1 Study Results. *J Thorac Oncol*, *18*(7), 940-951. https://doi.org/10.1016/j.jtho.2023.03.015

Liso, A., Bogliolo, A., Freschi, V., Martelli, M. P., Pileri, S. A., Santodirocco, M., Bolli, N., Martelli, M. F., & Falini, B. (2008). In human genome, generation of a nuclear export signal through duplication appears unique to nucleophosmin (NPM1) mutations and is restricted to AML. *Leukemia*, *22*(6), 1285-1289. https://doi.org/10.1038/sj.leu.2405045

Long, S. A., Amparo, A. M., Goodhart, G., Ahmad, S. A., & Waters, A. M. (2024). Evaluation of KRAS inhibitor-directed therapies for pancreatic cancer treatment. *Front Oncol*, *14*, 1402128. https://doi.org/10.3389/fonc.2024.1402128

Lopez, D. J., Rodriguez, J. A., & Banuelos, S. (2020). Nucleophosmin, a multifunctional nucleolar organizer with a role in DNA repair. *Biochim Biophys Acta Proteins Proteom*, *1868*(12), 140532. https://doi.org/10.1016/j.bbapap.2020.140532

Ma, X., Sloman, D. L., Duggal, R., Anderson, K. D., Ballard, J. E., Bharathan, I., Brynczka, C., Gathiaka, S., Henderson, T. J., Lyons, T. W., Miller, R., Munsell, E. V., Orth, P., Otte, R. D., Palani, A., Rankic, D. A., Robinson, M. R., Sather, A. C., Solban, N., . . . Han, Y. (2024). Discovery of MK-1084: An Orally Bioavailable and Low-Dose KRAS(G12C) Inhibitor. *J Med Chem*. https://doi.org/10.1021/acs.jmedchem.4c00572

Martinez Fiesco, J. A., Durrant, D. E., Morrison, D. K., & Zhang, P. (2022). Structural insights into the BRAF monomer-to-dimer transition mediated by RAS binding. *Nat Commun*, *13*(1), 486. https://doi.org/10.1038/s41467-022-28084-3

Mathieu, V., de Lassalle, E. M., Toelen, J., Mohr, T., Bellahcene, A., Van Goietsenoven, G., Verschuere, T., Bouzin, C., Debyser, Z., De Vleeschouwer, S., Van Gool, S., Poirier, F., Castronovo, V., Kiss, R., & Feron, O. (2012). Galectin-1 in melanoma biology and related neo-angiogenesis processes. *J Invest Dermatol*, *132*(9), 2245-2254. https://doi.org/10.1038/jid.2012.142

Michisaka, S., Sase, H., Tachibana, Y., Hasegawa, M., Fujii, T., Kuramoto, S., Shibahara, N., Ohta, A., Tanada, M., Shiraishi, T., Iikura, H., Kitazawa, T., & Tanaka, H. (2024). Combination of LUNA18, a novel RAS inhibitor, with KRAS G12C inhibitors augments anti-tumor activity via inhibition of MAPK pathway reactivation. *American Association for Cancer Research*. https://doi.org/https://doi.org/10.1158/1538-7445.AM2024-1664

Mo, S. P., Coulson, J. M., & Prior, I. A. (2018). RAS variant signalling. *Biochem Soc Trans*, *46*(5), 1325-1332. https://doi.org/10.1042/BST20180173

Nagashima, T., Inamura, K., Nishizono, Y., Suzuki, A., Tanaka, H., Yoshinari, T., & Yamanaka, Y. (2022). ASP3082, a First-in-class novel KRAS G12D degrader, exhibits remarkable anti-

tumor activity in KRAS G12D mutated cancer models. *European Journal of Cancer*, *174S1 (2022) S3–S128*.

Ostrem, J. M., Peters, U., Sos, M. L., Wells, J. A., & Shokat, K. M. (2013). K-Ras(G12C) inhibitors allosterically control GTP affinity and effector interactions. *Nature*, *503*(7477), 548-551. https://doi.org/10.1038/nature12796

Park, E., Rawson, S., Li, K., Kim, B. W., Ficarro, S. B., Pino, G. G., Sharif, H., Marto, J. A., Jeon, H., & Eck, M. J. (2019). Architecture of autoinhibited and active BRAF-MEK1-14-3-3 complexes. *Nature*, *575*(7783), 545-550. https://doi.org/10.1038/s41586-019-1660-y

Park, E., Rawson, S., Schmoker, A., Kim, B. W., Oh, S., Song, K., Jeon, H., & Eck, M. J. (2023). Cryo-EM structure of a RAS/RAF recruitment complex. *Nat Commun*, *14*(1), 4580. https://doi.org/10.1038/s41467-023-40299-6

Paul, A., Sarkar, A., Saha, S., Maji, A., Janah, P., & Kumar Maity, T. (2021). Synthetic and computational efforts towards the development of peptidomimetics and small-molecule SARS-CoV 3CLpro inhibitors. *Bioorg Med Chem*, *46*, 116301. https://doi.org/10.1016/j.bmc.2021.116301

Pavic, K., Chippalkatti, R., & Abankwa, D. (2022). Drug targeting opportunities en route to Ras nanoclusters. *Adv Cancer Res*, *153*, 63-99. https://doi.org/10.1016/bs.acr.2021.07.005

Peng, S. B., Henry, J. R., Kaufman, M. D., Lu, W. P., Smith, B. D., Vogeti, S., Rutkoski, T. J., Wise, S., Chun, L., Zhang, Y., Van Horn, R. D., Yin, T., Zhang, X., Yadav, V., Chen, S. H., Gong, X., Ma, X., Webster, Y., Buchanan, S., . . . Flynn, D. L. (2015). Inhibition of RAF Isoforms and Active Dimers by LY3009120 Leads to Anti-tumor Activities in RAS or BRAF Mutant Cancers. *Cancer Cell*, *28*(3), 384-398. https://doi.org/10.1016/j.ccell.2015.08.002

Pershing, N. L., Lampson, B. L., Belsky, J. A., Kaltenbrun, E., MacAlpine, D. M., & Counter, C. M. (2015). Rare codons capacitate Kras-driven de novo tumorigenesis. *J Clin Invest*, *125*(1), 222-233. https://doi.org/10.1172/JCI77627

Pfeffer, K., Ho, T. H., Grill, F. J., Ruiz, Y., & Lake, D. F. (2023). Generation and characterization of a monoclonal antibody that binds to Galectin-1. *Protein Expr Purif*, *210*, 106308. https://doi.org/10.1016/j.pep.2023.106308

Pfleger, K. D., & Eidne, K. A. (2006). Illuminating insights into protein-protein interactions using bioluminescence resonance energy transfer (BRET). *Nat Methods*, *3*(3), 165-174. https://doi.org/10.1038/nmeth841

Posada, I. M., Serulla, M., Zhou, Y., Oetken-Lindholm, C., Abankwa, D., & Lectez, B. (2016). ASPP2 Is a Novel Pan-Ras Nanocluster Scaffold. *PLoS One*, *11*(7), e0159677. https://doi.org/10.1371/journal.pone.0159677

Posada, I. M. D., Lectez, B., Sharma, M., Oetken-Lindholm, C., Yetukuri, L., Zhou, Y., Aittokallio, T., & Abankwa, D. (2017). Rapalogs can promote cancer cell stemness in vitro in a Galectin-1 and H-ras-dependent manner. *Oncotarget*, *8*(27), 44550-44566. https://doi.org/10.18632/oncotarget.17819

Potdar, S., Ianevski, F., Ianevski, A., Tanoli, Z., Wennerberg, K., Seashore-Ludlow, B., Kallioniemi, O., Ostling, P., Aittokallio, T., & Saarela, J. (2023). Breeze 2.0: an interactive web-tool for visual analysis and comparison of drug response data. *Nucleic Acids Res*, *51*(W1), W57-W61. https://doi.org/10.1093/nar/gkad390

Poulikakos, P. I., Persaud, Y., Janakiraman, M., Kong, X., Ng, C., Moriceau, G., Shi, H., Atefi, M., Titz, B., Gabay, M. T., Salton, M., Dahlman, K. B., Tadi, M., Wargo, J. A., Flaherty, K. T., Kelley, M. C., Misteli, T., Chapman, P. B., Sosman, J. A., . . . Solit, D. B. (2011). RAF inhibitor resistance is mediated by dimerization of aberrantly spliced BRAF(V600E). *Nature*, *480*(7377), 387-390. https://doi.org/10.1038/nature10662

Poulikakos, P. I., & Rosen, N. (2011). Mutant BRAF melanomas--dependence and resistance. *Cancer Cell*, *19*(1), 11-15. https://doi.org/10.1016/j.ccr.2011.01.008

Poulikakos, P. I., Zhang, C., Bollag, G., Shokat, K. M., & Rosen, N. (2010). RAF inhibitors transactivate RAF dimers and ERK signalling in cells with wild-type BRAF. *Nature*, *464*(7287), 427-430. https://doi.org/10.1038/nature08902

Prior, I. A., Hood, F. E., & Hartley, J. L. (2020). The Frequency of Ras Mutations in Cancer. *Cancer Res*, *80*(14), 2969-2974. https://doi.org/10.1158/0008-5472.CAN-19-3682

Prior, I. A., Lewis, P. D., & Mattos, C. (2012). A comprehensive survey of Ras mutations in cancer. *Cancer Res*, *72*(10), 2457-2467. https://doi.org/10.1158/0008-5472.CAN-11-2612

Rezaei Adariani, S., Kazemein Jasemi, N. S., Bazgir, F., Wittich, C., Amin, E., Seidel, C. A. M., Dvorsky, R., & Ahmadian, M. R. (2021). A comprehensive analysis of RAS-effector interactions reveals interaction hotspots and new binding partners. *J Biol Chem*, *296*, 100626. https://doi.org/10.1016/j.jbc.2021.100626

Roskoski, R., Jr. (2010). RAF protein-serine/threonine kinases: structure and regulation. *Biochem Biophys Res Commun*, *399*(3), 313-317. https://doi.org/10.1016/j.bbrc.2010.07.092

Rotblat, B., Niv, H., Andre, S., Kaltner, H., Gabius, H. J., & Kloog, Y. (2004). Galectin-1(L11A) predicted from a computed galectin-1 farnesyl-binding pocket selectively inhibits Ras-GTP. *Cancer Res*, *64*(9), 3112-3118. https://doi.org/10.1158/0008-5472.can-04-0026

Sacher, A., LoRusso, P., Patel, M. R., Miller, W. H., Jr., Garralda, E., Forster, M. D., Santoro, A., Falcon, A., Kim, T. W., Paz-Ares, L., Bowyer, S., de Miguel, M., Han, S. W., Krebs, M. G., Lee, J. S., Cheng, M. L., Arbour, K., Massarelli, E., Choi, Y., . . . Study, G. (2023). Single-Agent Divarasib (GDC-6036) in Solid Tumors with a KRAS G12C Mutation. *N Engl J Med*, *389*(8), 710-721. https://doi.org/10.1056/NEJMoa2303810

Sarkisian, C. J., Keister, B. A., Stairs, D. B., Boxer, R. B., Moody, S. E., & Chodosh, L. A. (2007). Dose-dependent oncogene-induced senescence in vivo and its evasion during mammary tumorigenesis. *Nat Cell Biol*, *9*(5), 493-505. https://doi.org/10.1038/ncb1567

Sase, H., Michisaka, S., Tachibana, Y., Hasegawa, M., Fujii, T., Takei, K., Kanei, T., Murao, N., Kuramoto, S., Shibahara, N., Ohta, A., Tanada, M., Shiraishi, T., Iikura, H., Kitazawa, T., & Tanaka, H. (2024). Anti-tumor activity of orally-available cyclic peptide LUNA18 through direct RAS inhibition in RAS-altered tumors. *American Association for Cancer Research*. https://doi.org/https://doi.org/10.1158/1538-7445.AM2024-1654

Schulze, C. J., Seamon, K. J., Zhao, Y., Yang, Y. C., Cregg, J., Kim, D., Tomlinson, A., Choy, T. J., Wang, Z., Sang, B., Pourfarjam, Y., Lucas, J., Cuevas-Navarro, A., Ayala-Santos, C., Vides, A., Li, C., Marquez, A., Zhong, M., Vemulapalli, V., . . . Lito, P. (2023). Chemical remodeling of a cellular chaperone to target the active state of mutant KRAS. *Science*, *381*(6659), 794-799. https://doi.org/10.1126/science.adg9652

Serrano, M., Lin, A. W., McCurrach, M. E., Beach, D., & Lowe, S. W. (1997). Oncogenic ras provokes premature cell senescence associated with accumulation of p53 and p16INK4a. *Cell*, *88*(5), 593-602. https://doi.org/10.1016/s0092-8674(00)81902-9

Shalom-Feuerstein, R., Plowman, S. J., Rotblat, B., Ariotti, N., Tian, T., Hancock, J. F., & Kloog, Y. (2008). K-ras nanoclustering is subverted by overexpression of the scaffold protein galectin-3. *Cancer Res*, *68*(16), 6608-6616. https://doi.org/10.1158/0008-5472.CAN-08-1117

Shaw, A. S., Kornev, A. P., Hu, J., Ahuja, L. G., & Taylor, S. S. (2014). Kinases and pseudokinases: lessons from RAF. *Mol Cell Biol*, *34*(9), 1538-1546. https://doi.org/10.1128/MCB.00057-14

Shi, Y., Tang, D., Li, X., Xie, X., Ye, Y., & Wang, L. (2022). Galectin Family Members: Emerging Novel Targets for Lymphoma Therapy? *Front Oncol*, *12*, 889034. https://doi.org/10.3389/fonc.2022.889034

Shi, Z., Weng, J., Niu, H., Yang, H., Liu, R., Weng, Y., Zhu, Q., Zhang, Y., Tao, L., Wang, Z., Huh, S. J., Jiang, Y., Mei, H., Dai, X., Zhang, L., & Wang, Y. (2023). D-1553: A novel KRAS(G12C) inhibitor with potent and selective cellular and in vivo antitumor activity. *Cancer Sci*, *114*(7), 2951-2960. https://doi.org/10.1111/cas.15829

Shimada, C., Xu, R., Al-Alem, L., Stasenko, M., Spriggs, D. R., & Rueda, B. R. (2020). Galectins and Ovarian Cancer. *Cancers (Basel)*, *12*(6). https://doi.org/10.3390/cancers12061421

Shu, L., Wang, D., Saba, N. F., & Chen, Z. G. (2020). A Historic Perspective and Overview of H-Ras Structure, Oncogenicity, and Targeting. *Mol Cancer Ther*, *19*(4), 999-1007. https://doi.org/10.1158/1535-7163.MCT-19-0660

Simanshu, D. K., Nissley, D. V., & McCormick, F. (2017). RAS Proteins and Their Regulators in Human Disease. *Cell*, *170*(1), 17-33. https://doi.org/10.1016/j.cell.2017.06.009

Smith, M. J. (2023). Defining bone fide effectors of RAS GTPases. *Bioessays*, *45*(9), e2300088. https://doi.org/10.1002/bies.202300088

Smith, M. J., Neel, B. G., & Ikura, M. (2013). NMR-based functional profiling of RASopathies and oncogenic RAS mutations. *Proc Natl Acad Sci U S A*, *110*(12), 4574-4579. https://doi.org/10.1073/pnas.1218173110

Steffen, C. L., Kaya, P., Schaffner-Reckinger, E., & Abankwa, D. (2023). Eliminating oncogenic RAS: back to the future at the drawing board. *Biochem Soc Trans*, *51*(1), 447-456. https://doi.org/10.1042/BST20221343

Steffen, C. L., Manoharan, G. B., Pavic, K., Yeste-Vazquez, A., Knuuttila, M., Arora, N., Zhou, Y., Harma, H., Gaigneaux, A., Grossmann, T. N., & Abankwa, D. K. (2024). Identification of an H-Ras nanocluster disrupting peptide. *Commun Biol*, *7*(1), 837. https://doi.org/10.1038/s42003-024-06523-9

Suire, S., Hawkins, P., & Stephens, L. (2002). Activation of phosphoinositide 3-kinase gamma by Ras. *Curr Biol*, *12*(13), 1068-1075. https://doi.org/10.1016/s0960-9822(02)00933-8

Sutton, M. N., Lu, Z., Li, Y. C., Zhou, Y., Huang, T., Reger, A. S., Hurwitz, A. M., Palzkill, T., Logsdon, C., Liang, X., Gray, J. W., Nan, X., Hancock, J., Wahl, G. M., & Bast, R. C., Jr. (2019). DIRAS3 (ARHI) Blocks RAS/MAPK Signaling by Binding Directly to RAS and Disrupting RAS Clusters. *Cell Rep*, *29*(11), 3448-3459 e3446. https://doi.org/10.1016/j.celrep.2019.11.045

Tanada, M., Tamiya, M., Matsuo, A., Chiyoda, A., Takano, K., Ito, T., Irie, M., Kotake, T., Takeyama, R., Kawada, H., Hayashi, R., Ishikawa, S., Nomura, K., Furuichi, N., Morita, Y., Kage, M., Hashimoto, S., Nii, K., Sase, H., . . . Shiraishi, T. (2023). Development of Orally Bioavailable Peptides Targeting an Intracellular Protein: From a Hit to a Clinical KRAS Inhibitor. *J Am Chem Soc*, *145*(30), 16610-16620. https://doi.org/10.1021/jacs.3c03886

Thijssen, V. L., Barkan, B., Shoji, H., Aries, I. M., Mathieu, V., Deltour, L., Hackeng, T. M., Kiss, R., Kloog, Y., Poirier, F., & Griffioen, A. W. (2010). Tumor cells secrete galectin-1 to enhance endothelial cell activity. *Cancer Res*, *70*(15), 6216-6224. https://doi.org/10.1158/0008-5472.CAN-09-4150

Troncoso, M. F., Elola, M. T., Blidner, A. G., Sarrias, L., Espelt, M. V., & Rabinovich, G. A. (2023). The universe of galectin-binding partners and their functions in health and disease. *J Biol Chem*, *299*(12), 105400. https://doi.org/10.1016/j.jbc.2023.105400

Vakana, E., Pratt, S., Blosser, W., Dowless, M., Simpson, N., Yuan, X. J., Jaken, S., Manro, J., Stephens, J., Zhang, Y., Huber, L., Peng, S. B., & Stancato, L. F. (2017). LY3009120, a panRAF inhibitor, has significant anti-tumor activity in BRAF and KRAS mutant preclinical models of colorectal cancer. *Oncotarget*, *8*(6), 9251-9266. https://doi.org/10.18632/oncotarget.14002

Van, Q. N., Prakash, P., Shrestha, R., Balius, T. E., Turbyville, T. J., & Stephen, A. G. (2021). RAS Nanoclusters: Dynamic Signaling Platforms Amenable to Therapeutic Intervention. *Biomolecules*, *11*(3). https://doi.org/10.3390/biom11030377

Vatansever, S., Gumus, Z. H., & Erman, B. (2016). Intrinsic K-Ras dynamics: A novel molecular dynamics data analysis method shows causality between residue pair motions. *Sci Rep*, *6*, 37012. https://doi.org/10.1038/srep37012

Verschuere, T., Toelen, J., Maes, W., Poirier, F., Boon, L., Tousseyn, T., Mathivet, T., Gerhardt, H., Mathieu, V., Kiss, R., Lefranc, F., Van Gool, S. W., & De Vleeschouwer, S. (2014). Glioma-derived galectin-1 regulates innate and adaptive antitumor immunity. *Int J Cancer*, *134*(4), 873-884. https://doi.org/10.1002/ijc.28426

Vetter, I. R., & Wittinghofer, A. (2001). The guanine nucleotide-binding switch in three dimensions. *Science*, *294*(5545), 1299-1304. https://doi.org/10.1126/science.1062023

Wang, L., Wang, N., Zhang, W., Cheng, X., Yan, Z., Shao, G., Wang, X., Wang, R., & Fu, C. (2022). Therapeutic peptides: current applications and future directions. *Signal Transduct Target Ther*, *7*(1), 48. https://doi.org/10.1038/s41392-022-00904-4

Wang, Y., Godin-Heymann, N., Dan Wang, X., Bergamaschi, D., Llanos, S., & Lu, X. (2013). ASPP1 and ASPP2 bind active RAS, potentiate RAS signalling and enhance p53 activity in cancer cells. *Cell Death Differ*, *20*(4), 525-534. https://doi.org/10.1038/cdd.2013.3

Weiss, A., Lorthiois, E., Barys, L., Beyer, K. S., Bomio-Confaglia, C., Burks, H., Chen, X., Cui, X., de Kanter, R., Dharmarajan, L., Fedele, C., Gerspacher, M., Guthy, D. A., Head, V., Jaeger, A., Nunez, E. J., Kearns, J. D., Leblanc, C., Maira, S. M., . . . Brachmann, S. M. (2022). Discovery, Preclinical Characterization, and Early Clinical Activity of JDQ443, a Structurally Novel,

Potent, and Selective Covalent Oral Inhibitor of KRASG12C. *Cancer Discov*, *12*(6), 1500-1517. https://doi.org/10.1158/2159-8290.CD-22-0158

Wright, L. P., & Philips, M. R. (2006). Thematic review series: lipid posttranslational modifications. CAAX modification and membrane targeting of Ras. *J Lipid Res*, *47*(5), 883-891. https://doi.org/10.1194/jlr.R600004-JLR200

Yan, J., Roy, S., Apolloni, A., Lane, A., & Hancock, J. F. (1998). Ras isoforms vary in their ability to activate Raf-1 and phosphoinositide 3-kinase. *J Biol Chem*, *273*(37), 24052-24056. https://doi.org/10.1074/jbc.273.37.24052

Yang, Y., Zhai, X., & El Hiani, Y. (2020). TRPML1-Emerging Roles in Cancer. *Cells*, *9*(12). https://doi.org/10.3390/cells9122682

Yu, X., Qian, J., Ding, L., Yin, S., Zhou, L., & Zheng, S. (2023). Galectin-1: A Traditionally Immunosuppressive Protein Displays Context-Dependent Capacities. *Int J Mol Sci*, *24*(7). https://doi.org/10.3390/ijms24076501

Zeng, S., Huang, W., Zheng, X., Liyan, C., Zhang, Z., Wang, J., & Shen, Z. (2021). Proteolysis targeting chimera (PROTAC) in drug discovery paradigm: Recent progress and future challenges. *Eur J Med Chem*, *210*, 112981. https://doi.org/10.1016/j.ejmech.2020.112981

Zhang, C., Spevak, W., Zhang, Y., Burton, E. A., Ma, Y., Habets, G., Zhang, J., Lin, J., Ewing, T., Matusow, B., Tsang, G., Marimuthu, A., Cho, H., Wu, G., Wang, W., Fong, D., Nguyen, H., Shi, S., Womack, P., . . . Bollag, G. (2015). RAF inhibitors that evade paradoxical MAPK pathway activation. *Nature*, *526*(7574), 583-586. https://doi.org/10.1038/nature14982

Zhang, F. L., Kirschmeier, P., Carr, D., James, L., Bond, R. W., Wang, L., Patton, R., Windsor, W. T., Syto, R., Zhang, R., & Bishop, W. R. (1997). Characterization of Ha-ras, N-ras, Ki-Ras4A, and Ki-Ras4B as in vitro substrates for farnesyl protein transferase and geranylgeranyl protein transferase type I. *J Biol Chem*, *272*(15), 10232-10239. https://doi.org/10.1074/jbc.272.15.10232

Zhou, Y., & Hancock, J. F. (2015). Ras nanoclusters: Versatile lipid-based signaling platforms. *Biochim Biophys Acta*, *1853*(4), 841-849. https://doi.org/10.1016/j.bbamcr.2014.09.008

Zhou, Y., & Hancock, J. F. (2018). Deciphering lipid codes: K-Ras as a paradigm. *Traffic*, *19*(3), 157-165. https://doi.org/10.1111/tra.12541

Zhou, Y., Prakash, P., Gorfe, A. A., & Hancock, J. F. (2018). Ras and the Plasma Membrane: A Complicated Relationship. *Cold Spring Harb Perspect Med*, *8*(10). https://doi.org/10.1101/cshperspect.a031831

Section C: Appendix of Original Publications

1. Manuscript (I)

Eliminating oncogenic RAS: back to the future at the drawing board

Candy Laura Steffen*, Pelin Kaya***,** Elisabeth Schaffner-Reckinger*, Daniel Abankwa

* These authors contributed equally.

Status: published

Personal contributions of Candy Laura Steffen

- Conducting literature research concerning macromolecular binders and peptides directly targeting RAS to generate Fig. 2
- Creation of Fig. 1 and 2, as well as table 1
- Assistance in conceptualizing Fig. 3
- Discussion and drafting of corresponding data contribution.

Biochemical Society Transactions (2023) **51** 447–456
https://doi.org/10.1042/BST20221343

Review Article

Eliminating oncogenic RAS: back to the future at the drawing board

Candy Laura Steffen*, Pelin Kaya*, Elisabeth Schaffner-Reckinger* and Daniel Abankwa

Cancer Cell Biology and Drug Discovery Group, Department of Life Sciences and Medicine, University of Luxembourg, L-4362 Esch-sur-Alzette, Luxembourg

Correspondence: Daniel Abankwa (daniel.abankwa@uni.lu)

RAS drug development has made enormous strides in the past ten years, with the first direct KRAS inhibitor being approved in 2021. However, despite the clinical success of covalent KRAS-G12C inhibitors, we are immediately confronted with resistances as commonly found with targeted drugs. Previously believed to be undruggable due to its lack of obvious druggable pockets, a couple of new approaches to hit this much feared oncogene have now been carved out. We here concisely review these approaches to directly target four druggable sites of RAS from various angles. Our analysis focuses on the lessons learnt during the development of allele-specific covalent and non-covalent RAS inhibitors, the potential of macromolecular binders to facilitate the discovery and validation of targetable sites on RAS and finally an outlook on a future that may engage more small molecule binders to become drugs. We foresee that the latter could happen mainly in two ways: First, non-covalent small molecule inhibitors may be derived from the development of covalent binders. Second, reversible small molecule binders could be utilized for novel targeting modalities, such as degraders of RAS. Provided that degraders eliminate RAS by recruiting differentially expressed E3-ligases, this approach could enable unprecedented tissue- or developmental stage-specific destruction of RAS with potential advantages for on-target toxicity. We conclude that novel creative ideas continue to be important to exterminate RAS in cancer and other RAS pathway-driven diseases, such as RASopathies.

Introduction

The small GTPase RAS operates as a switchable recruitment site of downstream effectors to the membrane. Thus GTP-binding triggers multiple intracellular signalling pathways, notably the MAPK pathway, which drives proliferation and differentiation [1]. This central position to orchestrate hallmarks of life may explain why RAS is so frequently exploited in cancer, where the three RAS genes, *KRAS*, *NRAS* and *HRAS* combined are mutated in 19% of cancer patients [2]. Mutations typically occur in hotspot codons 12, 13 or 61, which essentially keep RAS GTP-bound and thus constitutively active.

In 2021 the first direct RAS inhibitor, sotorasib (AMG 510), was approved after a 40 year long quest to inhibit this major oncogene. Impressive initial clinical data with a median overall survival of 12.5 months in smoking-associated KRAS-G12C mutant NSCLC patients supported this effort [3]. A number of other G12C-specific inhibitors are currently being evaluated in patients, including adagrasib (MRTX849), which is the second G12C-inhibitor to enter clinical assessment [4,5]. However, the application of these inhibitors is limited to KRAS-G12C mutant tumours, such as found in 14% of NSCLC patients, and <5% in colorectal and pancreatic cancers. Moreover, emerging resistances have stunted overall patient response and the initially high expectations. Resistance mechanisms include additional oncogenic KRAS mutations in codons 12, 13 or 61 that are not susceptible to G12C-inhibitors [6,7].

*These authors contributed equally to this work.

Received: 30 November 2022
Revised: 11 January 2023
Accepted: 12 January 2023

Version of Record published: 23 January 2023

PORTLAND PRESS

Biochemical Society Transactions (2023) **51** 447–456
https://doi.org/10.1042/BST20221343

Nonetheless, the first direct RAS inhibitors are a tremendous first milestone that demarcate the extraordinary achievements in RAS drug development during the past decade. They impressively demonstrate what happens, if specifically the oncogenic version of a major cancer driver is drug-targeted. Yet they also clarify that even with exquisite (covalent) on-target specificity, side effects cannot be ruled out [8]. Most importantly, these inhibitors provide unequivocal proof of KRAS as a cancer drug target in humans.

The KRAS-G12C inhibitor development story is testimony to not take no for an answer, and pursue the targeting of cancer drivers, even if they were considered undruggable. This justifies and encourages novel drug development efforts against RAS. We will here review, which approaches are on the drawing boards of researchers and give an outlook on potential future developments.

The development of allele-specific and pan-RAS inhibitors for clinical applications

Crystal structures of RAS show that GTP-binding induces conformational changes in two regions of RAS, called switch I and switch II, without revealing targetable pockets on RAS [1]. However, seminal work from the Shokat group published in 2013 identified the cryptic allosteric switch II-pocket (SII-P), which manifests only upon binding of KRAS-G12C inhibitors [9]. Their first proof-of-concept inhibitor introduced the acrylamide warhead for covalent engagement of the nucleophilic cysteine on position 12, thus creating a paradigm that has until today been widely utilized (Figure 1). Since then, essentially every major pharma company has developed KRAS-G12C inhibitors and we refer to recent reviews for details on their pre-/clinical progress [5,10].

The common chemical theme of these compounds in addition to their identical warhead is the 4-piperazin-1-yl-pyrimidine scaffold core that was essentially introduced with ARS-1620 [11]. Intriguingly, with the development of the scaffold of adagrasib a significant non-covalent binding to wild-type KRAS and to a number of KRAS mutants that carry hotspot mutations on codons 12, 13 and 61 was achieved [12]. In line

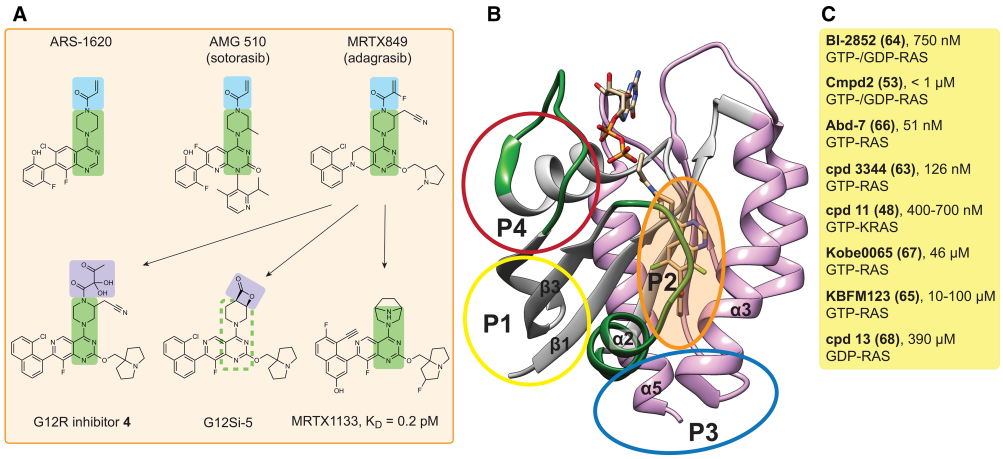

Figure 1. Overview of small molecule inhibitors targeting RAS.

(**A**) Selected SII-P small molecule inhibitors based on the 4-piperazin-1-yl-pyrimidine scaffold (green highlights). The common acrylamide warhead of KRAS-G12C inhibitors (top row) is highlighted in blue. Adagrasib served as a starting point for additional inhibitors (arrows), including covalent G12R- and G12S-inhibitors, with an α,β-diketoamide warhead or a strained β-lactone electrophile, respectively (purple). Note that the exact stereochemistry of displayed inhibitors has been largely omitted. (**B**) Crystal structure of GDP-KRAS-G12C in complex with ARS-1620 (PDB ID 5V9U). The RAS structure can be divided into the N-terminal effector lobe (grey), with the switch I and switch II regions labelled in green, and the allosteric lobe (pink). The allosteric binding sites P1–4 are indicated with circles. (**C**) Current experimental small molecule inhibitors (here those with an affinity <500 µM) target predominantly P1. The RAS affinity and selectivity is indicated for each compound (cpd). References are in brackets after the names [48,53,63–68]. The full list of small molecule inhibitors is contained in Supplementary File S1.

with this, the adagrasib scaffold served as a starting point for the development of the first covalent inhibitors of KRAS-G12S and KRAS-G12R in the GDP-bound OFF-state [13,14]. These carry instead of the acrylamide warhead, a strained β-lactone electrophile in the case of the G12S-inhibitor, while an α,β-diketoamide warhead was used in the G12R-inhibitor (Figure 1A). All of these SII-P targeting compounds lock KRAS in an inactive conformation by distorting switch I and switch II, thus typically blocking access of RAS activating GEFs, such as SOS, and of RAS effectors, notably RAF [9,11–14]. In agreement with the reuse of the pharmacologically validated adagrasib scaffold, inhibitors are furthermore active in cells, to suppress MAPK signalling and selectively the growth of cancer cells carrying the targeted mutation.

One initially puzzling finding was that all of these covalent inhibitors rely on the GDP-bound, inactive KRAS. However, oncogenic KRAS mutants are generally approximated to be constitutively GTP-bound and ON. While it is commonly assumed that the GTPase activating protein (GAP) neurofibromin (NF1) turns RAS OFF, the heterotrimeric G protein-associated GAP RGS3 was identified as the enzyme that sufficiently inactivates all major oncogenic KRAS alleles [15]. Consequently, ablation of RGS3 severely decreased the antitumorigenic effect of adagrasib in a mouse xenograft model. This can be explained by the distinct catalytic mechanisms of NF1 and RGS3. NF1 provides a catalytic arginine (the Arg-finger) to speed-up GTP hydrolysis of RAS, a mechanism that is crucially inhibited by oncogenic hotspot mutants of RAS [16]. In contrast, RGS3 is from a different family of GAPs, which likely bind RAS also involving its switch regions, but employ asparagine as catalytic residue [17,18].

It is astonishing, but not the first time in RAS/ MAPK biology that such a fundamental biological mechanism was only discovered after the first RAS inhibitors entered the clinic. Both failure of farnesyl transferase inhibitors and paradoxical RAF activation were only fully recognized at the clinical stage [10]. The RGS3-catalyzed hydrolysis of RAS furthermore begs the question, in which biological context then is the NF1-associated GAP-activity required, given that all hotspot mutants of RAS evade it.

The OFF-state dependency of SII-P inhibitors is also liable to major resistance mechanisms, which increase the ON-state, such as mutational activation of EGFR or up-regulation of other receptor tyrosine kinases [5]. Additional resistance mechanisms after sotorasib treatment include mutations that disrupt binding of the inhibitors to the SII-P, most notably Y96D, which also blocks access of adagrasib [6,19]. *In vitro* studies furthermore forecast evasive mutations, which increase GTP-levels of KRAS, such as Y40A, N116H and A146V [20]. Xenograft data furthermore suggest that MAPK pathway reactivation occurs sooner or later in particular by the emergence of clones with other oncogenic KRAS alleles or overactivation of other RAS isoforms, including MRAS [7].

Some of these resistance issues can be overcome by inhibiting the ON-state of KRAS. The adagrasib-derived non-covalent inhibitor MRTX-EX185 demonstrates this potential even for a SII-P binder [12]. The non-covalent inhibitor MRTX1133 exploited this further and introduced sub-picomolar targeting of the most common KRAS mutation, KRAS-G12D, with potent inhibition of signalling and xenograft growth [21].

Another embodiment is seen in a completely different RAS inhibition approach that is being evaluated in clinical trials. A whole panel of allele-specific and pan-RAS inhibitors has been commercially developed, which tie together KRAS in the ON-state and the ubiquitous and abundant chaperone protein cyclophilin A [22]. These 'molecular glue' compounds lead to an inhibitory tri-complex formation that sterically blocks RAS interactions and thus downstream signalling. Molecular glues are small molecules, which link two proteins in a non-native complex to inhibit or modify at least one of the binding partners [23]. The interesting potential of this approach is demonstrated by the covalent KRAS-G12C inhibitor RM-018, which can overcome the Y96D-dependent resistance encountered with sotorasib and adagrasib [19]. In addition to KRAS-G12C, the tri-complex approach has been utilized to covalently target KRAS-G12D, KRAS-G13C and multiple RAS alleles non-covalently, as recently reviewed elsewhere [5].

The exploration of novel binding sites and inhibition principles of RAS using macromolecular binders

In the commercial tri-complex approach, binding to the part of RAS that engages effectors is obstructed. This first half of the RAS protein (residues 1–85) is therefore also referred to as effector lobe, while the second half of the G-domain (residues 86–166) is called the allosteric lobe. The effector lobe makes major contacts not only with effectors, but all other major regulators of RAS, such as GEFs and GAPs.

Biochemical Society Transactions (2023) **51** 447–456
https://doi.org/10.1042/BST20221343

Therefore, high affinity macromolecular binders raised against the effector lobe can potently inhibit RAS signalling. In addition to classical antibodies (~150 kDa) and Fab-fragments (~50 kDa), much smaller specific binders can be raised by directed evolution *in vitro*, such as designed ankyrin repeat proteins (DARPins; ~20 kDa), Affimers (~12 kDa), which are based on the artificial phytocystatin-derived scaffold called Adhiron, and monobodies (~10 kDa), which originate from an artificial fibronectin type III domain [24–26]. Such binders exhibit typically affinities in the nanomolar range and encode high binding specificities to a small contact area. The small contact site can be exploited for pharmacophore based computational or *in vitro* competitive screening for small molecule functional analogues.

Obvious targets on the effector lobe are the switch regions, for which both GTP-specific binders (antibodies iDab#6, RT11, inRas37, monobody 12VC1, DARPin K55) [27–30], as well as GDP-specific binders (monobody JAM20, DARPin K27) have been identified [27,31] (Figure 2). Accordingly, these reagents typically repress RAS/ effector-binding and RAS-activation, respectively, and several were shown to block RAS-mutant cancer cell growth *in vitro* and in murine tumour models.

The truly exciting potential of these artificial binders lies in their ability to discover novel binding sites on RAS, which is notoriously binding cavity free. In support of this potential, affimer K3 was found to bind at the same site of KRAS, where current covalent G12C-inhibitors are lodging. Similarly, another affimer K6 binds to a pocket in between the switch I and switch II regions, a site that is also targeted by inhibitors DCAI and BI-2852 (Figure 1 and Supplementary File S1) [32–34].

Several other macromolecular binders engage with RAS on the allosteric lobe, hence in a nucleotide-independent manner. Complexation creates significant sterical bulk around RAS, which plausibly impacts on higher complex formation, such as transient dimers and nanoclustering. Nanoclusters are proteo-lipid complexes containing transient di-/trimeric RAS assemblies, which act as membrane recruitment sites of RAF-effectors and are therefore necessary for MAPK signalling [35]. In addition, the conformational mobility of RAS at the membrane impacts on MAPK signalling [35–38]. Given that a bulky binder would most probably restrain such conformational motions it is plausible to assume that they also affect associated RAS activities.

The monobody NS1 binds to HRAS and KRAS, but not NRAS, at an epitope comprising helices α4 and α5 [39]. These make up the most common interface that is assumed to partake in RAS self-organization into nanoclusters on the plasma membrane [40]. This interface was also recognized by the affimer K69 [32]. In contrast, the DARPins K13 and K19 bind to helices α3 and α4, which have also been suggested as interface for transient RAS dimers at the membrane [40]. While such macromolecular binders are *per se* not pharmacologically tractable for an intracellular target such as RAS, they nevertheless provide crucial proof-of-concept data for the target site in cellular and *in vivo* models.

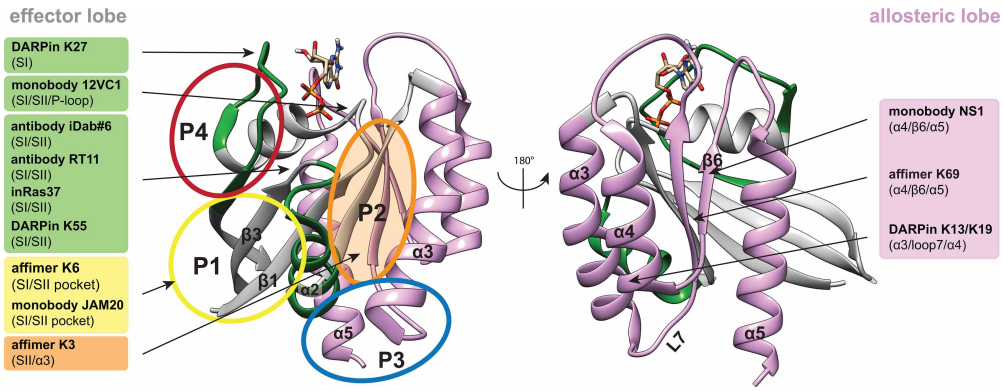

Figure 2. Overview of macromolecular RAS binders.
Crystal structure of GDP-KRAS (PDB ID 4OBE). Effector and allosteric lobes, as well as allosteric binding sites are indicated as in Figure 1. The names of macromolecular RAS binders are highlighted in the same colour as their binding sites, with more detailed binding site information given in brackets.

Moreover, they can be further functionalized to enable new modes of action. By genetically fusing E3-ligase subunits such as von Hippel-Lindau (VHL) tumour suppressor to the monobodies NS1 and 12VC1 or the DARPin K19, RAS degrader constructs were generated [30,41,42]. In general degraders realized potent RAS signalling suppression and anti-proliferative activities, and in the case of the 12VC1 were also more potent than the competitively binding monobody alone [30]. Given that these degraders emulate the proteolysis targeting chimera (PROTAC) mode of action, which will be discussed in the next chapter, they may be useful to forecast the potential of analogous PROTACs [43].

On the pathway to develop smaller RAS binders, peptides are a natural intermediate. A number of peptides or peptidomimetics that target the GTP-KRAS effector lobe typically with nanomolar affinity and compete with effector binding and downstream signalling of RAS have been developed. These peptides have a median size of ∼14 residues, can be either linear or cyclic, and contain non-natural amino acids or other chemical modifications (i.e. peptidomimetics) (Table 1). Cyclic peptides are entropically advantageous and are more resistant against exopeptidases [44]. So far, none of these peptides have been harnessed for degrader development.

What is the future of RAS inhibition? From small molecule binders to PROTAC-degraders

RAS is a small mono-domain protein with a shallow surface that has been considered undruggable due to the lack of obvious binding pockets. The nucleotide binding site remains problematic as a target, due to the high cellular GTP concentration in combination with the picomolar affinity of the guanine nucleotides to RAS [5]. However, computational approaches led by the Gorfe group, have identified already in 2011, hence well before the discovery of first covalent inhibitors, altogether four low affinity (sub-/millimolar) allosteric sites on RAS named P1 to P4 that have all been experimentally validated [45–47]. P1 and P4 are situated in the effector lobe, P3 in the allosteric lobe and P2 in between both lobes (Figure 1B).

The hydrophobic pocket P1 is located between switch II and β-strands 1–3 and is partially closed in crystal structures of GDP-RAS [48]. It essentially corresponds to the switch I/switch II region that is targeted by several experimental ON- and OFF-state binders (Figure 1C and Supplementary File S1). P2 is at the interface

Table 1 Overview of RAS binding peptides

Name (PDB ID)	RAS specificity	K_D (nM)	Site on RAS	Properties	Ref.
Linear					
RBDv1, RBDv12	GTP-RAS	3.35 2.52	P4	14 aa, inhibits RAS signalling, reduces cancer cell growth	[69]
SAH-SOS1	GDP-/GTP-RAS	106–175	near P4	16 aa, blocks nucleotide exchange, reduces cancer cell growth	[70]
225-11 (5WPL)	GTP-RAS	3.3	P4	32 aa, blocks effector interaction	[71]
R11.1.6 (5UFQ)	RAS-G12D	4	switch II	61 aa, blocks effector interaction, inhibits RAS signalling	[72]
Cyclic					
Cyclorasin 9A5	GTP-RAS	440	near P4	11 aa, blocks effector interaction, inhibits RAS signalling	[73]
Cyclorasin B4-27	GTP-RAS	21	near P4	16 aa, blocks effector interaction (cellular BRET-assay)	[74]
KRpep-2d (5XCO)	KRAS-G12D	51	P2	19 aa, inhibits RAS signalling, reduces cancer cell growth	[75–77]
KS-58	KRAS-G12D	22	P2	11 aa, inhibits RAS signalling, reduces cancer cell growth *in vivo*	[78,79]
KD2 (6WGN)	GTP-KRAS-G12D	none	near P2	15 aa, blocks effector interaction	[80]

Peptide and peptidomimetic RAS binders and their properties. The PDB ID is given if the complex with RAS was determined.

Biochemical Society Transactions (2023) **51** 447–456
https://doi.org/10.1042/BST20221343

of helix α2 with helix α3. This cryptic hydrophobic pocket is currently the most successfully targeted site, as it harbours the covalent OFF-state inhibitors targeting G12C, G12S, G12R and non-covalent inhibitors targeting G12D (Figure 1A). The polar P3 site is located between helix α5 and loop 7 and is accessible in both GTP- and GDP-states of KRAS, but less in the other RAS isoforms [46]. However, currently few binders target this site, such as metal cyclens and KAL-21404358 [49,50]. P4 is also polar and situated behind switch I and possesses andrographolide derivatives as the most interesting ligands currently [51]. It thus appears that the number of targetable sites on RAS is limited.

By combining computational and experimental approaches several small molecules have been identified that bind primarily to P1 and P2 (Figure 1C and Supplementary File S1). These ligands cover a broad range of affinities from milli- to nanomolar, typically lack RAS isoform selectivity and can disrupt binding of RAS interaction partners, such as RAF, and suppress MAPK signalling or cell viability. Only for compound 11 was KRAS-selective on-target binding demonstrated *in vitro* [48]. Therefore, cellular effects of low affinity compounds have to be taken with caution, as at the early stages of compound discovery off-target effects will contribute to these readouts.

With the exception of the covalent and non-covalent SII-P binding inhibitors, none of the small molecule binders has advanced toward clinical development. This may suggest that before a non-covalent inhibitor (such as MRTX1133) can flourish, a covalent counterpart that is anchored at the desired site may be advantageous during compound development [9].

Given their size, small molecules are less likely to block protein–protein interfaces such as needed to inhibit RAS nanoclustering. However, membrane-bound RAS also undergoes potentially RAS isoform specific conformational changes that impact on its nanoclustering [36,37]. Interestingly, some very rare cancer-associated and RASopathy mutations seem to affect nanoclustering by perturbing conformational dynamics of RAS [38,52]. A similar conformational shift may therefore also be achievable by small molecules, which was indeed demonstrated by the Ikura group. They showed that Cmpd2 stabilizes a non-productive conformation of KRAS at the membrane, by binding in between the membrane and the P1 site [53]. Another intriguing concept originated from the serendipitous discovery of a RAS-dimer stabilizer BI-2852, which was developed as RAS switch I/switch II pocket binder [33,54]. This nanomolar ligand illustrates the potential to modulate RAS oligomerization, specifically by locking it in a non-productive dimer.

As compared with competitive inhibitors, PROTACs instruct protein degradation by recruiting the ubiquitin-proteasome system to the target protein [55]. They can therefore bind outside of an active or allosteric site of a protein and after degradation abrogate any scaffolding functions of the target. This is enabled by their hybrid structure, which contains one binder (the warhead) for the target protein that is tethered via a linker to a moiety that recruits an E3-ligase, most commonly VHL and cereblon. The latter was enabled by the finding that immunomodulatory thalidomide derivatives alone work as 'molecular glues' that stick cereblon to IKAROS-family transcription factors and thus instruct their degradation [55].

Both concepts, molecular glues and PROTACs are thus not only historically related but bear similar capabilities, as both types of inhibitors can be potentially reused after reversible binding to and degradation of the target protein. Of note, molecular glues may also act by incapacitating a protein in a non-functional complex, such as illustrated by the tri-complex approach described earlier. Given that PROTACs follow an apparent 'plug-and-play' design, where the E3-ligase recruiting moiety can be utilized in several molecules, this approach currently predominates [55]. However, significant optimization for linker length and pharmacological properties of the relatively large molecules still requires substantial developmental efforts [56].

Current RAS-targeting PROTACs (XY-4-88, LC-2, KP-14) all build on the covalent G12C-inhibitors and as such cannot benefit from PROTAC degrader recycling, as these inhibitors are consumed due to the covalent cysteine engagement (Supplementary File S1) [57–59]. An interesting advancement in this regard is the development of reversible covalent inhibitor YF135, which employs a cyanoacrylamide for cysteine linkage [60]. Side-by-side comparison with the RAS-binding warhead alone furthermore demonstrates a 30-fold higher activity of the PROTAC. It remains to be seen, how and whether any of the exploratory RAS-ligands (Figure 1C and Supplementary File S1) can be converted into PROTACs. Given the distinct spatio-temporal expression of some E3-ligases in tissues and inside of cells, PROTACs may provide a more controlled drug action, which could reduce toxicity and new treatment mechanisms [61,62].

RAS drug development is in full motion since 2007 (Figure 3) and it can be hoped that novel creative ideas will continue to provide new RAS drugs for cancer therapy or other RAS-associated diseases, such as RASopathies.

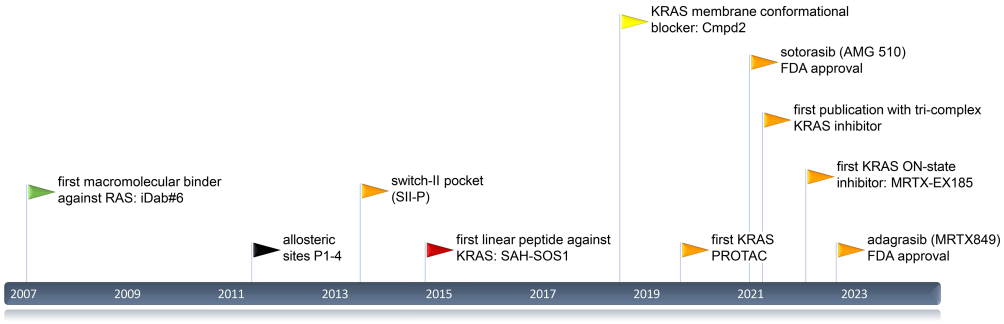

Figure 3. Timeline of notable RAS drug development events since 2007.

Arrowheads mark publications of binders and sites with colours corresponding to those used for binding sites in Figures 1 and 2.

Perspectives

- KRAS is the most frequently mutated oncogene and a major driver of cancer (stemness), which has finally become a clinically validated drug-target, thanks to KRAS-G12C targeting sotorasib and adagrasib. However, the performance of these compounds in the clinic warrants continuing efforts in RAS pathway drug development and further research to understand the essence of RAS in cancer.

- At least four targetable allosteric pockets and four surface areas on RAS have been identified and validated by the discovery of macromolecular-, peptidic- and small molecule-binders. These block upstream processes of RAS signalling, such as effector binding and nanoclustering.

- PROTAC degraders of RAS may offer new ways to inhibit RAS in a spatio-temporally (tissue type, differentiation stage, cell-cycle stage) more defined manner, with potential benefits for on-target toxicity. However, the viability of this approach awaits evaluation in the clinic.

Competing Interests

The authors declare that there are no competing interests associated with the manuscript.

Funding

This work was supported by grants from the Luxembourg National Research Fund (FNR): AFR individual grant 13589879 to P.K. and INTER/NWO/19/14061736 — HRAS-PPi to D.A.

Author Contributions

This review was jointly prepared by C.L.S., P.K., E.S.-R. and D.A.

Abbreviations

EGFR, Epidermal growth factor receptor; GEF, Guanine nucleotide exchange factor; MAPK, Mitogen-activated protein kinases; NSCLC, Non-small cell lung cancer; RGS3, Regulator of G-protein signalling 3; SOS, Son of sevenless guanine nucleotide exchange factor.

Biochemical Society Transactions (2023) **51** 447–456
https://doi.org/10.1042/BST20221343

References

1 Simanshu, D.K., Nissley, D.V. and McCormick, F. (2017) RAS proteins and their regulators in human disease. *Cell* **170**, 17–33 https://doi.org/10.1016/j.cell.2017.06.009

2 Prior, I.A., Hood, F.E. and Hartley, J.L. (2020) The frequency of Ras mutations in cancer. *Cancer Res.* **80**, 2969–2974 https://doi.org/10.1158/0008-5472.CAN-19-3682

3 Skoulidis, F., Li, B.T., Dy, G.K., Price, T.J., Falchook, G.S., Wolf, J. et al. (2021) Sotorasib for lung cancers with KRAS p.G12C mutation. *N. Engl. J. Med.* **384**, 2371–2381 https://doi.org/10.1056/NEJMoa2103695

4 Fell, J.B., Fischer, J.P., Baer, B.R., Blake, J.F., Bouhana, K., Briere, D.M. et al. (2020) Identification of the clinical development candidate MRTX849, a covalent KRAS(G12C) inhibitor for the treatment of cancer. *J. Med. Chem.* **63**, 6679–6693 https://doi.org/10.1021/acs.jmedchem.9b02052

5 Punekar, S.R., Velcheti, V., Neel, B.G. and Wong, K.K. (2022) The current state of the art and future trends in RAS-targeted cancer therapies. *Nat. Rev. Clin. Oncol.* **19**, 637–655 https://doi.org/10.1038/s41571-022-00671-9

6 Awad, M.M., Liu, S., Rybkin, I.I., Arbour, K.C., Dilly, J., Zhu, V.W. et al. (2021) Acquired resistance to KRAS(G12C) inhibition in cancer. *N. Engl. J. Med.* **384**, 2382–2393 https://doi.org/10.1056/NEJMoa2105281

7 Zhao, Y., Murciano-Goroff, Y.R., Xue, J.Y., Ang, A., Lucas, J., Mai, T.T. et al. (2021) Diverse alterations associated with resistance to KRAS(G12C) inhibition. *Nature* **599**, 679–683 https://doi.org/10.1038/s41586-021-04065-2

8 Kwan, A.K., Piazza, G.A., Keeton, A.B. and Leite, C.A. (2022) The path to the clinic: a comprehensive review on direct KRAS(G12C) inhibitors. *J. Exp. Clin. Cancer Res.* **41**, 27 https://doi.org/10.1186/s13046-021-02225-w

9 Ostrem, J.M., Peters, U., Sos, M.L., Wells, J.A. and Shokat, K.M. (2013) K-Ras(G12C) inhibitors allosterically control GTP affinity and effector interactions. *Nature* **503**, 548–551 https://doi.org/10.1038/nature12796

10 Moore, A.R., Rosenberg, S.C., McCormick, F. and Malek, S. (2020) RAS-targeted therapies: is the undruggable drugged? *Nat. Rev. Drug Discov.* **19**, 533–552 https://doi.org/10.1038/s41573-020-0068-6

11 Janes, M.R., Zhang, J., Li, L.S., Hansen, R., Peters, U., Guo, X. et al. (2018) Targeting KRAS mutant cancers with a covalent G12C-specific inhibitor. *Cell* **172**, 578–589.e517 https://doi.org/10.1016/j.cell.2018.01.006

12 Vasta, J.D., Peacock, D.M., Zheng, Q., Walker, J.A., Zhang, Z., Zimprich, C.A. et al. (2022) KRAS is vulnerable to reversible switch-II pocket engagement in cells. *Nat. Chem. Biol.* **18**, 596–604 https://doi.org/10.1038/s41589-022-00985-w

13 Zhang, Z., Guiley, K.Z. and Shokat, K.M. (2022) Chemical acylation of an acquired serine suppresses oncogenic signaling of K-Ras(G12S). *Nat. Chem. Biol.* **18**, 1177–1183 https://doi.org/10.1038/s41589-022-01065-9

14 Zhang, Z., Morstein, J., Ecker, A.K., Guiley, K.Z. and Shokat, K.M. (2022) Chemoselective covalent modification of K-Ras(G12R) with a small molecule electrophile. *J. Am. Chem. Soc.* **144**, 15916–15921 https://doi.org/10.1021/jacs.2c05377

15 Li, C., Vides, A., Kim, D., Xue, J.Y., Zhao, Y. and Lito, P. (2021) The G protein signaling regulator RGS3 enhances the GTPase activity of KRAS. *Science* **374**, 197–201 https://doi.org/10.1126/science.abf1730

16 Scheffzek, K., Ahmadian, M.R., Kabsch, W., Wiesmuller, L., Lautwein, A., Schmitz, F. et al. (1997) The Ras-RasGAP complex: structural basis for GTPase activation and its loss in oncogenic Ras mutants. *Science* **277**, 333–338 https://doi.org/10.1126/science.277.5324.333

17 Soundararajan, M., Willard, F.S., Kimple, A.J., Turnbull, A.P., Ball, L.J., Schoch, G.A. et al. (2008) Structural diversity in the RGS domain and its interaction with heterotrimeric G protein alpha-subunits. *Proc. Natl Acad. Sci. U.S.A.* **105**, 6457–6462 https://doi.org/10.1073/pnas.0801508105

18 Tesmer, J.J., Berman, D.M., Gilman, A.G. and Sprang, S.R. (1997) Structure of RGS4 bound to AlF4$^-$-activated Giα1: stabilization of the transition state for GTP hydrolysis. *Cell* **89**, 251–261 https://doi.org/10.1016/s0092-8674(00)80204-4

19 Tanaka, N., Lin, J.J., Li, C., Ryan, M.B., Zhang, J., Kiedrowski, L.A. et al. (2021) Clinical acquired resistance to KRAS(G12C) inhibition through a novel KRAS switch-II pocket mutation and polyclonal alterations converging on RAS-MAPK reactivation. *Cancer Discov.* **11**, 1913–1922 https://doi.org/10.1158/2159-8290.CD-21-0365

20 Lito, P., Solomon, M., Li, L.S., Hansen, R. and Rosen, N. (2016) Allele-specific inhibitors inactivate mutant KRAS G12C by a trapping mechanism. *Science* **351**, 604–608 https://doi.org/10.1126/science.aad6204

21 Hallin, J., Bowcut, V., Calinisan, A., Briere, D.M., Hargis, L., Engstrom, L.D. et al. (2022) Anti-tumor efficacy of a potent and selective non-covalent KRAS^{G12D} inhibitor. *Nat. Med.* **28**, 2171–2182 https://doi.org/10.1038/s41591-022-02007-7

22 Zhang, Z. and Shokat, K.M. (2019) Bifunctional small-molecule ligands of K-Ras induce its association with immunophilin proteins. *Angew. Chem. Int. Ed. Engl.* **58**, 16314–16319 https://doi.org/10.1002/anie.201910124

23 Geiger, T.M., Schäfer, S.C., Dreizler, J.K., Walz, M. and Hausch, F. (2022) Clues to molecular glues. *Curr. Res. Chem. Biol.* **2**, 14 https://doi.org/10.1016/j.crchbi.2021.100018

24 Koide, A., Bailey, C.W., Huang, X. and Koide, S. (1998) The fibronectin type III domain as a scaffold for novel binding proteins. *J. Mol. Biol.* **284**, 1141–1151 https://doi.org/10.1006/jmbi.1998.2238

25 Stumpp, M.T., Binz, H.K. and Amstutz, P. (2008) DARPins: a new generation of protein therapeutics. *Drug Discov. Today* **13**, 695–701 https://doi.org/10.1016/j.drudis.2008.04.013

26 Tiede, C., Tang, A.A., Deacon, S.E., Mandal, U., Nettleship, J.E., Owen, R.L. et al. (2014) Adhiron: a stable and versatile peptide display scaffold for molecular recognition applications. *Protein Eng. Des. Sel.* **27**, 145–155 https://doi.org/10.1093/protein/gzu007

27 Guillard, S., Kolasinska-Zwierz, P., Debreczeni, J., Breed, J., Zhang, J., Bery, N. et al. (2017) Structural and functional characterization of a DARPin which inhibits Ras nucleotide exchange. *Nat. Commun.* **8**, 16111 https://doi.org/10.1038/ncomms16111

28 Shin, S.M., Choi, D.K., Jung, K., Bae, J., Kim, J.S., Park, S.W. et al. (2017) Antibody targeting intracellular oncogenic Ras mutants exerts anti-tumour effects after systemic administration. *Nat. Commun.* **8**, 15090 https://doi.org/10.1038/ncomms15090

29 Tanaka, T., Williams, R.L. and Rabbitts, T.H. (2007) Tumour prevention by a single antibody domain targeting the interaction of signal transduction proteins with RAS. *EMBO J.* **26**, 3250–3259 https://doi.org/10.1038/sj.emboj.7601744

30 Teng, K.W., Tsai, S.T., Hattori, T., Fedele, C., Koide, A., Yang, C. et al. (2021) Selective and noncovalent targeting of RAS mutants for inhibition and degradation. *Nat. Commun.* **12**, 2656 https://doi.org/10.1038/s41467-021-22969-5

31 Wallon, L., Khan, I., Teng, K.W., Koide, A., Zuberi, M., Li, J. et al. (2022) Inhibition of RAS-driven signaling and tumorigenesis with a pan-RAS monobody targeting the switch I/II pocket. *Proc. Natl Acad. Sci. U.S.A.* **119**, e2204481119 https://doi.org/10.1073/pnas.2204481119

32 Haza, K.Z., Martin, H.L., Rao, A., Turner, A.L., Saunders, S.E., Petersen, B. et al. (2021) RAS-inhibiting biologics identify and probe druggable pockets including an Sll-α3 allosteric site. *Nat. Commun.* **12**, 4045 https://doi.org/10.1038/s41467-021-24316-0
33 Kessler, D., Gmachl, M., Mantoulidis, A., Martin, L.J., Zoephel, A., Mayer, M. et al. (2019) Drugging an undruggable pocket on KRAS. *Proc. Natl Acad. Sci. U.S.A.* **116**, 15823–15829 https://doi.org/10.1073/pnas.1904529116
34 Maurer, T., Garrenton, L.S., Oh, A., Pitts, K., Anderson, D.J., Skelton, N.J. et al. (2012) Small-molecule ligands bind to a distinct pocket in Ras and inhibit SOS-mediated nucleotide exchange activity. *Proc. Natl Acad. Sci. U.S.A.* **109**, 5299–5304 https://doi.org/10.1073/pnas.1116510109
35 Abankwa, D. and Gorfe, A.A. (2020) Mechanisms of Ras membrane organization and signaling: Ras rocks again. *Biomolecules* **10**, 1522 https://doi.org/10.3390/biom10111522
36 Abankwa, D., Gorfe, A.A., Inder, K. and Hancock, J.F. (2010) Ras membrane orientation and nanodomain localization generate isoform diversity. *Proc. Natl Acad. Sci. U.S.A.* **107**, 1130–1135 https://doi.org/10.1073/pnas.0903907107
37 Abankwa, D., Hanzal-Bayer, M., Ariotti, N., Plowman, S.J., Gorfe, A.A., Parton, R.G. et al. (2008) A novel switch region regulates H-ras membrane orientation and signal output. *EMBO J.* **27**, 727–735 https://doi.org/10.1038/emboj.2008.10
38 Solman, M., Ligabue, A., Blazevits, O., Jaiswal, A., Zhou, Y., Liang, H. et al. (2015) Specific cancer-associated mutations in the switch III region of Ras increase tumorigenicity by nanocluster augmentation. *Elife* **4**, e08905 https://doi.org/10.7554/eLife.08905
39 Spencer-Smith, R., Koide, A., Zhou, Y., Eguchi, R.R., Sha, F., Gajwani, P. et al. (2017) Inhibition of RAS function through targeting an allosteric regulatory site. *Nat. Chem. Biol.* **13**, 62–68 https://doi.org/10.1038/nchembio.2231
40 Van, Q.N., Prakash, P., Shrestha, R., Balius, T.E., Turbyville, T.J. and Stephen, A.G. (2021) RAS nanoclusters: dynamic signaling platforms amenable to therapeutic intervention. *Biomolecules* **11**, 377 https://doi.org/10.3390/biom11030377
41 Bery, N., Miller, A. and Rabbitts, T. (2020) A potent KRAS macromolecule degrader specifically targeting tumours with mutant KRAS. *Nat. Commun.* **11**, 3233 https://doi.org/10.1038/s41467-020-17022-w
42 Roth, S., Macartney, T.J., Konopacka, A., Chan, K.H., Zhou, H., Queisser, M.A. et al. (2020) Targeting endogenous K-RAS for degradation through the affinity-directed protein missile system. *Cell Chem. Biol.* **27**, 1151–1163.e1156 https://doi.org/10.1016/j.chembiol.2020.06.012
43 Lim, S., Khoo, R., Juang, Y.C., Gopal, P., Zhang, H., Yeo, C. et al. (2021) Exquisitely specific anti-KRAS biodegraders inform on the cellular prevalence of nucleotide-loaded states. *ACS Cent. Sci.* **7**, 274–291 https://doi.org/10.1021/acscentsci.0c01337
44 Choi, J.S. and Joo, S.H. (2020) Recent trends in cyclic peptides as therapeutic agents and biochemical tools. *Biomol. Ther. (Seoul)* **28**, 18–24 https://doi.org/10.4062/biomolther.2019.082
45 Gorfe, A.A. and Cho, K.J. (2021) Approaches to inhibiting oncogenic K-Ras. *Small GTPases* **12**, 96–105 https://doi.org/10.1080/21541248.2019.1655883
46 Grant, B.J., Lukman, S., Hocker, H.J., Sayyah, J., Brown, J.H., McCammon, J.A. et al. (2011) Novel allosteric sites on Ras for lead generation. *PLoS ONE* **6**, e25711 https://doi.org/10.1371/journal.pone.0025711
47 Prakash, P., Hancock, J.F. and Gorfe, A.A. (2015) Binding hotspots on K-ras: consensus ligand binding sites and other reactive regions from probe-based molecular dynamics analysis. *Proteins* **83**, 898–909 https://doi.org/10.1002/prot.24786
48 McCarthy, M.J., Pagba, C.V., Prakash, P., Naji, A.K., van der Hoeven, D., Liang, H. et al. (2019) Discovery of high-affinity noncovalent allosteric KRAS inhibitors that disrupt effector binding. *ACS Omega* **4**, 2921–2930 https://doi.org/10.1021/acsomega.8b03308
49 Feng, H., Zhang, Y., Bos, P.H., Chambers, J.M., Dupont, M.M. and Stockwell, B.R. (2019) K-Ras(G12D) Has a potential allosteric small molecule binding site. *Biochemistry* **58**, 2542–2554 https://doi.org/10.1021/acs.biochem.8b01300
50 Rosnizeck, I.C., Graf, T., Spoerner, M., Trankle, J., Filchtinski, D., Herrmann, C. et al. (2010) Stabilizing a weak binding state for effectors in the human ras protein by cyclen complexes. *Angew. Chem. Int. Ed. Engl.* **49**, 3830–3833 https://doi.org/10.1002/anie.200907002
51 Hocker, H.J., Cho, K.J., Chen, C.Y., Rambahal, N., Sagineedu, S.R., Shaari, K. et al. (2013) Andrographolide derivatives inhibit guanine nucleotide exchange and abrogate oncogenic Ras function. *Proc. Natl Acad. Sci. U.S.A.* **110**, 10201–10206 https://doi.org/10.1073/pnas.1300016110
52 Mazhab-Jafari, M.T., Marshall, C.B., Smith, M.J., Gasmi-Seabrook, G.M., Stathopulos, P.B., Inagaki, F. et al. (2015) Oncogenic and RASopathy-associated K-RAS mutations relieve membrane-dependent occlusion of the effector-binding site. *Proc. Natl Acad. Sci. U.S.A.* **112**, 6625–6630 https://doi.org/10.1073/pnas.1419895112
53 Fang, Z., Marshall, C.B., Nishikawa, T., Gossert, A.D., Jansen, J.M., Jahnke, W. et al. (2018) Inhibition of K-RAS4B by a unique mechanism of action: stabilizing membrane-dependent occlusion of the effector-binding site. *Cell Chem. Biol.* **25**, 1327–1336.e1324 https://doi.org/10.1016/j.chembiol.2018.07.009
54 Tran, T.H., Alexander, P., Dharmaiah, S., Agamasu, C., Nissley, D.V., McCormick, F. et al. (2020) The small molecule BI-2852 induces a nonfunctional dimer of KRAS. *Proc. Natl Acad. Sci. U.S.A.* **117**, 3363–3364 https://doi.org/10.1073/pnas.1918164117
55 Bekes, M., Langley, D.R. and Crews, C.M. (2022) PROTAC targeted protein degraders: the past is prologue. *Nat. Rev. Drug Discov.* **21**, 181–200 https://doi.org/10.1038/s41573-021-00371-6
56 Paiva, S.L. and Crews, C.M. (2019) Targeted protein degradation: elements of PROTAC design. *Curr. Opin. Chem. Biol.* **50**, 111–119 https://doi.org/10.1016/j.cbpa.2019.02.022
57 Bond, M.J., Chu, L., Nalawansha, D.A., Li, K. and Crews, C.M. (2020) Targeted degradation of oncogenic KRAS(G12C) by VHL-Recruiting PROTACs. *ACS Cent. Sci.* **6**, 1367–1375 https://doi.org/10.1021/acscentsci.0c00411
58 Li, L., Wu, Y., Yang, Z., Xu, C., Zhao, H., Liu, J. et al. (2021) Discovery of KRas G12C-IN-3 and pomalidomide-based PROTACs as degraders of endogenous KRAS G12C with potent anticancer activity. *Bioorg. Chem.* **117**, 105447 https://doi.org/10.1016/j.bioorg.2021.105447
59 Zeng, M., Xiong, Y., Safaee, N., Nowak, R.P., Donovan, K.A., Yuan, C.J. et al. (2020) Exploring targeted degradation strategy for oncogenic KRAS (G12C). *Cell Chem. Biol.* **27**, 19–31.e16 https://doi.org/10.1016/j.chembiol.2019.12.006
60 Yang, F., Wen, Y., Wang, C., Zhou, Y., Zhou, Y., Zhang, Z.M. et al. (2022) Efficient targeted oncogenic KRAS(G12C) degradation via first reversible-covalent PROTAC. *Eur. J. Med. Chem.* **230**, 114088 https://doi.org/10.1016/j.ejmech.2021.114088
61 Kannt, A. and Dikic, I. (2021) Expanding the arsenal of E3 ubiquitin ligases for proximity-induced protein degradation. *Cell Chem. Biol.* **28**, 1014–1031 https://doi.org/10.1016/j.chembiol.2021.04.007
62 Schapira, M., Calabrese, M.F., Bullock, A.N. and Crews, C.M. (2019) Targeted protein degradation: expanding the toolbox. *Nat. Rev. Drug Discov.* **18**, 949–963 https://doi.org/10.1038/s41573-019-0047-y

Biochemical Society Transactions (2023) **51** 447–456
https://doi.org/10.1042/BST20221343

63 Bery, N., Cruz-Migoni, A., Bataille, C.J., Quevedo, C.E., Tulmin, H., Miller, A. et al. (2018) BRET-based RAS biosensors that show a novel small molecule is an inhibitor of RAS-effector protein-protein interactions. *Elife* **7**, e37122 https://doi.org/10.7554/eLife.37122
64 Kessler, D., Bergner, A., Bottcher, J., Fischer, G., Dobel, S., Hinkel, M. et al. (2020) Drugging all RAS isoforms with one pocket. *Future Med. Chem.* **12**, 1911–1923 https://doi.org/10.4155/fmc-2020-0221
65 Matsumoto, S., Hiraga, T., Hayashi, Y., Yoshikawa, Y., Tsuda, C., Araki, M. et al. (2018) Molecular basis for allosteric inhibition of GTP-bound H-Ras protein by a small-molecule compound carrying a naphthalene ring. *Biochemistry* **57**, 5350–5358 https://doi.org/10.1021/acs.biochem.8b00680
66 Quevedo, C.E., Cruz-Migoni, A., Bery, N., Miller, A., Tanaka, T., Petch, D. et al. (2018) Small molecule inhibitors of RAS-effector protein interactions derived using an intracellular antibody fragment. *Nat. Commun.* **9**, 3169 https://doi.org/10.1038/s41467-018-05707-2
67 Shima, F., Yoshikawa, Y., Ye, M., Araki, M., Matsumoto, S., Liao, J. et al. (2013) In silico discovery of small-molecule Ras inhibitors that display antitumor activity by blocking the Ras-effector interaction. *Proc. Natl Acad. Sci. U.S.A.* **110**, 8182–8187 https://doi.org/10.1073/pnas.1217730110
68 Sun, Q., Burke, J.P., Phan, J., Burns, M.C., Olejniczak, E.T., Waterson, A.G. et al. (2012) Discovery of small molecules that bind to K-Ras and inhibit Sos-mediated activation. *Angew. Chem. Int. Ed. Engl.* **51**, 6140–6143 https://doi.org/10.1002/anie.201201358
69 Wiechmann, S., Maisonneuve, P., Grebbin, B.M., Hoffmeister, M., Kaulich, M., Clevers, H. et al. (2020) Conformation-specific inhibitors of activated Ras GTPases reveal limited Ras dependency of patient-derived cancer organoids. *J. Biol. Chem.* **295**, 4526–4540 https://doi.org/10.1074/jbc.RA119.011025
70 Leshchiner, E.S., Parkhitko, A., Bird, G.H., Luccarelli, J., Bellairs, J.A., Escudero, S. et al. (2015) Direct inhibition of oncogenic KRAS by hydrocarbon-stapled SOS1 helices. *Proc. Natl Acad. Sci. U.S.A.* **112**, 1761–1766 https://doi.org/10.1073/pnas.1413185112
71 McGee, J.H., Shim, S.Y., Lee, S.J., Swanson, P.K., Jiang, S.Y., Durney, M.A. et al. (2018) Exceptionally high-affinity Ras binders that remodel its effector domain. *J. Biol. Chem.* **293**, 3265–3280 https://doi.org/10.1074/jbc.M117.816348
72 Kauke, M.J., Traxlmayr, M.W., Parker, J.A., Kiefer, J.D., Knihtila, R., McGee, J. et al. (2017) An engineered protein antagonist of K-Ras/B-Raf interaction. *Sci. Rep.* **7**, 5831 https://doi.org/10.1038/s41598-017-05889-7
73 Upadhyaya, P., Qian, Z., Selner, N.G., Clippinger, S.R., Wu, Z., Briesewitz, R. et al. (2015) Inhibition of Ras signaling by blocking Ras-effector interactions with cyclic peptides. *Angew. Chem. Int. Ed. Engl.* **54**, 7602–7606 https://doi.org/10.1002/anie.201502763
74 Buyanova, M., Cai, S., Cooper, J., Rhodes, C., Salim, H., Sahni, A. et al. (2021) Discovery of a bicyclic peptidyl pan-Ras inhibitor. *J. Med. Chem.* **64**, 13038–13053 https://doi.org/10.1021/acs.jmedchem.1c01130
75 Niida, A., Sasaki, S., Yonemori, K., Sameshima, T., Yaguchi, M., Asami, T. et al. (2017) Investigation of the structural requirements of K-Ras(G12D) selective inhibitory peptide KRpep-2d using alanine scans and cysteine bridging. *Bioorg. Med. Chem. Lett.* **27**, 2757–2761 https://doi.org/10.1016/j.bmcl.2017.04.063
76 Sakamoto, K., Kamada, Y., Sameshima, T., Yaguchi, M., Niida, A., Sasaki, S. et al. (2017) K-Ras(G12D)-selective inhibitory peptides generated by random peptide T7 phage display technology. *Biochem. Biophys. Res. Commun.* **484**, 605–611 https://doi.org/10.1016/j.bbrc.2017.01.147
77 Sogabe, S., Kamada, Y., Miwa, M., Niida, A., Sameshima, T., Kamaura, M. et al. (2017) Crystal structure of a human K-Ras G12D mutant in complex with GDP and the cyclic inhibitory peptide KRpep-2d. *ACS Med. Chem. Lett.* **8**, 732–736 https://doi.org/10.1021/acsmedchemlett.7b00128
78 Sakamoto, K., Lin, B., Nunomura, K., Izawa, T. and Nakagawa, S. (2022) The K-Ras(G12D)-inhibitory peptide KS-58 suppresses growth of murine CT26 colorectal cancer cell-derived tumors. *Sci. Rep.* **12**, 8121 https://doi.org/10.1038/s41598-022-12401-3
79 Sakamoto, K., Masutani, T. and Hirokawa, T. (2020) Generation of KS-58 as the first K-Ras(G12D)-inhibitory peptide presenting anti-cancer activity *in vivo*. *Sci. Rep.* **10**, 21671 https://doi.org/10.1038/s41598-020-78712-5
80 Zhang, Z., Gao, R., Hu, Q., Peacock, H., Peacock, D.M., Dai, S. et al. (2020) GTP-state-selective cyclic peptide ligands of K-Ras(G12D) block its interaction with Raf. *ACS Cent. Sci.* **6**, 1753–1761 https://doi.org/10.1021/acscentsci.0c00514

2. Manuscript (II)

Identification of an H-Ras nanocluster disrupting peptide

Candy Laura Steffen[*]**,** Ganesh babu Manoharan[*], Karolina Pavic, Alejandro Yeste-Vázquez, Matias Knuuttila, Neha Arora, Yong Zhou, Harri Härmä, Anthoula Gaigneaux, Tom N. Grossmann, Daniel Kwaku Abankwa

* These authors contributed equally.

Status: published

Personal contributions of Candy Laura Steffen

- Purified proteins and designed, collected, and evaluated BRET, FP signalling and cell viability data to then generate the below listed figures submitted for this manuscript:
  - Figure 2 (d, e)
  - Figure 3 (b, c)
  - Figure 4 (b, c)
  - Figure 5 (a-d)
  - Figure 6 (a-e)
  - Figure S2c
  - Figure S3a-f
- Designed the schematics:
  - Figure 1a, e
  - Figure 2f
  - Figure 3a
  - Figure 4a
  - Figure S1a
- The personal contributions of all authors to the manuscript are listed in the author's contribution section at the end of the corresponding manuscript.

communications biology

Article

https://doi.org/10.1038/s42003-024-06523-9

Identification of an H-Ras nanocluster disrupting peptide

Check for updates

Candy Laura Steffen [1,8], Ganesh babu Manoharan [1,8], Karolina Pavic[1], Alejandro Yeste-Vázquez[2,3], Matias Knuuttila [4], Neha Arora[5], Yong Zhou [5], Harri Härmä[6], Anthoula Gaigneaux [7], Tom N. Grossmann [2,3] & Daniel Kwaku Abankwa [1,4] ✉

Hyperactive Ras signalling is found in most cancers. Ras proteins are only active in membrane nanoclusters, which are therefore potential drug targets. We previously showed that the nanocluster scaffold galectin-1 (Gal1) enhances H-Ras nanoclustering via direct interaction with the Ras binding domain (RBD) of Raf. Here, we establish that the B-Raf preference of Gal1 emerges from the divergence of the Raf RBDs at their proposed Gal1-binding interface. We then identify the L5UR peptide, which disrupts this interaction by binding with low micromolar affinity to the B- and C-Raf-RBDs. Its 23-mer core fragment is sufficient to interfere with H-Ras nanoclustering, modulate Ras-signalling and moderately reduce cell viability. These latter two phenotypic effects may also emerge from the ability of L5UR to broadly engage with several RBD- and RA-domain containing Ras interactors. The L5UR-peptide core fragment is a starting point for the development of more specific reagents against Ras-nanoclustering and -interactors.

Ras is a major oncogene and recent advances in its direct targeting have validated its high therapeutic significance[1,2]. The three cancer-associated Ras genes encode four different protein isoforms: K-Ras4A, K-Ras4B (hereafter K-Ras), N-Ras, and H-Ras. These membrane-bound small GTPases operate as switchable membrane recruitment sites for downstream interaction partners, called effectors. Downstream of mitogen and growth factor sensing receptors, inactive GDP-bound Ras is activated by guanine nucleotide exchange factors (GEFs), which facilitate GDP/ GTP-exchange[3,4]. The two switch regions of GTP-Ras undergo significant conformational changes upon activation, thus enabling binding to the Ras binding domain (RBD) or Ras association (RA) domain of effectors, such as Raf, PI3Kα, and RASSF proteins. These effectors are implicated in cell proliferation, growth, and apoptosis, respectively[5,6].

Current evidence suggests that Ras proteins promiscuously interact with any of the three Raf paralogs, A-, B- and C-Raf. Raf proteins reside as autoinhibited complexes with 14-3-3 proteins in the cytosol and are activated by a series of structural rearrangements that are still not understood in full detail[7,8]. The first crucial step is the displacement of the RBD from the cradle formed by the 14-3-3 dimer[7]. Simultaneous binding of Ras and 14-3-3 to the N-terminal region of Raf is incompatible due to steric clashes and electrostatic repulsion, which is only relieved if the RBD and adjacent cysteine-rich domain of Raf are released from 14-3-3 for binding to membrane-anchored Ras. Allosteric coupling between the N-terminus of Raf and its C-terminus then causes dimerization of the C-terminal kinase domains, which is necessary for their catalytic activity[8–10].

The Ras-induced dimerization of the Raf proteins requires di-/oligomeric assemblies of Ras, called nanoclusters[11]. Initially it was estimated that 5–20 nm sized nanoclusters contain 6–8 Ras proteins and that nanoclustering was necessary for MAPK-signal transmission[12–14]. More recent data revealed that nanoclusters are dominated by Ras dimers[11,15]. Intriguingly, Ras nanoclustering can be increased by Raf-ON-state inhibitors that induce Raf dimerization and increase Ras–Raf interaction, suggesting that Raf dimers are integral components of nanocluster[16,17]. The reinforced nanoclustering may thus contribute to the paradoxical MAPK-activation that is observed with these inhibitors[18].

Currently, less than a dozen proteins are known that can modulate Ras nanoclustering[19]. These proteins do not share any structural or functional similarities, suggesting that their mechanisms of nanocluster modulation

[1]Cancer Cell Biology and Drug Discovery group, Department of Life Sciences and Medicine, University of Luxembourg, 4362 Esch-sur-Alzette, Luxembourg. [2]Department of Chemistry and Pharmaceutical Sciences, VU University Amsterdam, Amsterdam, The Netherlands. [3]Amsterdam Institute of Molecular and Life Sciences (AIMMS), VU University Amsterdam, Amsterdam, The Netherlands. [4]Turku Bioscience Centre, University of Turku and Åbo Akademi University, 20520 Turku, Finland. [5]Department of Integrative Biology and Pharmacology, McGovern Medical School, UT Health, Houston, TX 77030, USA. [6]Chemistry of Drug Development, Department of Chemistry, University of Turku, 20500 Turku, Finland. [7]Bioinformatics Core, Department of Life Sciences and Medicine, University of Luxembourg, 4367 Esch-sur-Alzette, Luxembourg. [8]These authors contributed equally: Candy Laura Steffen, Ganesh babu Manoharan. ✉e-mail: daniel.abankwa@uni.lu

are diverse. The best understood nanocluster scaffold is the small lectin galectin-1 (Gal1), which specifically increases nanoclustering and MAPK-output of active or oncogenic H-Ras[20–22]. Consistently, upregulation of galectins has been linked to more severe cancer progression[23]. For many years, it was mechanistically unclear, how this protein that is best known for binding β-galactoside sugars in the extracellular space affects Ras membrane organization on the inner leaflet of the plasma membrane[24,25]. While it was first suggested that the farnesyl tail of Ras is engaged by Gal1[26], it was later on shown that neither Gal1 nor related galectin-3, which is a nanocluster scaffold of K-Ras, bind farnesylated Ras-derived peptides[27,28].

We previously proposed a model of stacked dimers of GTP-H-Ras and Raf as the minimal unit of active nanocluster that can be further enhanced by Gal1[29]. We confirmed that Gal1 does not directly interact with the farnesyl tail of Ras proteins, but instead engages indirectly with Ras via direct binding to the RBD of Raf proteins (K_D = 106 ± 40 nM)[29]. Given that Gal1 is a dimer at low micromolar concentrations in cells (K_D = 7 μM)[30,31], we hypothesized that dimeric Gal1 stabilizes Raf-dimers on active H-Ras nanocluster. In line with this, in particular B-Raf-dependent membrane translocation of the tumor suppressor SPRED1 by dimer inducing Raf-inhibitors was emulated by expression of Gal1[32]. Our mechanistic model suggests that dimeric Gal1 stabilizes the dimeric form of Raf-effectors downstream of H-Ras. This enhances H-Ras/ Raf signaling output, not only by facilitation of Raf-dimerization, but also by an allosteric feedback mechanism that enhances the nanoclustering of H-Ras. Altogether, a transient stacked dimer complex of H-Ras, Raf and Gal1 is formed, which also shifts the H-Ras activity from the PI3K to the MAPK pathway[29]. Current galectin inhibitor developments focus on its carbohydrate-binding pocket, which is necessary for its lectin activity in the extracellular space[33,34]. Inhibitors that would target the nanocluster enhancing function of Gal1 are missing.

Here we describe the identification of a 23-residue peptide that interferes with the binding of Gal1 to the RBD of Raf and disrupts H-Ras nanoclustering. Interestingly, this peptide broadly engages with a number of other RBD- and RA-domain containing Ras effectors, modulates Ras signaling and decreases cell viability.

Results

Galectin-1 binds via the RBD preferentially to B-Raf and stabilizes H-RasG12V nanoclustering

We previously provided evidence that Gal1, which can dimerize at higher concentrations, binds to the Ras binding domain (RBD) of Raf proteins to stabilize active H-Ras nanocluster[29] (Fig. 1a). We first corroborated some features of this stacked-dimer model using Bioluminesence Resonance Energy Transfer (BRET)-experiments. To this end, interaction partners

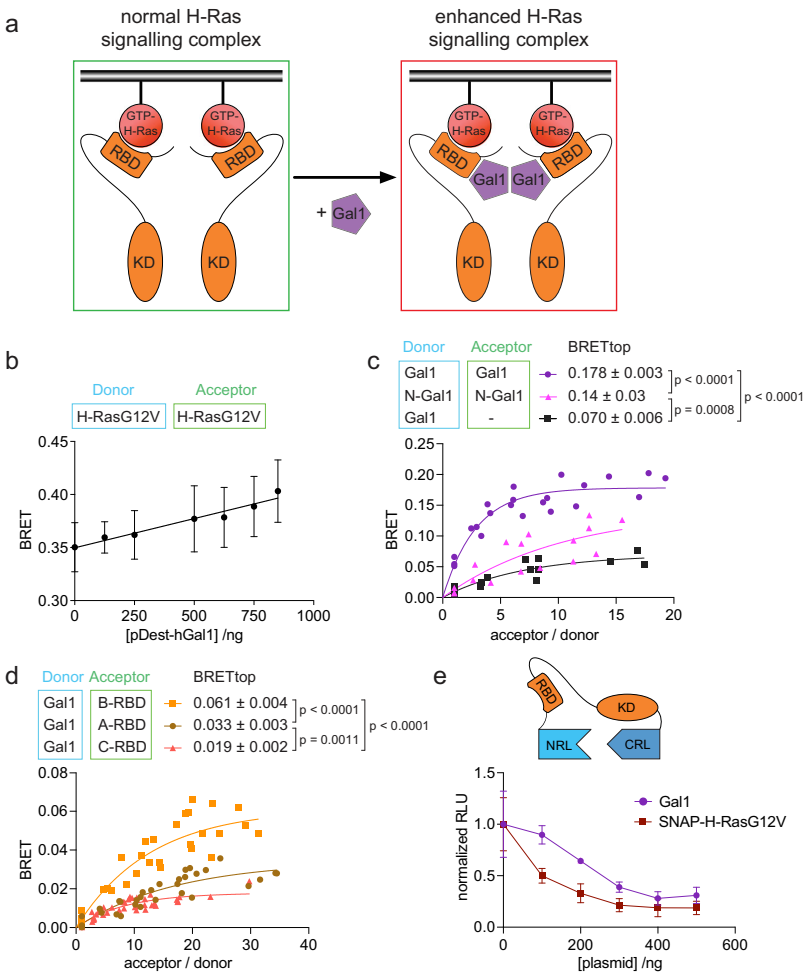

Fig. 1 | The B-Raf preference of the H-Ras nanocluster scaffold Gal1 emerges within the RBD. a Schematic of our model for Gal1 stabilized H-Ras nanocluster. **b** Dose-dependent effect of human Gal1 expression (48 h) on H-RasG12V nanoclustering-BRET (donor:-acceptor plasmid ratio = 1:5); $n = 4$. **c** BRET-titration curves of the Gal1/ Gal1-interaction as compared to that of dimer-interface mutated N-Gal1. RLuc8-Gal1 was titrated with GFP2 as a control (black); $n = 3$. **d** BRET-titration curves of the Gal1-interaction with the RBDs of A-, B-, and C-Raf; $n = 3$. **e** Split-luciferase KinCon B-Raf biosensor response after expression of SNAP-H-RasG12V or Gal1; $n = 3$.

were tagged with RLuc8 or NanoLuc as donor and GFP2 or mNeonGreen as acceptor, and constructs were transiently expressed in HEK293-EBNA (hereafter HEK) cells to monitor the interaction by the increased BRET-signal. In BRET-titration experiments, the characteristic BRET-parameter BRETmax is typically determined. It is a measure for the maximal number of binding sites and the interaction strength, if other interaction parameters, such as complex geometry, are constant[35]. However, actual binding saturation is typically not reached in cells, and therefore BRETmax cannot be faithfully determined. Hence, we introduced the BRETtop value, which is the maximal BRET-ratio that is reached within a defined range of acceptor/donor signal-ratios, which is kept constant for BRET-pairs that are being compared[36].

In agreement with our earlier results obtained via Förster/fluorescence resonance energy transfer (FRET)[29], Gal1 expression increased H-RasG12V nanoclustering-BRET in a dose-dependent manner (Fig. 1b). Mutating four residues at the Gal1 dimer interface (N-Gal1) significantly reduced the BRETtop, suggesting that Gal1 is active as a dimer under our expression conditions[31] (Fig. 1c). BRET-experiments also confirmed the previously noted interaction preference of Gal1 for B-Raf[29] (Supplementary Fig. 1a), which was already seen with the RBDs of the corresponding Raf paralogs (Fig. 1d). Using computational docking that was based on experimentally determined constraints, we previously proposed a structural model for the binding of Gal1 to the RBD of C-Raf (C-RBD)[29] (Supplementary Fig. 1b). This model was validated by demonstrating that D113A, D117A mutations in the C-RBD significantly reduced binding to Gal1[29]. To further confirm these structural data, we here introduced analogous charge-neutralizing mutations D211A and D213A in the B-Raf-derived RBD (B-RBD), and mutation D75A in the A-Raf-derived RBD (A-RBD) (Supplementary Fig. 1c). In support of our docking data, the BRETtop of the interaction between Gal1 and either mutant was significantly reduced (Supplementary Fig. 1d, e). Consistent with the Raf-paralog specific interaction preference of Gal1, the mutated residues reside in a stretch that is least conserved between the RBDs (Supplementary Fig. 1c), which is in agreement with the significant difference in their Gal-1 BRET-interaction data (Fig. 1d).

Split-luciferase KinCon Raf-biosensors can report on the effect of mutations and modulators on the conformational state of Raf proteins[37] (Fig. 1e). The expression of SNAP-tagged oncogenic H-RasG12V (SNAP-H-RasG12V) reduces the luminescence signal, consistent with a relief of the closed autoinhibited state (Fig. 1e). Expression of increasing amounts of Gal1 likewise reduced the luminescence signal, suggesting that Gal1 facilitates the open state of B-Raf, although less than H-RasG12V (Fig. 1e).

Taken together with our previously published results[29], these data suggest a model wherein Gal1 binds to the RBD of Raf proteins, notably B-Raf, thus potentially destabilizing their autoinhibition. This could facilitate dimeric Ras–Raf engagement, which however requires a number of other modifications and conformational rearrangements[17]. When present as a dimer, Gal1 may further stabilize the active H-Ras/Raf stacked-dimer complex and thus an active H-Ras nanocluster, similar to what was observed with ON-state inhibitors of Raf[16].

Identification of the L5UR-peptide as a disruptor of the Raf-RBD/galectin-1 interface

Gal1 increases H-Ras-driven MAPK output, and its elevated expression correlates with poorer survival in *HRAS* mutant cancers, such as head and neck squamous cell carcinoma, which frequently displays elevated Gal1 levels[22,29] (Supplementary Fig. 2a). Taken together with our H-Ras nanocluster model, these data support targeting of the interface between Gal1 and the Raf-RBD as a new strategy against oncogenic H-Ras. We hypothesized that the 52-mer L5UR peptide, which was derived from a Gal1 interaction partner, could act as a Raf-RBD/Gal1-interface inhibitor. Its residues 22–45 were previously shown to bind with a low affinity (K_D = 310 μM) to the opposite side of the carbohydrate binding site of Gal1[38]. This back-site overlaps with the one we had predicted as RBD-binding site on Gal1[29]. We thus expected that the L5UR-peptide would disrupt the Raf-RBD/Gal1-interaction and consequently the Gal1-augmented H-RasG12V-nanoclustering and MAPK-signaling.

In line with this, expression of untagged L5UR decreased the FRET between mGFP-Gal1 and mRFP-C-RBD in HEK cells (Fig. 2a). This effect was comparable to the loss observed in the C-RBD-D117A mutant with reduced Gal1-binding (Fig. 2a)[29]. For comparison, we tested the effect of Anginex and its topomimetic small molecule analog OTX-008[39]. Anginex is a 33-mer angiostatic peptide that binds to Gal1 at an unknown site[40–42]. Competitive fluorescence polarization experiments with FITC-tagged full-length L5UR (F-L5UR) as a probe, established that it can be displaced from purified His-tagged Gal1 by the Anginex peptide (Supplementary Fig. 2b). However, neither Anginex nor OTX-008 disrupted the Gal1/C-RBD interaction as measured by FRET in cells (Fig. 2a), suggesting that the Anginex binding site only partially overlaps with the L5UR-binding site, but not sufficiently with the C-RBD binding site on Gal1. By contrast, expression of the L5UR-peptide decreased the Gal1-augmented H-RasG12V nanoclustering-FRET (Fig. 2b). In agreement with previous data[29], dimerization-deficient N-Gal1 did not increase nanoclustering-FRET, and co-expression of the L5UR-peptide had no additional effect (Fig. 2b).

Next, we aimed to confirm that L5UR engages directly with the Raf-RBD/Gal1 interface. We purified His-tagged Gal1 and the GST-tagged B-RBD and performed pulldown experiments with a biotin-tagged L5UR (bio-L5UR) peptide (Fig. 2c). Interestingly, L5UR pulled down Gal1 and the GST-B-RBD independently from each other (Fig. 2c). Indeed, fluorescence polarization binding experiments determined a micromolar (K_D = 7.3 ± 0.7 μM) binding of F-L5UR to the GST-B-RBD (Fig. 2d), but no binding to GST alone (Supplementary Fig. 2c). Using a Quenching Resonance Energy Transfer (QRET)-assay, we independently confirmed the micromolar binding to B-RBD, even with the shortened 22–44 residue core fragment of L5UR labeled with a europium-chelate (Eu-L5URcore) (Table 1, Supplementary Fig. 2d). By contrast, no saturation of Eu-L5URcore binding to Gal1 could be observed at the technically highest possible concentration of 135 μM (Supplementary Fig. 2e).

Competitive fluorescence polarization experiments, using F-L5UR as a probe, established that the full-length peptide of L5UR could be displaced from the GST-B-RBD with an IC_{50} = 2 ± 1 μM (Fig. 2e), and likewise from the C-RBD (Table 1, Supplementary Fig. 2f). As expected, the shorter L5URcore could displace F-L5UR from the C-RBD with a slightly reduced potency (IC_{50} = 14 ± 6 μM) (Supplementary Fig. 2f). The L5UR has a high proportion of six positively charged arginine residues in its core region, which may indicate that binding of the peptide to the RBD of Raf is influenced by electrostatic interactions. We therefore introduced several negatively charged, acidic residues to mostly replace basic and hydrophobic residues in the core-region of the L5UR peptide to generate a non-binding mutant (mutL5UR) (Fig. 2f). Indeed, mutL5UR did not have any displacement activity in the competitive fluorescence polarization assay (Fig. 2e, Supplementary Fig. 2f). Circular dichroism spectra of the L5UR, L5URcore and mutL5URcore peptides suggested they were mostly random coil with ~25% antiparallel β-sheet (Supplementary Fig. 2g).

In conclusion, L5UR binds with low micromolar affinity to the RBDs of B-Raf and C-Raf (Table 1). This interaction is significantly determined by residues in its core region, as binding is attenuated in the mutL5UR variant.

SNAP-tagged L5UR disrupts the B-RBD/ galectin-1 complex, and H-RasG12V nanoclustering in cells and binds to multiple Ras interactors

To improve the readout of L5UR-variant expression in cells and eventually enable further functionalization, we designed genetic constructs where a SNAP-tag was added via a long linker to the C-terminus of the peptide (Fig. 3a).

The L5UR-SNAP dose-dependently decreased BRET between Gal1 and the B-RBD to a similar extent as the untagged L5UR, confirming that the SNAP-tag did not increase activity further (Fig. 3b). In agreement with the binding data (Fig. 2e), mutL5UR-SNAP did not decrease the BRET signal, nor did the SNAP-tag alone (Fig. 3b). Immunoblotting confirmed an

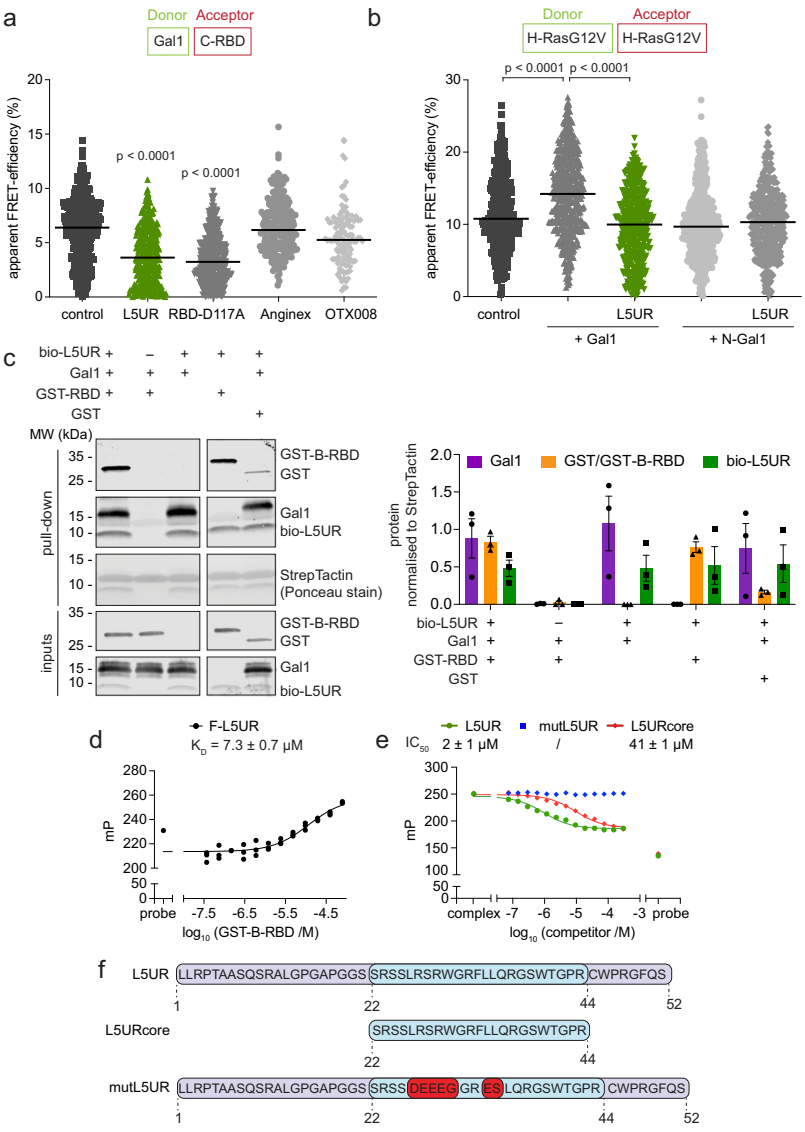

Fig. 2 | The L5UR-peptide binds to the Raf-RBD and disrupts the Raf-RBD/ Gal1-complex. a Effect of L5UR expression (24 h) on Gal1/C-RBD FRET (donor:acceptor plasmid ratio = 1:3); $n = 3$. **b** Effect of L5UR expression (24 h) on Gal1-augmented H-RasG12V nanoclustering-FRET (donor:acceptor plasmid ratio = 1:3); $n = 3$. **c** Immunoblot data from pull-down assay with biotinylated L5UR and purified Gal1, GST-B-RBD or GST-only control with example blots (left) and quantification of repeat data (right); $n = 3$. **d** Binding of 10 nM F-L5UR to GST-B-RBD detected in a fluorescence polarization assay; $n = 3$. **e** Displacement of F-L5UR (10 nM) from GST-B-RBD (15 µM) by L5UR-derived peptides; $n = 3$. **f** Sequences of L5UR-derived peptides as used for in vitro and in cellulo assays. The stretch of the core peptide is highlighted in blue, mutations are in red.

Table 1 | Overview of L5UR/ Raf-RBD in vitro binding data

Protein	Probe	K_D[b] or IC_{50}/µM
GST-B-RBD	L5UR	7.3 ± 0.7[b]
GST-B-RBD	L5UR[a]	2 ± 1
GST-B-RBD	L5URcore[a]	41 ± 1
B-RBD	L5URcore (QRET)	18 ± 1
C-RBD	L5UR[a]	4 ± 1
C-RBD	L5URcore[a]	14 ± 6

[a]In competitive fluorescence polarization assay with F-L5UR.
[b]Marks actual K_D, while otherwise IC_{50} are reported.

initially linear increase of L5UR-SNAP variant expression with increasing amounts of transfected constructs (Supplementary Fig. 3a, b). Consistent with the Gal1/ B-RBD disruption, the L5UR-SNAP construct decreased Gal1-enhanced H-RasG12V nanoclustering-BRET to a similar extent as the untagged L5UR, while again mutL5UR or the SNAP-tag alone had no effect (Fig. 3c). In line with the higher affinity of L5UR for the Raf-RBD, we observed very similar effects even without co-expression of Gal1 in HEK cells that are otherwise comparatively devoid of Gal1 (Supplementary Fig. 3c, d). L5UR or L5UR-SNAP reduced the nanoclustering-BRET by ~33% (Fig. 3c), while co-expression of SNAP-H-RasG12V led to a ~85% reduction (Supplementary Fig. 3e). Neither of the L5UR-constructs significantly perturbed K-RasG12V nanoclustering-BRET, suggesting a potential Ras isoform selectivity (Supplementary Fig. 3f).

The disruption of H-RasG12V nanoclustering specifically by L5UR-SNAP, but not the SNAP-tag alone, was furthermore confirmed by the classical electron microscopy-based Ras nanoclustering analysis performed

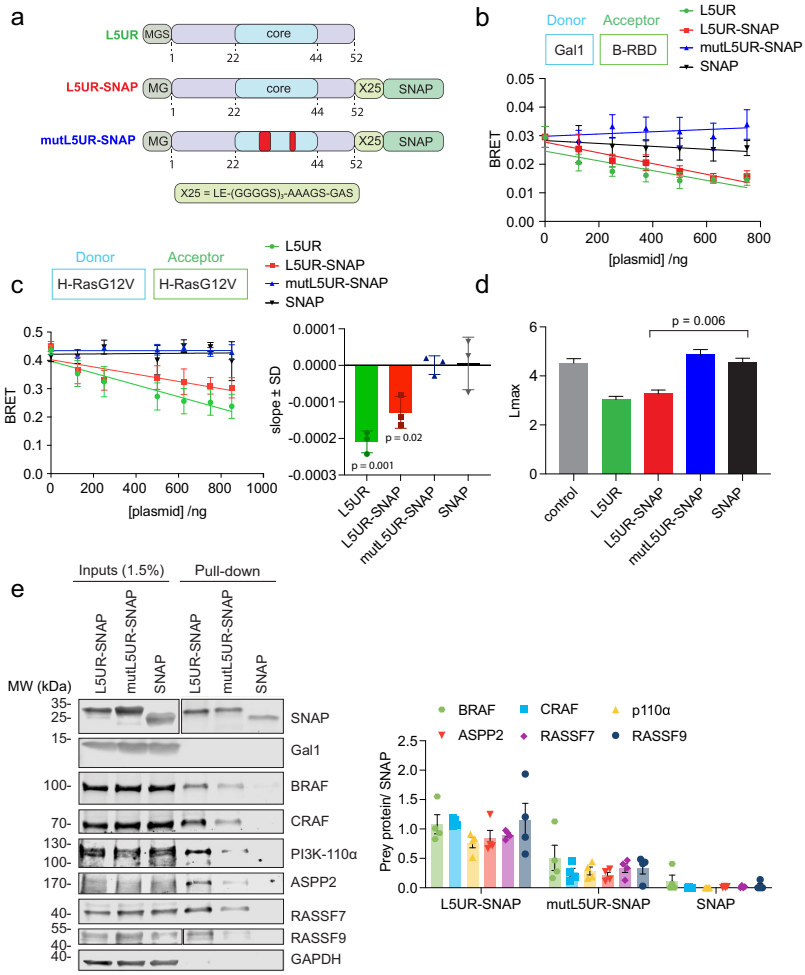

Fig. 3 | The L5UR and L5UR-SNAP peptides disrupt H-RasG12V nanoclustering. a Schematics of L5UR derived constructs expressed in cellular assays. The stretch of the core peptide is highlighted in blue, loss-of-function mutations are indicated red. **b** Effect of expression of L5UR constructs (48 h) on Gal1/B-RBD BRET (donor:acceptor plasmid ratio = 1:10); $n = 3$. **c** Effect of L5UR construct expression (48 h) on H-RasG12V nanoclustering-BRET with co-transfection of 200 ng Gal1 plasmid (donor:acceptor plasmid ratio = 1:5); $n = 3$. Statistical comparison was done against the SNAP-only sample. **d** Electron microscopy-based analysis of H-RasG12V nanoclustering in BHK cells showing the effects of L5UR-construct expression and controls; $n = 15$. Higher Lmax values indicate higher nanoclustering. **e** Immunoblot data from pull-down assays with L5UR-SNAP and control constructs from HEK cells co-expressing Gal1 with example blots (left) and quantification of repeat data (right); n = 4 (left).

on membrane sheets of Gal1-expressing BHK cells (Fig. 3d)[21]. These data therefore confirmed the disruption of H-RasG12V nanoclustering by L5UR- and L5UR-SNAP construct expression.

While Gal1 appears to have a preference for B-Raf, it readily engages with the RBD of other Raf proteins (Fig. 1d, Supplementary Fig. 1a). We therefore tested if L5UR can also bind to other RBD- and RA-containing proteins by performing pull-down experiments. The SNAP-tag enabled covalent coupling of L5UR or mutL5UR to beads that were incubated with lysates of Gal1-transfected HEK cells. While the SNAP-tag alone did not interact with any of the examined proteins (Fig. 3e), L5UR-SNAP pulled down not only full-length B-Raf and C-Raf, but also the catalytic subunit of PI3Kα. ASPP2 contains an RBD, interacts with oncogenic H-Ras and is a pan-Ras nanocluster scaffold that can neutralize Gal1 nanoclustering and can switch from a Gal1 promoted growth to a senescence phenotype[43–45]. Like the other RBD-containing proteins it was pulled down by L5UR-SNAP, as were its two RA-domain containing interaction partners, RASSF7 and RASSF9, which do not directly bind to Ras[5,46]. Quantification confirmed that the mutL5UR-SNAP was ≤50% more efficient than L5UR-SNAP in pulling down any of these proteins (Fig. 3e). It is therefore likely that downstream of Ras and other small GTPases several pathways are affected by L5UR.

TAT-tagged L5UR modulates Ras-signaling and weakly inhibits cell proliferation

Peptides can be rendered cell-permeable by the addition of cell penetrating sequences, which facilitate their characterization as prototypic and proof-of-concept reagents[47]. The 12-residue cell penetrating TAT-peptide that is derived from a Human Immunodeficiency Virus (HIV)-protein, can facilitate cellular peptide uptake[48–50]. We therefore chemosynthetically added the TAT-peptide via a PEG2-linker to the 23-residue long L5URcore peptide (TAT-L5URcore) and the corresponding loss-of-function mutant (TAT-mutL5URcore) (Fig. 4a).

To verify cell penetration and on-target activity, we tested the effect of the TAT-peptides in our on-target BRET-assays. Both the BRET between Gal1 and the B-RBD (Fig. 4b), as well as H-RasG12V-nanoclustering BRET (Fig. 4c), were dose-dependently decreased by the TAT-L5URcore peptide with $EC_{50} = 16 \pm 1$ μM and $EC_{50} = 19 \pm 1$ μM, respectively. Neither the TAT-peptide alone, nor the mutant TAT-mutL5URcore, or the non-TAT peptides L5URcore and mutL5URcore decreased the BRET-signal in either assay (Fig. 4b, c).

Based on our model and mechanistic data, signaling, and proliferation of *HRAS* mutant cancer cell lines with high Gal1 levels were expected to respond best to the nanocluster disrupting TAT-L5URcore peptide. Cancer

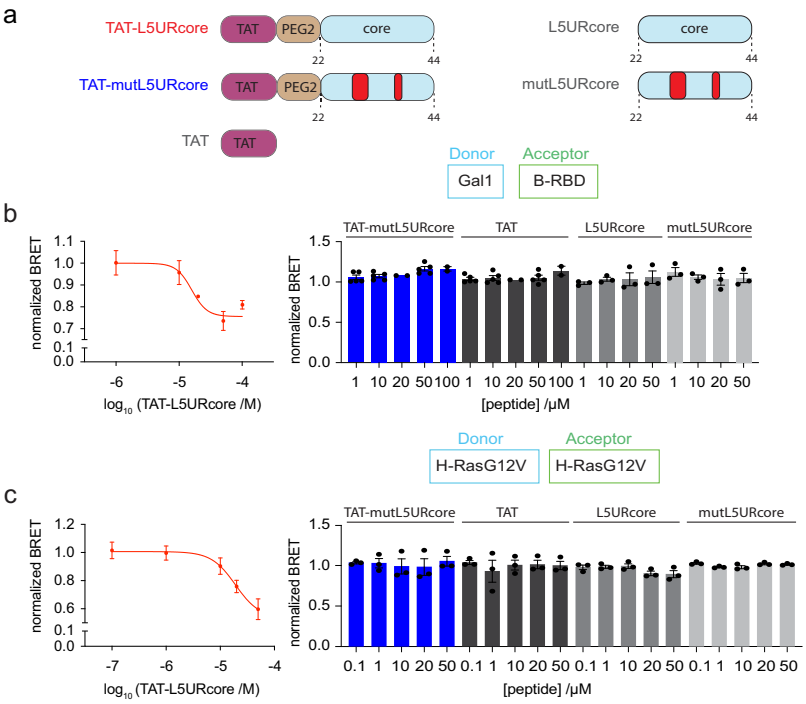

Fig. 4 | The TAT-tagged L5URcore peptide disrupts H-RasG12V nanoclustering. a Schematics of TAT-functionalized L5URcore-derived peptides and controls as applied in cellular assays. Loss-of-function mutations of L5UR are indicated in red. Non-TAT peptides are acetylated at the N-terminus. **b**, **c** Effect of cell-penetrating derivatives of L5URcore and control peptides on Gal1/B-RBD BRET (**b** donor:acceptor plasmid ratio = 1:10; $n \geq 2$) or H-RasG12V nanoclustering-BRET (**c** donor:acceptor plasmid ratio = 1:5, co-transfection of 200 ng Gal1 plasmid; $n = 3$). After 24 h expression of plasmids, peptides were added to cells at specified concentrations and incubated for 2 h.

cell lines Hs 578 T (*HRAS-G12D*) and T24 (*HRAS-G12V*), as well as the *KRAS-G12C* mutant MIA PaCa-2, express high levels of Gal1, while HEK cells have, in comparison undetectably low levels of Gal1 (Supplementary Fig. 3d).

Indeed, treatment of the *HRAS*-mutant cell lines Hs 578 T (Fig. 5a, e) and T24 (Fig. 5b, f) specifically with the TAT-L5URcore peptide at 1–20 µM reduced EGF-induced cellular pERK-and pAkt-levels in a dose-dependent manner. In MIA PaCa-2 pERK remained unaffected, while pAkt-levels were reduced at 20 µM (Fig. 5c, g). Interestingly, in non-transformed HEK cells pERK-levels were slightly induced by TAT-L5URcore, as were pAkt-levels, which were however also upregulated by trametinib (Fig. 5d, h). Furthermore, an apparently non-specific increase in pERK- and/or pAkt-levels was observed at intermediate concentrations of TAT-mutL5URcore and TAT notably in Hs 578 T and MIA PaCa-2. TAT-L5URcore effects on signaling were still relatively weak, which can be attributed to the immaturity of this reagent with only micromolar activity.

We then examined the effect of the TAT-enabled peptides on the viability of these cell lines. The proliferation of *HRAS*-mutant cancer cell lines Hs 578 T (Fig. 6a, e) and T24 (Fig. 6b, e) was specifically reduced by TAT-L5URcore, but not the control TAT-peptides. However, this was also observed for *KRAS*-mutant MIA PaCa-2 (Fig. 6c, e) and non-transformed HEK cells (Fig. 6d, e). To quantitate the relatively weak effect of the peptides on cell proliferation more accurately, we applied the normalized area under the curve DSS3-analysis, where a higher DSS3-score corresponds to higher anti-proliferative activity (Fig. 6e). While we observed a higher anti-proliferative effect of TAT-L5URcore as compared to TAT-mutL5URcore, the broad effect on cell proliferation may indicate that the TAT-L5URcore interferes with several signaling pathways that are relevant for cell proliferation and survival.

Discussion

We here demonstrate that the 23-residue L5URcore peptide binds with micromolar affinity to the Raf-RBD at a site that enables it to disrupt the interaction with Gal1. The peptide interferes with nanocluster of active H-Ras and inhibits Ras-signaling and cell proliferation. The fact that L5UR reduces nanoclustering of H-Ras even in HEK cells that have very low Gal1 levels, is consistent with its higher affinity to Raf-RBDs than to Gal1. Yet, it is plausible that by interfering at the Raf-RBD/ Gal1 interface, L5UR can unfold a higher and more selective activity in *HRAS*-mutant cells with high Gal1 levels, such as observed for Hs 578 T and T24 (Fig. 5). However, the broad impact on cell proliferation (Fig. 6), its engagement of several Ras interactors (Fig. 3e), and its mixed effect on signaling (Fig. 5), suggest that L5URcore is still an immature tool reagent. It nevertheless represents a starting point for the development of novel Ras-nanocluster disrupting reagents that engage with one or more Ras-interactors to affect Ras-signaling and cancer cell proliferation.

How selectively L5UR disrupts the H-Ras nanocluster remains unclear. It is currently unknown how Gal1 positively regulates H-Ras nanocluster but negatively K-Ras nanocluster[29]. Vice versa, how the related galectin-3 (Gal3) increases, specifically K-Ras nanocluster is not known[51–53]. In the context of our stacked-dimer model (Fig. 1a) and our KinCon-data (Fig. 1e), it is conceivable that galectins facilitate the activation of Raf and/or stabilize specific Raf-dimers to facilitate nanoclustering of specific Ras isoforms. Indeed, Gal1 distinguishes between the RBDs from A-, B-, and C-Raf and most strongly engages the B-Raf-RBD. For K-Ras, evidence exists that it binds preferentially with B-/C-Raf-dimers[16,54], while for Gal1 augmented H-Ras nanocluster our previous data suggested a particular relevance for B-/A-Raf dimers[29]. One would, therefore, predict that these dimers are specifically stabilized by Gal3 and Gal1, respectively. However, it is not entirely plausible how symmetrical dimers of galectins, or in the case of Gal3 potentially even oligomers[25], would stabilize asymmetric dimers of Raf proteins. Heterodimerization of galectins could provide a solution to this problem. In humans, 15 different galectins are found and only Gal1 and Gal3 are characterized as nanocluster scaffolds so far[25]. Given the relatedness in this protein family, it is plausible to assume that other galectins have a similar activity and potentially mixed galectin-dimers could form that then

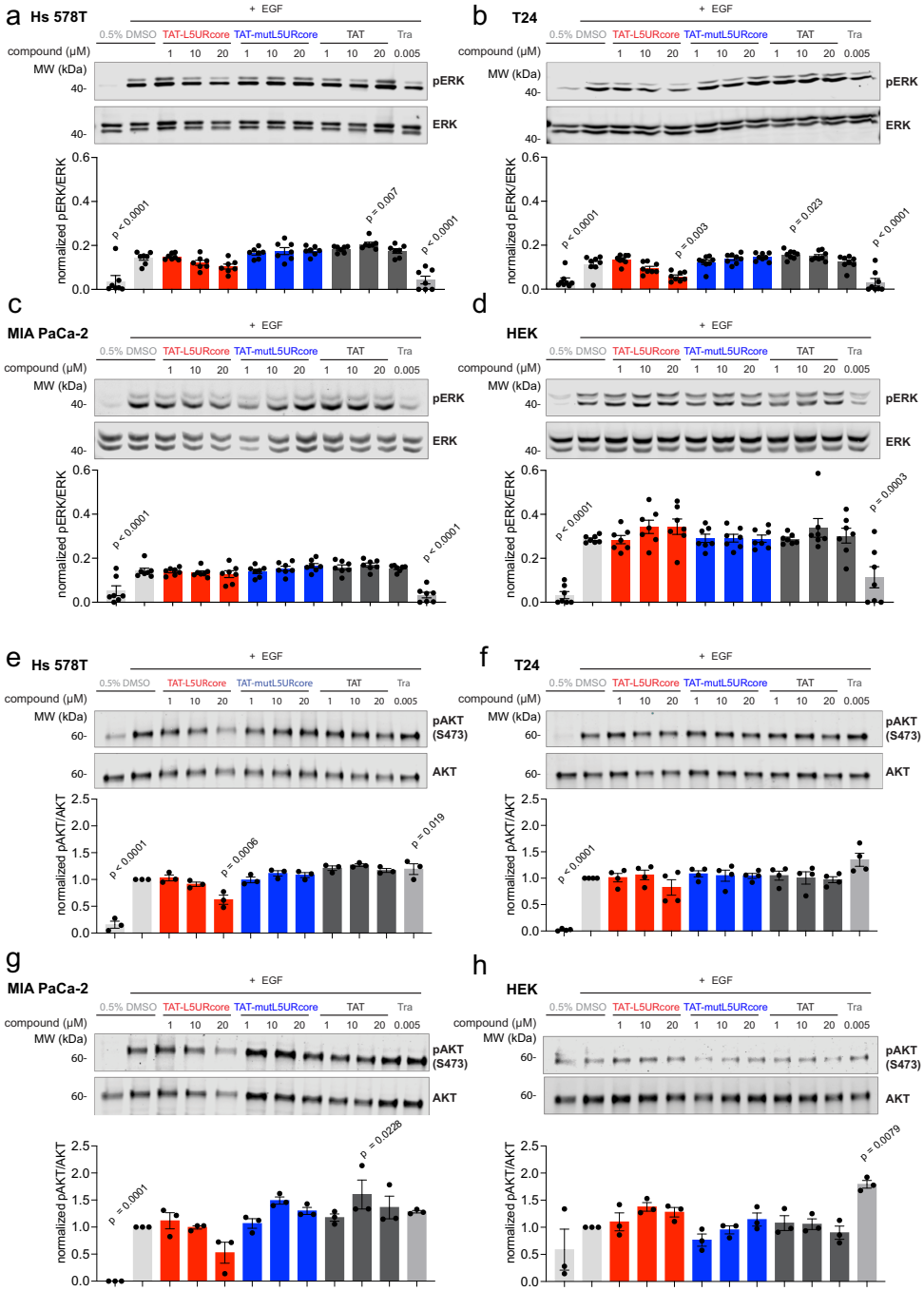

Fig. 5 | The TAT-tagged L5URcore peptide impacts on Ras-signaling. a–h Immunoblot analysis of lysates from Hs 578 T (**a**, **e**), T24 (**b**, **f**), MIA PaCa-2 (**c**, **g**), and HEK (**d**, **h**) cells after EGF-stimulation and treatment with L5URcore-derived peptides with and without TAT-tag or control compound, trametinib (Tra), for 2 h; $n = 3–8$.

stabilize the asymmetric dimers of Raf. Therefore, a complex equilibrium of mixed oligomers that partly stabilize and partly compete and sequester could be the answer to the intricate problem of Ras-isoform specific nanoclustering effect of galectins.

The TAT-L5URcore peptide provides a unique tool to investigate the functioning of Ras nanocluster further. In contrast to current galectin inhibitors, which target the carbohydrate-binding pocket[33,34], the L5UR-peptide acts via a novel mode-of-action that at least in part exploits the role

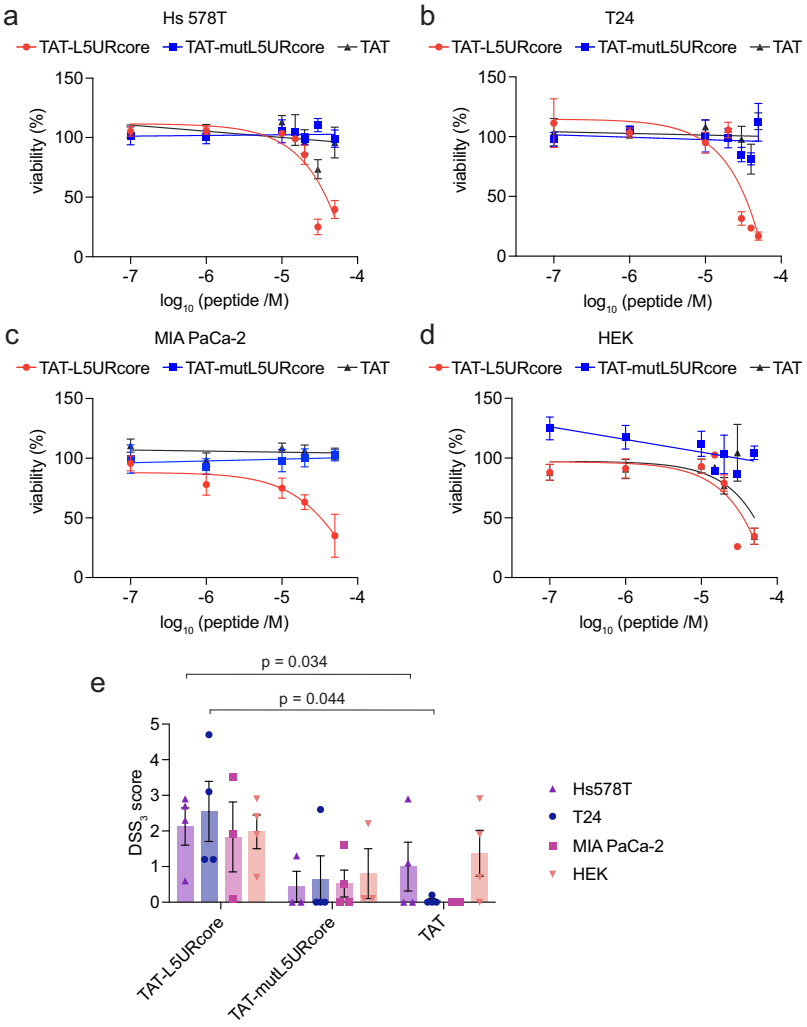

Fig. 6 | HRAS-mutant cancer cell proliferation is decreased by TAT-L5UR peptides. a–d 2D cell viability of Hs 578 T (**a**), T24 (**b**), MIA PaCa-2 (**c**), and HEK (**d**) cells in response to 48 h treatment with TAT-L5URcore peptides and TAT-control; $n = 3$. **e** Drug sensitivity score (DSS3), an area under the curve metric, calculated for the viability data in (**a–d**). A higher value indicates a stronger anti-proliferative effect. TAT-control was used as a reference for statistical comparisons.

of the Raf-RBD/ Gal1 interface in nanocluster stabilization. The intermediate size below 3 kDa of the TAT-L5URcore peptide represents a relevant starting point for the development of smaller molecules with analogous mode-of-action[55,56]. The properties of this peptide and the putative target site suggest that not a distinct pocket, but an assembly of charged and hydrophobic interactions are the major driving force for its affinity. Regarding size, mechanism-of-action, and specificity, L5URcore contrasts with the NS1-monobody, which specifically binds to the allosteric lobe of K-Ras and H-Ras to disrupt nanoclustering[57]. Given the size of the monobody of ~10 kDa it is likely that the steric hindrance caused by this large ligand is mostly responsible for the interference with nanoclustering. With the identification of the targetable site on the Raf-RBD and with more insight into the structure of the Gal1/RBD complex, it will be possible to identify improved binders with higher affinity and specificity in the future. Both competitive screening as well as the structure-based design of peptidomimetics present opportunities for future improvements. The fact that multiple RBD- and RA-domain proteins are bound by L5UR may in this context at first appear as a liability but may hold the opportunity to develop novel RBD- and RA-binders that could affect a broad range of effectors.

Targeting of the H-Ras nanocluster scaffold Gal1 is quite different from approaches focusing on the main nodes of the Ras-MAPK pathway. Both mechanistic and genetic evidence suggest that Gal1 acts as a positive modifier that is associated with a worse progression of *HRAS* mutant cancers, notably head and neck cancers that are frequently associated with high Gal1 levels (Supplementary Fig. 2a). While *HRAS* is overall the least frequently mutated *RAS* gene (in 1.3% of cancer patients), it is mutated in >5% of head and neck squamous cell carcinomas (HNSC)[58]. The prognosis for patients with recurrent and metastatic HNSC is still poor[59]. While tipifarnib, a farnesyltransferase inhibitor shows promising efficacy in HNSC patients, there is still a need for potent treatments[60]. By interfering at the interface of Raf-proteins with Gal1, one may not eliminate other functions of Gal1 and modulate Raf in an unconventional manner that may allow for a normalization of the signaling activity. This would be beneficial regarding side effects, as normal tissue functions could continue to progress.

We expect that our L5UR peptide work will provide new perspectives on how to target Ras nanocluster and potentially also several Ras interactors in a different way.

Methods

Expression constructs

Here we refer to the 52-mer fragment derived from residues 38–89 of the unique region of the λ5-chain (λ5-UR) of the pre-B-cell receptor as L5UR. This unique region bears no similarity to known proteins[38]. The pClontech-L5UR was made by excising L5UR cDNA from pET28a-L5UR (gift from Dr. Elantak), using NheI–XhoI sites and subcloned into pmCherrry-C1 (Clontech, #632524). This removed the mCherry cDNA from the expression vector leaving only the full-length L5UR. Vector pcDNA-Hygro-Anginex was a gift from Prof. Thijssen[42,61]. Expression clones were mostly produced by multi-site gateway cloning as described in our previous studies[36,62,63]. Some expression clone genes were synthesized and cloned into desired vectors by the company GeneCust, France. The B-Raf KinCon sensor encoded by the pcDNA3-RLucF1-BRAF-RLucF2 plasmid was described previously by others[37]. A listing of all plasmid constructs and their sources is provided in Supplementary Table 1.

Cell culture

Hs 578 T, T24, MIA PaCa-2, and BHK-21 cells were obtained from DSMZ-German Collection of Microorganisms and Cell Cultures GmbH or ATCC. HEK293-EBNA cells were a gift from Prof. Florian M. Wurm, EPFL, Lausanne. All cell lines were cultured in a humidified incubator maintained at 37 °C and 5% CO_2, in Dulbecco's modified Eagle Medium (DMEM) (Gibco, #41965039) supplemented with 9% (v/v) Fetal Bovine Serum (FBS) (Gibco, #10270106), 2 mM L-Glutamine (Gibco, #25030081) and penicillin-streptomycin (Gibco, #15140122) 10,000 units/mL (complete growth medium), in T75 culture flasks (Greiner, #658175). Cells were regularly passaged 2–3 times a week and routinely tested for mycoplasma contamination using MycoAlert Plus mycoplasma Detection kit (Lonza, #LT07-710).

Bacterial strains

Competent *E. coli* BL21 Star (DE3)pLysS and *E. coli* DH10B were grown in Luria–Bertani (LB) medium (Sigma, #L3022) at 37 °C, with appropriate antibiotics unless otherwise stated.

Peptide synthesis

Reagents were purchased from Iris Biotech GmbH, Sigma Aldrich, and Carl Roth and used without additional purification. Synthetic protocols were adapted from previously reported protocols[64–66]. All reaction steps were performed in a syringe reactor at room temperature on an orbital shaker. Unless stated otherwise, all procedures were performed with 1 mL of solvent or reagent solution per 50 mg resin. For all scales (10–100 µmol), H-Rink amide ChemMatrix® resin (Sigma-Aldrich, Art. No. 727768) was swollen in dimethylformamide (DMF) for 30 min. For amino acid (aa) coupling a solution of 4 eq. N-α-fluorenylmethyloxycarbonyl (Fmoc) protected amino acid, 4 eq. (1-cyano-2-ethoxy-2-oxoethyliden-aminooxy)dimethylamino-morpholino-carbenium hexafluorophosphate (COMU) and 4 eq. ethyl cyano (hydroxyimino) acetate (Oxyma) in DMF was prepared (0.3 mL per 50 mg resin). Then 8 eq. N,N-diisopropylethylamine (DIPEA) were added to the coupling solution. Subsequently, resin and coupling solution were mixed in a syringe reactor on an orbital shaker. After 30 min, the reaction solution was discarded, and the amino acid coupling was repeated once. After washing the resin with DMF (3×), dichloromethane (DCM) (3×), and DMF (3×), Fmoc removal was performed by adding a solution of piperidine in DMF (2:8, v/v). After 5 min, the solution was discarded and the Fmoc removal was repeated. The resin was washed with DMF (3×), DCM (3×), and DMF (3×). Afterwards, subsequent amino acids were added by repeating cycles of amino acid coupling and Fmoc removal. Peptide synthesis was supported by automated solid-phase synthesis (SPPS), using the peptide synthesis robot Syro I (MultiSynTech), with a double coupling protocol of 4 eq. benzotriazol-1-yl-oxytripyrrolidinophosphonium hexafluorophosphate (PyBOP, 1st 40 min coupling,) and 4 eq. hexafluorophosphate azabenzotriazole tetramethyl uronium (HATU, 2nd 40 min coupling) as coupling reagents and DMF as solvent. Additionally, the coupling reaction with 4 eq. The Fmoc-protected amino acid was supplemented with 4 eq. Oxyma and 8 eq. DIPEA. Before Fmoc removal was conducted with 25% (v/v) piperidine in DMF, a capping step using Ac_2O (acetic anhydride) and DIPEA in NMP (1:1:8, v/v/v) was performed. In between reaction steps, the resin was washed with DMF.

N-terminal acetylated peptides were synthesized by adding a solution of acetic anhydride, DIPEA, and DMF (1:1:8, v/v/v) to the immobilized peptide on resin. The reaction solution was discarded after 10 min, and the acetylation was repeated. Subsequently, the resin was washed with DMF (3×), DCM (3×), and DMF (3×).

N-terminal biotin labeled peptides were prepared by coupling the linker 18-(9-Fluorenylmethyloxycarbonylamino)-4,7,10, 13-tetraoxa-octadecanoic acid (Fmoc-PEG5-OH) as described above onto the N-terminus. After Fmoc removal (see above), biotin was coupled as described above but increasing to 6 eq. of biotin. Subsequently, the resin was washed DMF (3×), DCM (3×) and DMF (3×).

Peptide cleavage and removal of side chain protecting groups were performed simultaneously by adding a solution of trifluoroacetic acid (TFA), triisopropylsilane (TIPS), 1,8-octanedithiol (ODT), and water (94:2.5:2.5:1, v/v/v/v) to the resin. After 2 h, the cleavage solution was collected and evaporated. The crude peptides were obtained by precipitation in diethyl ether with subsequent centrifugation (10 min, 4000 rcf). After the removal of the supernatant, the crude peptide was dissolved in acetonitrile (ACN) and water (1:4, v/v).

Peptide purification was carried out via reverse-phase HPLC (high-performance liquid chromatography) on an Agilent semi-preparative system 1100 (Column: Macherey-Nagel Nucleodur C18, 10 × 125 mm, 110 Å, 5 µm) using various gradients of solvent A (H_2O + 0.1% TFA) and solvent B (ACN + 0.1% TFA) over 20–40 min with a flow rate of 6 mL min^{-1}.

Peptides were analyzed by analytical reverse-phase HPLC coupled to ESI-MS (Agilent 1260 + quadrupole 6120, Column: Eclipse XDB-C18, 4.6 × 150 mm, 5 µm) with solvent A (H_2O + 0.1% FA + 0.01% TFA) and solvent B (ACN + 0.1% FA + 0.01% TFA) via a 10 min gradient from 5% to 95% solvent B. An overview of peptides synthesized by us in this study is given in Supplementary Table 2.

Protein purification

For protein expression, a 16 h culture was set by inoculating colonies into an appropriate volume of antibiotic-supplemented LB media incubated 16 h at 37 °C. The next day, 25 mL of the culture was added to 1 L of LB and incubated at 37 °C until OD at 600 nm reached 0.6–0.9, at which point protein expression was induced by adding isopropyl β-D-1-thiogalactopyranoside (IPTG) (VWR, #437145X) at the final concentration of 0.5 mM. GST-tagged B-Raf-RBD (residues 155–227 of human B-Raf) and GST-tagged C-Raf-RBD (residues 50–134 of human C-Raf) protein expression was induced for 4 h at 23 °C, and the His-tagged protein expression was induced for 16 h at 25 °C. Afterward, the cell pellet was collected by centrifugation, rinsed in PBS, and stored at −20 °C until purification.

For GST-tagged protein purification, cells were lysed by resuspending the pellet in a buffer consisting of 50 mM Tris-HCl pH 7.5, 150 mM NaCl, 2 mM DTT, 0.5% (v/v) Triton-X 100, 1× Protease Inhibitor Cocktail (Thermo Scientific Pierce Protease Inhibitor Mini Tablets, EDTA-free, #A32955) and by sonication on ice using a Bioblock Scientific Ultrasonic Processor instrument (Elmasonic S 40 H, Elma). Lysates were cleared by centrifugation at ~18,500×*g* for 30 min at 4 °C. For GST-tagged proteins, the cleared lysate was incubated with 500 µL glutathione agarose slurry (GE Healthcare, #17-0756-01) (resuspended 1:1 in lysis buffer) for 3 h at 4 °C with gentle rotation. Next, the supernatant was removed, and beads were washed five times with 1 mL of washing buffer consisting of 50 mM Tris-HCl at pH 7.5, 500 mM NaCl, 5 mM DTT, 0.5% (v/v) Triton-X 100. Next, beads were rinsed three times with 1 mL of equilibration buffer (50 mM Tris-HCl pH 7.5, 150 mM NaCl, 2 mM DTT). GST-tagged protein was eluted off the beads by using a 20 mM glutathione solution (Sigma-Aldrich, #G4251-5G). Fractions were analyzed by resolving on 4–20% gradient SDS-

PAGE (BioRAD #4561094 or #4651093), stained with Roti Blue (Carl Roth Roti-Blue quick, #4829-2), and dialyzed into a final dialysis buffer (50 mM Tris-HCl at pH 7.5, 150 mM NaCl, 2 mM DTT, 10% (v/v) glycerol) by using a D-Tube Dialyzer with MWCO 6–8 kDa (Millipore, #71507-M) for 16 h at 4 °C. Protein concentration was measured using NanoDrop 2000c Spectrophotometer (Thermo Fischer Scientific) and stored at −80 °C.

For GST-tag removal, the cleared lysate was incubated with 500 µL of glutathione agarose slurry (resuspended 1:1 in lysis buffer) for 5 h at 4 °C with gentle rotation, then proceeded to washing steps as described above. The beads were rinsed with equilibration buffer and then with dialysis buffer before the excess was drained as much as possible. The beads were then resuspended in 650 µL of dialysis buffer and 100 U of Thrombin (GE Healthcare, #GE27-0846-01), to a final volume of 1 mL. The next day, the untagged protein was collected by applying supernatant to 1 mL polypropylene column, and the flow-through was collected as fraction 1. The beads were washed once more with 1 mL of dialysis buffer, and the flow-through was collected as fraction 2. The two fractions were analyzed by resolving on 4–20% gradient SDS-PAGE and stained with Roti Blue. Protein concentration was measured using NanoDrop and stored at −80 °C.

For His-tagged protein purification, the cells were resuspended in lysis buffer (50 mM Tris-HCl at pH 7.4, 150 mM NaCl, 5 mM $MgSO_4$, 4 mM DTT, 100 mM β-lactose, 100 µM phenylmethylsulfonyl fluoride) with ~5 mg of DNAseI (Merck, #10104159001) and ~5 mg of lysozyme (Thermo Fisher Scientific, #89833). Cells were lysed using an LM10 microfluidizer (Microfluidics, USA) at 18000 PSI, and cell debris was separated by centrifugation (4 °C, 30 min, 75,600×*g*, JA25.50 rotor Beckman Coulter). The supernatant was loaded on an affinity chromatography column (GE Healthcare, His-Trap FF crude, #17-5286-01) with a flow rate of 1 mL/min. A total amount of 10 column volumes 10% elution buffer (50 mM Tris-HCl pH 7.4, 150 mM NaCl, 5 mM $MgSO_4$, 100 mM β-lactose, 4 mM DTT, 1 M Imidazole) and 90% lysis buffer (50 mM Tris-HCl pH 7.4, 150 mM NaCl, 5 mM $MgSO_4$, 4 mM DTT, 100 mM β-lactose) with a flow rate of 2 mL/min was applied. The protein was then eluted using 5 column volumes of elution buffer (50 mM Tris-HCl pH 7.4, 150 mM NaCl, 5 mM $MgSO_4$, 100 mM β-lactose, 4 mM DTT, 1 M Imidazole). Afterwards, the protein was injected into a size exclusion chromatography system (GE Healthcare, HiLoad 16/600 Superdex 75 pg, #28-9893-33) using SEC buffer (20 mM HEPES pH 7.4, 150 mM NaCl, 5 mM $MgSO_4$, 100 mM β-lactose, 4 mM DTT) and a flow rate of 1 mL/min. Protein-containing fractions were pooled, concentrated (MWCO = 3 kDa) to 16.1 mg/mL, snap-frozen in liquid nitrogen, and stored at −80 °C. The protein concentration was measured using NanoDrop 2000c Spectrophotometer (Thermo Fisher Scientific).

Fluorescence polarization assays

The fluorescence polarization assay was adapted from our previously established protocol[62,67]. The non-labeled L5UR and their derivatives and FITC-labeled peptides were obtained from Pepmic Co., China. F-L5UR was synthesized by attaching fluorescein to the N-terminus amino group, leucine of L5UR peptide via aminohexanoic acid linker.

For the direct binding assay, the GST-B-RBD, or GST, was 2-fold diluted in an assay buffer composed of 50 mM Tris HCl pH 7.4, 50 mM NaCl, 5 mM DTT, and 0.005% (v/v) Tween 20 in a black low volume, round bottom 384-well plate (Corning, #4514). Then 10 nM F-L5UR peptide was added to each well and incubated for 20 min at ~22 °C on a horizontal shaker. The fluorescence polarization measurement was performed on the Clariostar (BMG Labtech) plate reader, using a fluorescence polarization module ($\lambda_{excitation}$ 482 ± 8 nm and $\lambda_{emission}$ 530 ± 20 nm). The milli fluorescence polarization, mP, was determined from the measured fluorescence intensities, calculated according to,

$$mP = 1000 \times \frac{I_h - I_v}{I_h + I_v}$$

where I_v and I_h are the fluorescence emission intensities detected with vertical and horizontal polarization, respectively. The mP was plotted against the concentration of the GST-RBD and the K_D value of the F-L5UR was calculated using a quadratic equation,

$$y = \frac{Af + (Ab - Af) * (Lt + K_D + x - \sqrt{(Lt + K_D + x)^2 - 4 * Lt * x}}{2Lt}$$

Af is the polarization value of the free fluoresce nt probe, *Ab* is the polarization value of the fluorescent probe/protein complex, *Lt* is the total concentration of the fluorescent probe, K_D is the equilibrium dissociation constant, *x* is total concentration of protein and y is measured polarization value[36,67]. K_D is measured in the same unit as *x*. For competitive fluorescence polarization experiments, the non-labeled peptides were threefold diluted in the assay buffer and then a complex of 5 nM F-L5UR peptide and 200 nM RBD was added to the dilution series to a final volume of 20 µL per well in 384-well plate. After 30 min incubation at ~22 °C, the fluorescence polarization was read. The logarithmic concentration of peptide was plotted against the mP-value and the data were fit with the log (inhibitor) vs response four parameters equation in GraphPad, and the IC_{50} values were derived. Some IC_{50} values were converted into K_D values as described earlier[68].

QRET assays

The QRET assays were modified from our previously described quenching luminescence assays[69–71]. Ac-K-L5URcore was conjugated with nonadentate europium chelate, {2,2′,2″,2‴-{[4′-(4‴-isothiocyanatophenyl)-2,2′,6′,2″-terpyridine-6,6″-diyl]bis(methylene-nitrilo)}tetrakis(acetate)}europium(III) (QRET Technologies, Finland) via the epsilon amine of the N-terminal lysine that was added to the L5UR-core peptide sequence and purified with analytical reverse-phase HPLC. The current homogeneous QRET binding assay is based on the quenching of non-bound Eu-K-L5URcore with MT2 quencher (QRET Technologies), while bound labeled peptide is luminescent. In the assay, purified B-RBD or Gal1 were twofold diluted in an assay buffer containing 10 mM HEPES pH 7.4 and 10 mM NaCl added in 5 µL to a white low-volume, round bottom 384-well plate. Eu-K-L5UR core peptide (29 nM), mixed with MT2 according to the manufacturer's instructions in the assay buffer supplemented with 0.01% (v/v) Triton X-100, was added in 5 µL volume to wells, and incubated for 30 min at ~22 °C on a shaker. The luminescence was measured with Tecan Spark multimode microplate reader (Tecan, Austria) in time-resolved mode using $\lambda_{excitation}$ 340 ± 40 nm and $\lambda_{emission}$ 620 ± 10 nm with 800 µs delay and 400 µs window times.

Circular dichroism spectra

Acetylated peptides were dissolved in buffer (1× PBS pH 7.5) to a final concentration of 25 µM. Measurements were performed using a Jasco Circular Dichroism spectrometer (J-1500) in a quartz cuvette (1 mm pathlength, Hellma) at 20 °C. Spectra were recorded in 5 continuous scans at a scanning speed of 100 nm min^{-1} (1 mdeg sensitivity, 0.5 nm resolution, 1.0 nm bandwidth, 2 s integration time). From each measurement, values from a blank control containing only the buffer were subtracted to obtain the final ellipticity (mdeg), which was transformed into the mean residue ellipticity (MRE/deg cm^2 $dmol^{-1}$).

In vitro pull-down assays with recombinant proteins

Biotinylated L5UR (bio-L5UR) peptide was synthesized as described above with a PEG5-linker to link the biotin to the L5UR peptide. GST, GST-B-Raf-RBD (155–227), and His-Gal1 were prepared as described above. Each protein in the assay was used at 2 µM concentration, and the peptide was at 4 µM in a reaction of 150 µL. First, peptide and Gal1 were pre-incubated for 30 min at 37 °C, then GST-B-RBD or GST alone was added, and the reaction continued for another hour. Control reaction mixes contained DMSO-vehicle instead of the peptide. At the end of the reaction time, 10 µL of each sample was withdrawn for SDS-PAGE analysis as inputs. For pull-downs,

5 µL of the beads were taken per sample. To prepare the beads, an appropriate volume of the slurry was pipetted into 15 mL falcon tubes and centrifuged at 830×*g* for 1 min to remove the ethanol-containing supernatant. The falcon tube was topped up to 15 mL with distilled water and centrifuged for 1 min to remove water. This washing step was repeated three times. Finally, the beads were resuspended in distilled water so that the final bead volume was 4× diluted i.e., 20 µL were pipetted to each tube. Pull-down was conducted by incubating samples on a rotating wheel at room temperature (20–25 °C) for 1 h. Then, the samples were centrifuged for 1 min at 830×*g* at 4 °C. The supernatant was discarded, and the beads were rinsed with 250 µL of washing buffer (50 mM Tris HCl pH 7.5, 150 mM NaCl, 4 mM β-mercaptoethanol, 0.05% (v/v) NP-40, 10% (v/v) Glycerol) for the total of 1 h at 4 °C, with four exchanges of the washing buffer. The bound material was eluted off the beads by adding 2× SDS-PAGE sample buffer and incubating for 5 min at 95 °C. The analysis was done by resolving the samples (8 µL of the input samples and 10 µL of the eluted material) on 4–20% gradient SDS-PAGE gels and analyzed by Western blotting. A list of all the antibodies used in the study and their sources are given in Supplementary Table 1.

SNAP-tag mediated pull-downs

For the pull-down of interactors of L5UR-SNAP and control constructs, HEK293 EBNA cells were plated on 10 cm dishes. For each dish, 5 µg of pDest305-CMV-hGal1 and pEF-L5UR-SNAP, pEF-mutL5UR-SNAP, or pEF-SNAP were transfected. Transfection was done at ≥70% confluency using 2 µL jetPRIME per 1 µg DNA transfected, according to the manufacturer's instructions. After about 24 h, the growth medium was removed, cells were rinsed twice in cold PBS, and each dish was lysed in 1 mL lysis buffer, consisting of 20 mM HEPES pH 7.5, 4 mM β-mercaptoethanol, 0.05% Igepal, 1× Protease Inhibitor (Thermo Scientific, #A32955) and 1× PhosSTOP (Roche, #04 906 837 001). The cells were scraped and transferred to Eppendorf tubes, then incubated on ice for 30 min, with occasional mixing by inverting the tube. The lysate was cleared by centrifugation for 15 min at 4 °C and 16,363 rcf. Cleared lysate was transferred to a clean tube, 15 µL sample was withdrawn as "Input" for Western blot analysis, and 25 µL of SNAP-capture magnetic beads (New England Biolabs, #S9145S) suspension (diluted 1:1 in lysis buffer) was added. The samples were further incubated for 2 h at room temperature (20–25 °C) on a rotating wheel. Next, the supernatant was discarded, and the beads were rinsed 3× 10 min with 1 mL of washing buffer consisting of 50 mM Tris pH 7.5, 150 mM NaCl, 2 mM EDTA, 2 mM DTT, 0.5% NP-40, 1× Protease Inhibitor, and 1× PhoSTOP. The bound material was released off the beads by adding 25 µL of 2× SDS-PAGE sample buffer and incubating for 5 min at 95 °C. The samples were resolved on 4–20% SDS-PAGE gels in Tris-Gly buffer and analyzed by Western blotting. A list of all the antibodies used in the study and their sources are given in Supplementary Table 1.

Electron microscopic analysis of Ras-nanoclustering

To quantify the nanoclustering of a component integral to the plasma membrane (PM), the apical PM sheets of baby hamster kidney (BHK) cells expressing a GFP-tagged H-Ras construct were fixed with 4% (w/v) PFA and 0.1% (w/v) glutaraldehyde. GFP anchored to the PM sheets was probed with 4.5 nm gold particles pre-coupled to anti-GFP antibody. Following embedment with methyl cellulose, the PM sheets were imaged using transmission electron microscopy (JEOL JEM-1400). Using the coordinates of every gold particle, Ripley's K-function calculated the extent of nanoclustering of gold particles within a selected 1 µm^2 PM area:

$$K(r) = An^{-2}\sum_{i\neq j} w_{ij} 1(\|x_i - x_j\| \le r)$$

$$L(r) - r = \sqrt{\frac{K(r)}{\pi}} - r$$

where n gold particles populate in an intact area of A; r is the length between 1 and 240 nm; $\|\cdot\|$ indicates Euclidean distance where $1(\cdot) = 1$ if $\|x_i - x_j\| \le r$ and $1(\cdot) = 0$ if $\|x_i - x_j\| > r$; $K(r)$ specifies the univariate K-function. w_{ij}^{-1} is a parameter used for an unbiased edge correction and characterizes the proportion of the circumference of a circle that has the center at x_i and radius $\|x_i\text{-}x_j\|$. Monte Carlo simulations estimate the 99% confidence interval (99% C.I.), which is then used to linearly transform $K(r)$ into $L(r) - r$. On a nanoclustering curve of $L(r) - r$ vs. r, the peak $L(r) - r$ value is used as summary statistics for nanoclustering and is termed as *Lmax*. For each condition, at least 15 PM sheets were collected for analysis. To analyze statistical significance between conditions, bootstrap tests compare our point patterns against 1000 bootstrap samples.

Immunoblotting

Routinely, 4–20% Mini-PROTEAN TGX Precast Protein Gels, 10-well, 50 µL, or 30 µL (BioRad, #4561094 or #4651093) were used, unless stated otherwise. For protein size reference, Precision Plus Protein All Blue Prestained Protein Standards (BioRad, #1610373) or Page Ruler Prestained (Thermo Fisher Scientific, #26616) were used. For ERK activity studies, Hs 578 T, T24, MIA PaCa-2 and HEK cells were grown in a 6-well plate for 24 h. After 16 h serum starvation, the cells were treated for 2 h with the L5UR derived TAT-peptides or DMSO control, before they were stimulated with 200 ng/ mL EGF for 10 min. The cell lysates were then prepared using a buffer composed of 150 mM NaCl, 50 mM Tris-HCl pH 7.4, 0.1% (w/v) SDS, 1% (v/v) Triton X-100, 1% (v/v) NP40, 1% (w/v) Na-deoxycholate, 5 mM EDTA pH 8 and 10 mM NaF completed with 1× protease inhibitor cocktail (Pierce, #A32955) and 1× phosphatase inhibitor cocktail (Roche PhosSTOP, #490684001). The total protein concentration was determined using Bradford assay (Protein Assay Reagent, BioRad, #5000006) and 25 µg cell lysate was loaded on a 10% homemade SDS-PAGE gel.

For immunoblotting, gels were transferred onto 0.2 µm pore-size nitrocellulose membrane by using Trans-Blot Turbo RTA Midi 0.2 µm Nitrocellulose Transfer Kit, for 40 blots (BioRad, #1704271). The membranes were blocked with TBS or PBS with 0.2% (v/v) Tween20 and 2% BSA. Primary antibodies were incubated at 4 °C for 16 h or for 1–3 h at room temperature (20–25 °C). All secondary antibodies were diluted at 1:10,000 in a blocking buffer and were incubated for 1 h at room temperature (20–25 °C). A detailed list of all the antibodies used in the study and their sources are given in Supplementary Table 1.

Fluorescence lifetime imaging microscopy (FLIM)-FRET analysis

FLIM-FRET experiments were conducted as described previously[29,30,72]. About 120,000 HEK cells were seeded per well in a 6-well plate (Greiner, #657160) with a cover slip (Carl Roth, #LH22.1) and grown for 18–24 h. For H-RasG12V nanoclustering-FRET, the cells were transfected with a total of 1 µg of mGFP/mCherry-tagged H-RasG12V at a donor (D):acceptor (A)-plasmid ratio of 1:3. In addition, 0.75 µg of other plasmids encoding L5UR, rat (rt) Gal1 or N-rtGal1 (dimerization-deficient mutant) were co-transfected. For Gal1/C-RBD FRET-interaction, the cells were transfected with 2 µg mGFP-rtGal1 and mRFP-C-RBD (D:A, 1:3) or mGFP-rtGal1 and mRFP-C-RBD-D117A pair (D:A, 1:3). In addition, cells were co-transfected with 1.5 µg pClontech-C-L5UR, the pcDNA-Hygro-Anginex or compound OTX008 (Cayman Chemicals, #23130). All transfections were done using jetPRIME (Polyplus, #114-75) transfection reagent according to the manufacturer's instructions. After 4 h of transfection the medium was changed. The next day, the cells were fixed with 4% w/v PFA. The cells were mounted with Mowiol 4–88 (Sigma-Aldrich, #81381). An inverted microscope (Zeiss AXIO Observer D1) with a fluorescence lifetime imaging attachment (Lambert Instruments) was used to measure fluorescence lifetimes of mGFP. Fluorescein (0.01 mM, pH 9) was used as a fluorescence lifetime reference ($\tau = 4.1$ ns). Averaged fluorescence lifetimes were used to calculate the apparent FRET efficiency as described[30,72].

Split-luciferase KinCon B-Raf biosensor measurements

HEK 293-EBNA cells were seeded in a 12-well plate (Greiner Bio-One, #665180) in 1 ml complete DMEM and grown for 24 h. The next day 0.5 µg

of KinCon sensor plasmid pcDNA-RlucF1-BRAF-RlucF2 was transfected along with 0.1–0.5 µg of modulator plasmid encoding either SNAP-H-RasG12V or Gal1) using jetPRIME as per manufacturer protocol; pcDNA3.1(−) Thermo Fisher Scientific, #V79520) was used to buffer the total amount of plasmid load per well to 1 µg. After 48 h of expression cells were collected and washed in PBS. Cells from one well of the 12-well plate were resuspended in 200 µL of PBS and 2× 90 µL were pipetted into a white 96-well plate (Nunc, Thermo Fisher Scientific, #236108). Then coelenterazine h was added to a final concentration of 5 µM and the luminescence signal at 480 ± 10 nm was collected for 10 s. The basically background-free signal was normalized against the signal without modulator plasmid.

BRET assays

We employed the BRET2 system where RLuc8 and GFP2 luminophores were predominantly used as the donor and acceptor, respectively, with coelenterazine 400a as the substrate. A CLARIOstar plate reader from BMG Labtech was used for BRET and fluorescence intensity measurement. The BRET protocol was adapted as described by us[73].

In brief, 150,000–200,000 HEK293-EBNA cells were seeded per well of a 12-well plate and grown for 24 h in 1 mL of complete DMEM. The next day, the cells were transfected with ~1 µg of plasmid DNA per well using a 3 µL jetPRIME transfection reagent. For the donor saturation titration, 25 ng of the donor plasmid was transfected with an acceptor plasmid concentration ranging from 25 to 1000 ng. The pcDNA3.1(−) plasmid (was used to top up the amount of DNA per well. 48 h after transfection, cells were collected in PBS and plated in a white 96-well plate.

First, the fluorescence intensity of GFP2 was measured ($\lambda_{excitation}$ 405 ± 10 nm and $\lambda_{emission}$ 515 ± 10 nm), which is directly proportional to the acceptor expression (RFU). Then 10 µM of coelenterazine 400a (GoldBio, #C-320) was added to the cells, and BRET readings were recorded simultaneously at $\lambda_{emission}$ 410 ± 40 nm (RLU) and 515 ± 15 nm (BRET signal). Emission intensity measured at 410 nm is directly proportional to the donor expression. The raw BRET ratio was calculated as the ratio of BRET signal/RLU. The background BRET ratio was obtained from cells expressing only the donor. The background BRET ratio was subtracted from the raw BRET ratio to obtain the BRET ratio, plotted here as 'BRET'. The relative expression was calculated as the ratio of RFU/RLU. The relative expression, acceptor/ donor, plotted in the *x*-axis in corresponding figures, was obtained by normalizing RFU/RLU values to those from cells transfected with 1:1 donor and acceptor plasmid ratio[54].

Alternatively, the fluorescence intensity of mNeonGreen was measured at $\lambda_{excitation}$ 485 ± 10 nm and $\lambda_{emission}$ 535 ± 10 nm. Then 2.9 µM of coelenterazine 400a was added to the cells and the BRET readings for mNeonGreen and NanoLuc were recorded simultaneously at $\lambda_{emission}$ 460 ± 25 nm (RLU) and 535 ± 25 nm (BRET signal).

The BRET ratio and acceptor/donor values from various biological repeats were plotted together and the data were fitted with a hyperbolic equation in Prism (GraphPad). The one phase association equation of Prism 9 (GraphPad) was used to predict the top asymptote Ymax-value, which was taken as the BRETtop. The BRETtop value represents the top asymptote of the BRET ratio reached within the defined acceptor/donor range.

For the dose-response BRET assays, the donor and acceptor plasmid concentration were kept constant, as indicated in the corresponding figure legends. HEK293-EBNA cells were grown in 12-well plate for 24 h in complete DMEM. The next day, donor and acceptor plasmids were transfected along with modulator plasmid ranging from 125 to 850 ng. After 48 h of expression the cells were collected in PBS and BRET measurements were carried out.

For treatment with peptides, HEK cells were batch-transfected. After 24 h of transfection, cells were re-plated in a white 96-well plate in phenol red-free DMEM. After another 48 h, peptides were added to cells at concentrations ranging from 0.1 µM to 100 µM. After 2 h incubation at 37 °C, the plate was brought to room temperature (20–25 °C) before taking BRET measurements as indicated above. The concentration of the transfected L5UR-modulator plasmid or applied peptide was plotted against the BRET value and the data were fitted with a straight-line equation using Prism.

Cell viability assay and drug sensitivity score (DSS) analysis

The cells were seeded in low attachment, suspension cell culture 96-well plates (Greiner, #655185). About 2000 T24, MIA PaCa-2, and HEK cells and 5000 Hs 578 T cells were seeded per well in a 50 µL complete growth medium. 24 h later, the cells were treated with 50 µL 2× peptide diluted in the growth medium or 0.2% (v/v) of the positive control, benzethonium chloride stock at 100 mM in H_2O (Sigma-Aldrich, #B8879). Forty-eight hours after the peptide treatment 10% (v/v) of alamarBlue reagent (Thermo Fisher Scientific, #DAL1100) was added to each well and incubated for 4 h at 37 °C. Using a CLARIOstar plate reader the fluorescence signal ($\lambda_{excitation}$ 560 ± 5 nm and $\lambda_{emission}$ 590 ± 5 nm) was recorded. The florescence signal was normalized against the negative control, here DMSO in buffer, representing 100% viability. Additionally, the data was analyzed using Breeze 2.0 to determine a drug sensitivity score (DSS), a normalized area under the curve (AUC). Here we plot only one of the output values from the Breeze pipeline[74], the DSS3 value, which was calculated as

$$DSS_3 = DSS_2 \frac{x_2 - x_1}{C_{max} - C_{min}}$$

where DSS_2 is given by the equation $DSS_2 = \frac{DSS_1}{\log a}$

And DSS_1 is given by the equation $DSS_1 = \frac{AUC - t(x_2 - x_1)}{(100 - t)(C_{max} - C_{min})}$

After dose–response inhibition data fitting with a logistic function, the area under the curve (AUC) was determined. The activity threshold (t) was set to ≥10%. The maximum (C_{max}) and minimum (C_{min}) concentrations used for screening of the inhibitors, with $C_{max} = x_2$ and x_1 concentration with minimal activity *t*. The parameter a is the value of the top asymptote, which can be different from 100% inhibition as obtained from the benzethonium chloride positive control value.

Statistics and reproducibility

Data were analyzed using Graph Pad prism 9.0 software. The number of independent biological repeats (n) for each dataset is provided in the figure legends. If not stated otherwise means and standard errors (SEM) are plotted. The statistical significance of differences between Lmax-values determined in the nanoclustering analysis by electron microscopy was determined using bootstrap tests. All BRETtop data were compared using the extra sum-of-squares *F* test. All other statistical analyses were performed using one-way ANOVA. A *p*-value of <0.05 was considered statistically significant, and the statistical significance levels were annotated.

Reporting summary

Further information on research design is available in the Nature Portfolio Reporting Summary linked to this article.

Data availability

All data supporting the findings of this study are available within the manuscript and its Supplementary Information. Uncropped and unedited blot images with references to respective figures are provided in Supplementary Figs. 4–19. All source data for graphs in this manuscript are provided in Supplementary Data 1. All unique/stable reagents generated in this study are available from the corresponding author with a completed materials transfer agreement. This study did not report standardized datatypes.

Received: 7 October 2023; Accepted: 28 June 2024;
Published online: 09 July 2024

References

1. Steffen, C. L., Kaya, P., Schaffner-Reckinger, E. & Abankwa, D. Eliminating oncogenic RAS: back to the future at the drawing board. *Biochem. Soc. Trans.* **51**, 447–456 (2023).
2. Punekar, S. R., Velcheti, V., Neel, B. G. & Wong, K. K. The current state of the art and future trends in RAS-targeted cancer therapies. *Nat. Rev. Clin. Oncol.* **19**, 637–655 (2022).
3. Simanshu, D. K., Nissley, D. V. & McCormick, F. RAS proteins and their regulators in human disease. *Cell* **170**, 17–33 (2017).
4. Spiegel, J., Cromm, P. M., Zimmermann, G., Grossmann, T. N. & Waldmann, H. Small-molecule modulation of Ras signaling. *Nat. Chem. Biol.* **10**, 613–622 (2014).
5. Smith, M. J. Defining bone fide effectors of RAS GTPases. *Bioessays* **45**, e2300088 (2023).
6. Kiel C., Matallanas D. & Kolch W. The ins and outs of RAS effector complexes. *Biomolecules* **11**, 236 (2021).
7. Simanshu, D. K. & Morrison, D. K. A structure is worth a thousand words: new insights for RAS and RAF regulation. *Cancer Discov.* **12**, 899–912 (2022).
8. Lavoie, H. & Therrien, M. Regulation of RAF protein kinases in ERK signalling. *Nat. Rev. Mol. Cell Biol.* **16**, 281–298 (2015).
9. Martinez Fiesco, J. A., Durrant, D. E., Morrison, D. K. & Zhang, P. Structural insights into the BRAF monomer-to-dimer transition mediated by RAS binding. *Nat. Commun.* **13**, 486 (2022).
10. Rajakulendran, T., Sahmi, M., Lefrancois, M., Sicheri, F. & Therrien, M. A dimerization-dependent mechanism drives RAF catalytic activation. *Nature* **461**, 542–545 (2009).
11. Abankwa D., Gorfe A. A. Mechanisms of Ras membrane organization and signaling: Ras rocks again. *Biomolecules* **10**, 1522 (2020).
12. Abankwa, D., Gorfe, A. A. & Hancock, J. F. Ras nanoclusters: molecular structure and assembly. *Semin. Cell Dev. Biol.* **18**, 599–607 (2007).
13. Plowman, S. J. & Hancock, J. F. Ras signaling from plasma membrane and endomembrane microdomains. *Biochim. Biophys. Acta* **1746**, 274–283 (2005).
14. Tian, T. et al. Plasma membrane nanoswitches generate high-fidelity Ras signal transduction. *Nat. Cell Biol.* **9**, 905–914 (2007).
15. Sarkar-Banerjee, S. et al. Spatiotemporal analysis of K-Ras plasma membrane interactions reveals multiple high order homo-oligomeric complexes. *J. Am. Chem. Soc.* **139**, 13466–13475 (2017).
16. Cho, K. J. et al. Raf inhibitors target ras spatiotemporal dynamics. *Curr. Biol.* **22**, 945–955 (2012).
17. Jin, T. et al. RAF inhibitors promote RAS-RAF interaction by allosterically disrupting RAF autoinhibition. *Nat. Commun.* **8**, 1211 (2017).
18. Holderfield, M., Deuker, M. M., McCormick, F. & McMahon, M. Targeting RAF kinases for cancer therapy: BRAF-mutated melanoma and beyond. *Nat. Rev. Cancer* **14**, 455–467 (2014).
19. Pavic, K., Chippalkatti, R. & Abankwa, D. Drug targeting opportunities en route to Ras nanoclusters. *Adv. Cancer Res.* **153**, 63–99 (2022).
20. Rotblat, B. et al. H-Ras nanocluster stability regulates the magnitude of MAPK signal output. *PLoS ONE* **5**, e11991 (2010).
21. Prior, I. A., Muncke, C., Parton, R. G. & Hancock, J. F. Direct visualization of Ras proteins in spatially distinct cell surface microdomains. *J. Cell Biol.* **160**, 165–170 (2003).
22. Elad-Sfadia, G., Haklai, R., Ballan, E., Gabius, H. J. & Kloog, Y. Galectin-1 augments Ras activation and diverts Ras signals to Raf-1 at the expense of phosphoinositide 3-kinase. *J. Biol. Chem.* **277**, 37169–37175 (2002).
23. Timoshenko, A. V. Towards molecular mechanisms regulating the expression of galectins in cancer cells under microenvironmental stress conditions. *Cell Mol. Life Sci.* **72**, 4327–4340 (2015).
24. Rabinovich, G. A. Galectin-1 as a potential cancer target. *Br. J. Cancer* **92**, 1188–1192 (2005).
25. Johannes L., Jacob R. & Leffler H. Galectins at a glance. *J. Cell Sci.* **131**, jcs208884 (2018).
26. Belanis, L., Plowman, S. J., Rotblat, B., Hancock, J. F. & Kloog, Y. Galectin-1 is a novel structural component and a major regulator of h-ras nanoclusters. *Mol. Biol. Cell* **19**, 1404–1414 (2008).
27. Mejuch, T., van Hattum, H., Triola, G., Jaiswal, M. & Waldmann, H. Specificity of lipoprotein chaperones for the characteristic lipidated structural motifs of their cognate lipoproteins. *Chembiochem* **16**, 2460–2465 (2015).
28. Lakshman, B. et al. Quantitative biophysical analysis defines key components modulating recruitment of the GTPase KRAS to the plasma membrane. *J. Biol. Chem.* **294**, 2193–2207 (2019).
29. Blazevits, O. et al. Galectin-1 dimers can scaffold Raf-effectors to increase H-ras nanoclustering. *Sci. Rep.* **6**, 24165 (2016).
30. Guzman, C. et al. The efficacy of Raf kinase recruitment to the GTPase H-ras depends on H-ras membrane conformer-specific nanoclustering. *J. Biol. Chem.* **289**, 9519–9533 (2014).
31. Cho, M. & Cummings, R. D. Galectin-1, a beta-galactoside-binding lectin in Chinese hamster ovary cells. I. Physical and chemical characterization. *J. Biol. Chem.* **270**, 5198–5206 (1995).
32. Siljamaki, E. & Abankwa, D. SPRED1 interferes with K-ras but Not H-ras membrane anchorage and signaling. *Mol. Cell Biol.* **36**, 2612–2625 (2016).
33. Stegmayr, J. et al. Extracellular and intracellular small-molecule galectin-3 inhibitors. *Sci. Rep.* **9**, 2186 (2019).
34. Chan, Y. C. et al. Dissecting the structure-activity relationship of galectin-ligand interactions. *Int. J. Mol. Sci*. **19**, 392 (2018).
35. Marullo, S. & Bouvier, M. Resonance energy transfer approaches in molecular pharmacology and beyond. *Trends Pharm. Sci.* **28**, 362–365 (2007).
36. Manoharan G. B., Laurini C., Bottone S., Ben Fredj N. & Abankwa D. K. K-Ras binds calmodulin-related Centrin1 with potential implications for K-Ras driven cancer cell stemness. *Cancers (Basel)* **15**, 3087 (2023).
37. Rock, R. et al. BRAF inhibitors promote intermediate BRAF(V600E) conformations and binary interactions with activated RAS. *Sci. Adv*. **5**, eaav8463 (2019).
38. Elantak, L. et al. Structural basis for galectin-1-dependent pre-B cell receptor (pre-BCR) activation. *J. Biol. Chem.* **287**, 44703–44713 (2012).
39. Dings, R. P. et al. Antitumor agent calixarene 0118 targets human galectin-1 as an allosteric inhibitor of carbohydrate binding. *J. Med. Chem.* **55**, 5121–5129 (2012).
40. Astorgues-Xerri, L. et al. OTX008, a selective small-molecule inhibitor of galectin-1, downregulates cancer cell proliferation, invasion and tumour angiogenesis. *Eur. J. Cancer* **50**, 2463–2477 (2014).
41. Brandwijk, R. J. et al. Cloning an artificial gene encoding angiostatic anginex: from designed peptide to functional recombinant protein. *Biochem. Biophys. Res. Commun.* **333**, 1261–1268 (2005).
42. Thijssen, V. L. et al. Galectin-1 is essential in tumor angiogenesis and is a target for antiangiogenesis therapy. *Proc. Natl Acad. Sci. USA* **103**, 15975–15980 (2006).
43. Posada, I. M. et al. ASPP2 is a novel pan-RAS nanocluster scaffold. *PLoS ONE* **11**, e0159677 (2016).
44. Posada, I. M. D. et al. Rapalogs can promote cancer cell stemness in vitro in a Galectin-1 and H-ras-dependent manner. *Oncotarget* **8**, 44550–44566 (2017).
45. Wang, Y. et al. ASPP1 and ASPP2 bind active RAS, potentiate RAS signalling and enhance p53 activity in cancer cells. *Cell Death Differ.* **20**, 525–534 (2013).
46. Dhanaraman, T. et al. RASSF effectors couple diverse RAS subfamily GTPases to the Hippo pathway. *Sci. Signal.* **13**, eabb4778 (2020).
47. Jauset, T. & Beaulieu, M. E. Bioactive cell penetrating peptides and proteins in cancer: a bright future ahead. *Curr. Opin. Pharm.* **47**, 133–140 (2019).

48. Dietrich, L. et al. Cell permeable stapled peptide inhibitor of Wnt signaling that targets beta-catenin protein-protein interactions. *Cell Chem. Biol.* **24**, 958–968.e955 (2017).
49. Vives, E., Brodin, P. & Lebleu, B. A truncated HIV-1 Tat protein basic domain rapidly translocates through the plasma membrane and accumulates in the cell nucleus. *J. Biol. Chem.* **272**, 16010–16017 (1997).
50. Adihou, H. et al. A protein tertiary structure mimetic modulator of the Hippo signalling pathway. *Nat. Commun.* **11**, 5425 (2020).
51. Siddiqui F. A., Vukic V., Salminen T. A., Abankwa D. Elaiophylin is a potent Hsp90/ Cdc37 protein interface inhibitor with K-Ras nanocluster selectivity. *Biomolecules* **11**, 836 (2021).
52. Siddiqui, F. A. et al. Novel small molecule Hsp90/Cdc37 interface inhibitors indirectly target K-Ras-signaling. *Cancers (Basel)* **13**, 927 (2021).
53. Shalom-Feuerstein, R. et al. K-ras nanoclustering is subverted by overexpression of the scaffold protein galectin-3. *Cancer Res.* **68**, 6608–6616 (2008).
54. Terrell, E. M. et al. Distinct binding preferences between Ras and Raf family members and the impact on oncogenic Ras signaling. *Mol. Cell* **76**, 872–884.e875 (2019).
55. Cromm, P. M. et al. Protease-resistant and cell-permeable double-stapled peptides targeting the Rab8a GTPase. *ACS Chem. Biol.* **11**, 2375–2382 (2016).
56. Pelay-Gimeno, M., Glas, A., Koch, O. & Grossmann, T. N. Structure-based design of inhibitors of protein-protein interactions: mimicking peptide binding epitopes. *Angew. Chem. Int. Ed. Engl.* **54**, 8896–8927 (2015).
57. Spencer-Smith, R. et al. Inhibition of RAS function through targeting an allosteric regulatory site. *Nat. Chem. Biol.* **13**, 62–68 (2017).
58. Prior, I. A., Hood, F. E. & Hartley, J. L. The frequency of Ras mutations in cancer. *Cancer Res.* **80**, 2969–2974 (2020).
59. Burtness, B. et al. Pembrolizumab alone or with chemotherapy versus cetuximab with chemotherapy for recurrent or metastatic squamous cell carcinoma of the head and neck (KEYNOTE-048): a randomised, open-label, phase 3 study. *Lancet* **394**, 1915–1928 (2019).
60. Ho, A. L. et al. Tipifarnib in head and neck squamous cell carcinoma with HRAS mutations. *J. Clin. Oncol.* **39**, 1856–1864 (2021).
61. Brandwijk, R. J. et al. Anti-angiogenesis and anti-tumor activity of recombinant anginex. *Biochem. Biophys. Res. Commun.* **349**, 1073–1078 (2006).
62. Okutachi, S. et al. A covalent calmodulin inhibitor as a tool to study cellular mechanisms of K-Ras-driven stemness. *Front. Cell Dev. Biol.* **9**, 665673 (2021).
63. Manoharan, G. B., Okutachi, S. & Abankwa, D. Potential of phenothiazines to synergistically block calmodulin and reactivate PP2A in cancer cells. *PLoS ONE* **17**, e0268635 (2022).
64. Wendt, M. et al. Bicyclic beta-sheet mimetics that target the transcriptional coactivator beta-catenin and inhibit Wnt signaling. *Angew. Chem. Int. Ed. Engl.* **60**, 13937–13944 (2021).
65. Paulussen, F. M. et al. Covalent proteomimetic inhibitor of the bacterial FtsQB divisome complex. *J. Am. Chem. Soc.* **144**, 15303–15313 (2022).
66. Kuepper, A. et al. Constrained peptides mimic a viral suppressor of RNA silencing. *Nucleic Acids Res.* **49**, 12622–12633 (2021).
67. Manoharan, G. B., Kopra, K., Eskonen, V., Harma, H. & Abankwa, D. High-throughput amenable fluorescence-assays to screen for calmodulin-inhibitors. *Anal. Biochem.* **572**, 25–32 (2019).
68. Sinijarv, H. et al. Binding assay for characterization of protein kinase inhibitors possessing sub-picomolar to sub-millimolar affinity. *Anal. Biochem.* **531**, 67–77 (2017).
69. Harma, H. et al. A new simple cell-based homogeneous time-resolved fluorescence QRET technique for receptor-ligand interaction screening. *J. Biomol. Screen* **14**, 936–943 (2009).
70. Kopra, K. & Harma, H. Quenching resonance energy transfer (QRET): a single-label technique for inhibitor screening and interaction studies. *N. Biotechnol.* **32**, 575–580 (2015).
71. Kopra, K. et al. A homogeneous quenching resonance energy transfer assay for the kinetic analysis of the GTPase nucleotide exchange reaction. *Anal. Bioanal. Chem.* **406**, 4147–4156 (2014).
72. Guzman, C., Oetken-Lindholm, C. & Abankwa, D. Automated high-throughput fluorescence lifetime imaging microscopy to detect protein-protein interactions. *J. Lab Autom.* **21**, 238–245 (2016).
73. Babu Manoharan, G., Guzman, C., Najumudeen, A. K. & Abankwa, D. Detection of Ras nanoclustering-dependent homo-FRET using fluorescence anisotropy measurements. *Eur. J. Cell Biol.* **102**, 151314 (2023).
74. Potdar, S. et al. Breeze 2.0: an interactive web-tool for visual analysis and comparison of drug response data. *Nucleic Acids Res*. **51(W1)** W57–W61 (2023).

Acknowledgements

The study was supported by the grant INTER/NWO/19/14061736-HRAS-PPi of the Luxembourg National Research Fund (FNR) and OCENW.KLEIN.228 of the Dutch Research Council (NWO) to DA and TG, respectively, as well as FNR-grant INTER/Mobility/2021/BM/15591725/panRAFi-PB to GM. Prof. Marc Therrien (IRIC, Université de Montréal, Canada) is gratefully acknowledged for hosting GM in his laboratory. Dr. Hugo Lavoie and Dr. Ting Jin (IRIC, Université de Montréal, Canada) are thanked for their support and advice to GM during his sabbatical. Geneviève Arseneault (IRIC, Université de Montréal, Canada) is thanked for the technical support. pET28a-L5UR was a gift from Dr. Latifa Elantak (CNRS Marseille, France). pcDNA-Hygro-Anginex was a gift from Prof. Victor L. Thijssen (VU Amsterdam, Netherlands). The KinCon plasmid was obtained from Dr. Eduard Stefan (University of Innsbruck, Austria).

Author contributions

D.K.A. and T.N.G. conceived the study. C.L.S. collected and evaluated BRET, FP, signaling, and cell viability data and purified proteins. G.M. collected and evaluated BRET, FP, and KinCon data. K.P. purified proteins and performed and evaluated pull-down experiments and signaling data. A.Y.V. synthesized all of the peptides in Supplementary Table 2 and performed CD spectra. MK collected and evaluated FLIM-FRET data. Y.Z. and N.A. collected and evaluated EM-nanoclustering data. H.H. collected and evaluated QRET data. A.G. performed bioinformatics analysis of survival and cancer type frequency. T.N.G. and D.K.A. jointly supervised the study. G.M., C.L.S., K.P., A.Y.V., T.N.G., and D.K.A. wrote the paper.

Competing interests

The authors declare no competing interests.

Additional information

Supplementary information The online version contains supplementary material available at https://doi.org/10.1038/s42003-024-06523-9.

Correspondence and requests for materials should be addressed to Daniel Kwaku Abankwa.

Peer review information *Communications Biology* thanks the anonymous, reviewer(s) for their contribution to the peer review of this work. Primary Handling Editor: Tobias Goris. A peer review file is available.

Supplementary Information

Identification of an H-Ras nanocluster disrupting peptide

Candy Laura Steffen [1,*], Ganesh babu Manoharan [1,*], Karolina Pavic [1], Alejandro Yeste-Vázquez [2,3], Matias Knuuttila [4], Neha Arora [5], Yong Zhou [5], Harri Härmä [6], Anthoula Gaigneaux [7], Tom N. Grossmann [2,3], Daniel Kwaku Abankwa [1,4]

[1] Cancer Cell Biology and Drug Discovery group, Department of Life Sciences and Medicine, University of Luxembourg, 4362 Esch-sur-Alzette, Luxembourg.

[2] Department of Chemistry and Pharmaceutical Sciences, VU University Amsterdam, Amsterdam, The Netherlands.

[3] Amsterdam Institute of Molecular and Life Sciences (AIMMS), VU University Amsterdam, Amsterdam, The Netherlands.

[4] Turku Bioscience Centre, University of Turku and Åbo Akademi University, 20520 Turku, Finland.

[5] Department of Integrative Biology and Pharmacology, McGovern Medical School, UT Health, Houston, TX 77030, USA.

[6] Chemistry of Drug Development, Department of Chemistry, University of Turku, 20500 Turku, Finland.

[7] Bioinformatics Core, Department of Life Sciences and Medicine, University of Luxembourg, 4367 Esch-sur-Alzette, Luxembourg

[*] These authors contributed equally

Correspondence: daniel.abankwa@uni.lu

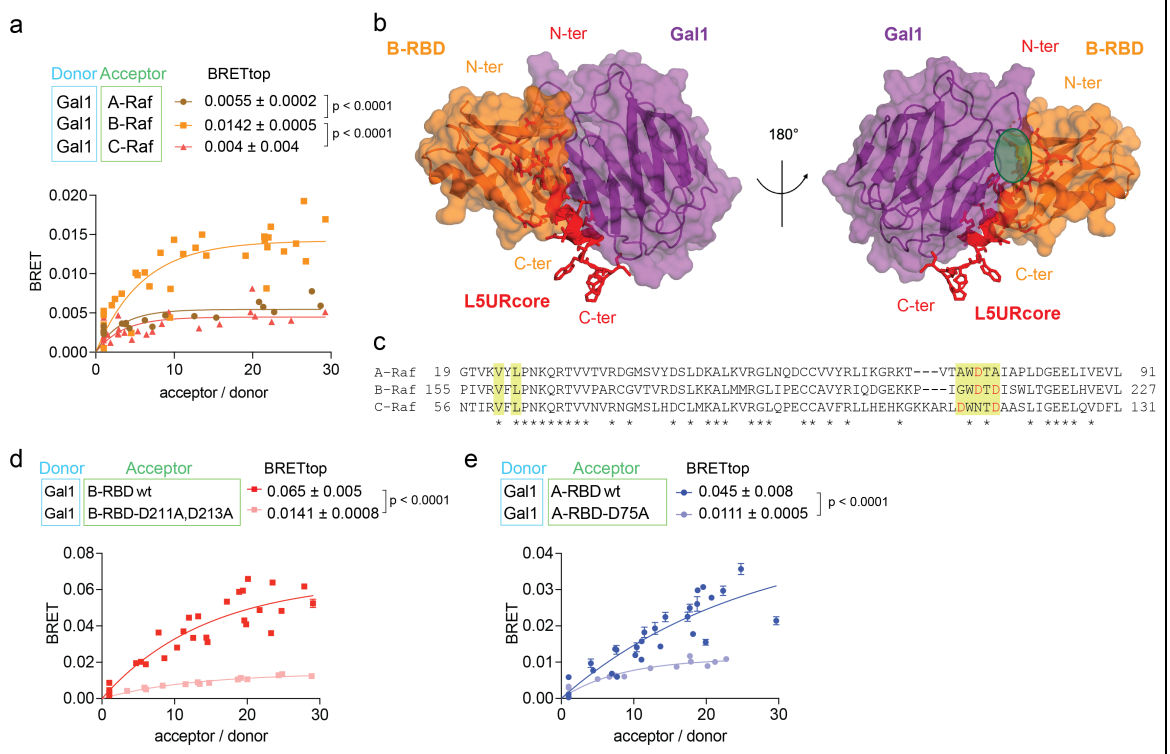

Supplementary Figure 1. Related to main Figure 1.

(**a**) BRET-titration curves of Gal1 and full-length Raf proteins; n = 3.

(**b**) Computational model of hypothetical Gal1/ B-RBD/ L5UR (22-45) complex indicating the carbohydrate binding site of Gal1 (PDB ID 3W58) in green. The structural model was created with PyMOL Molecular Graphics System (Version 2.5.1) using the published Gal1/ C-RBD docking model [1], the Haddock model of Gal1/ L5UR(22-45) [2] and the RBD structure of B-Raf (PDB ID 3NY5).

(**c**) Multiple sequence alignment of RBDs of A-, B- and C-Raf. The protein sequences of RBDs from the three human Raf proteins, A-Raf (P10398), B-Raf (P15056) and C-Raf (P04049) were essentially as employed in the cellular assays; in brackets Uniprot database (http://uniprot.org/) accession numbers. Multiple sequence alignment was performed using Clustal Omega (https://www.ebi.ac.uk/Tools/msa/clustalo/). Yellow highlighted residues were identified as possible interaction sites with Gal1 before [1], and mutations tested in the BRET experiments in (d, e) are in red.

(**d, e**) BRET-titration curves of Gal1 with wild-type (wt) A-RBD and A-RBD-D75A mutant (d); n = 3, or with wt B-RBD and B-RBD-D211A, D213A mutant (e); n = 3.

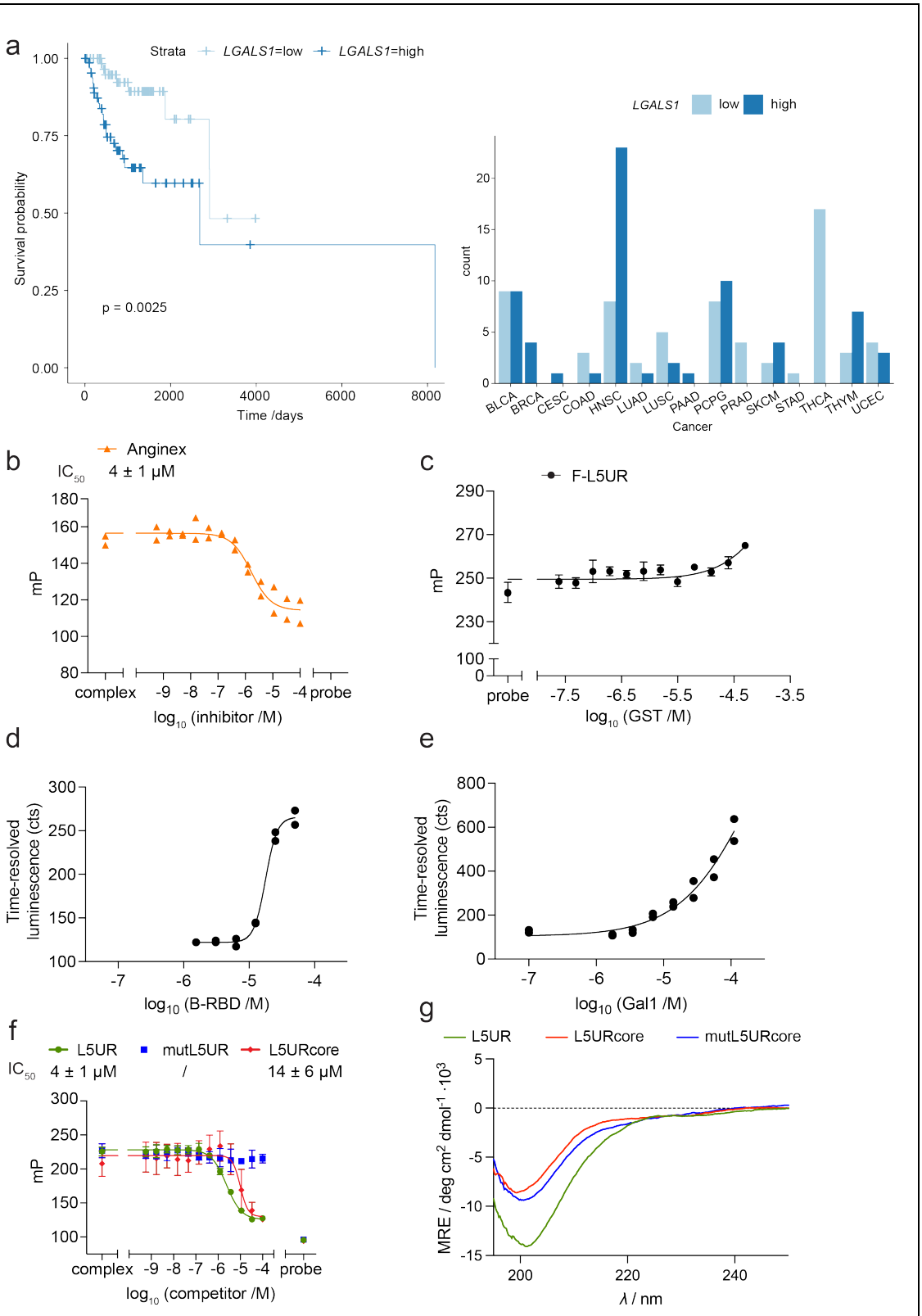

Supplementary Figure 2. Related to main Figures 2 and 3.
(**a**) PanCanAtlas data analysis reveals that high Gal1 (gene *LGALS1*) levels significantly decrease survival in HRAS mutant cancer cases (left). Higher Gal1 levels are more often found in head and neck (HNSC) cancers and to some extent in skin (SKCM) and thymus (THYM) cancers. These cancer types could therefore be particularly interesting for treatment with a Gal1/ Raf-interface inhibitor, which would abrogate the stimulating effect of Gal1 on oncogenic H-Ras nanoclustering and thus MAPK-signalling.
(**b**) Displacement of F-L5UR (5 nM) from Gal1 (5 μM) by Anginex; n = 2.

(**c**) Control showing negligible binding of 10 nM F-L5UR to GST measured by fluorescence polarisation; n = 3.
(**d**) Eu-L5URcore (29 nM) binding to B-RBD measured in the QRET assay using time-resolved luminescence detection; n = 2.

(**e**) Eu-L5URcore (29 nM) binding to Gal1 measured in the QRET assay using time-resolved luminescence detection; n = 2.

(**f**) Displacement of F-L5UR (5 nM) from C-RBD (200 nM) by L5UR-derived peptides; n = 3.

(**g**) Circular dichroism spectra of 25 μM of indicated L5UR-derived peptides in 1x PBS (pH 7.5).

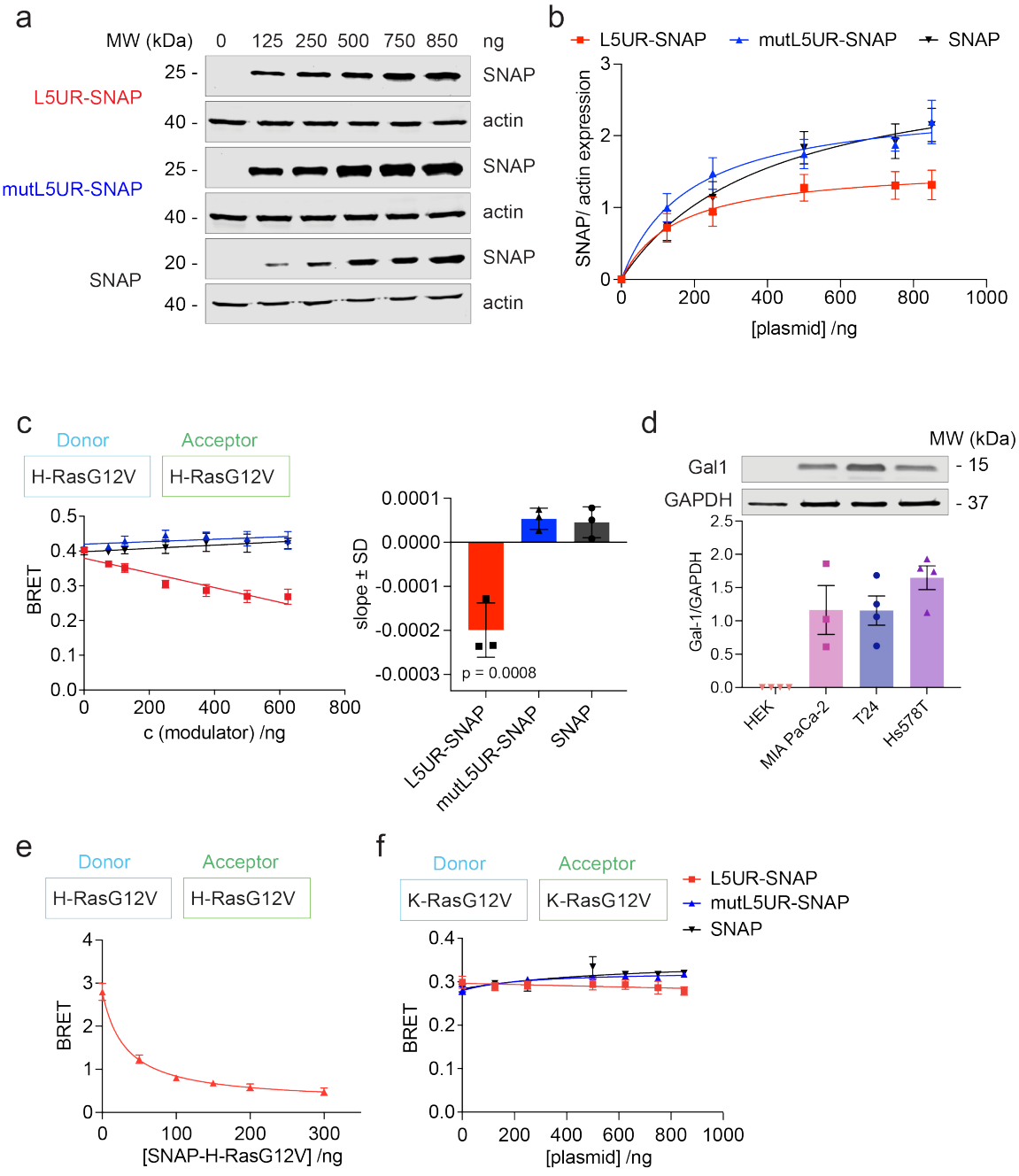

Supplementary Figure 3. Related to main Figures 3, 4 and 5.
(**a, b**) Representative immunoblots (c) and quantification of all repeats (d) showing dose-dependent expression of L5UR constructs (48 h); n = 3.
(**c**) Effect of L5UR construct expression (48 h) on H-RasG12V nanoclustering-BRET (donor:acceptor plasmid ratio = 1:5); n = 3.
(**d**) Immunoblot data and quantification of endogenous Gal1 expression in employed cell lines; n = 3.
(**e**) Effect of SNAP-H-RasG12V on NanoLuc/ mNeonGreen-H-RasG12V nanoclustering-BRET (donor:acceptor plasmid ratio = 1:5); n = 3.
(**f**) Negligible effect of L5UR construct expression (48 h) on K-RasG12V nanoclustering-BRET (donor:acceptor plasmid ratio = 1:10); n = 3.

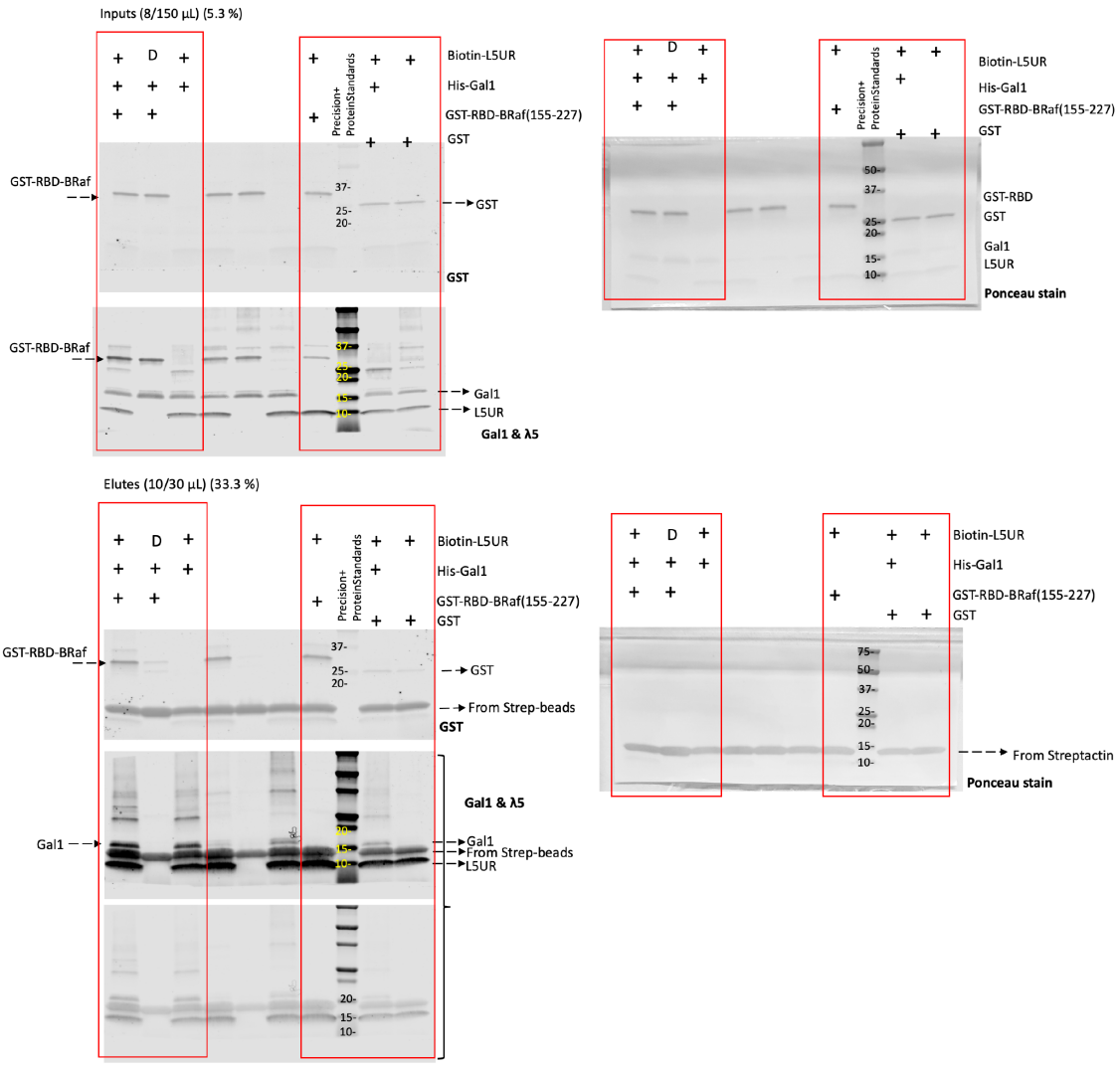

Supplementary Figure 4. Original Western blotting data of Figure 2c, repeat 1.

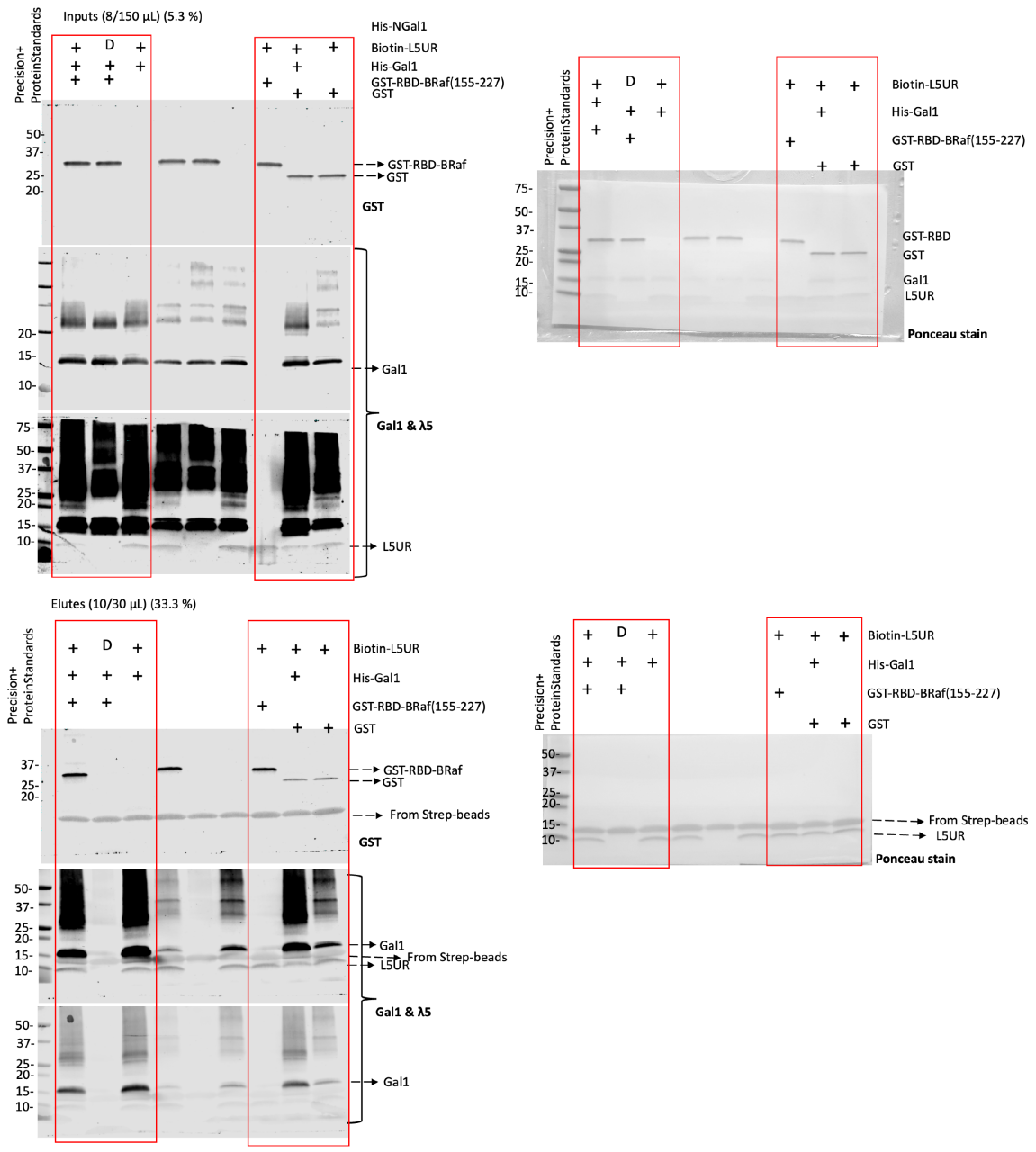

Supplementary Figure 5. Original Western blotting data of Figure 2c, repeat 2.

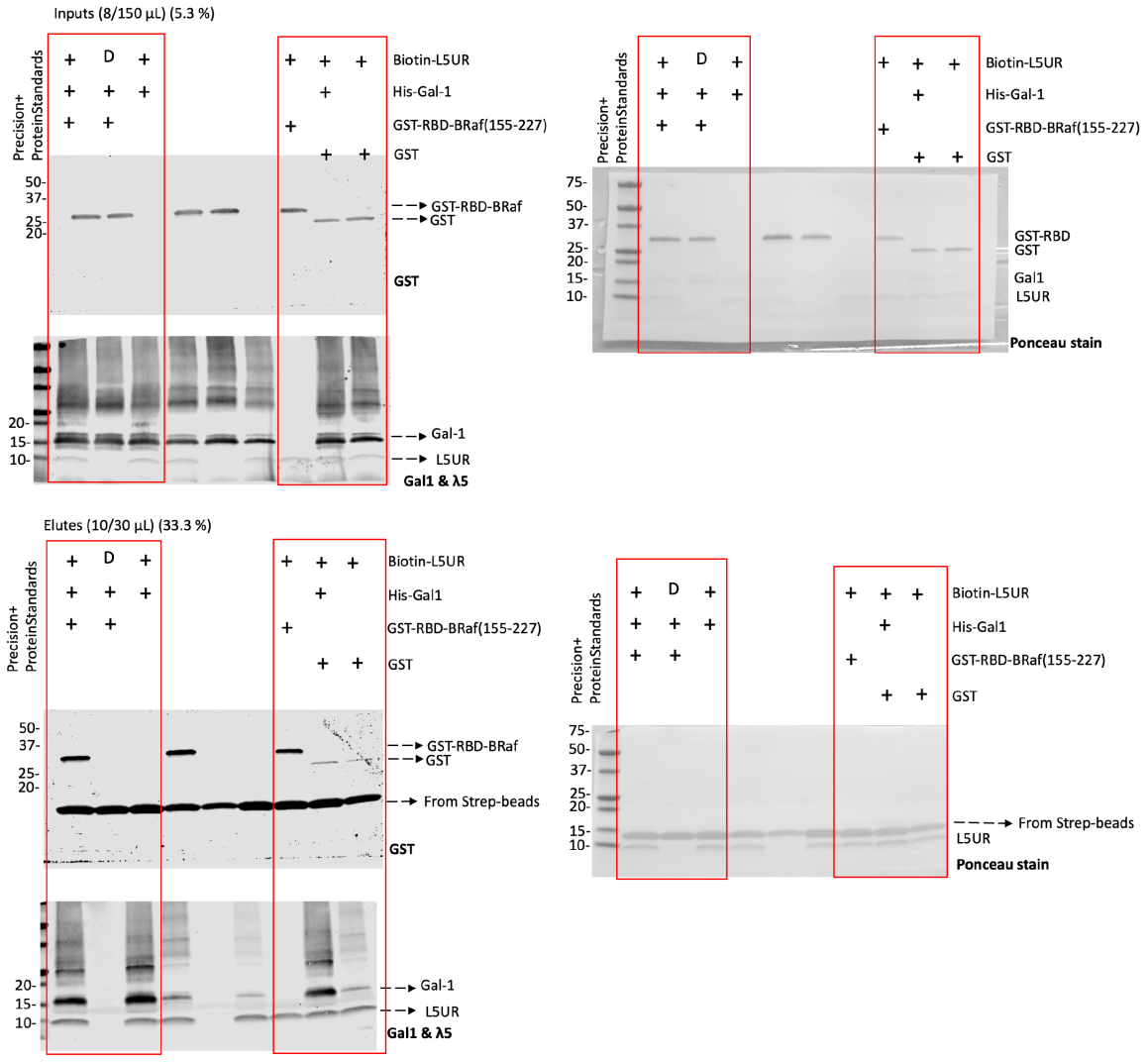

Supplementary Figure 6. Original Western blotting data of Figure 2c repeat 3.

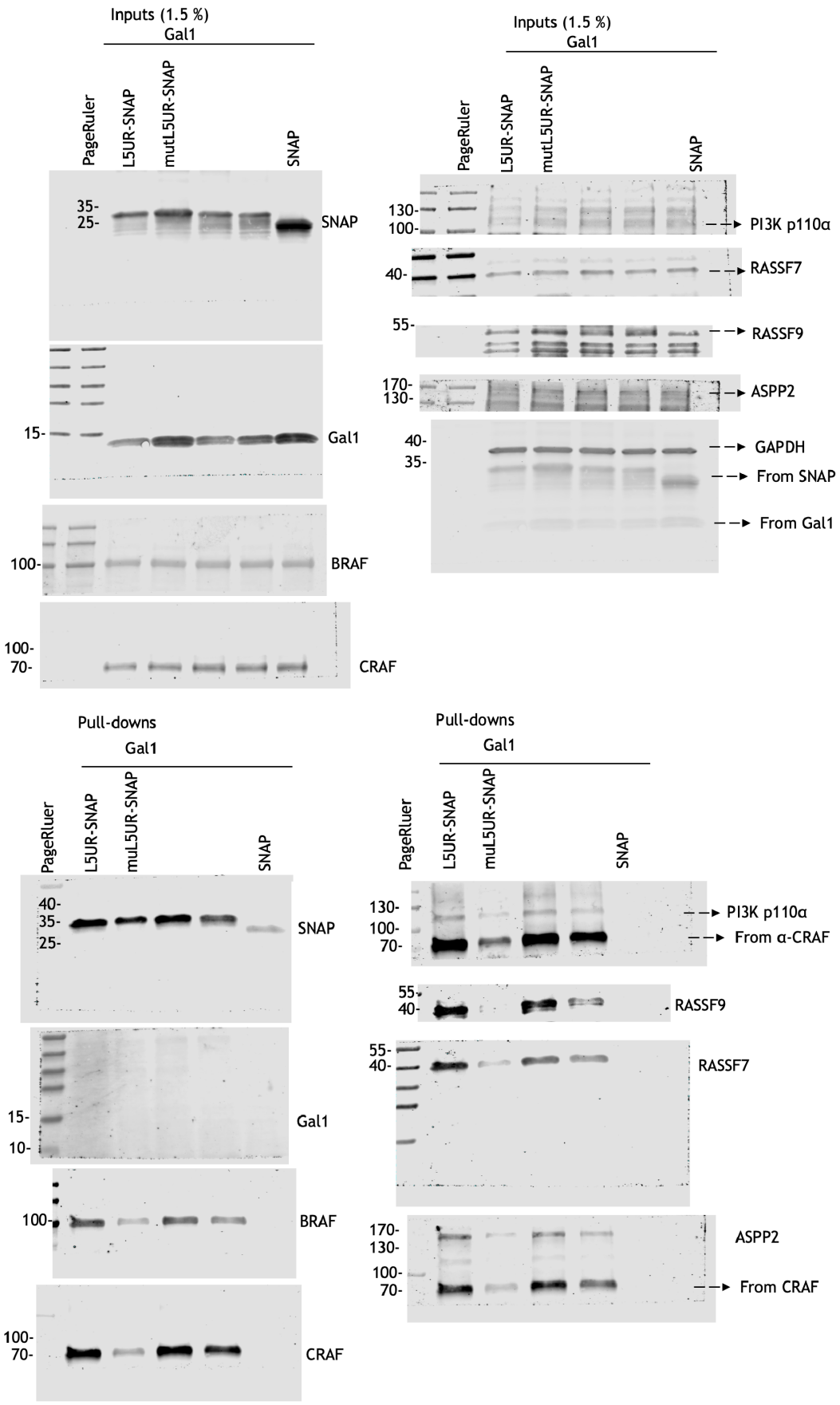

Supplementary Figure 7. Original Western blotting data of Figure 3e.

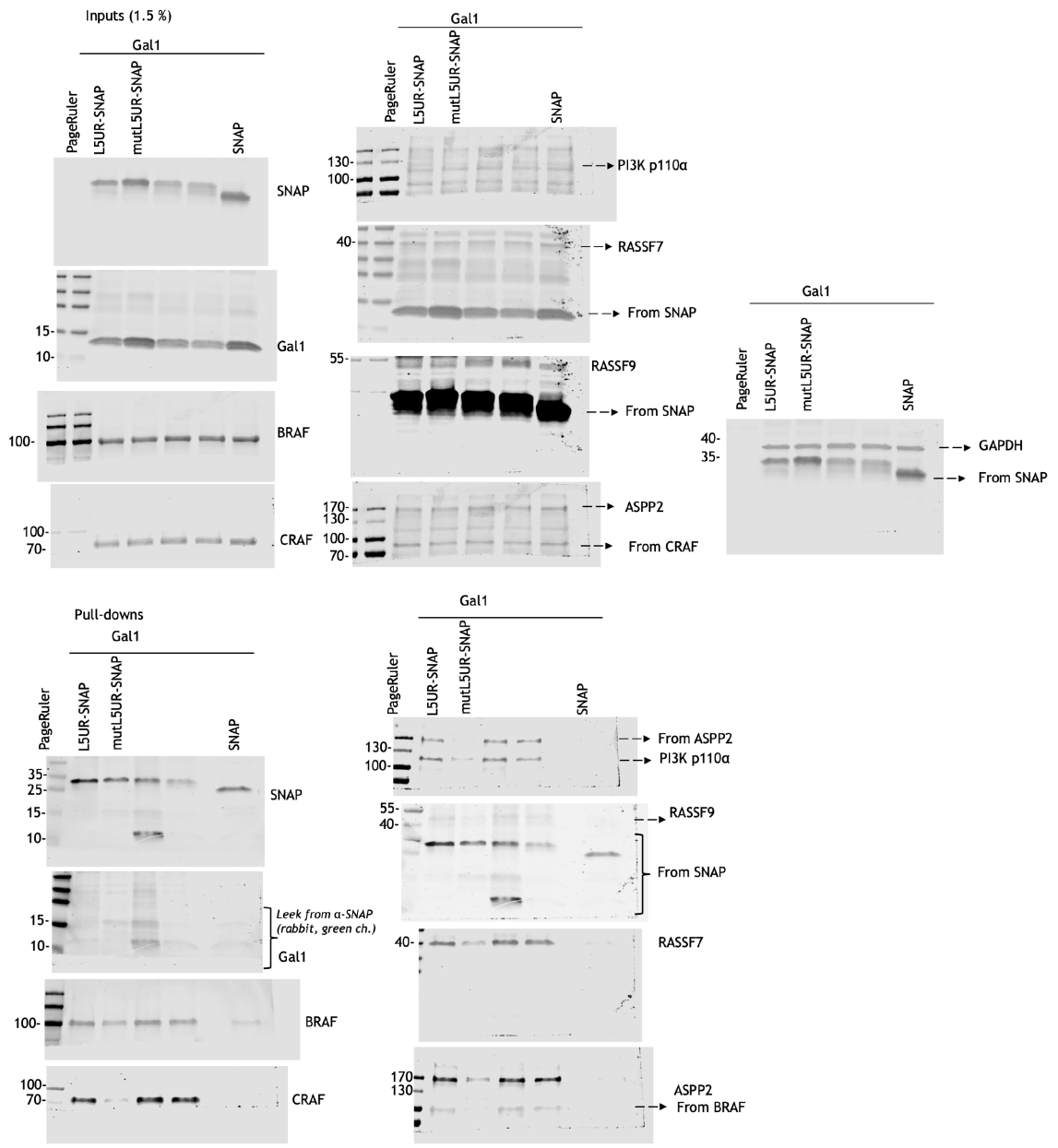

Supplementary Figure 8. Original Western blotting data of Figure 3e.

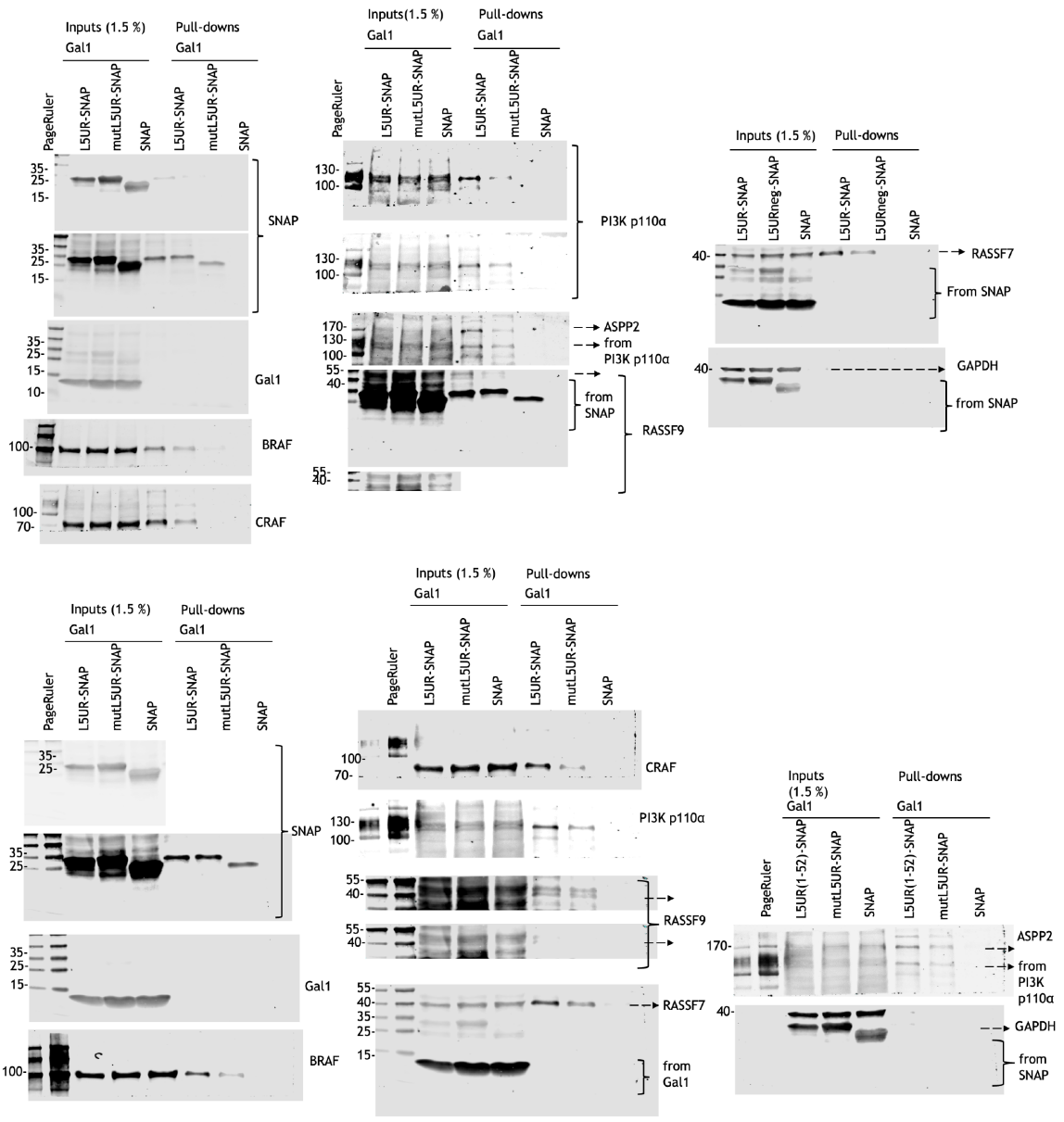

Supplementary Figure 9. Original Western blotting data of Figure 3e.

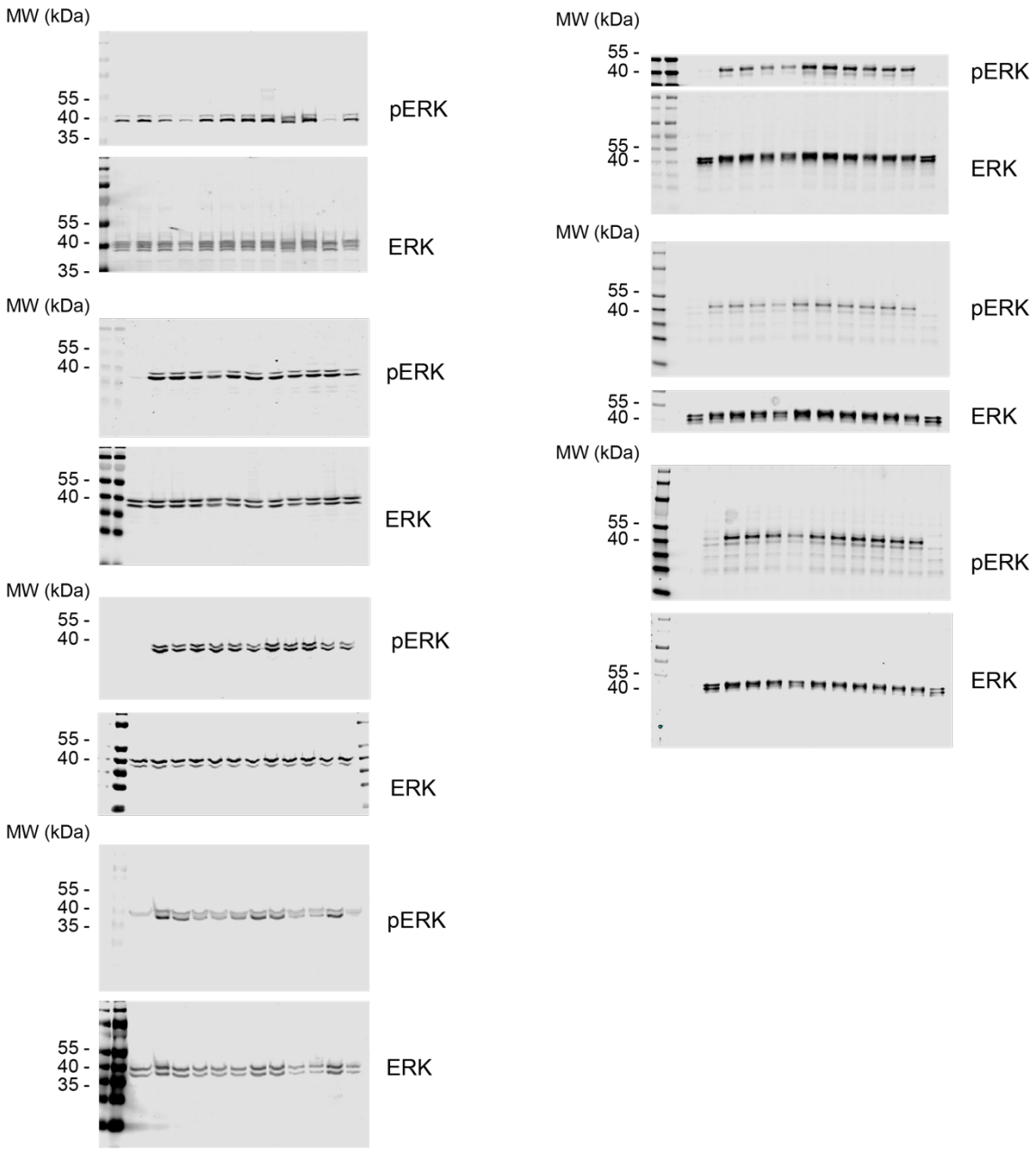

Supplementary Figure 10. Original Western blotting data of Figure 5a.

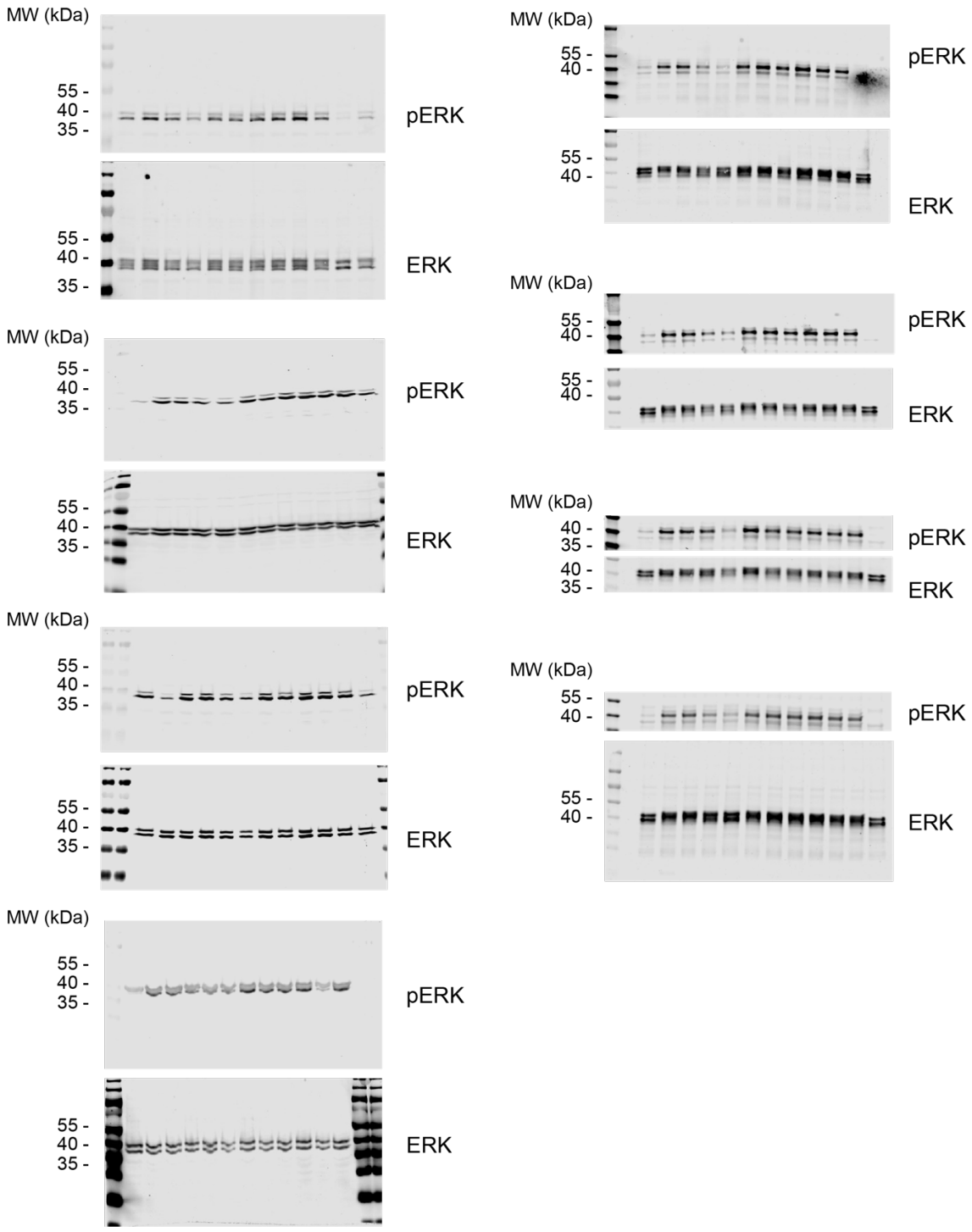

Supplementary Figure 11. Original Western blotting data of Figure 5b.

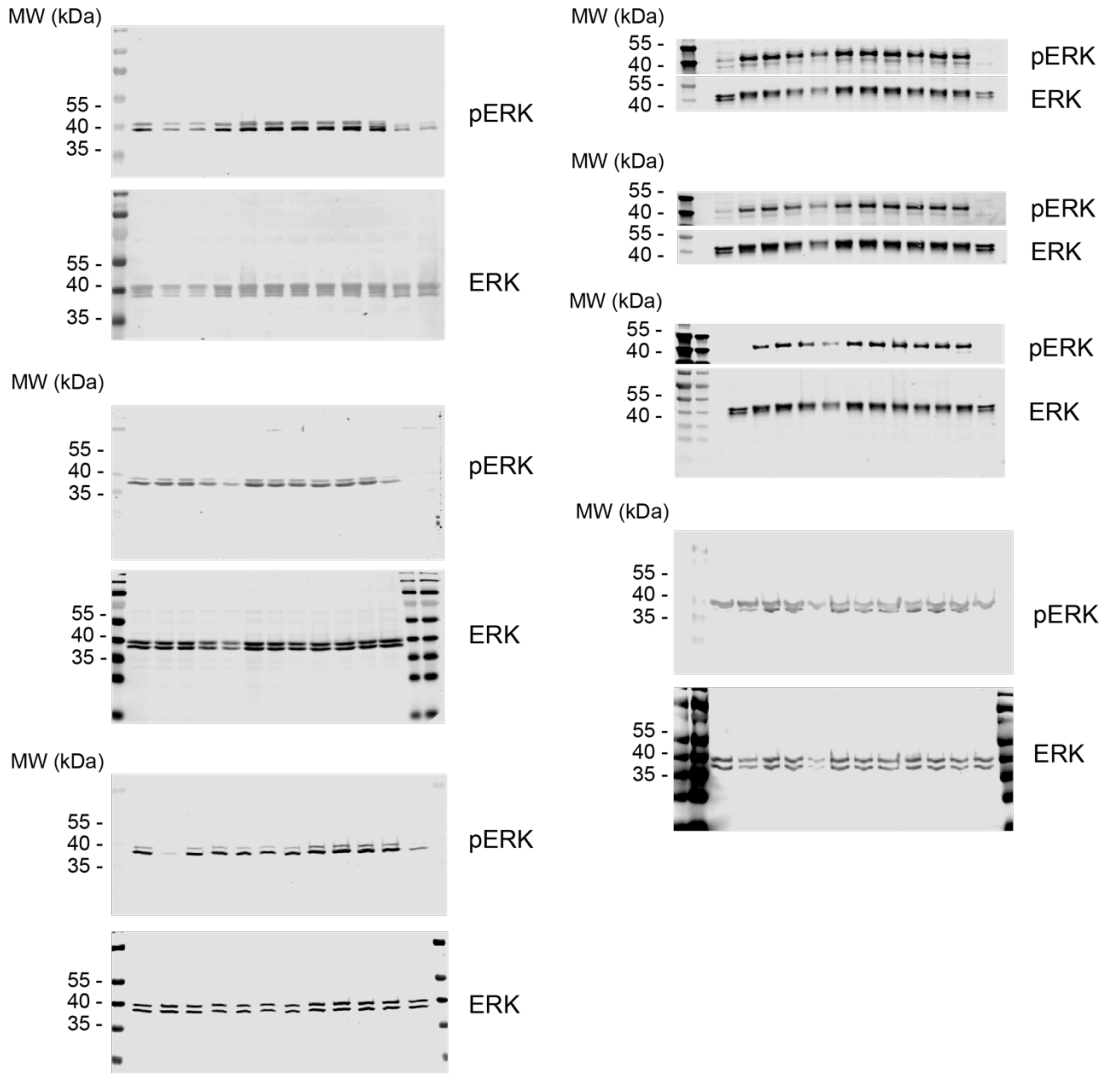

Supplementary Figure 12. Original Western blotting data of Figure 5c.

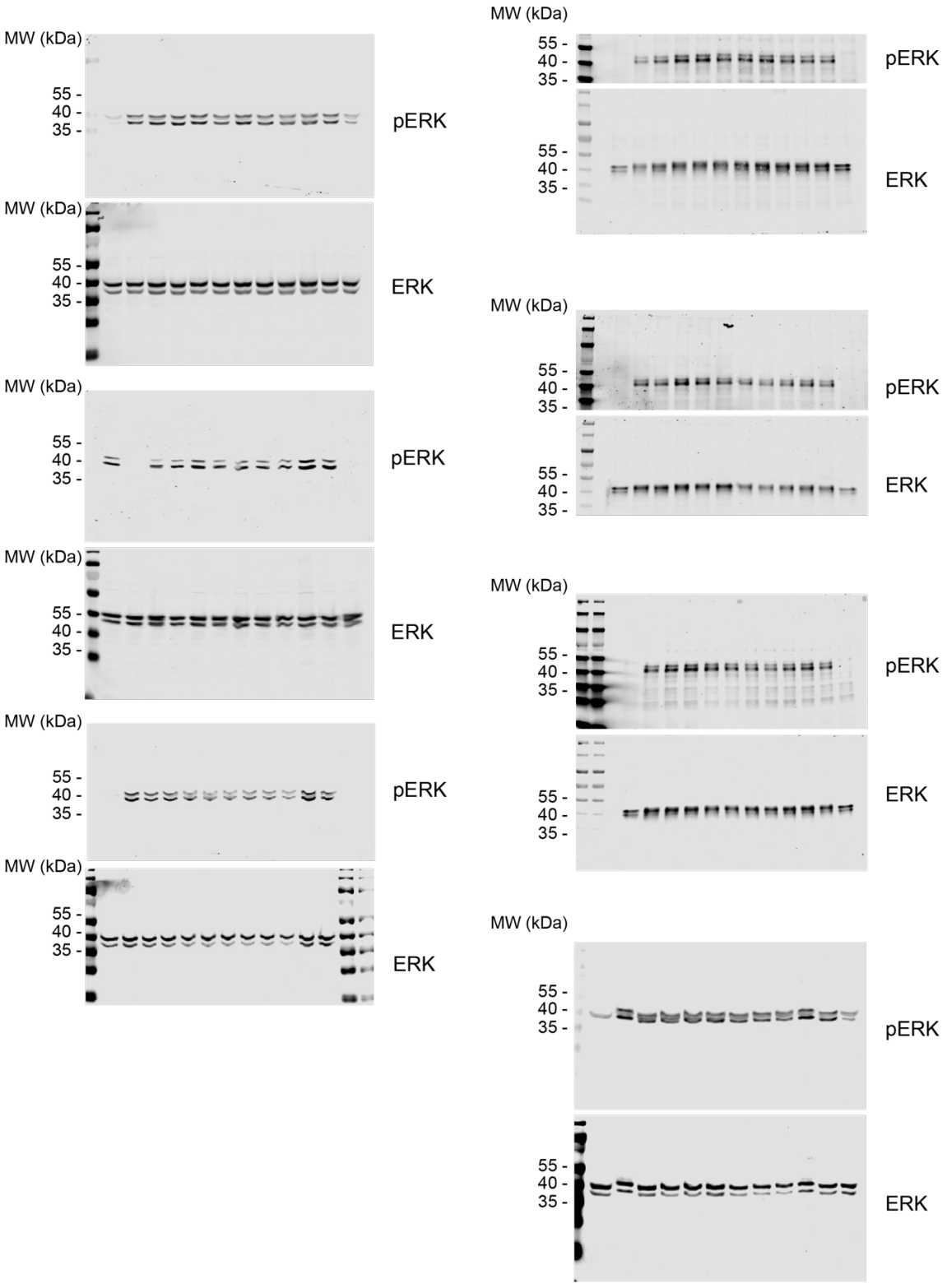

Supplementary Figure 13. Original Western blotting data of Figure 5d.

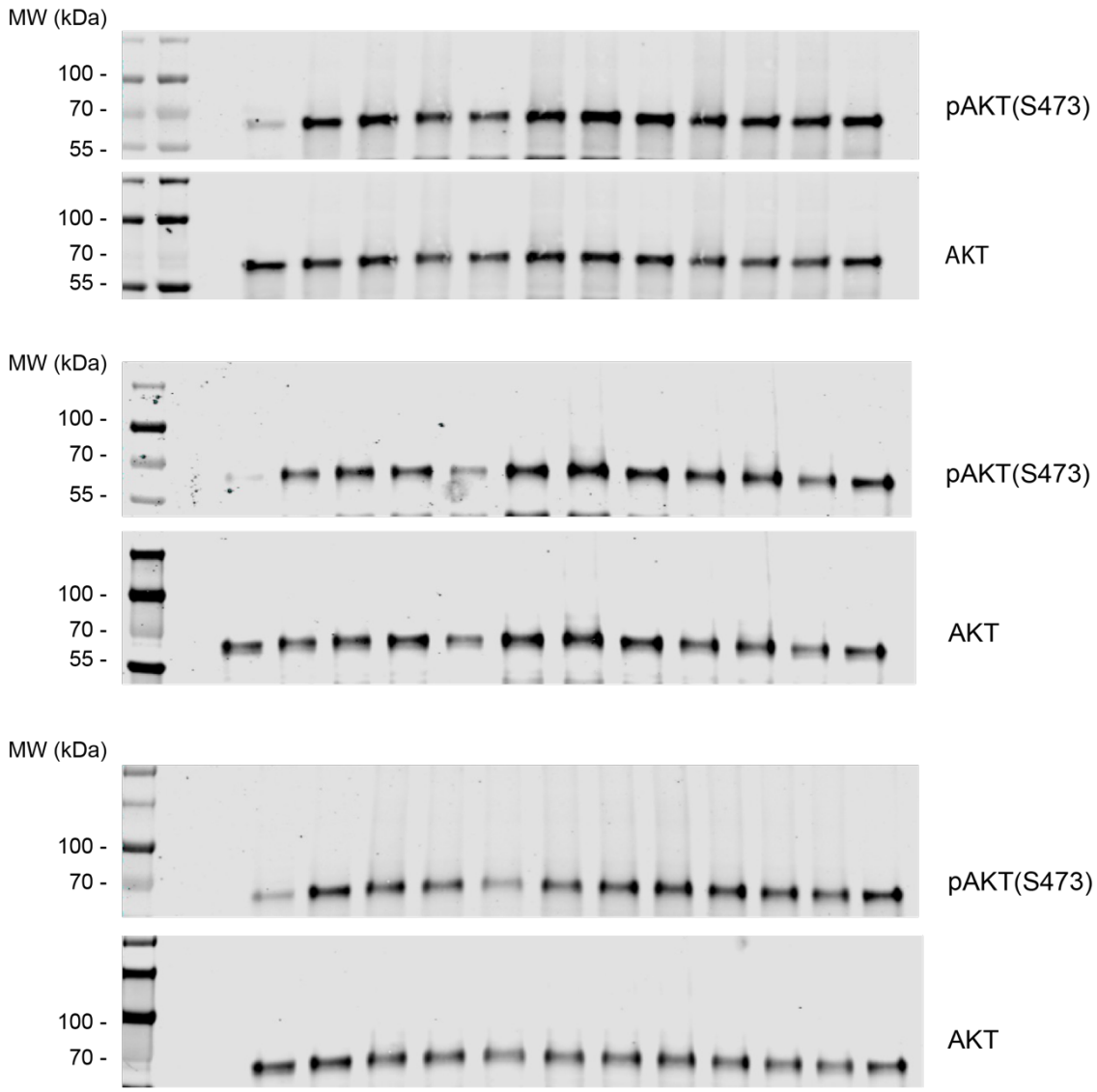

Supplementary Figure 14. Original Western blotting data of Figure 5e.

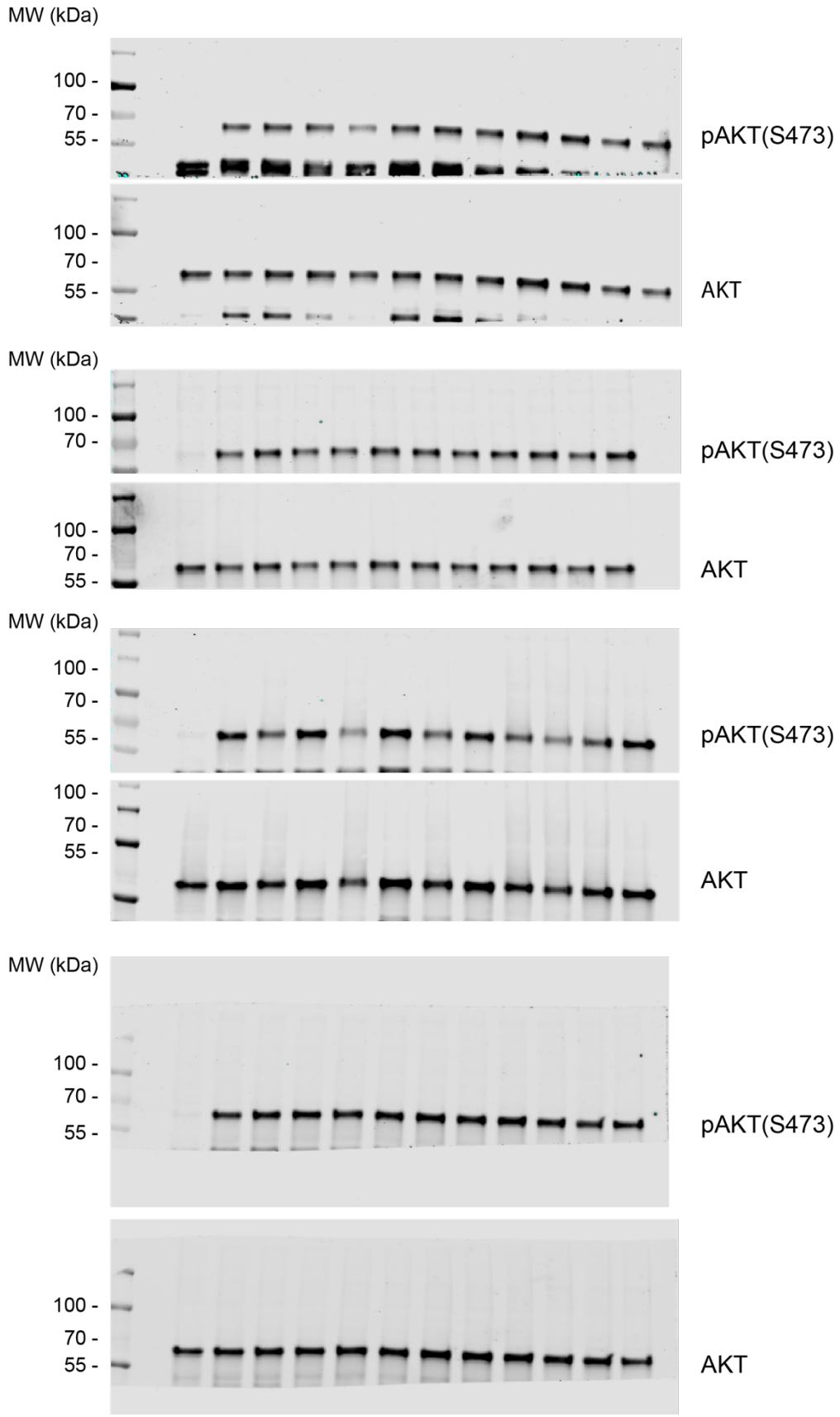

Supplementary Figure 15. Original Western blotting data of Figure 5f.

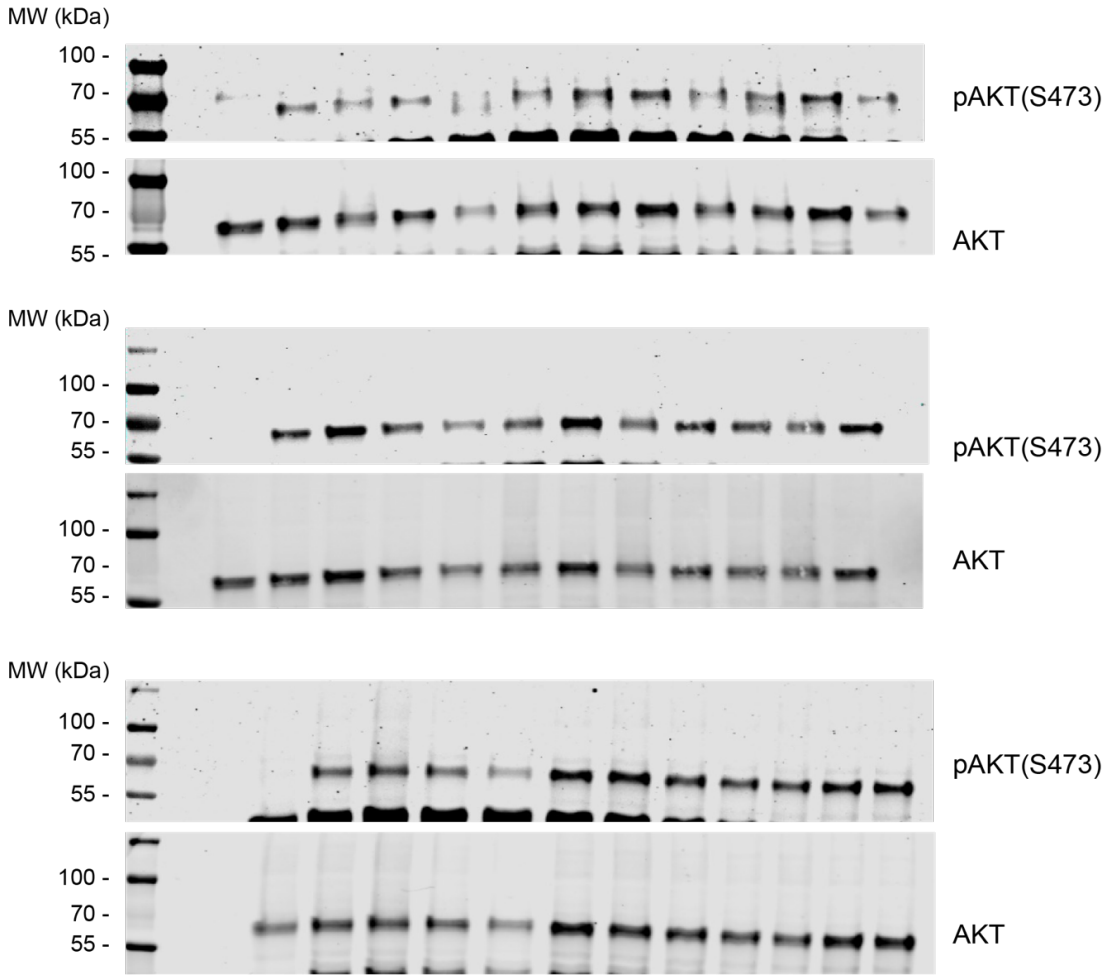

Supplementary Figure 16. Original Western blotting data of Figure 5g.

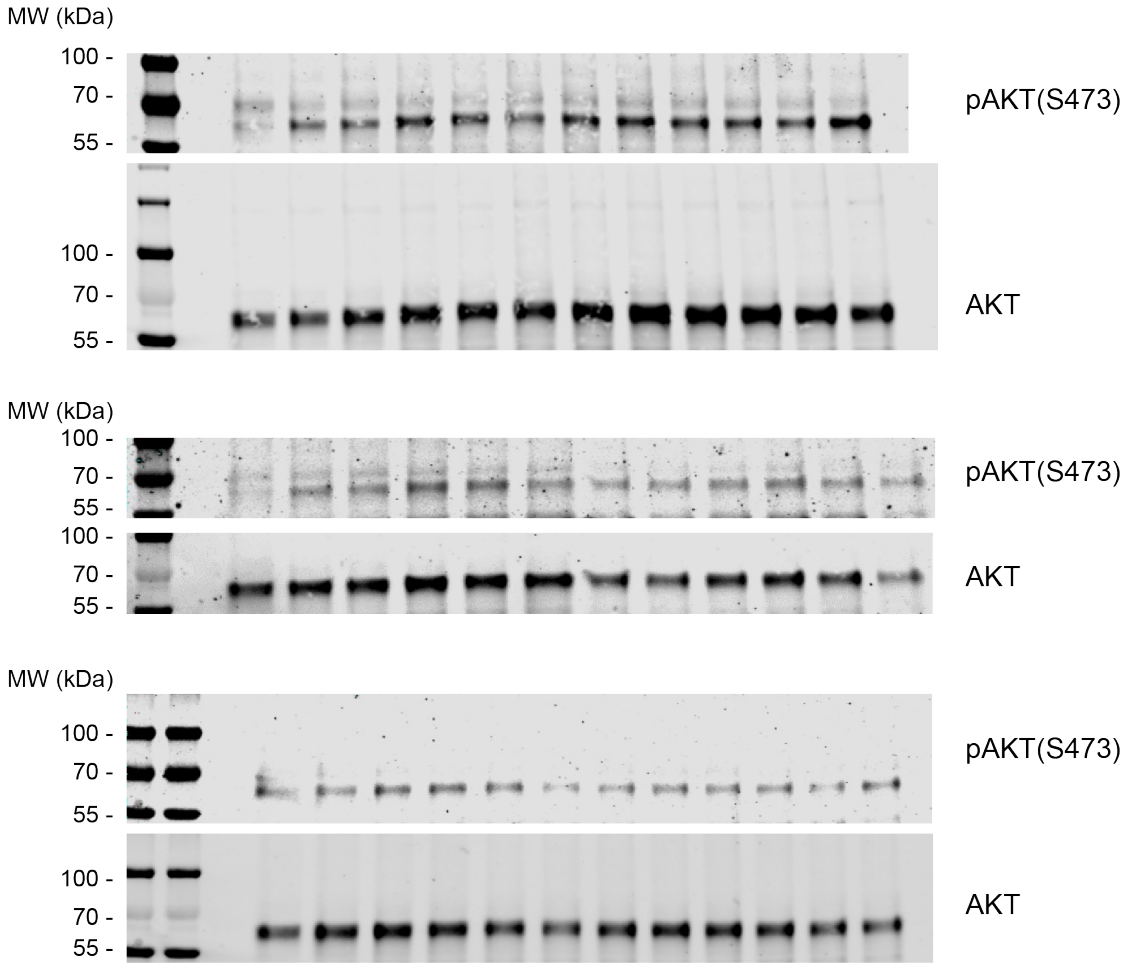

Supplementary Figure 17. Original Western blotting data of Figure 5h.

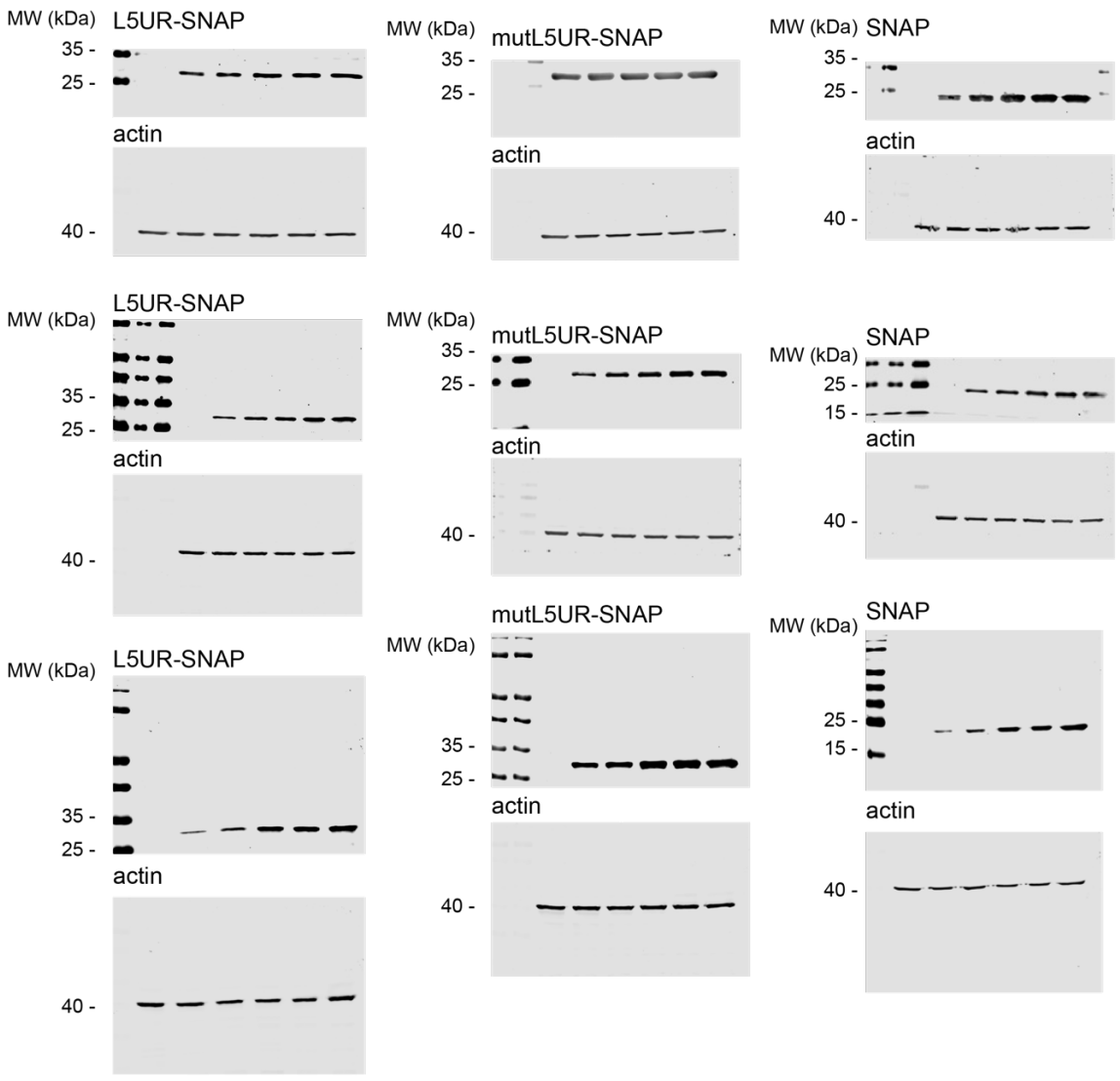

Supplementary Figure 18. Original Western blotting data of Figure S3a.

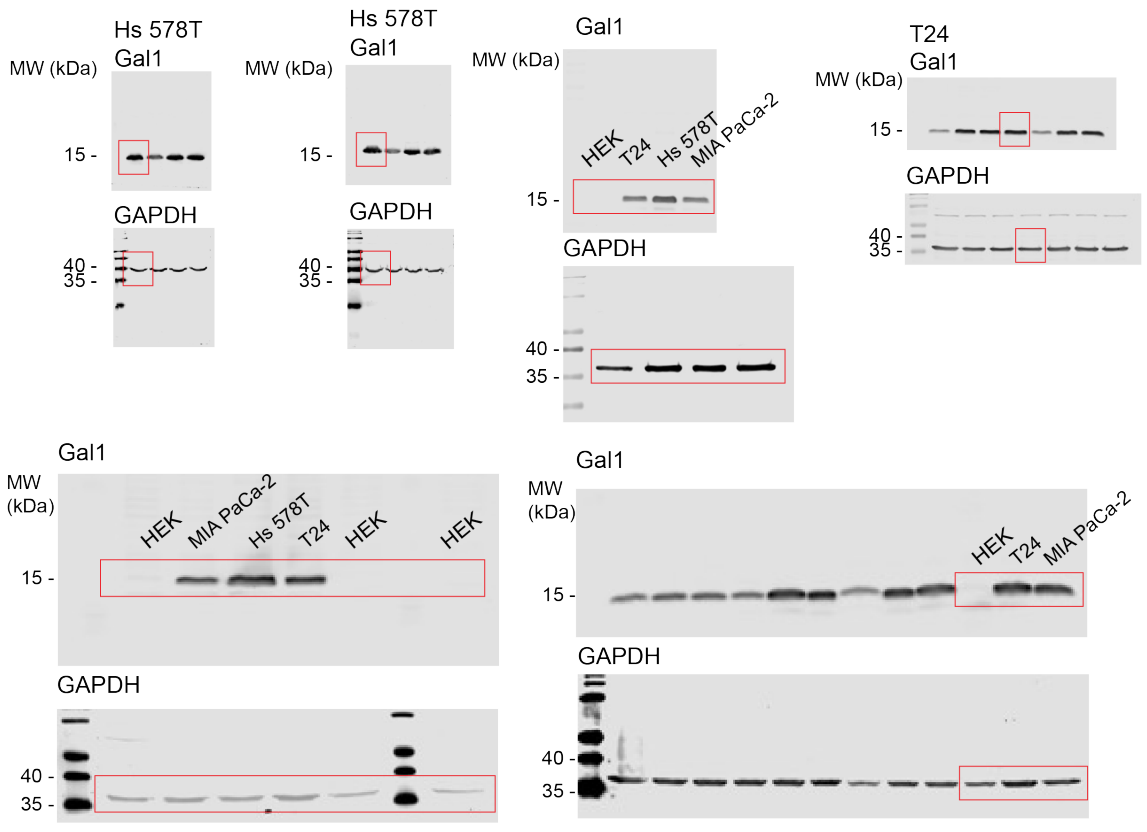

Supplementary Figure 19. Original Western blotting data of Figure S3d.

Supplementary Table 1: Materials and equipment employed in the study.

REAGENT or RESOURCE	SOURCE	IDENTIFIER
Antibodies		
mouse monoclonal anti-Galectin 1 (E2)	Santa Cruz Biotechnology	sc-166619 RRID:AB_2136629
mouse monoclonal Lambda 5 (A-1), λ5	Santa Cruz Biotechnology	sc-398932 RRID: N/A
rabbit polyclonal GST	Cell Signaling	2622S RRID: N/A
rabbit polyclonal anti-SNAP	New England Biolabs	P9310S RRID:AB_10631145
mouse monoclonal anti-B-Raf (F-7)	Santa Cruz Biotechnology	sc-5284 RRID:AB_626760
rabbit polyclonal anti-C-Raf (C-12)	Santa Cruz Biotechnology	sc-133 RRID:AB_632305
rabbit polyclonal anti-PI3K p110α	Cell Signaling	4255 RRID:AB_659888
mouse monoclonal anti-RASSF7 (C-6)	Santa Cruz Biotechnology	sc-374431 RRID:AB_10989731
rabbit polyclonal anti-RASSF9	Invitrogen	PA5-58878 RRID: N/A
rabbit polyclonal anti-ASPP2	Bethyl	A300-819A RRID:AB_597858
rabbit polyclonal anti-GAPDH	Sigma-Aldrich	G9545, RRID:AB_796208
mouse monoclonal anti-β-actin	Sigma-Aldrich	A5441 RRID:AB_476744
mouse monoclonal anti-phospho-p44/42 MAPK (Erk1/2) (Thr202/Tyr204) (E10)	Cell Signaling Technology	9106 RRID:AB_331768
rabbit polyclonal anti 44/42 MAPK (Erk1/2)	Cell Signaling Technology	9102 RRID:AB_330744
rabbit monoclonal anti-phospho-AKT(S473) (D9E)	Bioke	4060S RRID: N/A
mouse monoclonal anti-AKT(pan) (40D4)	Bioke	2920S RRID: N/A
IRDye 680LT Goat anti-Mouse IgG1-Specific Secondary Antibody	Li-Cor Biosciences	926-68052 RRID:AB_2783644
IRDye 800CW Goat anti-Mouse IgG Secondary Antibody	Li-Cor Biosciences	926-32210 RRID:AB_621842
IRDye 680RD Goat anti-Rabbit IgG Secondary Antibody	Li-Cor Biosciences	926-68071, RRID:AB_10956166
IRDye 800CW Goat anti-Rabbit IgG Secondary Antibody	LI-Cor Biosciences	926-32212, RRID:AB_621847
Bacterial and virus strains		
E. coli DH10B	New England Biolabs	C3019I
E. coli BL21 Star (DE3)pLysS	Thermo Fisher Scientific	C602003
Biological samples		
N/A	N/A	N/A
Chemicals, peptides, and recombinant proteins		
Fluorescein-isothiocyanate labelled L5UR	Pepmic Co., China	N/A
L5UR	Pepmic Co., China	N/A
mutL5UR	Pepmic Co., China	N/A
L5URcore	Pepmic Co., China	N/A
Biotinylated L5UR	This paper	N/A
TAT-L5URcore	This paper	N/A

TAT-mutL5URcore	This paper	N/A
TAT	This paper	N/A
Eu-L5URcore	This paper	N/A
Benzethonium chloride	Sigma-Aldrich	53751-50G; CAS121-54-0
Trametinib	MedChem Express	SC-364639; CAS871700-17-3
Pierce Protease Inhibitor Mini Tablets, EDTA-free	Thermo Scientific	#A32955
PhosSTOP	Roche	04 906 837 001
Critical commercial assays		
Gateway LR Clonase II enzyme mix	Thermo Fisher Scientific	11791020
jetPRIME transfection reagent	Polyplus	101000046
Coelenterazine 400a; 2,8-Dibenzyl-6-phenyl-imidazo[1,2a]pyrazin-3-(7H)-one; DeepBlueC	Gold Biotechnology	C-320-1
Coelenterazine h	Sanbio bv	16894-1
alamarBlue cell viability reagent	Thermo Fisher Scientific	DAL1100
SNAP-capture magnetic beads	New England Biolabs	S9145S
Experimental models: Cell lines		
Human cell line, HEK293-EBNA (HEK)	Prof. Florian M. Wurm, EPFL	RRID:CVCL_6974
Human cell line, MIA PaCa-2	ATCC	CRM-CRL-1420, RRID:CVCL_0428
Human cell line, Hs 578T	DSMZ	ACC 781, RRID:CVCL_0332
Human cell line, T24	DSMZ	ACC 376, RRID:CVCL_0554
BHK-21	DSMZ	CCL-10, RRID:CVCL_1914
Experimental models: Organisms/strains		
N/A		
Oligonucleotides		
N/A		
Recombinant DNA		
C413-E36_CMV promoter	3	Addgene, #162927
C453-E04_CMV promoter	3	Addgene, #162973
pDest-305	3	Addgene, #161895
pDest-312	3	Addgene, #161897
pDest-527		Addgene, #11518
C231-E13_RLuc8-stop	3	Addgene, FNL Combinatorial Cloning Platform, kit #1000000211
C511-E03_RLuc8-no stop	3	Addgene, FNL Combinatorial Cloning Platform, kit #1000000211
pDONR235-GFP2_stop	4	N/A
pDONR257-GFP2_no stop	4	N/A
Hs. K-Ras4B G12V (mutated P01116-2)	RAS mutant collection V2.0, RAS-Initiative	Addgene, #83132
Hs. H-Ras G12V (mutated P01112-1)	RAS mutant collection V2.0, RAS-Initiative	Addgene, #83184
Hs. ARAF (P10398)	RAS mutant collection V2.0, RAS-Initiative	Addgene, #70293

Hs. BRAF (P15056)	RAS mutant collection V2.0, RAS-Initiative	Addgene, #70299
Hs. RAF1 (P04049)	RAS mutant collection V2.0, RAS-Initiative	Addgene, #70497
pDONR221-hGal1 (P09382)	This paper	N/A
pDONR221-hNGal1 (mutated P09382)	This paper	N/A
pDONR221-C-RBD (P04049)	GeneCust (Boynes, France)	N/A
pDONR221-B-RBD (aa 155-227 of P15056)	GeneCust (Boynes, France)	N/A
pDest305-CMV-GFP2- K-Ras4BG12V (mutated P01116-2)	4	N/A
pDest305-CMV-RLuc8- K-Ras4BG12V (mutated P01116-2)	4	N/A
pDest305-CMV-GFP2- H-RasG12V (mutated P01112-1)	4	N/A
pDest305-CMV-RLuc8- H-RasG12V (mutated P01112-1)	4	N/A
pDest305-CMV-hGal1 (P09382)	This paper	N/A
pDest305-CMV-RLuc8-Gal1 (P09382)	This paper	N/A
pDest305-CMV-GFP2-Gal1 (P09382)	This paper	N/A
pDest305-CMV-RLuc8-N-hGal1 (mutated P09382)	This paper	N/A
pDest305-CMV-GFP2-N-hGal1 (mutated P09382)	This paper	N/A
pEF-A-RBD-GFP2 (aa 19-91 of P10398)	This paper	N/A
pEF-B-RBD-GFP2 (aa 155-227 of P15056)	This paper	N/A
pEF-C-RBD-GFP2 (aa 56-131 of P04049)	This paper	N/A
pClontech-C-L5UR (P15814-1)	This paper	N/A
pEF-L5UR-SNAP (aa 38-89 of P15814-1)	GeneCust (Boynes, France)	N/A
pEF-mutL5UR-SNAP (mutated aa 38-89 of P15814-1)	GeneCust (Boynes, France)	N/A
pEF-SNAP	GeneCust (Boynes, France)	N/A
pDest305-CMV-GFP2-B-Raf (P15056)	This paper	N/A
pDest305-CMV-GFP2-C-Raf (P04049)	This paper	N/A
pDest305-CMV-GFP2-A-Raf (P10398)	This paper	N/A
pEF-A-RBD-D75A-GFP2 (mutated aa 19-91 of P10398)	This paper	N/A
pEF-B-RBD-D211,213A-GFP2 (mutated aa 155-227 of P15056)	This paper	N/A
mGFP-rtGal1 (P11762)	1	N/A
mRFP-C-RBD (aa 56-131 of P04049)	5	N/A
mGFP-H-RasG12V (mutated P01112-1)	6	N/A
mCherry-H-RasG12V (mutated P01112-1)	7	N/A
mRFP-C-RBD-D117A (mutated, aa 56-131 of P04049)	1	N/A
pcDNA3-rtGal1 (P11762)	8	N/A
pcDNA3-N-rtGal-1 (mutated P11762)	1	N/A

pcDNA-Hygro-Anginex	9, 10	N/A
pDest527-His-hGal1 (P09382)	This paper	N/A
pGEX4T2-B-RBD (aa 155-227 of P15056)	This paper	N/A
pGEX2T-C-RBD (aa 50-134 of P04049)	This paper	N/A
pGEX4T2	Addgene	27458101
pcDNA3.1(-)	ThermoFisher Scientific	V79520
pDest305-CMV-mNeonGreen- H-RasG12V (mutated P01112-1)	This paper	N/A
pDest305-CMV-NanoLuc- H-RasG12V (mutated P01112-1)	This paper	N/A
pcDNA3-RLucF1-BRAF-RLucF2	11	N/A
Software and algorithms		
BREEZE pipeline	12	https://breeze.fimm.fi/
PyMol	The PyMOL Molecular Graphics System	https://pymol.org/2/
GraphPad Prism v9.5.1	GraphPad by Dotmatics,	https://www.graphpad.com/
Other		
CLARIOstar Plus Microplate Reader	BMG LABTECH	https://www.bmglabtech.com/en/clariostar-plus/
Odyssey CLx Infrared Imaging System	LI-COR Biosciences	https://www.licor.com/bio/odyssey-clx/
ÄKTA pure chromatography system	Cytiva	https://www.cytivalifesciences.com/en/us/shop/chromatography/chromatography-systems/akta-pure-p-05844
Elmasonic S 40 H	Elma	https://www.elma-ultrasonic.com/
Tecan Spark multimode microplate reader	Tecan Austria GmbH	https://lifesciences.tecan.com/multimode-plate-reader
Electron microscope	JEOL	JEOL JEM-1400
Inverted microscope AXIO Observer D1	Zeiss	https://www.zeiss.com/microscopy/en/products/light-microscopes/widefield-microscopes/axio-observer-for-life-science-research.html#features
Lambert Instruments FLIM Attachment (LIFA)	Lambert Instruments	https://www.lambertinstruments.com/lifa#lifa-introduction
LM10 Microfluidizer Processor	(Microfluidics, USA)	https://www.microfluidics-mpt.com/microfluidizers/lm10

Supplementary Table 2: Sequences, N-terminal modifications, calculated and found m/z values of synthesized peptides. All the peptides bear a C-terminal amide. (Ac: Acetylated)

Peptide	Sequence	N-term.	Purity / %	m/z calc.	m/z found
L5UR	LLRPTAASQSRALGPGAPGGSSRSSLRSRWGRFLLQRGSWTGPRCWPRGFQS	Ac Biotin-PEG5	90 >95	949.8 1234.6	950.2 $[M+6H]^{+6}$ 1235.4 $[M+5H]^{+5}$
L5URcore	SRSSLRSRWGRFLLQRGSWTGPR	Ac	>95	929.8	930.2 $[M+3H]^{+3}$
L5URcore-nK	KSRSSLRSRWGRFLLQRGSWTGPR	Ac	>95	1458.1	1458.2 $[M+2H]^{+2}$
mutL5URcore	SRSSDEEEGGRESLQRGSWTGPR	Ac	>95	868.7	869.0 $[M+3H]^{+3}$
TAT	GRKKRRQRRRPQ	Ac	>95	555.0	555.1 $[M+3H]^{+3}$
TAT-PEG2-L5URcore	GRKKRRQRRRPQ-PEG2-SRSSLRSRWGRFLLQRGSWTGPR	Ac	>95	648.8	649.1 $[M+7H]^{+7}$
TAT-PEG2-mutL5URcore	GRKKRRQRRRPQ-PEG2-SRSSDEEEGGRESLQRGSWTGPR	Ac	>95	1088.8	1089.3 $[M+4H]^{+4}$

Supplementary Information References

1. Blazevits O*, et al.* Galectin-1 dimers can scaffold Raf-effectors to increase H-ras nanoclustering. *Sci Rep* **6**, 24165 (2016).

2. Elantak L*, et al.* Structural basis for galectin-1-dependent pre-B cell receptor (pre-BCR) activation. *J Biol Chem* **287**, 44703-44713 (2012).

3. Wall VE, Garvey LA, Mehalko JL, Procter LV, Esposito D. Combinatorial assembly of clone libraries using site-specific recombination. *Methods Mol Biol* **1116**, 193-208 (2014).

4. Okutachi S*, et al.* A Covalent Calmodulin Inhibitor as a Tool to Study Cellular Mechanisms of K-Ras-Driven Stemness. *Front Cell Dev Biol* **9**, 665673 (2021).

5. Abankwa D, Gorfe AA, Inder K, Hancock JF. Ras membrane orientation and nanodomain localization generate isoform diversity. *Proc Natl Acad Sci U S A* **107**, 1130-1135 (2010).

6. Abankwa D*, et al.* A novel switch region regulates H-ras membrane orientation and signal output. *EMBO J* **27**, 727-735 (2008).

7. Solman M*, et al.* Specific cancer-associated mutations in the switch III region of Ras increase tumorigenicity by nanocluster augmentation. *Elife* **4**, e08905 (2015).

8. Paz A, Haklai R, Elad-Sfadia G, Ballan E, Kloog Y. Galectin-1 binds oncogenic H-Ras to mediate Ras membrane anchorage and cell transformation. *Oncogene* **20**, 7486-7493 (2001).

9. Thijssen VL*, et al.* Galectin-1 is essential in tumor angiogenesis and is a target for antiangiogenesis therapy. *Proc Natl Acad Sci U S A* **103**, 15975-15980 (2006).

10. Brandwijk RJ, Dings RP, van der Linden E, Mayo KH, Thijssen VL, Griffioen AW. Anti-angiogenesis and anti-tumor activity of recombinant anginex. *Biochem Biophys Res Commun* **349**, 1073-1078 (2006).

11. Rock R*, et al.* BRAF inhibitors promote intermediate BRAF(V600E) conformations and binary interactions with activated RAS. *Sci Adv* **5**, eaav8463 (2019).

12. Potdar S*, et al.* Breeze 2.0: an interactive web-tool for visual analysis and comparison of drug response data. *Nucleic Acids Res*, (2023).

3. Manuscript (III)

Protocol to measure and analyze protein interactions in mammalian cells using Bioluminescence Resonance Energy Transfer

Carla Jane Duval*, **Candy Laura Steffen***, Karolina Pavic, Daniel Kwaku Abankwa

* These authors contributed equally.

Status: accepted in STAR protocols on 05.09.2024, preprint available on bioRxiv

doi: https://doi.org/10.1101/2024.07.05.602189

Personal contributions of Candy Laura Steffen

- Designed and analysed experiments and data to generate the below listed figures submitted for this manuscript:
  - Graphical abstract
  - Table 1
  - Fig. 2
  - Fig. 3
  - Fig. 4
- Implicated in discussions, drafting of corresponding data contribution.
- Involved in writing and conceptualization of the study.
- The personal contributions of all authors to the manuscript are listed in the author's contribution section at the end of the corresponding manuscript.

STAR ✦ Protocols

CellPress

Protocol to measure and analyze protein interactions in mammalian cells using Bioluminescence Resonance Energy Transfer

Carla Jane Duval[1,2,3,*], **Candy Laura Steffen**[1,2], **Karolina Pavic** [1] **and Daniel Kwaku Abankwa**[1,4,**]

[1]Cancer Cell Biology and Drug Discovery Group, Department of Life Sciences and Medicine, University of Luxembourg, 4362 Esch-sur-Alzette, Luxembourg

[2]These authors contributed equally

[3]Technical contact

[4]Lead contact

* Correspondence: carla.duval@uni.lu

**Correspondence: daniel.abankwa@uni.lu

Summary

Bioluminescence resonance energy transfer (BRET) allows to quantitate protein interactions in intact cells. Here, we present a protocol for measuring BRET due to transient interactions of oncogenic K-RasG12V in plasma membrane nanoclusters of HEK293-EBNA cells. We describe steps for seeding, transfecting and replating cells. We then detail procedures for their preparation for BRET-measurements on a CLARIOstar microplate reader and detailed data analysis. For complete details on the use and execution of this protocol, please refer to Steffen et al., 2024 [1].

Graphical abstract

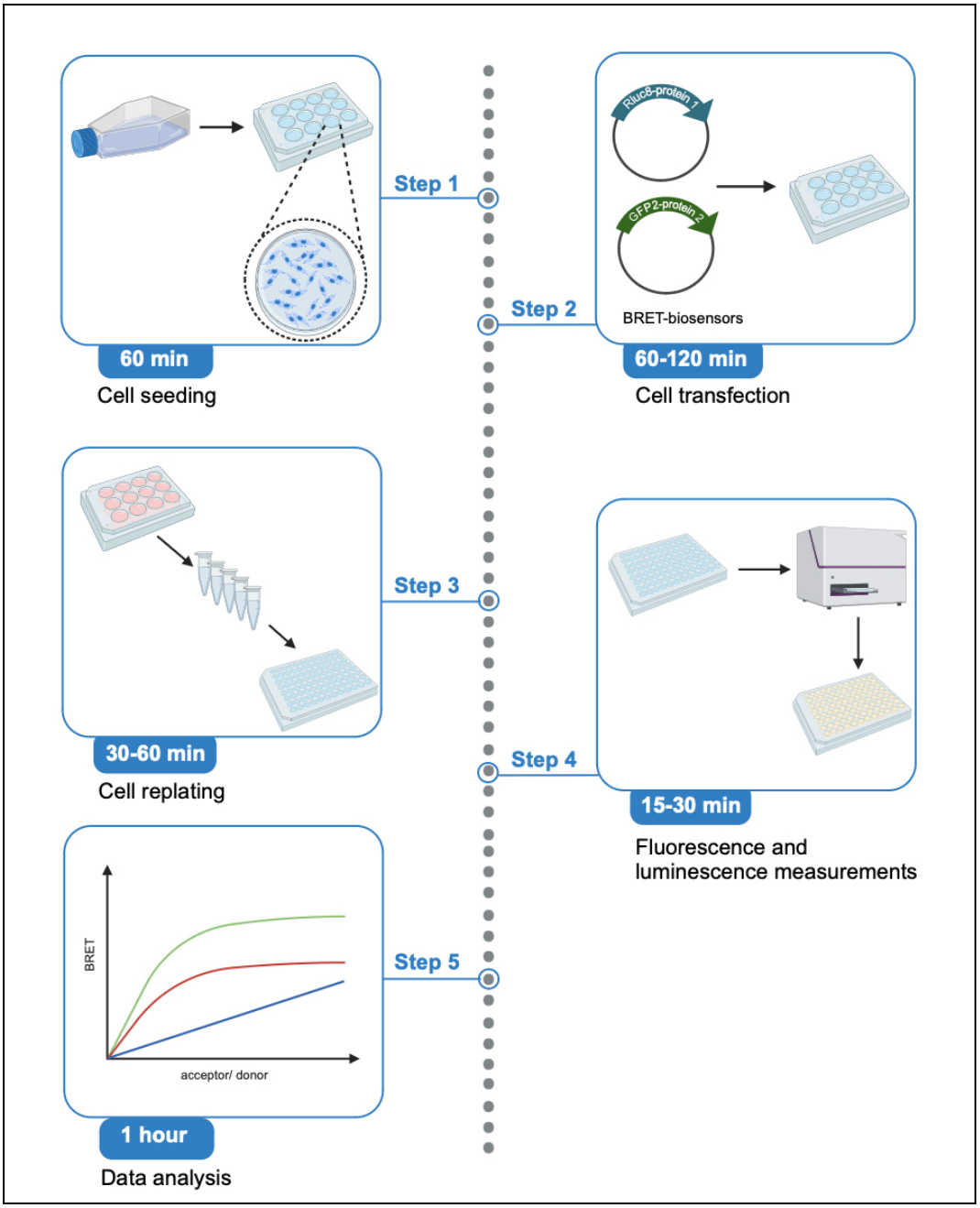

Before you begin

Background

Bioluminescence resonance energy transfer (BRET) enables quantitative molecular interaction experiments in the native cellular environment. BRET has thus been used to investigate diverse protein interactions in the cytosol, nucleus and cellular membranes [2].

BRET refers to the radiation-free transfer of the donor energy, provided in our case by the Renilla luciferase mutant RLuc8-catalyzed conversion of the luciferase substrate coelenterazine 400a, to the acceptor, green fluorescent protein 2 (GFP2). The donor and acceptor together form the BRET-pair, for which various combinations have been established, including more recently NanoLuc and mNeonGreen [3]. For BRET to occur, several conditions must be fulfilled, such as an overlap of the emission spectrum of the donor and excitation spectrum of the acceptor [2]. Furthermore, donor and acceptor must be in molecular proximity (here 4 - 12 nm) for a change in the BRET-signal, which is the emission by the acceptor after the donor excitation is generated from the conversion of the substrate by Rluc8 [4].

By genetically fusing proteins or their domains to donor and acceptor, BRET-biosensors can be constructed, where the interaction is mediated by the fused proteins. As an example, we use the Rluc8-K-RasG12V/ GFP2-K-RasG12V BRET-biosensor, where BRET emerges due to the transient approximation of K-RasG12V in proteo-lipid complexes at the plasma membrane, called nanocluster [5]. Design and optimization of such biosensors can be challenging and was discussed elsewhere [6].

Our protocol provides detailed instructions on conducting donor saturation-titration BRET experiments on a conventional microplate reader that can detect both fluorescence and luminescence. In these experiments the BRET-ratio is plotted as a function of the acceptor/ donor-ratio, where a constant amount of RLuc8-tagged donor-construct is co-expressed with increasing amounts of GFP2-tagged acceptor-construct. While it is common to plot the BRET-ratio against the plasmid ratio of transfected BRET-constructs, the plasmid ratio does not correspond to the actual molecular acceptor/ donor-ratio. It is therefore preferrable to plot against the expression signal ratio, as we explain in more detail in the expected outcomes section. To obtain the expression signal ratio, the acceptor fluorescence signal is measured and compiled with the donor-luminescence signal. To calculate the BRET-ratio, the donor- and BRET-signal of the BRET-biosensor sample and a donor-only control are compiled. Detection channels for all raw signals are set up on the plate reader, which is in our case a CLARIOstar microplate reader. Classically, the BRETmax- and BRET50-values are determined from fitting a saturation function to the BRET-ratio *vs.* expression signal ratio plot. Both values essentially characterize the strength or probability of the interaction [7]. However, true saturation is typically not reached in cells and we therefore introduced the BRETtop value, which is the highest BRET-ratio within a defined range of acceptor/ donor-expression signal ratios [8].

Preparation

1. Prepare mammalian expression vectors encoding donor- and acceptor- constructs.
   Note: New constructs require significant optimization and testing for uncompromised biological activity. Our example BRET-biosensor, RLuc8-K-RasG12V/ GFP2-K-RasG12V, was constructed by multi-site gateway cloning [9].

2. Prepare cell culture medium and coelenterazine 400a substrate needed for the assay.

3. Verify that your fluorescence and luminescence microplate reader allows for the definition of three BRET-pair specific detection channels for the acceptor- (excitation at 405 ± 10 nm, emission at 515 ± 10 nm), donor- (emission at 410 ± 40 nm), and the BRET-signal (emission at 515 ± 40 nm) (**Figure 1**), and has ideally an injector for dispensing microliter amounts of the luciferase substrate to 96-well plates.
   Note: We here describe the setup and operation using a CLARIOstar microplate reader for the RLuc8/ GFP2 BRET-pair.
   Critical: Any other plate reader employed for this protocol needs to allow for the setup of three BRET-pair specific detection channels as described in detail in **Part 4**.

Key resources table

REAGENT or RESOURCE	SOURCE	IDENTIFIER
Chemicals, peptides, and recombinant proteins		
Dulbecco's phosphate-buffered saline (PBS) (1 ×)	Thermo Fisher Scientific	Cat# 14040091
Dulbecco's modified Eagle's medium (DMEM)	Thermo Fisher Scientific	Cat# 41965039
Trypsin EDTA (0.05%)	Thermo Fisher Scientific	Cat# 25300054
Fetal bovine serum (FBS)	Thermo Fisher Scientific	Cat# 10270106
Penicillin-Streptomycin (10,000 U/mL)	Thermo Fisher Scientific	Cat# 15140122
L-glutamine (200 mM)	Thermo Fisher Scientific	Cat# 25030024
Dimethyl sulfoxide (DMSO) ≥ 99.5%	VWR	Cat# A3672
ISOTON II diluent	Beckman Coulter	Cat# 8448011
Coelenterazine 400a/ DeepBlue C ™, (2,8-Dibenzyl-6-phenylimidazo[1,2a]pyrazin-3-(7H)-one)	Cayman Chemical	Cat# 16894
Mevastatin	Alfa Aesar	J61357
Critical commercial assays		
jetPRIME	Polyplus-transfection	Cat# 101000001
Lipofectamine RNAiMAX	Invitrogen	Cat# 13778-150
Experimental models: Cell lines		
Human cell line, HEK293-EBNA (HEK)	ATCC	CRL-10852
Oligonucleotides		
human *FNTA* siRNA (Hs_FNTA_6 FlexiTube siRNA) 5'-3'-sequence CCGGGATGCTATTGAGTTAAA	QIAGEN	Cat# SI02661995|S1/ 1027417

Negative control siRNA	QIAGEN	Cat# 1027310 GeneGlobe ID: SI03650325
Recombinant DNA		
pDest305-CMV- RLuc8-K-RasG12V	Okutachi et al., 2021[5]	N/A
pDest305-CMV- GFP2-K-RasG12V	Okutachi et al., 2021[5]	N/A
pDest305-CMV- RLuc8	Okutachi et al., 2021[5]	N/A
pDest312-CMV- GFP2	Okutachi et al., 2021[5]	N/A
pcDNA3.1(-)	ThermoFisher Scientific	V79520
Software and algorithms		
CLARIOstar software	BMG LABTECH	N/A
Microsoft Excel	Microsoft Corporation	N/A
GraphPad Prism	GraphPad Software	N/A
Other		
CO_2 incubator	Panasonic	Cat#MCO-170AICUVL-PA
Microcentrifuge Micro Star 17R	VWR	Cat# 521-1647
Microcentrifuge MiniStar blueline	VWR	Cat# 521-2321P
CLARIOstar microplate reader	BMG LABTECH	N/A
Z1 particle counter	Beckman Coulter	Cat# 9914591
Cuvette for Coulter counter	VWR	Cat# 720-0812
T75 flask	Greiner Bio-One	Cat# 658175
Reaction tube 1.5 mL	Greiner Bio-One	Cat# 616201
Reaction tube 1.5 mL, brown	Greiner Bio-One	Cat# 616283
Falcon 15 mL	Greiner Bio-One	Cat# 188271
Falcon 50 mL	Greiner Bio-One	Cat# 227261
12-well plates	Greiner Bio-One	Cat# 655180
White flat bottom 96-well plate	Thermo Fisher Scientific	Cat# 236108

Materials and equipment setup

- Growth medium

Reagent	**Final concentration**	**Amount**
DMEM	1	500 mL
Fetal Bovine Serum	~9%	50 mL
L-glutamine	2 mM	5 mL
Penicillin/ streptomycin (10,000 U/ mL)	100 U/ mL	5 mL
Total	**N/A**	**560 mL**

[Store at 4°C for up to 1 month.]

Note: The addition of penicillin/ streptomycin is recommended to avoid cell culture contamination.

- Prepare a stock solution of the luciferase substrate coelenterazine 400a in 100% ethanol to a final concentration of 1 mM. The stock can be stored in brown reaction tubes at -30°C for several months.
  Note: Coelenterazine 400a is sensitive to oxidation, therefore, dissolve it fresh before use and keep protected from light.

Step-by-step method details

Part 1: Cell seeding

Timing: 60 min

This part describes the preparation of a HEK293-EBNA cell culture for the transfection.

1. Prewarm DMEM, PBS and trypsin EDTA in a 37°C water bath.
2. Prepare the cell counter, here Beckman Coulter Z1 Counter, by flushing it twice with Milli-Q water, followed by two flushes with ISOTON II Diluent before use.
3. Grow HEK293-EBNA cells in a T75 flask under humidified 5% CO_2 at 37°C in complete growth medium until they reach 80 - 90% confluency.
   Note: Instead of HEK293-EBNA, also HEK293T, HEK293A or other well expressing cell lines can be used.
4. Aspirate the growth medium and gently rinse the cells once with 5 mL sterile PBS.
5. Aspirate the PBS and detach the cells by adding 4 mL of trypsin EDTA. Incubate at 37°C until the cells have detached (approximately 3 - 5 min).
6. To neutralize the trypsin EDTA, add 8 mL of growth medium and resuspend by pipetting until all the cells have been washed off from the T75 flask bottom.
7. Transfer the cell suspension to a 15 mL Falcon tube and pellet the cells by centrifugation for 3 min at 200 × *g* and 22°C - 25°C.
8. Aspirate the supernatant and resuspend the cell pellet in 1 mL of fresh growth medium.
9. To measure the cell concentration, dilute 50 µL of the cell suspension in 10 mL ISOTON II Diluent.
   Note: This will make a 1:200 cell dilution.
   Critical: Before measuring the cell concentration on the cell counter, make sure that the value specifying the cell dilution on the counter is set to 1:200.
   Note: The number displayed at the end of the measurement will show the number of cells/ mL.
10. Seed 200,000 cells in 1 mL per well of a 12-well plate.
11. Culture the cells until the desired cell confluency for transfection is reached.

Optional: To study the impact of a specific gene knock-down on the BRET-biosensor, HEK293-EBNA can be transfected with siRNA after seeding. As an example, consider the knock-down of the alpha-subunit of farnesyl- and geranylgeranyl-transferase I (*FNTA*), as described in **Table S1**. Growth medium containing siRNA and RNA-transfection reagent needs to be removed before transfecting plasmids encoding the BRET-biosensor constructs.

Part 2: Cell transfection

Timing: 60 - 120 min

BRET-biosensor constructs are transfected into the HEK293-EBNA plated in a 12-well plate, so that each well contains one distinct biological sample (e.g. construct-ratio, drug treatment or constructs with mutation of interest). The amounts of example BRET-biosensor constructs that need to be transfected for a donor saturation-titration BRET experiment example are given in **Table 1**.

12. Make sure that the cells are approximately 50 - 60% confluent before the transfection with jetPRIME.
    Note: Other transfection reagents can be used for which specific optimal transfection conditions may apply.
13. Dilute your plasmid stocks to 100 ng/ µL.
14. The total amount of DNA to be transfected in each well is 1025 ng.
15. For each well, prepare one 1.5 mL reaction tube with the DNA mix. As a BRET-control, transfect cells with only the donor construct (**Table 1**).
16. Dilute the appropriate volume of DNA, indicated in the "volume/ µL from 100 ng/ µL stock" column, in 100 µL jetPRIME buffer and mix by vortexing for 10 s.
17. Before using the jetPRIME reagent, mix it by vortexing 1 - 2 s and spin down in a tabletop microcentrifuge for ~5 s at 2000 × *g* to collect the droplets possibly retained inside the tube lid.
18. Add jetPRIME reagent at a 1:3 ratio per µg of DNA. For 1025 ng DNA, use 3 µL jetPRIME reagent.
    Note: If using another transfection reagent, consult its instruction manual for specific requirements.
19. Incubate at 22°C - 25°C without shaking for 10-15 min before adding the DNA mix dropwise to the corresponding well.
20. Incubate the well-plate with transfected cells in the incubator (37°C, 5% CO_2) for up to 48 h of BRET-biosensor expression.

Optional: A drug treatment that modulates the BRET-biosensor interaction can be applied to the cells 24 h after transfection for a maximum of another 24 h within this protocol. Here, we treat some BRET-biosensor samples with 5 µM mevastatin in vehicle (0.1% DMSO/ growth medium). Mevastatin is a competitive inhibitor of 3-hydroxy-3-methylglutaryl-coenzyme A (HMG-CoA) reductase, which catalyzes the rate-limiting step in the synthesis not only of cholesterol but also of prenyl-

pyrophosphates. Thus, Ras prenylation is blocked and consequently its plasma membrane anchorage, which also results in the inhibition of the transient interactions associated with nanoclustering [9,10]. For our example BRET-biosensor, RLuc8-K-RasG12V/ GFP2-K-RasG12V, the mevastatin treatment would therefore reduce the BRET-ratio.

Table 1. Example amounts of transfected BRET-biosensor and donor-only (BRET-control) plasmids for donor saturation-titration BRET experiments. "A/D ratio" refers to ratio between the GFP2-tagged acceptor construct (GFP2-K-RasG12V) and the RLuc8-tagged donor construct (RLuc8-K-RasG12V). The pcDNA3.1-plasmid is used as empty vector to top up the transfected DNA amount to the same total per well.

well number	A/D ratio		plasmid amounts/ ng			volume/ µL from 100 ng/ µL plasmid stock		
	GFP2-K-RasG12V	RLuc8-K-RasG12V	GFP2-K-RasG12V	RLuc8-K-RasG12V	pcDNA 3.1	GFP2-K-RasG12V	RLuc8-K-RasG12V	pcDNA 3.1
1	1	1	25	25	975	0.25	0.25	9.75
2	4	1	100	25	900	1	0.25	9
3	8	1	200	25	800	2	0.25	8
4	12	1	300	25	700	3	0.25	7
5	16	1	400	25	600	4	0.25	6
6	24	1	600	25	400	6	0.25	4
7	32	1	800	25	200	8	0.25	2
8	40	1	1000	25	0	10	0.25	0
9 BRET-control	0	4	0	100	900	0	1	9

Part 3: Cell replating to prepare for the measurement

Timing: 30 - 60 min (depending on the number of 12-well plates)

Next, each 12-well sample is replated in quadruplicate into a white flat bottom 96-well plate for the measurements on the plate reader.

21. Carefully aspirate the medium from the cells.
    Critical: Handle the plate gently to avoid cell detachment.
    Note: If extensive cell detachment is observed under a cell culture microscope, we recommend to detach all cells from the bottom of the 12-well-plate by pipetting the growth medium up- and down, and then centrifuge the suspension for 10 min at 900 × *g* and 4°C in 1.5 mL reaction tubes before directly proceeding to **step 24** followed by a PBS washing step as described in **steps 22,23**.

22. Rinse the cells by adding 1 mL PBS per well, detach the cells by pipetting and collect in 1.5 mL reaction tubes.
23. Pellet the cells by centrifugation for 10 min at 900 × *g* and 4°C.
24. Aspirate the supernatant.
25. Resuspend the cells in a slight excess of 380 µL of PBS.
26. For each sample, dispense 4 × 90 µL of cell suspension into four adjacent wells of a white flat bottom 96-well plate as quadruplicate technical repeats.
    Note: It may also be possible to employ black plates. However, in that case we observed a four-fold loss of luminescence signal, while the fluorescence signal in white plates was just more variable.

Part 4: Fluorescence and luminescence measurements on a plate reader

Timing: 15 - 30 min (depending on the number of white flat bottom 96-well plates)

In this part, we first describe the setup of the three RLuc8/ GFP2 BRET-pair specific detection channels for the acceptor- (excitation at 405 ± 10 nm, emission at 515 ± 10 nm), donor- (emission at 410 ± 40 nm), and the BRET-signal (emission at 515 ± 40 nm) on the CLARIOstar microplate reader (**Figure 1**). We then explain how to conduct the measurements starting with the acceptor channel, followed by injection of the luciferase substrate and simultaneous acquisition of the donor- and BRET-channel signals.

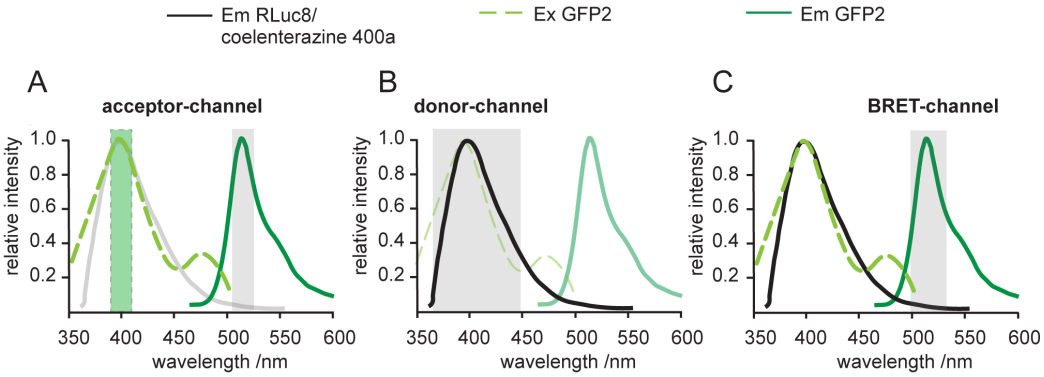

Figure 1: Definition of the three detection channels for BRET-experiments.
(**A-C**) The acceptor- (A), donor- (B) and BRET-channels (C) are indicated relative to the emission (Em) and excitation (Ex) spectra of the donor RLuc8/ coelenterazine 400a (grey/ black) and the acceptor GFP2 (green). The excitation bandwidth is marked with a light green dashed box (A), while the detection bandwidths are marked with a light grey box (A-C).

27. First, set up the three detection channels as "**Test Protocols**" within the CLARIOstar software.
    a. Open the CLARIOstar software on the computer that controls the plate reader.
    b. Click on "**Microplate**" and "**Manage Protocols**", which opens the "**Test Protocols**" window.
    c. Click on "**New**", which opens the "**Measurement Method and Mode**" window.
    d. Make sure that "**Fluorescence Intensity**" is selected in the "**Measurement Method**" selection and "**Endpoint**" in the "**Reading Mode**" selection (feature 1 in **Fixed_Image_1**) and then click "**OK**".
    Note: This will open the "**Fluorescence Intensity – Endpoint**" window.
    e. In the "**Fluorescence Intensity – Endpoint**" window, open on its **"Basic Parameters"** tab, type in the name of the new protocol and select for "**Microplate**" "**NUNC 96**" in the drop-down menu, which is the appropriate setting for the 96-well microplates.
    Note: Adjust this if another plate type is used (feature 2 in **Fixed_Image_1**).
    f. In the "**Presets**" tab, enter the following monochromator-filter settings for the acceptor-channel (feature 3 in **Fixed_Image_1**):
        - Excitation: 405-20
        - Dichroic: 462.5
        - Emission: 515-20

    and confirm by clicking "**OK**".
    Note: The CLARIOstar microplate reader allows to freely chose excitation and emission detection windows, due to its monochromator technology. In the specifications e.g. **"**405-20," 20 refers to the bandwidth of the monochromator-filter centered at 405 nm, i.e. for detection between 395-415 nm or 405 ± 10 nm.
    Note: Keep all other features, in the protocol set-up steps not highlighted here at default settings. Specifically, keep "**Optic**" at "**Top optic**". In the "**General Settings**" field, "**Settling time**" is the time after the microplate moves to the next well and before the measurement begins. It is set to 0.2 s. "**No. of flashes per well**" is set at 50 but can be increased up to 200. All the measurements per flash will be averaged and one intensity value will be obtained per well.

[*Insert **Fixed_Image_1** here]

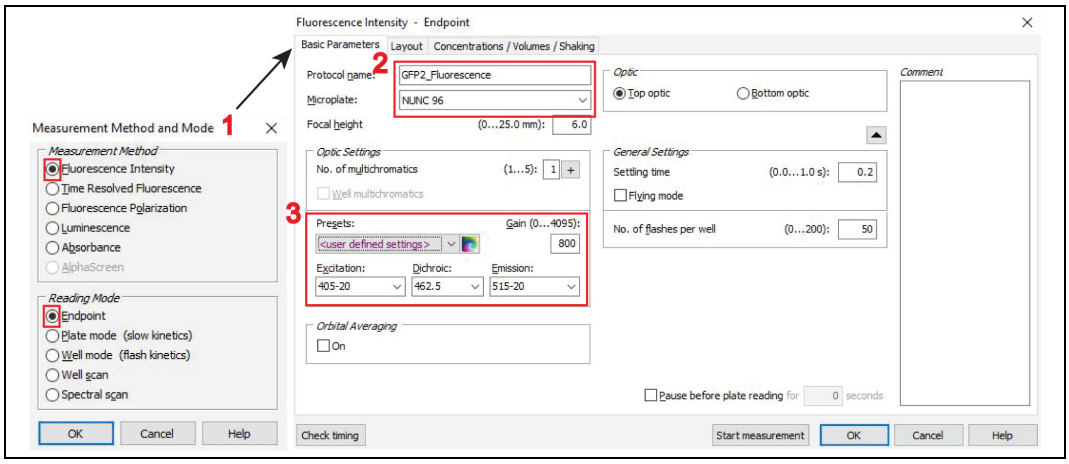

g. Next, create a two-channel protocol for donor- and BRET-channel acquisition.
   i Open another "**Test Protocols**" window and click on "**New**".
   ii Select in the "**Measurement Method and Mode**" window "**Luminescence**" and "**Well mode**" (feature 4 in **Fixed_Image_2**) and then click "**OK**".
   Note: By selecting "**Well mode**", the luminescence signals will be measured immediately after the injection of the luciferase substrate coelenterazine 400a, with both injection and measurement done well-by-well.

h. In the "**Luminescence – Well mode**" window open on its **"Basic Parameters"** tab, go to the "**Optic Settings**" and change the "**No. of multichromatics**" to "2" (feature 5 in **Fixed_Image_2**).

[*Insert Fixed_Image_2 here]

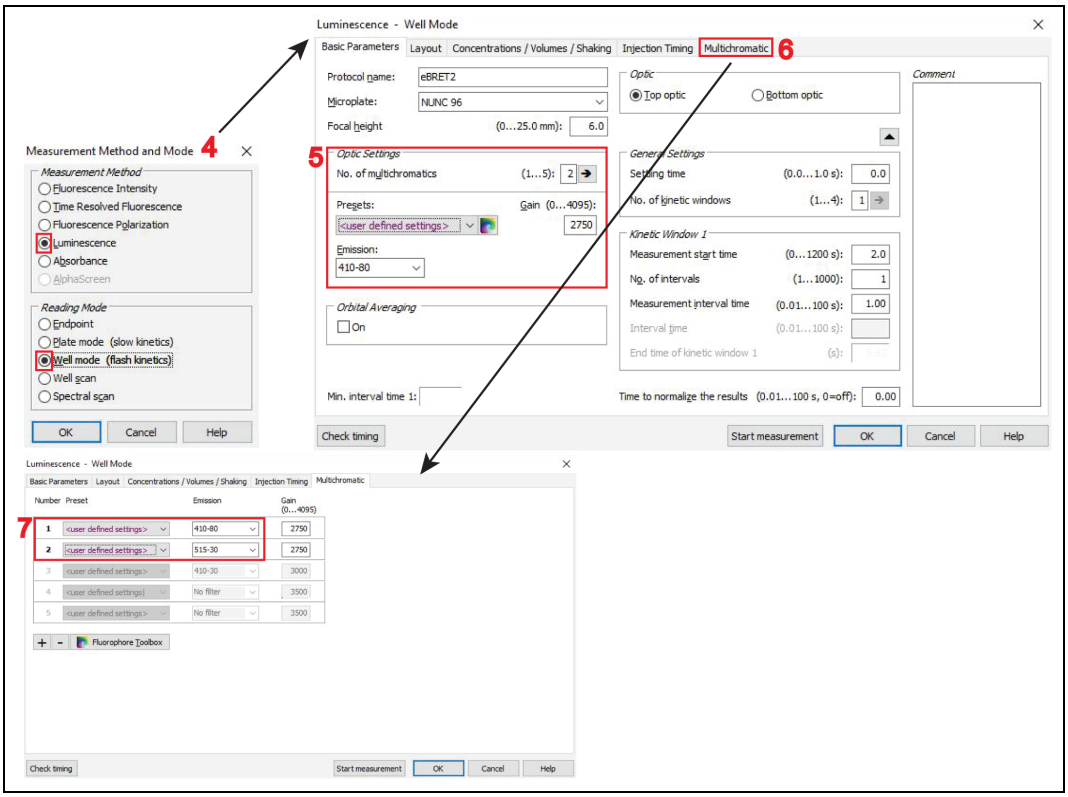

i. In the "**Multichromatic**" tab of the "**Luminescence – Well mode**" window (feature 6 in **Fixed_Image_2**), define the donor- and BRET-channel, by entering the two monochromator-filter values "410-80" for the donor- and "515-30" for the BRET-channel (feature 7 in **Fixed_Image_2**).

Note: Keep again all other settings, not highlighted here in the protocol set-up steps, at displayed default settings. Notably, the "**Settling time**" is set to 0 s. There is no settling time implemented due to the fast substrate conversion.

CRITICAL: Before beginning with the actual BRET measurements of the target BRET-biosensor samples, set up optimal gain settings for the photomultiplier tube detector of the microplate reader. See **Troubleshooting 1** for details on how to set up correct gain settings.

28. To start with the measurement of BRET-samples, turn on the CLARIOstar microplate reader and press the button to eject the tray.
29. Place the white flat bottom 96-well plate on it and press the button again to retract the tray.
30. Start the CLARIOstar software from the computer desktop, click on "**Manage Protocols**" and select to display protocols for fluorescence intensity in the "**Test protocols**".

31. Click on the created protocol to measure the acceptor-channel and click on "**Edit**". Verify all parameters correspond to those specified in **step 27**.
Note: This opens the "**Fluorescence Intensity – Endpoint**" window.

[*Insert **Fixed_Image_3** here]

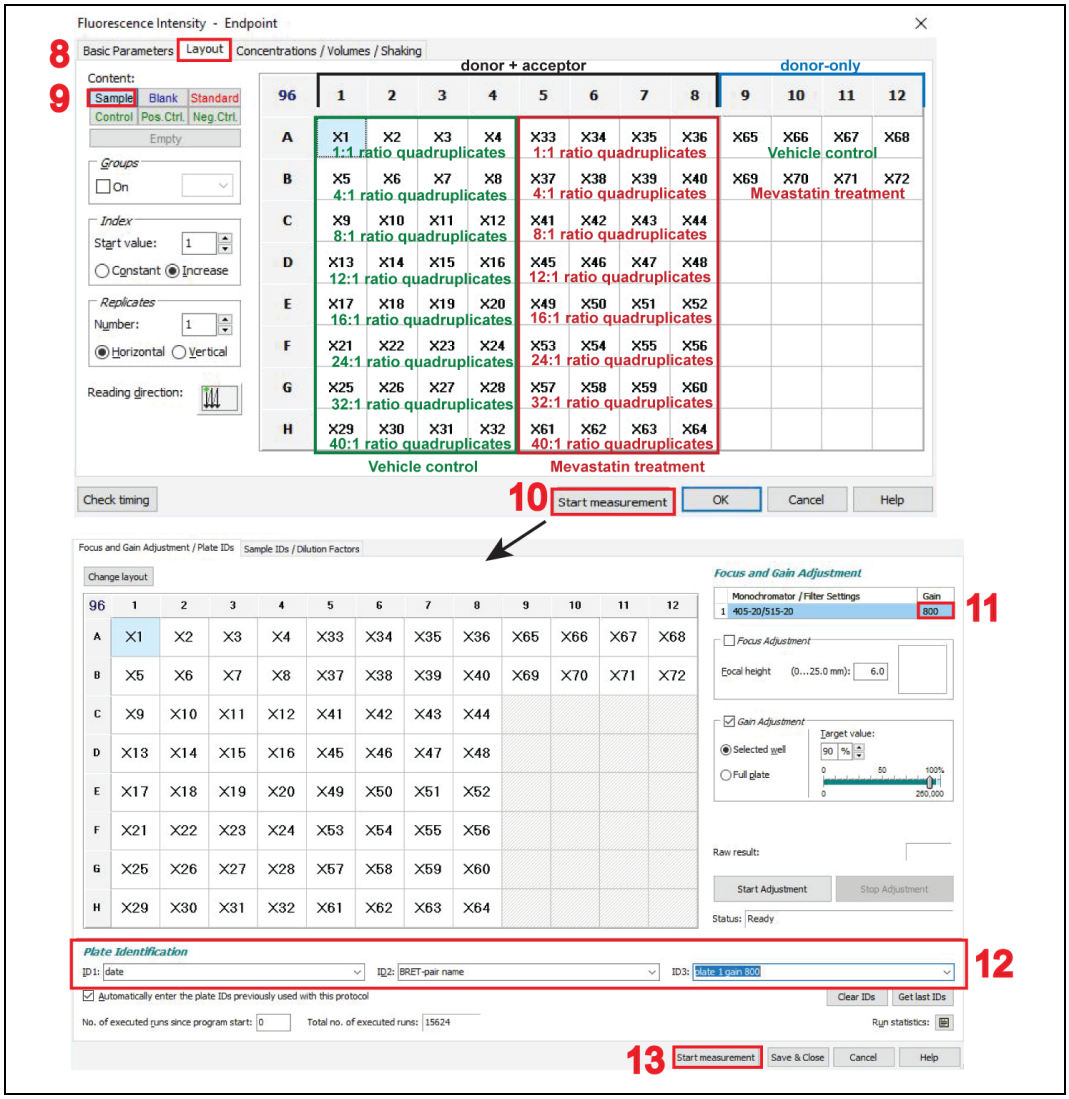

32. In the "**Layout**" tab (feature 8 in **Fixed_Image_3**), click on "**Sample**" (feature 9 in **Fixed_Image_3**) and select all wells on the 96-well plate grid that contain samples to be measured.

Note: The 96-well plate setup screenshot shows the samples annotated. The vehicle control samples are in green and the mevastatin-treated samples are in red. Plasmid ratios of quadruplicates are also indicated. The donor-only samples are added to the right.

33. Click on "**Start measurement**" (feature 10 in **Fixed_Image_3**).
    Note: The "**Concentrations/ Volumes/ Shaking**" tab is not used in this protocol as nothing is injected and no shaking is needed, therefore keep at default.
34. In the "**Start measurement"** window, which opens automatically, enter the optimal gain settings as determined in **Troubleshooting 1** (feature 11 in **Fixed_Image_3**)
35. Fill out the plate identification ID1, ID2 and ID3 (feature 12 in **Fixed_Image_3**), then click on "**Start measurement**" (feature 13 in **Fixed_Image_3**).
    Note: Plate identification ID1, ID2 and ID3 are user defined and should be annotated so that the results can be traced back to the corresponding plate and experiment date, e.g. enter ID1: date, ID2: BRET-biosensor, ID3: plate number and gain.
36. For Luminescence measurements, start by preparing a volume of 100 µM coelenterazine 400a appropriate for your sample number by diluting the stock in PBS in a 15 mL Falcon.
    Critical: For a full 96-well plate, prepare 2 mL of coelenterazine 400a.
    Note: To each well of a white flat bottom 96-well plate, 10 µL of coelenterazine 400a will be added, thus resulting in a final concentration of 10 µM luciferase substrate. Consider that approximately 500 µL of the substrate will be spent when preparing the injection system, described in **step 37**. Additional amounts further account for volume loss when dispensing the substrate from the Falcon into the wells.
37. Prepare the pump and the injection system.
    a. Open the lid of the CLARIOstar plate reader, position the input tube end into a Falcon tube with rinsing liquids (b.-d.) and place a small beaker underneath the displaced reagent injector for liquid waste collection.
    b. Rinse with 100% ethanol by double-clicking the button corresponding to the pump 1, 3 to 4 times (feature 14 in **Fixed_Image_4**).
    c. Rinse 3 - 4 times with Milli-Q water
    d. Rinse 3 - 4 times with PBS
    e. Place the Falcon containing the substrate in the designated place in the instrument and rinse the injection system once with the substrate.
    f. Place the reagent injector back in its operating position (feature 15 in **Fixed_image_4**).

    Note: If you have to measure multiple 96-well plates, perform the pump and injection system preparation just before the first injection of coelenterazine 400a. As the substrate precipitates quickly, rinse the injection system with ethanol if the next luminescence reading is more than 20 min later. Consider preparing fresh substrate when precipitates are visible.

[*Insert **Fixed_Image_4** here]

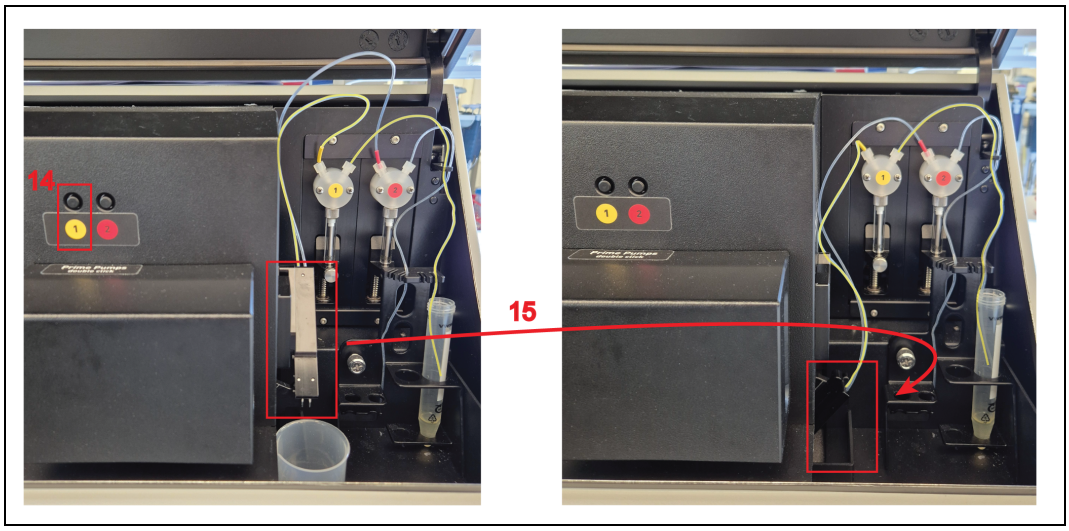

38. To measure donor- and BRET-channel, click on "**Manage Protocols**" to open the "**Test Protocols**" tab.
    a. Click on "**Luminescence**", select the protocol "eBRET2" and click on "**Edit**".
       Note: This opens "**Luminescence - Well Mode**" window.
    b. Verify all parameters correspond to those specified in **step 27**.
39. In the "**Layout**", select all the wells containing BRET-samples of the 96-well plate (refer to **step 32**).
40. Click on the "**Concentrations/ Volumes/ Shaking**" tab (feature 16 in **Fixed_Image_5**) and type in "**10**" in the "**Start volume**" (feature 17 in **Fixed_Image_5**) for a luciferase substrate injection volume of 10 µL per well.
    Critical: Select the pump 1 (feature 18 in **Fixed_Image_5**), which was primed for use in **step 37**.
    Note: In the "**Injection Timing**" and "**Multichromatic**" tabs, keep all other parameters at default settings as specified in **step 27**. Default parameters specify a 1 s substrate injection window, 2 s wait for optic movement, followed by a 2.6 s measurement.
    Note: It is possible to add the substrate manually e.g. with a multi-pipette and mix by agitation. However, the luminescence signal needs to be stable during the measurement, which is typically the case for at least 60 min after substrate addition.
41. Click "**Start measurement**" (feature 19 in **Fixed_Image_5**).
42. In the "**Start measurement**" window, input the optimal gain settings (feature 20 in **Fixed_Image_5**)
43. Fill out the plate identification ID1, ID2 and ID3, then click on "**Start measurement**" (feature 21 in **Fixed_Image_5**).
    Note: Specify the plate identification ID1, ID2 and ID3 analogous to **step 35**.

[*Insert **Fixed_Image_5** here]

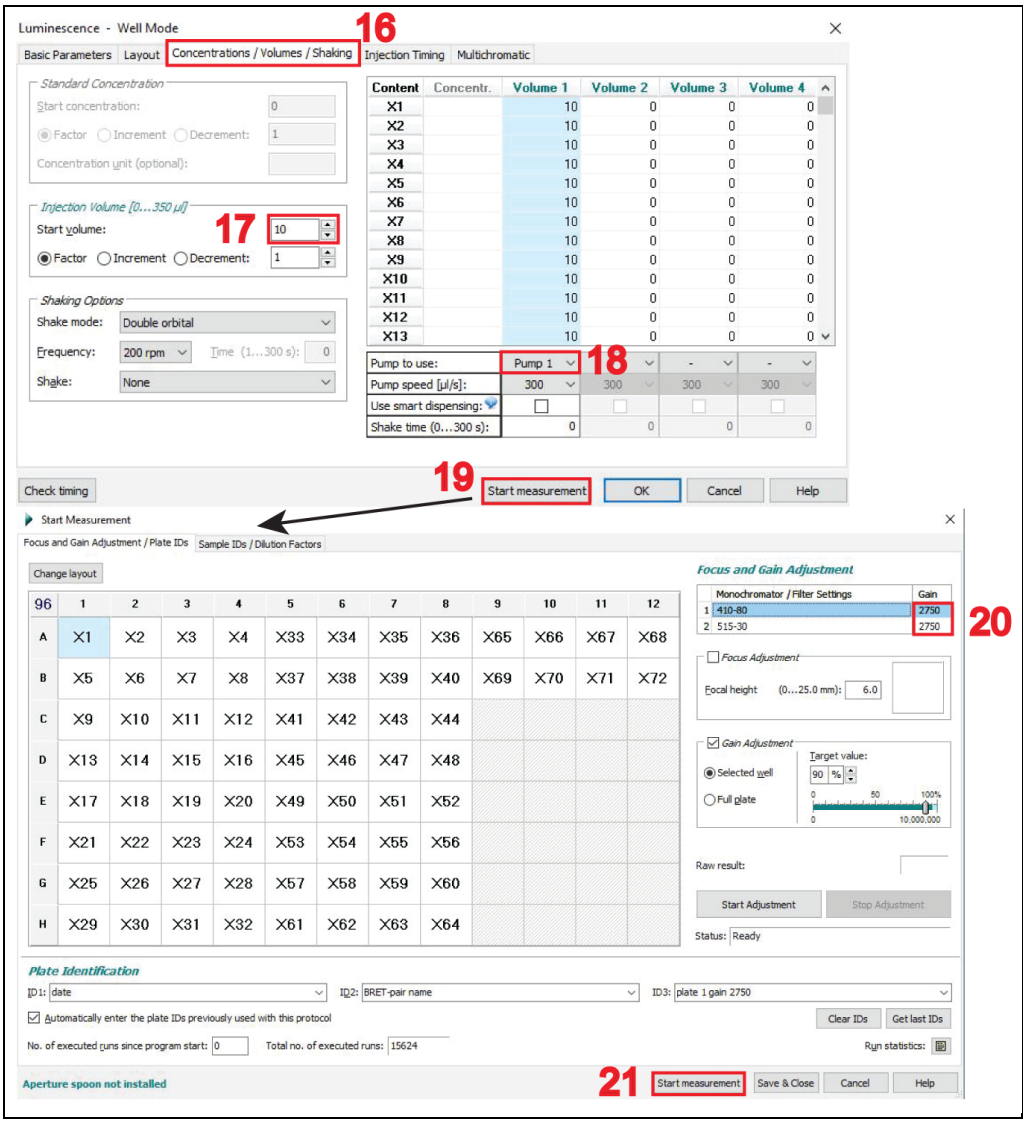

44. After the measurements, open the CLARIOstar MARS Data Analysis Software (feature 22 in **Fixed_Image_6**), where under "**Measurement Method**" either "**Luminescence**" or "**Fluorescence**" is identified.
    a. Select and open your pair of measurement files (feature 23 in **Fixed_Image_6**)
    b. Click on the small Excel icon (feature 24 in **Fixed_Image_6**) to export the displayed results as Excel workbook files.

[*Insert **Fixed_Image_6** here]

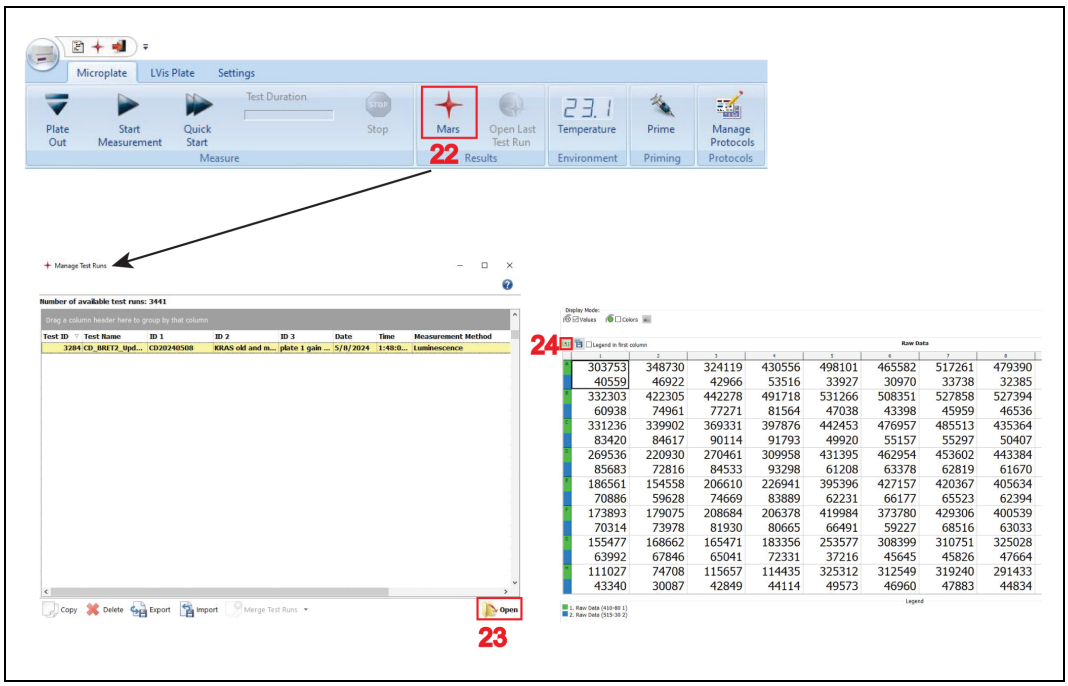

Part 5: Data analysis in Excel and GraphPad Prism

Timing: 60 min

In this part, the BRET ratio, the expression signal ratio [11] and the normalized expression signal ratio [12] are calculated. Curve fitting of the data can yield the classical BRETmax and BRET50-parameters, alternatively, we here also determine the BRETtop value, which represents the top asymptote of the BRET ratio reached within a defined acceptor/ donor range [8].

[*Insert **Fixed_Image_7** here]

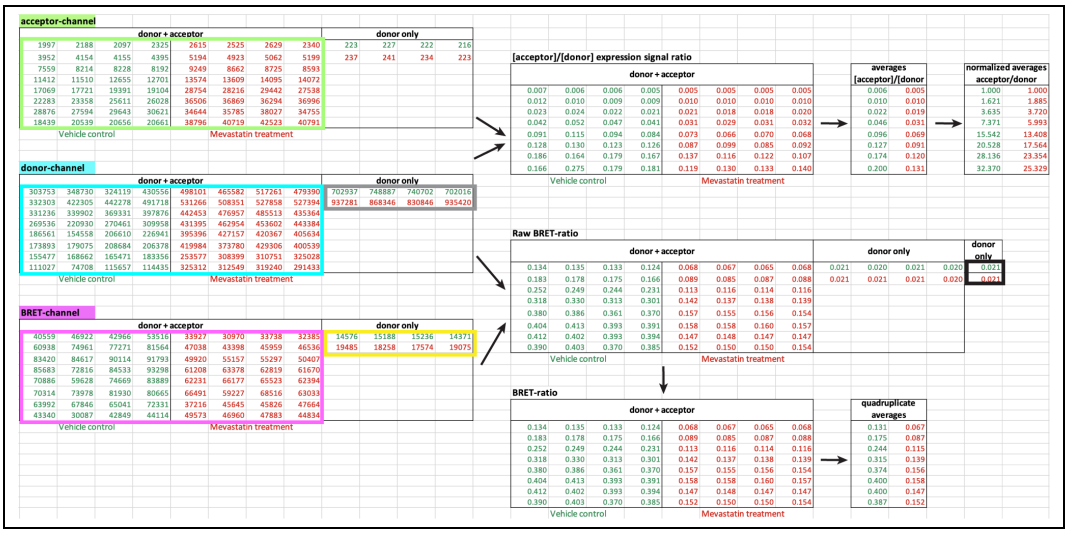

45. Merge the exported raw signals for all three channels into one Excel workbook file as shown above.

    Note: The example here contains two sets of saturation-titration data as specified in **Tables 1 and S2** with vehicle control (in dark green) and mevastatin treatment (in red). Each sample is present in quadruplicates in the tables. Samples to the right are donor-only BRET-control samples. See **Troubleshooting 2** for verification of raw signals in acceptor, donor-, and BRET-channels after correct gain setting.

46. The BRET ratio is calculated as the raw BRET ratio of each BRET-biosensor sample (donor + acceptor) from which the raw BRET ratio of donor-only samples is subtracted.

    Note: The formula to obtain the BRET ratio is:

$$BRET\ ratio = \frac{BRET\ channel_{(donor+acceptor)}}{donor\ channel_{(donor+acceptor)}} - \frac{BRET\ channel_{(donor-only)}}{donor\ channel_{(donor-only)}}$$

    The colors in the formula refer to the colors of the boxes in the Excel sheet screenshot.

47. Calculate the raw BRET-ratio of the BRET-samples per well and subtract the average of the raw BRET ratio of donor-only samples.

    Note: Calculate then from the quadruplicate technical repeats the averages of the BRET-ratios.

48. Next, calculate the expression signal ratio, indicated as [acceptor]/[donor], per well by dividing the acceptor-channel values (boxed in light green) by the donor-channel values (boxed in blue) for all BRET-biosensor samples.

49. For the normalized expression signal ratio, further divide each expression signal ratio by the value corresponding to 1:1 A/D-plasmid ratio, here 1:1 plasmid amounts of GFP2-K-RasG12V and RLuc8-K-RasG12V.
50. To plot the data, open GraphPad Prism and create an "XY" table.
    a. Plot the averages across all technical and biological repeats from BRET ratio data as Y-values against the acceptor/ donor plasmid ratios from 1:1 to 40:1 (**Figure 2A**).
    b. To fit the data with a hyperbolic equation, click on the "**Analyze"** tab, then under "**XY analyses**" select "**nonlinear regression**" and select "**Hyperbola** (x is a concentration)".
    Note: The formula for the saturation binding curve or rectangular hyperbola is:
    $$y = \frac{BRETmax \times x}{BRET50 + x}$$
    where x is a measure of the relative expression of the acceptor to the donor, and y is the BRET ratio. BRETmax represents the maximum saturation BRET signal and depends on the structural parameters (distance and orientation) of the BRET-biosensor complex. BRET50 corresponds to the acceptor/ donor ratio required to attain 50% of the maximum BRET signal and is a measure of the effective interaction probability between the interacting BRET-constructs.
    c. Alternatively, use the BRET-ratio averages from technical quadruplicate repeats as y-values and plot against the averages of the corresponding expression signal ratios (**Figure 2B**) or the normalized expression signal ratios as x-values (**Figure 2C**). Fit the same hyperbolic equation (**step 50**).
    Note: Given that the concentration of expressed constructs is proportional to their signal, we denote their signals in squared brackets, i.e. [acceptor] and [donor] for the signals acquired in the acceptor and donor channels, respectively. The expected results of raw signals from each channel are discussed in **Troubleshooting 2.**
    d. In order to obtain the characteristic BRETtop value for data plotted as shown in **Figure 2B and C**, we employ fitting with another function.
    Note: This is merely to obtain this parameter, which is not achievable with the saturation binding curve as it extrapolates the BRETmax value.
        i. First, duplicate the above data table in GraphPad Prism. In the "**Analysis**" tab, select the symbol for "**Fit a curve with a nonlinear regression**" and click on the "**one phase association**" equation.
        ii. In the "**Table of result**", click on "**Nonlin fit**" in the upper left corner to open the "**Parameters: Nonlinear Regression**" tab.
        iii. Select "**Constrain**" and set the Y0 constant equal to 0.
        iv. In the "**Confidence**" section of the parameters, select "**Symmetrical (asymptotic) approximate CI**" and "**Show SE of parameters**".
        v. Go back to the "**Table of results**". The BRETtop value is the "**Plateau**" value given with its standard error.

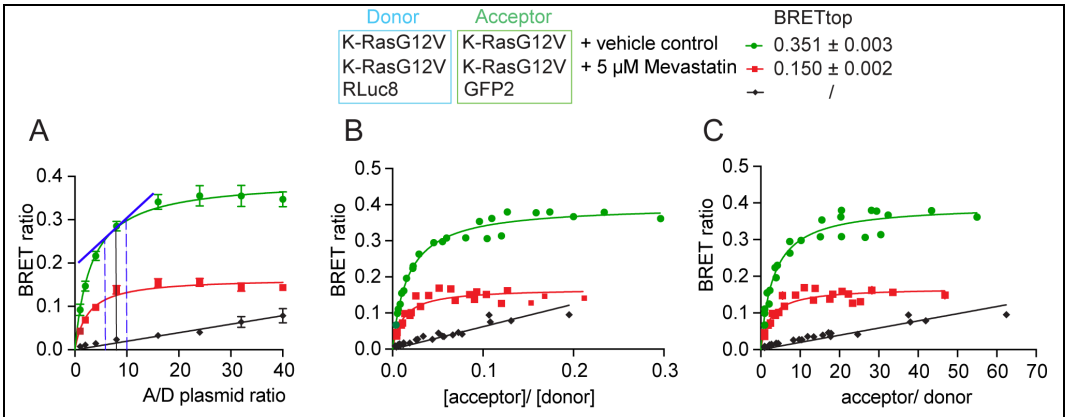

Figure 2: Three formats to visualize the donor saturation-titration curves of the example BRET-biosensor with and without drug treatment as compared to a background-BRET control.

(**A-C**) Different representations of the same dataset from the BRET-biosensor RLuc8-K-RasG12V/ GFP2-K-RasG12V with vehicle (green), and the same with 5 µM mevastatin treatment for 24h (red). As a non-interacting control, the donor and acceptor without fused K-RasG12V were analyzed (black). Data were fit with a saturation binding curve (green, red) or linear function (black). Means ± SEM across all technical and independent biological repeats (n=3) are plotted, resulting in larger errors of BRET-ratio values (A). By contrast, in (B,C) means ± SEM of the quadruplicates from n=3 independent biological repeats are plotted individually in one plot. Note that errors are too small to be recognized (B,C). From the plot in (A) one can determine the optimal A/D-plasmid ratio for dose-response testing of e.g. a drug (not shown). The best dynamic range is found in the pseudo-linear regime of the curve, as indicated in blue (A). The preferred plot employs the '[acceptor]/[donor]' expression signal ratio on the x-axis. Given that the concentration of expressed constructs is proportional to their signal, we denote their signals in squared brackets (B). From this the normalized expression signal ratio, 'acceptor/ donor', is derived (C). The BRETtop values were determined with a different fit function and are indicated next to the legend.

Expected outcomes

To illustrate this protocol, we performed donor saturation-titration BRET experiments with the BRET-biosensor RLuc8-K-RasG12V/ GFP2-K-RasG12V (**Figure 2**). We show three plots, to illustrate the differences in appearance of the data depending on the selected x-axis values. When assessing the BRET-ratio as a function of the A/D-plasmid ratio, curves appear smoothest (**Figure 2A**). These x-axis values are not calculated based on actual protein expression levels but suppose that the ratio of transfected plasmid DNA is translated into corresponding protein ratios. When combining biological repeats, the uncertainty of this assumption manifests itself in a higher error of the BRET-ratio values. From this representation one can also identify the optimal A/D-plasmid ratio (here at A/D = ~10:1) for dose-response experiments (**Figure 2A**). Under these conditions, the BRET-ratio response of the BRET-

biosensor depends pseudo-linearly on manipulations that affect the interaction, such as drug-treatments [10].

The preferred format employs the expression signal ratio on the x-axis, as it is derived from measured signal values (**Figure 2B**). When all instrument settings are kept constant, both parameters, the BRET-ratio and the [acceptor]/[donor] expression signal ratio are values that should maintain a fixed relation between biological repeats, as they relate to actual biophysical parameters. Thus, averages of technical repeats can be visualized in one plot, without averaging biological repeat data. As an alternative in cases where the ranges of the expression signal ratio values differ much between conditions that are to be compared (e.g. different mutants of a protein that express differently), it can be advantageous to employ the normalized expression signal ratio (**Figure 2C**). However, the decision to use this representation needs to be taken in context with the specific biology.

We furthermore demonstrate that the saturation-titration curve can detect the impact of a drug treatment, here mevastatin, which prevents the lipid modification of the expressed Ras constructs and thus reduces their membrane anchorage, nanoclustering and nanoclustering-dependent BRET (**Figure 2, red curves**). With complete inhibition, all of the BRET-biosensor constructs would be cytoplasmic and should therefore behave as the tags only (**Figure 2, black curves**). Their BRET is only driven by random collisions in the cellular cytoplasm and therefore linearly depends on the acceptor/donor ratio in the attainable expression regime. The comparison with a control, where only the tags RLuc8 and GFP2 are expressed (**Figure 2, black curves**), suggests that the mevastatin treatment does not completely inhibit membrane anchorage of all BRET-biosensors (**Figure 2, red curves**).

Limitations

In this K-Ras-based BRET-biosensors assay, a drop in BRET such as observed by the mevastatin treatment can be due to any process upstream of Ras nanoclustering. Thus, any manipulation that impacts on Ras lipid modification, its proper trafficking or its lateral organization in nanoclusters can be detected in this assay [13]. It is not possible to conclude that Ras or related proteins are present as dimers or other oligomers based on BRET-assay results alone. To conclude on stable di-/oligomers, proteins would have to be purified and their interaction and affinity be determined with appropriate methods, such as surface plasmon resonance spectroscopy [14]. In addition, crystal structures of the complex provide atomic resolution details of interface residues.

The method can be further improved by calibrating the expression signal ratio for actual protein-stoichiometries and total expression levels. This could be achieved by using a fusion-protein of the BRET-pair with a long linker that prevents BRET as its signal ratio can be associated with a fixed 1:1 protein stoichiometry. Furthermore, using a purified acceptor protein preparation of known concentration could help to relate the signals with actual concentration equivalents.

Troubleshooting

Problem 1:

A possible error message "**Overflow of the signal**" could result if the gain was set too high after **steps 35** or **43**, resulting in signals higher than 260,000 relative units. Therefore, in **step 27**, the gain settings have to be adjusted accurately.

Potential solution:

An optimal detector gain linearly amplifies the signal relative to the input concentration. Here we employ the transfected acceptor- (i.e. GFP2-K-RasG12V) and donor- (i.e. RLuc8-K-RasG12V) plasmid amounts as proxies for the input concentrations. Both constructs should ideally be biologically identical and correspond to the target condition to be studied i.e., here being K-RasG12V-based constructs to ensure equal expression. We individually express increasing amounts of these target BRET-biosensor constructs for the same time and using the same total DNA-amounts as later in the BRET-experiments. It is important to use actual target constructs, which will display the expression properties later found in BRET-experiments. Do not use the tags only i.e., RLuc8 and GFP2.

By following the steps described in **Part 4**, we acquire a series of measurements from cells expressing the acceptor-construct using different gain settings for the acceptor channel (**Figure 3A**). The optimal acceptor-channel gain is identified as the highest gain that still linearly correlates with the amount of transfected acceptor-construct. The same will then be done for the donor channel, where the optimal donor-channel gain is identified in an analogous fashion (**Figure 3B**). For the BRET-channel, we approximate the same settings as determined for the donor-channel.

Detector gain settings usually need to be established only once for a given BRET-pair and microplate reader. Importantly, the determined gain settings have to be maintained across biological repeats that will be combined or compared. This is necessary to ascertain that the expression signal ratio scales with the stoichiometry change of expressed donor- and acceptor-constructs.

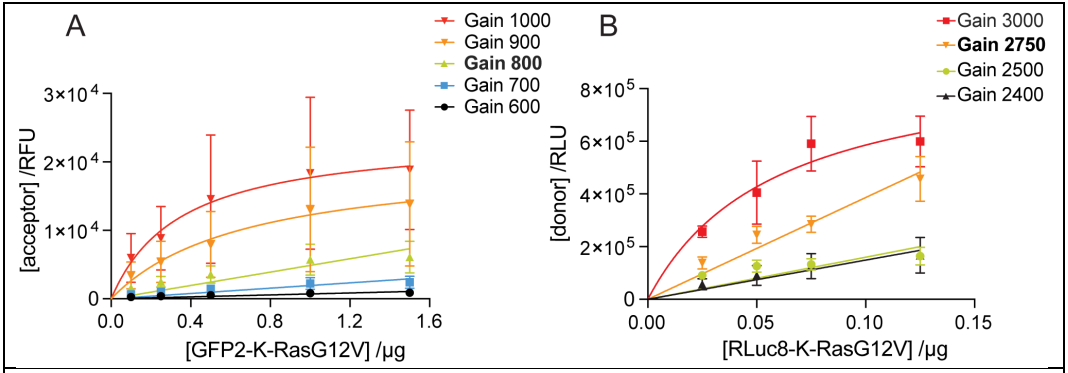

Figure 3: Detection channel signal gain exploration.

(**A**) Acceptor-channel signals are plotted as a function of the transfected GFP2-K-RasG12V plasmid amounts at different gain values. (**B**) Donor-channel signals are plotted as a function of the

transfected RLuc8-K-RasG12V plasmid amounts at different gain values. The best gain values are in bold. Curves were fit with a linear or saturation function. Plotted are means ± SEM from n = 3 independent biological repeats (A,B).

Problem 2

The raw signals in acceptor, donor-, and BRET-channels have not been verified after correct gain setting (**Part 4**).

Potential solution:

The signals in acceptor, donor-, and BRET-channel should be above background and follow approximately the trends shown in **Figure 4**.

Verify that the instrument is properly set up, notably the gain settings are correct (see **Troubleshooting 1**). Start BRET-experimentation with trusted and validated BRET-biosensor constructs. The design of novel BRET-biosensors requires more experience and knowledge.

If low signals are detected, the transfection of your construct could have been insufficient, consider optimization by monitoring the expression of your BRET-constructs also by alternative means, such as flow cytometry, fluorescence microscopy or Western blotting. A low transfection efficiency can also result from sub-optimal culture conditions, such as a too dense culture or too high cell passage number. Furthermore, the cell line for heterologous expression could be relevant. It is necessary to employ a cell line with a high transfectability, as each cell should ideally be transfected with the specified A/D-plasmid ratio. We routinely use HEK293-EBNA cells for their ease of handling, transfection efficiency and high expression yields.

To increase the acceptor/ donor expression signal ratio range, consider expressing donor or acceptor construct at different ratios from those given in the example i.e., lower or higher ranges, so that the raw signals in the acceptor- and donor-channels are of similar magnitude. Alternatively, express constructs for different amounts of time e.g., express the donor-construct for a shorter time (by transfecting it later) than the acceptor-construct.

The biological impact of the BRET-construct on protein expression and cell viability or proliferation can ultimately be limiting for a successful experiment. Protein products that are toxic or cell cycle inhibitory cannot be expressed at high levels and may not be suitable for cellular BRET-measurements.

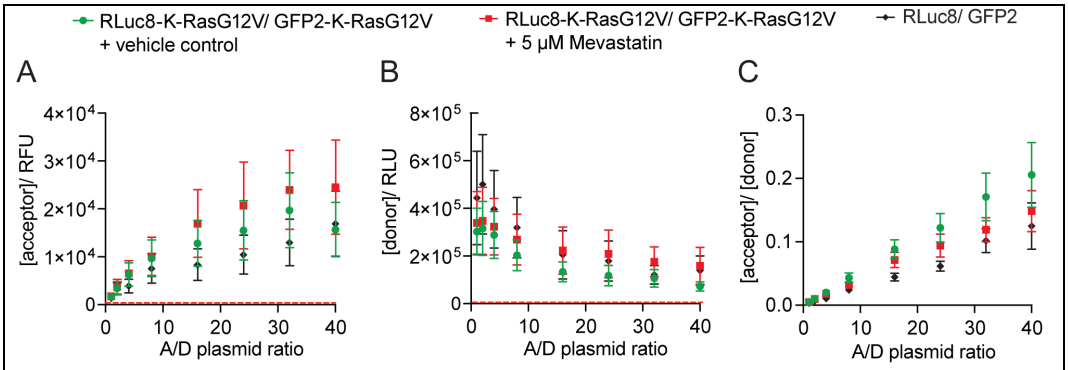

Figure 4: Plots to verify the good expression of the transfected BRET-biosensor constructs.

(**A-C**) The raw signals from the acceptor- (A), donor- (B) and BRET-channels (C) are plotted against the A/D-plasmid ratio of transfected RLuc8-K-RasG12V/ GFP2-K-RasG12V BRET-biosensor plasmid amounts at optimal gain settings. Verify that the acceptor signal approximately linearly increases along the x-axis (A). Ideally, the signal of the donor remains constant and should be of a similar relative unit magnitude as the acceptor signals. However, here we observe that at higher A/D-plasmid ratios, the signal is reduced but somewhat constant. This is due to BRET occurring, but probably also due to the limited amount of overexpression the cell can realize. As the acceptor construct is highly overexpressed, the expression of the donor construct may somewhat be suppressed (B). The raw BRET-signal should increase with increasing A/D-plasmid ratios (C). Red dashed lines indicate the very low background signal levels of non-transfected cells. Here the acceptor-channel has merely 234 RFU and the donor-channel 34 RLU background signal. Given these values are well below those of the biosensor samples, a subtraction of this background signal from our raw signals has been omitted in our protocol.

Resource availability

- **Lead contact**: Further information and requests for resources and reagents should be directed to and will be fulfilled by the lead contact, Prof. Dr. Daniel Kwaku Abankwa (daniel.abankwa@uni.lu).
- **Technical contact**: Questions about the technical specifics of performing the protocol should be directed to and will be answered by the technical contact, Carla Jane Duval (carla.duval@uni.lu).
- **Materials availability**: This study did not generate new unique reagents.
- **Data and code availability**: The protocol includes all datasets generated or analyzed during this study.

Acknowledgments

This work was supported by grants from the National Research Fund Luxembourg (FNR) INTER/UKRI/19/14174764-RAS-NANOME and INTER/NWO/19/14061736 - HRAS-PPi to DKA and AFR/17927850/Duval C./KRuptor to CJD. We are grateful to Dr. Ganesh babu Manoharan for

implementing the BRET-technology in the Abankwa lab. The graphical abstract was created using BioRender.com.

Author contributions

C.L.S. participated in the initial conceptualization. C.L.S. and C.J.D. designed and carried out the experiments. C.L.S. and C.J.D. analyzed the data. C.L.S., C.J.D. and K.P. wrote the first draft of the manuscript. D.K.A. edited the manuscript and supervised the entire study.

Declaration of interests

The authors declare no competing interests.

References

1. Steffen, C.L., Manoharan, G.B., Pavic, K., Yeste-Vazquez, A., Knuuttila, M., Arora, N., Zhou, Y., Harma, H., Gaigneaux, A., Grossmann, T.N., and Abankwa, D.K. (2024). Identification of an H-Ras nanocluster disrupting peptide. Commun Biol *7*, 837. 10.1038/s42003-024-06523-9.
2. Bacart, J., Corbel, C., Jockers, R., Bach, S., and Couturier, C. (2008). The BRET technology and its application to screening assays. Biotechnol J *3*, 311-324. 10.1002/biot.200700222.
3. den Hamer, A., Dierickx, P., Arts, R., de Vries, J., Brunsveld, L., and Merkx, M. (2017). Bright Bioluminescent BRET Sensor Proteins for Measuring Intracellular Caspase Activity. ACS Sens *2*, 729-734. 10.1021/acssensors.7b00239.
4. Dacres, H., Michie, M., Wang, J., Pfleger, K.D., and Trowell, S.C. (2012). Effect of enhanced Renilla luciferase and fluorescent protein variants on the Forster distance of Bioluminescence resonance energy transfer (BRET). Biochem Biophys Res Commun *425*, 625-629. 10.1016/j.bbrc.2012.07.133.
5. Abankwa, D., and Gorfe, A.A. (2020). Mechanisms of Ras Membrane Organization and Signaling: Ras Rocks Again. Biomolecules *10*. 10.3390/biom10111522.
6. Lindenburg, L., and Merkx, M. (2014). Engineering genetically encoded FRET sensors. Sensors (Basel) *14*, 11691-11713. 10.3390/s140711691.
7. Hamdan, F.F., Percherancier, Y., Breton, B., and Bouvier, M. (2006). Monitoring protein-protein interactions in living cells by bioluminescence resonance energy transfer (BRET). Curr Protoc Neurosci *Chapter 5*, Unit 5 23. 10.1002/0471142301.ns0523s34.
8. Manoharan, G.B., Laurini, C., Bottone, S., Ben Fredj, N., and Abankwa, D.K. (2023). K-Ras Binds Calmodulin-Related Centrin1 with Potential Implications for K-Ras Driven Cancer Cell Stemness. Cancers (Basel) *15*. 10.3390/cancers15123087.
9. Okutachi, S., Manoharan, G.B., Kiriazis, A., Laurini, C., Catillon, M., McCormick, F., Yli-Kauhaluoma, J., and Abankwa, D. (2021). A Covalent Calmodulin Inhibitor as a Tool to Study Cellular Mechanisms of K-Ras-Driven Stemness. Front Cell Dev Biol *9*, 665673. 10.3389/fcell.2021.665673.
10. Kaya, P., Schaffner-Reckinger, E., Manoharan, G.B., Vukic, V., Kiriazis, A., Ledda, M., Burgos Renedo, M., Pavic, K., Gaigneaux, A., Glaab, E., and Abankwa, D.K. (2024). An Improved PDE6D Inhibitor Combines with Sildenafil To Inhibit KRAS Mutant Cancer Cell Growth. J Med Chem *67*, 8569-8584. 10.1021/acs.jmedchem.3c02129.
11. Lavoie, H., Thevakumaran, N., Gavory, G., Li, J.J., Padeganeh, A., Guiral, S., Duchaine, J., Mao, D.Y., Bouvier, M., Sicheri, F., and Therrien, M. (2013). Inhibitors that stabilize a closed RAF kinase domain conformation induce dimerization. Nat Chem Biol *9*, 428-436. 10.1038/nchembio.1257.
12. Terrell, E.M., Durrant, D.E., Ritt, D.A., Sealover, N.E., Sheffels, E., Spencer-Smith, R., Esposito, D., Zhou, Y., Hancock, J.F., Kortum, R.L., and Morrison, D.K. (2019). Distinct Binding Preferences

between Ras and Raf Family Members and the Impact on Oncogenic Ras Signaling. Mol Cell *76*, 872-884 e875. 10.1016/j.molcel.2019.09.004.

13. Parkkola, H., Siddiqui, F.A., Oetken-Lindholm, C., and Abankwa, D. (2021). FLIM-FRET Analysis of Ras Nanoclustering and Membrane-Anchorage. Methods Mol Biol *2262*, 233-250. 10.1007/978-1-0716-1190-6_13.

14. Siddiqui, F.A., Alam, C., Rosenqvist, P., Ora, M., Sabt, A., Manoharan, G.B., Bindu, L., Okutachi, S., Catillon, M., Taylor, T., et al. (2020). PDE6D Inhibitors with a New Design Principle Selectively Block K-Ras Activity. ACS Omega *5*, 832-842. 10.1021/acsomega.9b03639.

Supporting Information

Supplementary Tables

Table S1. Example amounts of transfected siRNA a day before transfection of BRET-biosensor and donor-only (BRET-control) plasmids for donor saturation-titration BRET experiments, related to Part 1. "A" refers to the GFP2-tagged acceptor construct (GFP2-K-RasG12V) and "D" to the RLuc8-tagged donor construct (RLuc8-K-RasG12V). The pcDNA3.1-plasmid is used as empty vector to top up the transfected DNA amount to the same total per well.

siRNA	well number	A/D ratio		plasmid amounts/ ng			volume/ µL from 100 ng/ µL plasmid stock			siRNA/ nM*
		A	D	A	D	empty vector	A	D	empty vector	
FNTA siRNA	1	1	1	25	25	975	0.25	0.25	9.75	100
	2	4	1	100	25	900	1	0.25	9	100
	3	8	1	200	25	800	2	0.25	8	100
	4	12	1	300	25	700	3	0.25	7	100
	5	16	1	400	25	600	4	0.25	6	100
	6	24	1	600	25	400	6	0.25	4	100
	7	32	1	800	25	200	8	0.25	2	100
	8	40	1	1000	25	0	10	0.25	0	100
	9 BRET-control	0	4	0	1	9	0	1	9	0
negative control siRNA	10	1	1	25	25	975	0.25	0.25	9.75	100
	11	4	1	100	25	900	1	0.25	9	100
	12	8	1	200	25	800	2	0.25	8	100
	13	12	1	300	25	700	3	0.25	7	100
	14	16	1	400	25	600	4	0.25	6	100
	15	24	1	600	25	400	6	0.25	4	100
	16	32	1	800	25	200	8	0.25	2	100
	17	40	1	1000	25	0	10	0.25	0	100
	18 BRET-control	0	4	0	1	9	0	1	9	0

* The siRNA e.g. targeting the gene *FNTA* is transfected using Lipofectamine RNAiMAX a day before the transfection of BRET-biosensor constructs and the donor-only control which is not transfected with any siRNA but only receives RNAiMAX. Growth medium containing siRNA and RNA-transfection reagent needs to be removed before transfecting plasmids. Subsequently, cells are DNA transfected as described in **part 2**. Two saturation-titration curves can then be obtained and compared, one transfected with *FNTA* siRNA and the other with negative control siRNA.

Table S2. Example amounts of transfected BRET-biosensor and donor-only (BRET-control) plasmids for donor saturation-titration BRET experiments with drug treatment, related to Part 2. "A" refers to the GFP2-tagged acceptor construct (GFP2-K-RasG12V) and "D" to the RLuc8-tagged donor construct (RLuc8-K-RasG12V). The pcDNA3.1-plasmid is used as empty vector to top up the transfected DNA amount to the same total per well. Two 12-well plates are needed for the saturation-titration curves, one for the vehicle-control and one for the treatment with 5 µM mevastatin in 0.1% DMSO/ growth medium. For the Mevastatin treatment, prepare a 5 mM stock solution diluted in DMSO. Take two Falcon tubes containing each 9 mL of growth medium in which you add 9 µL of mevastatin in the first and 9 µL of DMSO in the second one, and vortex thoroughly to mix the medium with the compounds. Then, replace the 1 mL medium in each well with 1 mL from the corresponding DMSO or Mevastatin treatment.

		A/D ratio		volume/ µL from 100 ng/ µL plasmid stock			
treatment	well number	A	D	A	D	empty vector	drug stock / µL**
vehicle control	1	1	1	0.25	0.25	9.75	1
	2	4	1	1	0.25	9	1
	3	8	1	2	0.25	8	1
	4	12	1	3	0.25	7	1
	5	16	1	4	0.25	6	1
	6	24	1	6	0.25	4	1
	7	32	1	8	0.25	2	1
	8	40	1	10	0.25	0	1
	9 BRET-control	0	4	0	1	9	0
5 µM Mevastatin	10	1	1	0.25	0.25	9.75	1
	11	4	1	1	0.25	9	1
	12	8	1	2	0.25	8	1
	13	12	1	3	0.25	7	1
	14	16	1	4	0.25	6	1
	15	24	1	6	0.25	4	1
	16	32	1	8	0.25	2	1
	17	40	1	10	0.25	0	1
	18 BRET-control	0	4	0	1	9	0

** Drug treatment is done the day after the DNA transfection for a total of 24 hours.